Leibniz-Institut für Katalyse e.V.

an der Universität Rostock

Development of Fe- and Co-based catalysts for sustainable organic synthesis

Dissertation

In Kumulativer Form

zur Erlangung des akademischen Grades

Doctor rerum Naturalien (Dr. rer. nat.)

der Mathematisch-Naturwissenschaftlichen Fakultät

der Universität Rostock

vorgelegt von

Vishwas G. Chandrashekhar

geb. am 12. 10. 1991 in Karnataka, India

Rostock, 17.03.2022

https://doi.org/10.18453/rosdok_id00003899

Die vorliegende Arbeit entstand in der Zeit von November 2018 bis März 2022 am Leibniz-Institut für Katalyse e.V. an der Universität Rostock.

This thesis has been performed in Leibniz Institute for Catalysis at the University of Rostock in the period from November 2018 to March 2022 and was supervised by Prof. Dr. Matthias Beller and Prof. Dr. Jagadeesh Rajenahally

1. Gutachter:

Prof. Dr. Matthias Beller

Leibniz-Institut für Katalyse e. V. an der Universität Rostock

Albert-Einstein-Str. 29a, 18059 Rostock, Deutschland

2. Gutachter:

Prof. Dr. José Pérez Sestelo

Centro de Investigaciones Científicas Avanzadas, University of A Coruña

As Carballeiras, s/n, Campus de Elviña, 15071 A Coruña, España

Tag der Einreichung: March 2022

Tag der Verteidigung: July 2022

Acknowledgement

At the very beginning, I would like to express my sincere gratitude to my supervisors **Prof. Matthias Beller, Prof. Jagadeesh Rajenahally** and **Dr. Helfried Neumann** for giving me this wonderful opportunity to peruse my PhD research studies in LIKAT. This work could not be possible without their constant guidance, continuous support, and encouragement throughout the course of the doctoral study. They not only have provided me the opportunities to enhance my abilities as a researcher and responsibilities as a team member but also created nice research atmosphere as well as scientific freedom.

I profusely thank Dr. Kathiravan Murugesan for his constant encouragement and inspiration during this study. I also thank Dr. Thirusangumurugan Senthamarai and Dr. Narayana Kalevaru for helpful research discussion and their kind support. My thanks also go to Dr. David Linke, LIKAT, Dr. Ahmad Alshammari, KACST Saudi Arabia and Dr. Kishore Natte, CSIR-IIP India cooperation.

I extend my thanks to Dr. Ralf Jackstell, Dr. Thomas Schareina and Sandra Leiminger for their constant help in the laboratory and equipment, which enabled to perform research in more convenient manner. I want to thank our group members, Dr. Maximillian Marx, Bei Zhou, Fairoosa Poovan, Sara Kopf, Zhuang Ma, Yue Hu, Jie Gao, Rui Ma, Dr. Xinmin Li, Dr. Qiang Wang, Dr. Peng Wang, Kangkang Sun, Zhusong Cao for all the scientific discussions. I am grateful to Anne Tonn and Nicole Aulerich, Dr. Bernd Müller, Martha Höhne for their administration and timely help and suggestions.

I take this opportunity to acknowledge the work of the analytical department of LIKAT, especially Dr. Wolfgang Baumann, Dr. Carsten Kreyenschulte, Dr. Nils Rockstroh, Dr. Henrik Lund, Dr. Christine Fischer, Dr. Marcus Klahn, Dr. Anke Spannenberg, Susann Buchholz, Susanne Schareina, and Andreas Koch for their excellent service in characterization and analysis. Also, I thank Andeas Hutter, Dr. Torsten Dwars and Torsten Weiss for their excellent technical and purchasing service.

I thank my colleagues, Soumyadeep Chakrabortty, Priyanka Gupta, Shasha Zheng, Zahra Mazloomi, Dr. Rauf Razzaq, Dr. Xin Liu, Claas Schünemann, and other members LIKAT for useful discussions and friendship which made my stay a pleasant and worthwhile experience in Germany.

I owe my gratitude to Prof. K.M. Lokanath Rai, Prof. D. Channe Gowda, University of Mysore, India, Ms. Shantala, Mr. H.T. Vijaykumar, Dr. P.J. Geeta for their constant inspiration.

I also want to mention my thanks to my former industrial group leaders and collegues, Dr. Santosh Kulkarani, Dr. Runa, Dr. Rahul, Dr. Awadut, Dr. Joydeep, Dr. Subba, and Sushma, Sarvanan, Kaushik, Rashmi, Senthil, Sumathi, Ganapathy, Rajasekar, Gilesh, Narasimha, Vaishnavi, Manasa, Pooja, and Asha. Also, I thank my friends Karthik, Gurudev, Tejaswini, and Varadaman their continuous encouragement made me to work hard during my research.

Finally, I dedicate this PhD thesis to my late Grandmother Smt. Vinoda Nagesh Bhat and to my parents, Smt. Aruna Chandrashekhar, and Shri. Sathyanarayana Chandrashekhar. I am thankful to my family members, aunt Smt. Anupama Chandramanja, and my brother Shree Harsha Bhat and Smt. Vismaya Shree Harsha Bhat for their moral support and encouragement through this study. I also appreciate the support of my other family members and relatives.

Abstract

Development of Fe- and Co-based catalysts for sustainable organic synthesis

Vishwas G. Chandrashekhar

Leibniz-Institut für Katalyse e.V. an der Universität Rostock

In this thesis, the development of Fe- and Co-based nanoparticle and molecularly defined catalysts for sustainable organic synthesis is reported. For this synthesis, mainly catalytic hydrogenations and reductive aminations are used, which allows for the cost-effective and practical access to different kinds of amines including drug targets and intermediates. First, the preparation of iron-nanoparticles was reported for the catalytic hydrogenation of nitriles in combination with aluminium additives to synthesize structurally diverse and functionalized primary amines. Next, molecularly defined cobalt-triphos catalyst has been applied for the reductive amination of aldehydes and ketones using ammonia and molecular hydrogen to prepare linear and branched primary amines. In addition, valorization renewable feedstock such as HMF by Co-NPs catalyzed reductive amination, to prepare bio-based primary, secondary and tertiary amines including N-methyl amines as well as N-heterocycles is reported. Finally, the hydrogenation of pyridines and other *N*-heterocycles to produce saturated cyclic amines is described. The detailed characterization of nanostructured catalytic materials by TEM, EDX, XPS, XRD, EPR and Mössbauer spectroscopy as well as molecularly defined complexes by NMR and X-ray crystal structure is presented. To design suitable catalysts and to accomplish these synthetic reactions, a number of optimization studies and control experiments including kinetic and mechanistic investigations have been performed.

Entwicklung Fe- und Co-basierter Katalysatoren für nachhaltige organische Synthese

Vishwas G. Chandrashekhar

Leibniz-Institut für Katalyse e.V. an der Universität Rostock

In dieser Doktorarbeit wird über die Entwicklung Fe- und Co-basierter Nanopartikel sowie molekular definierter Katalysatoren für nachhaltige organische Synthese berichtet. Für diese Synthese werden vor allem katalytische Hydrierungen und reduktive Aminierungen verwendet, was einen kosteneffizienten und praktischen Zugang zu verschiedenen Arten von Aminen, inklusive Arzneistoff-Targets und Intermediaten, ermöglicht. Zunächst wurde über die Herstellung von Eisen-Nanopartikeln für die katalytische Hydrierung von Nitrilen in Kombination mit Aluminium-Additiven für die Synthese strukturell diverser und funktionalisierter primärer Amine berichtet. Als nächstes wurde der molekular definierte Kobalt-Triphos-Katalysator für die reduktive Aminierung von Aldehyden und Ketonen mit Ammoniak und molekularem Wasserstoff für die Herstellung linearer und verzweigter primärer Amine angewandt. Zusätzlich wird über die Wertschöpfung erneuerbarer Rohstoffe wie HMF durch Co-NP-katalysierte reduktive Aminierung zur Herstellung bio-basierter primärer, sekundärer und tertiärer Amine einschließlich N-Methylaminen sowie N-Heterozyklen berichtet. Schließlich wird die Hydrierung von Pyridinen und anderen N-Heterozyklen für die Produktion gesättigter zyklischer Amine beschrieben. Die detaillierte Charakterisierung der nanostrukturierten katalytischen Materialien durch TEM-, EDX-, XPS-, XRD-, EPR- und Mössbauer-Spektroskopie sowie der molekular definierten Komplexe durch NMR-Spektroskopie und Röntgeneinkristallstrukturanalyse wird präsentiert. Um passende Katalysatoren zu designen und diese synthetischen Reaktionen zu bewerkstelligen, wurden mehrere Optimierungsstudien und Kontrollexperimente einschließlich kinetischer und mechanistischer Untersuchungen durchgeführt.

List of Abbreviation

ACN	Acetonitrile
Al-foil	Aluminium foil
AMF	5-(Aminomethyl)-2-furanmethanol
Ar	Argon
BDC	Benzene-1,4-dicarboxylic acid
BET	Brunauer–Emmett–Teller
BHMF	2,5-Bis(hydroxymethyl)furan
Cat.	Catalyst
CAGR	Compound annual growth rate
CP	Coordination polymer
COD	Cycloocta-1,5-diene
CTAB	Cetyl trimethyl ammonium bromide
DABCO	1,4-Diazabicyclo[2.2.2]octane
DFT	Density Functional Theory
DMF	*N,N*-Dimethylformamide
dppe	1,2-Bis(diphenylphosphino)ethane
EELS	Electron Energy Loss Spectroscopy
EDXS	Energy Dispersive X-Ray Spectroscopy
E.g.,	Example
EPR	Electron Paramagnetic Resonance
EtOH	Ethanol
et al.	*Et alii*
HAADF	High Angle Annular Dark-Field imaging
HMDA	Hexan-1,6-diamine
HMF	5-Hydroxymethylfurfural
HRTEM	High-Resolution Transmission Electron Microscopy
H_2TPDC	[p-Terphenyl]-4,4''-dicarboxylic acid
h	Hour
IL	Ionic liquid
IPA	Isopropanol or 2-Propanol
L	Ligand
MC	Mesoporous carbon
MeOH	Methanol
ml	Milliliter

mmol	Millimole
MOF	Metal organic framework
mol	Mole
$NaBEt_3H$	Sodium triethyl borohydride
NMR	Nuclear Magnetic Resonance
NPs	Nanoparticles
NTf_2	Bis(trifluoromethylsulfonyl)imide
PCy_3	Tricyclohexylphosphine
Ph	Phenyl
PMA	Pyromellitic acid
PPh_3	Triphenylphosphine
POP	Porous organic polymer
PZ	Piperazine
r.t	Room temperature
SAED	Selected Area Electron Diffraction
STEM	Scanning Transmission Electron Microscopy
TA	Tartaric acid
t-BuOH	tert-Butyl alcohol
TEM	Transmission Electron Microscopy
Tetraphos	Tris[2-(diphenylphosphino)ethyl]phosphine
TFE	2,2,2-Trifluoroethanol
THF	Tetrahydrofuran
Linear Triphos	Bis(2-diphenylphosphinoethyl)phenylphosphine
Tripod triphos	1,1,1-Tris(diphenylphosphinomethyl)ethane
TON	Turnover number
TPA	Terephthalic acid
TPPTS	3,3′,3″-Phosphanetriyltris(benzenesulfonicacid) trisodium salt
XRD	X-ray Powder Diffraction
XPS	X-ray Photoelectron Spectroscopy

Table of Contents

List of schemes

List of Figures

List of Tables

1. Introduction

Organic synthesis provides the basis for many important areas in chemistry. In general, it involves the construction of compounds related to hydrocarbons and their derivatives.[1-4] Nowadays it represents a powerful toolbox, which can be applied to produce an array of different kinds of organic molecules found in nature and used in daily life.[1-4] By understanding the synthetic processes and nature of the molecules, analogues or new compounds can be prepared, which allow for improved applications in different areas of technology, science, and everyday life.[1-7] Starting from the laboratory synthesis of urea[5] in 1828 by German chemist Friedrich Wöhler the chemistry world has been radically transformed by new synthetic methods. In general, these developments have led to the synthesis of numerous useful products including pharmaceuticals, agrochemicals, cosmetics, and polymers.[2-7] While in the past century, traditional organic synthetic methodologies often involved stochiometric reagents or hazardous reagents, which obviously generate substantial amounts of waste and suffer from low atom-economy.[8-11] Thus, to overcome these limitations and to achieve organic synthesis in more efficient and sustainable manner, catalytic methodologies became important.[8-11]

Nowadays, catalysis constitutes an indispensable tool in the chemical, pharmaceutical and agrochemical industries as well as material sciences and energy related technologies.[12] Thus, today >80% of all commercial chemical products involve at least one catalytic step during their manufacture.[13] In the present and past two centuries numerous catalytic methodologies have been developed to produce all kinds of chemicals.[12-13] Starting from Ostwald (1909) for his notable work on the basic principles of catalysis and his investigations of chemical equilibria and reaction rates many Nobel prizes have been awarded to the development of catalytic methodologies.[14] Examples include Ziegler and Natta (1963) for catalysis in polymer synthesis, Wilkinson and Fischer (1973) for organometallic compounds and catalysts, Knowles and Noyori (2001) in catalytic hydrogenation including Sharpless (2001) for catalytic asymmetric oxidation, Chauvin, Grubbs and Schrock (2005) for catalytic olefin metathesis, and Heck, Negishi and Suzuki (2010) for cross-coupling reactions, and finally last year Benjamin List and David MacMillan (2021) for the development of asymmetric organocatalysis.

A major success in catalysis is based on the development of precious metal based heterogeneous materials and molecularly defined complexes.[12,15] However, their availability and comparably high price inspired scientists to look for alternative catalysts, especially based on 3d-metals (*e.g.,* Mn, Fe, Co, Ni).[16-18] The inherent features of these 3d-metals such as abundancy, lower cost and sometimes reduced toxicity makes them promising metal candidates for catalysis (**Figure 1**). Among all metals, iron is the second-most abundant metal in the earth′s crust (4.7 %) and constitutes the active center in numerous biocatalysts.[17]

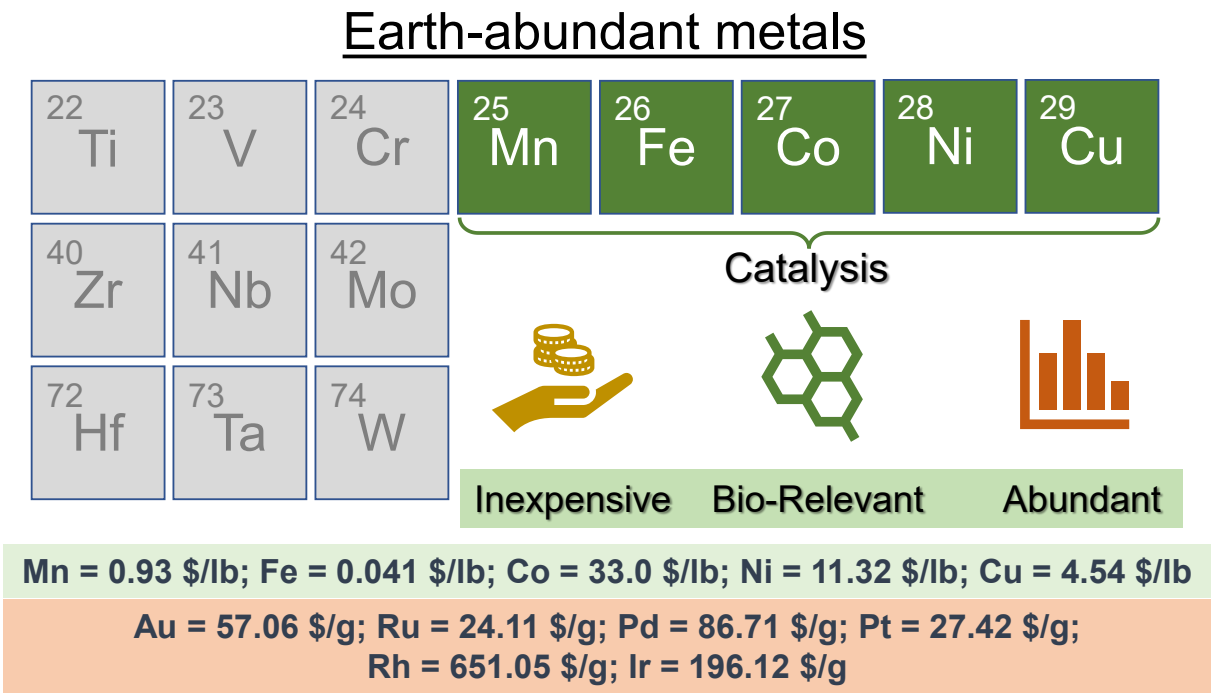

Figure 1. *Overview of earth abundant metals.*

The major challenge in 3d-metal based catalysis is to generate highly active and selective as well as stable catalytic species, as they often undergo multiple oxidation states. For this purpose, creating a suitable environment with metal-phosphorous or metal-nitrogen interactions is crucial.[19] As an example, in case of homogeneous Fe catalysts, chelating ligand-based systems are known to provide a stable ligand environment, which provides high activity and selectivity for different reactions.[20] Similarly, to improve the activity and selectivity of heterogeneous materials, creating nanoparticles or single atoms with a suitable micro-environment on the surface is interesting research field.[21]

Among the various catalytic reactions, hydrogenations constitute an important synthetic toolbox applied both in research laboratories and industries to access fine and bulk chemicals as well as pharmaceuticals and agrochemicals.[12c,20a,21c-e,22] These reactions are highly valued in organic synthesis as they are 100% atom-efficient and economical.[20a] Also, molecular hydrogen is easily available, and the reaction produces only water as by-product.[21c-e] A first breakthrough in catalytic hydrogenation reactions was established already in 1897, in which Paul Sabatier used heterogeneous Ni-catalysts for the synthesis of methane from CO_2.[23] Many decades after this seminal work, Geoffrey Wilkinson and co-workers pioneered homogeneous Rh-catalyzed hydrogenation of alkenes.[24] Among the many other notable discoveries, the artificial N_2 fixation for the synthesis of NH_3 using heterogeneous iron catalysts by Haber-Bosch is worth noting.[25]

The synthetic applicability of catalytic hydrogenation in the words of Rylander:[26]

"Catalytic hydrogenation is one of the most useful and versatile tools available to the organic chemist. The scope of the reaction is very broad; most functional groups can be made to undergo reduction, frequently in high yield, to any of several products. Multifunctional molecules can often be reduced selectively at any of several functions. A high degree of stereochemical control is possible with considerable predictability, and products free of contaminating reagents are obtained easily. Scale up of laboratory experiments to industrial processes presents little difficulty."-Paul Rylander (1979)

In general, catalytic hydrogenation reactions are frequently used for the synthesis of amines by catalytic hydrogenation of nitroarenes and nitriles as well as reductive aminations, which will be discussed in more detail in the next chapters.

1.1 Amines

Amines are considered as privileged organic compounds.[27] In 2019, the global amine market value was $17.57 billion, due to the increasing demand for high-quality food, clothing and changing lifestyles, with annual growth rate of 8% its estimated to reach $32.98 billion (**Figure 2**).[28] Today, >6 million metric tons per year of amine based valuable fine and bulk chemicals are produced (**Figure 2**).[28] For instance, more than 75% of top 200 selling drugs contain amine/nitrogen moieties, which play crucial roles in their activities.[27d] Also, the synthesis of new drugs, and improved personal care products, demands practical synthesis of new amine building blocks.[27e-i]

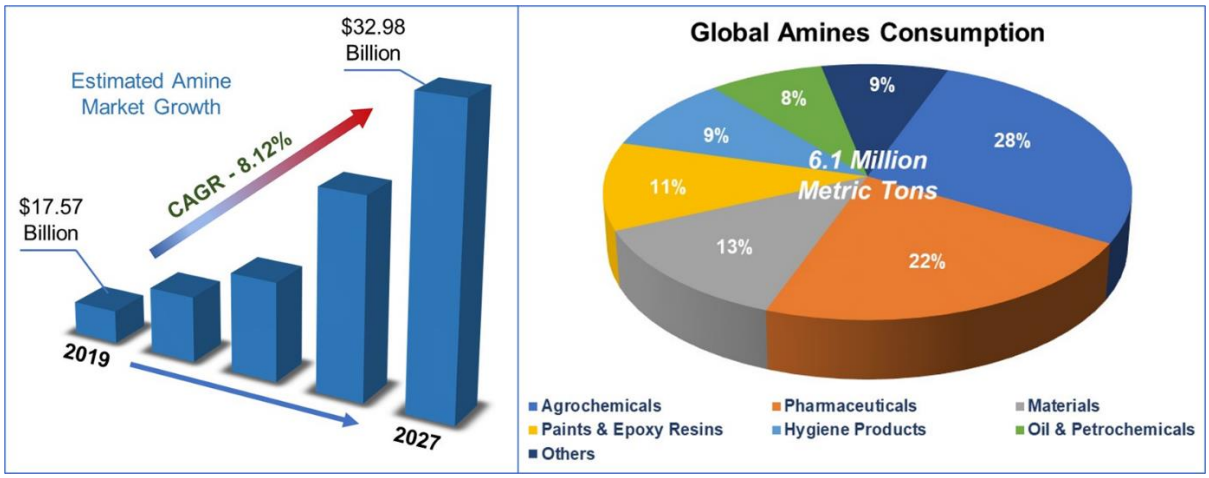

Figure 2. *Amines global market insight.*

Obviously, amines can be synthesized by using many different synthetic and catalytic methods.[29-34] Over the years, respective catalytic methods like nitrile hydrogenation,[30] reductive amination,[21e,31] hydrogenation of nitro-compounds,[18f,21c-d] C-N cross coupling,[32] hydroamination,[33] and alcohol amination[34] have been developed for the synthesis of various

amines (**Figure 3**).[29-34] Among all these methods, catalytic nitrile hydrogenation and catalytic reductive amination has gained substantial importance in industry and academia.[21e,30-31]

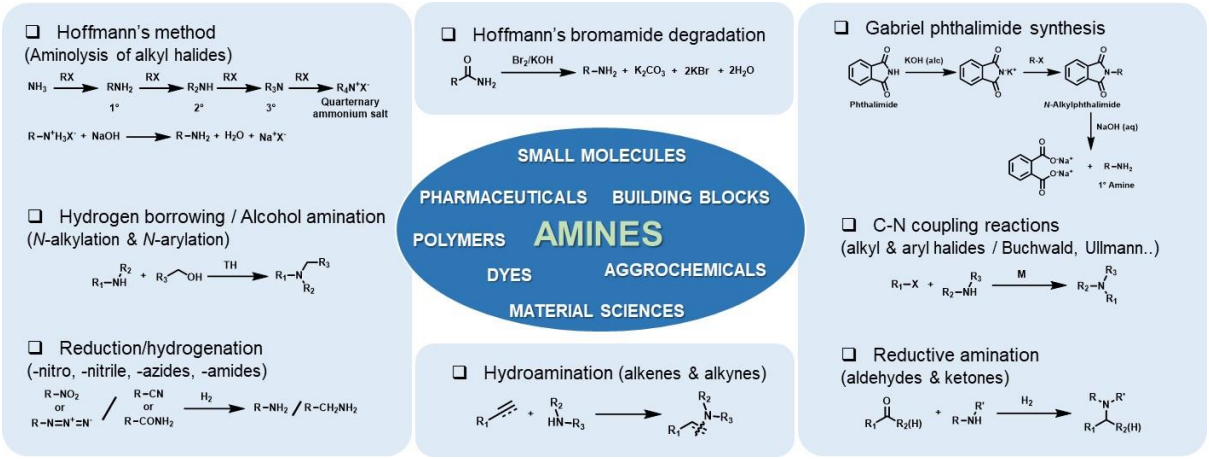

Figure 3. *General methods employed for the synthesis of amines.*

1.2 Catalytic nitrile hydrogenation

Among all hydrogenation reactions, catalytic hydrogenation of nitriles to primary benzylic and aliphatic amines allows for cost-effective and 100% atom economical industrial processes.[30,35-38] For the hydrogenation of nitriles to primary amines in an efficient and selective manner, design of suitable catalyst systems is crucial.[30a-b,

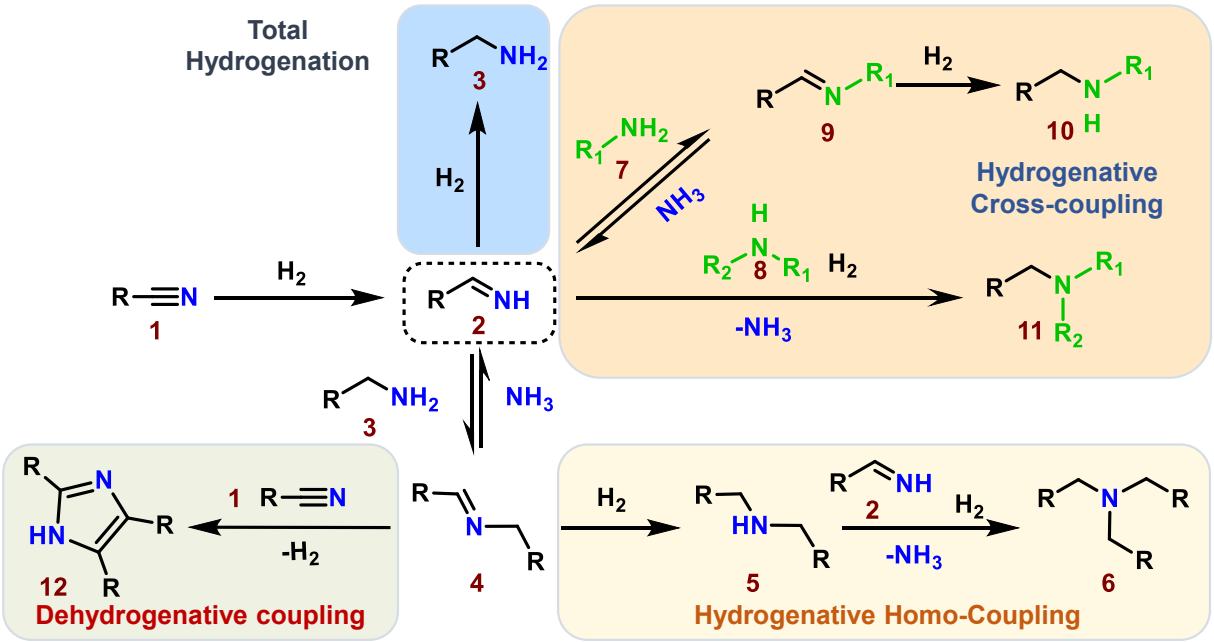

Scheme 1. *General reaction pathways for catalytic nitrile hydrogenation.*

As shown in **Scheme 1**, first hydrogenation of nitrile **1** generates primary imine **2**. This intermediate is hydrogenated to form primary amine **3** following total hydrogenation pathway. If the hydrogenation rate of primary imine **2** is slow, then the primary amine **3** can react with **2** to produce secondary imine **4**. Successive hydrogenation leads to secondary amine **5**,

following the same homo-coupling pathway, the corresponding tertiary amine **6** can be formed. Instead, in the presence of alternative primary or secondary amines **7** and **8**, imine **2** can undergo hydrogenative cross-coupling to form corresponding secondary or tertiary amines **10** and **11**. In addition, synthesis of 2,4,5-substituted imidazoles by the reaction of secondary imine **4** with nitrile **1** under dehydrogenative coupling pathway has been described too.[30a-b,]

The historic overview of heterogeneous catalysts developed for nitrile hydrogenations over the past century is shown in **Figure 4**.[35-38] Soon after the discovery of benzonitrile hydrogenation with nickel salts in 1905 by Sabatier,[35a] Paal & Gerum reported using colloidal Pd for nitrile hydrogenation in 1909.[35b] After the discovery of Raney Ni,[35c-d] many catalyst systems classified as supported catalysts, metal borides, metal alloys were reported for nitrile hydrogenations, too.[36] Most of these catalyst systems are based on noble metals and their limited availability and higher price constitute major drawbacks. Consequently, state-of-the-art catalysts for nitrile hydrogenation in industry continue to be Raney-Ni,[35c-e,36b,d] and copper chromite,[35i] which need drastic conditions. To overcome these issues in recent years 3d-metals based heterogeneous catalysts have been reported (**Figure 4**).[37-38] Herein, we discuss only cobalt and iron-based hydrogenation systems.

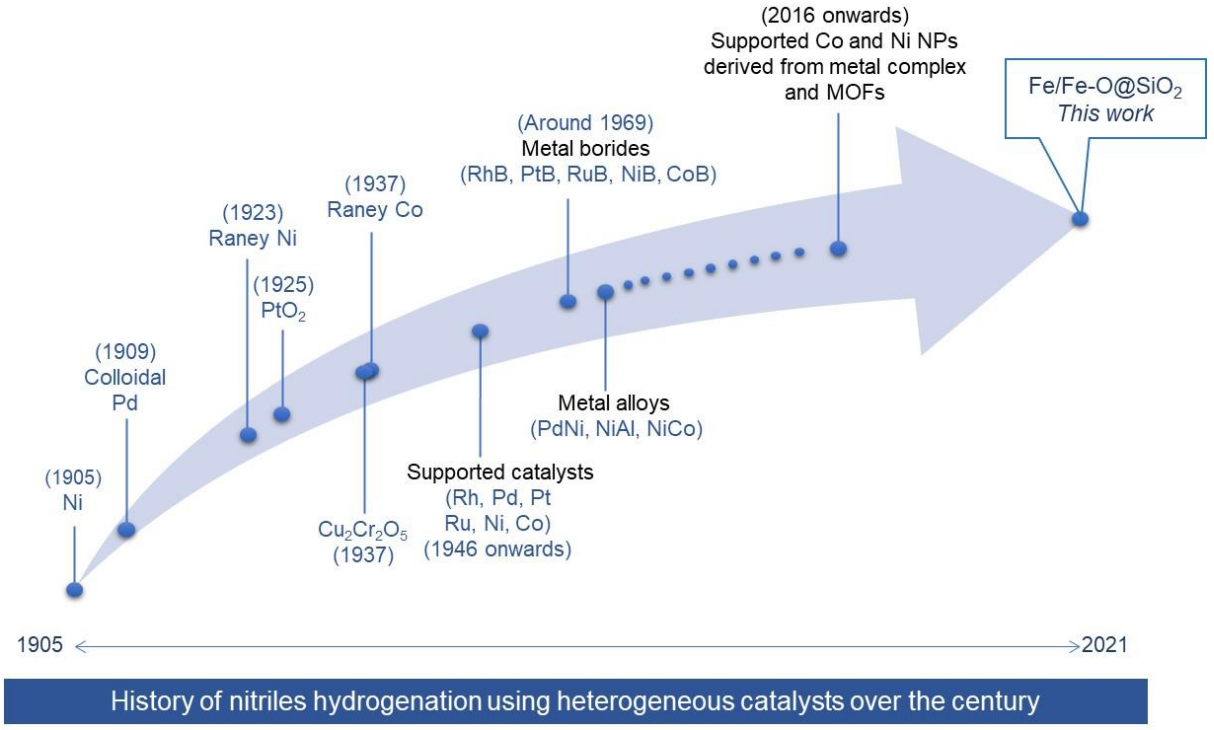

Figure 4. *Overview of heterogeneous catalysts developed for nitrile hydrogenation.*

1.3 Heterogeneous cobalt and iron catalyzed nitrile hydrogenation

Apart from Raney-Co and Co-supported catalysts. In 2016, our group[38a] reported a heterogeneous cobalt-based catalyst by pyrolysis of a $Co(OAc)_2.4H_2O$ - 1,10-phen complex

on α-Al_2O_3 at 800 °C for the hydrogenation of nitriles to primary amines under mild conditions. Here, aromatic, heterocyclic, aliphatic and, dinitriles were converted to the respective primary amines with an optimal amount of ammonia. It was also demonstrated that the reaction can be done with 5 bar hydrogen at 85 °C (**Scheme 2**). Notably, even after 8 runs, no significant drop-in activity or selectivity was observed. The authors demonstrated that the hydrogenation property of Co-catalyst is highly influenced by modification of support and nitrogen containing ligands. STEM analysis of the optimal catalyst showed different types of cobalt structures. Here, major metallic-Co NPs are covered by several graphitic layers and Co-oxide particles without graphitic layers were observed in close contact to metallic-Co.

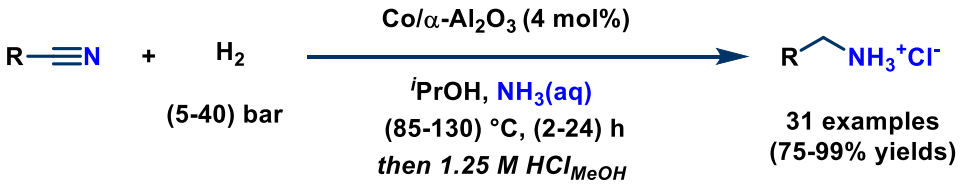

Scheme 2. *Cobalt catalyzed hydrogenation of nitriles.*

In 2017, Lin and co-workers[38b] reported single-site cobalt catalysts on Zr_{12}-based MOF nodes for the effective hydrogenation of nitriles. First, Zr_{12}-TPDC-MOF was prepared from triphenyldicarboxylic acid (H_2TPDC) and $Zr_{12}(\mu_3\text{-}O)_8(\mu_3\text{-}OH)_8(\mu_2\text{-}OH)_6$ nodes, which are used as ligand platform and linked with $CoCl_2$ to form Zr_{12}-TPDC-CoCl, which was then reduced with $NaBEt_3H$ to obtain a reusable Zr_{12}-TPDC-Co catalyst. This catalyst at 0.5 mol% was able to hydrogenate few aromatic nitriles with 94-98% yield (**Scheme 3**). The Zr_{12}-TPDC-Co catalyst was reused for seven times without loss of catalytic activity. The catalyst was synthesized in glove box prior to reaction by the reduction with $NaBEt_3H$, which could be a drawback for this methodology on larger scale.

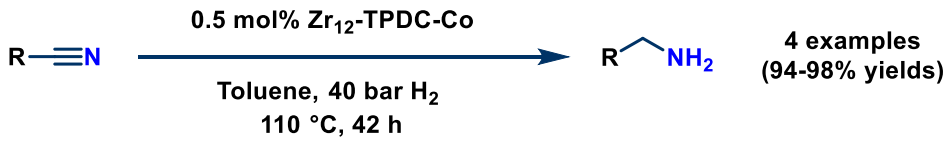

Scheme 3. *Zr-MOF supported single-site cobalt catalyzed hydrogenation of nitriles.*

After that, in 2018, Ferraccioli *et al.*[38c] reported ceria supported carbonaceous cobalt particles derived from vitamin B_{12}. This material was prepared by wet impregnation of cyanocobalamin on CeO_2 and pyrolysis at 800 °C under argon atmosphere. STEM, EDX analysis revealed two different Co phases, one with cobalt oxide particles of larger size dispersion compared to other finely dispersed phase. The catalyst showed excellent performance with 1.6 mol% Co loading for hydrogenation of industrial relevant nitriles (aromatic, heterocyclic and, aliphatic) in presence of aq. NH_3 and *i*-PrOH as solvent at 120 °C (**Scheme 4**). The catalyst can be recycled up to four runs with 90-94% yield, in fifth run moderate drop in yield observed.

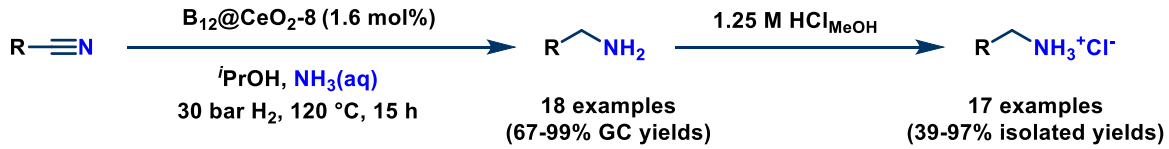

Scheme 4. *Carbonaceous cobalt particles catalyzed hydrogenation of nitriles.*

Later in the same year, our group[38d] developed graphene encapsulated Co-NPs supported on carbon (VULCAN-XC72R) for the hydrogenation of various structurally diverse and functionalized nitriles using gaseous ammonia. In this work, we also showcased gram scale synthesis and catalyst recycling. The catalyst was prepared by synthesis of Co-MOF template on carbon using $Co(NO_3)_2.6H_2O$ and terephthalic acid and subsequent pyrolysis at 800 °C under argon (**Scheme 5**). The STEM, XRD, EPR and XPS analysis support the formation of Co_3O_4 particles (5-30 nm) and metallic Co-NPs both encapsulated by graphene shells.

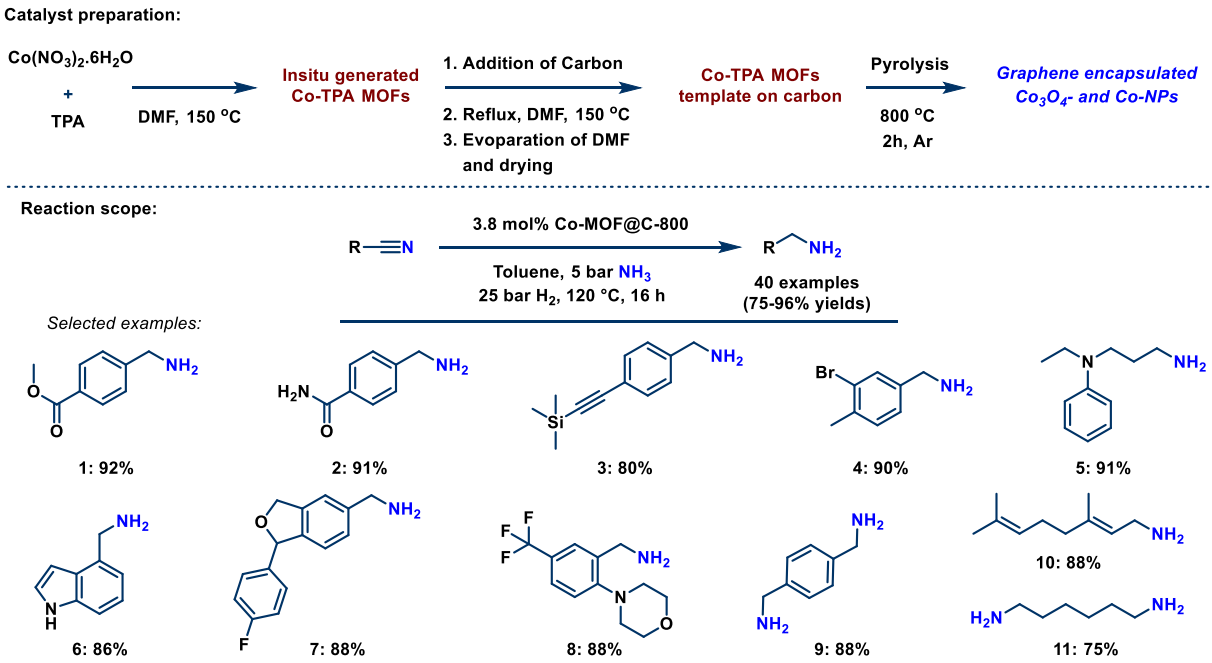

Scheme 5. *Co-MOF@C catalyzed hydrogenation of nitriles.*

In 2020, our group[38e] reported Co-NPs supported on carbon-magnesium oxide hybrid materials. The optimal catalyst was prepared by anchoring $Co(OAc)_2.4H_2O$ on chitin and then supported on MgO, successive pyrolysis at 700 °C to give carbon supported Co-NPs decorated on MgO nano cubes. The best catalyst allows hydrogenation of industrially relevant nitrile substrates (*e.g.*, adiponitrile, picolinonitrile and fatty nitriles) under mild conditions in high yields (**Scheme 6**). The Co-catalyst outperforms existing commercial catalyst like Raney-Ni, Pd/C, $Pd(OH)_x/C$, Pt/C, Ru/C in high selectivity towards primary amine. In addition, no loss in catalytic activity was detected when catalyst reused for six runs.

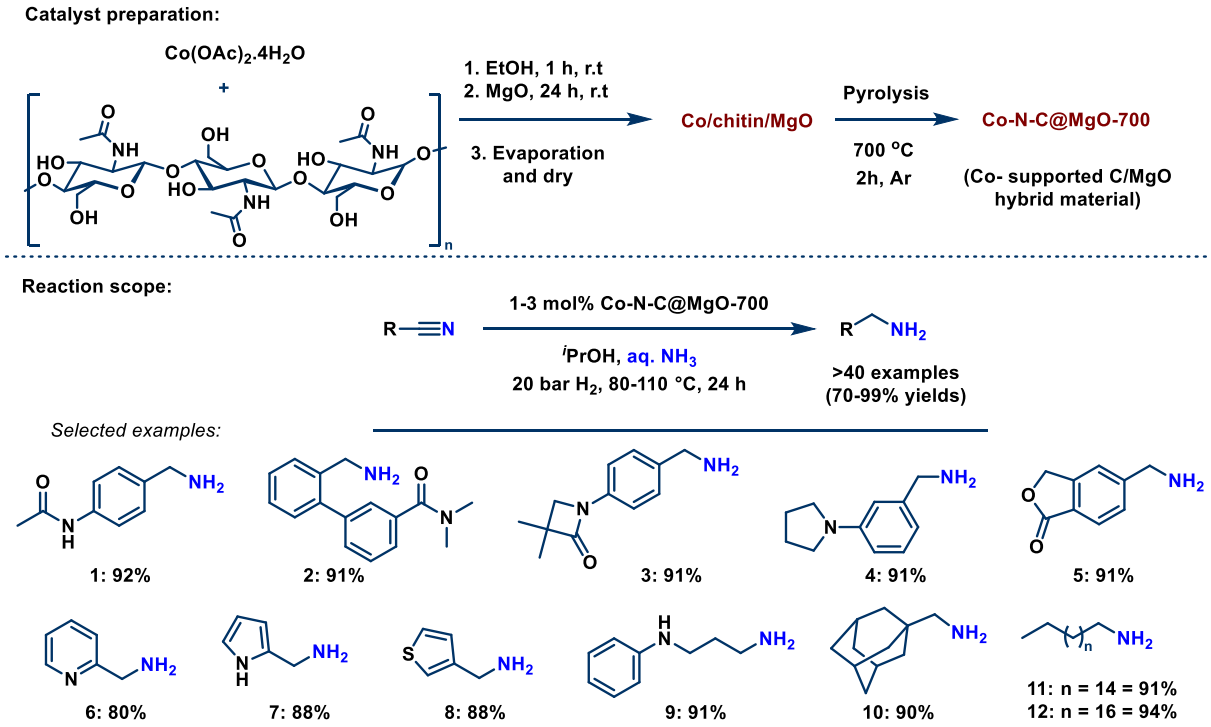

Scheme 6. *Co-N-C@MgO catalyzed hydrogenation of nitriles.*

In the beginning of 2020, Mitsudome *et al.*[38f] reported for the first time the use of metal-phosphide catalysts for hydrogenation of nitriles. The catalyst material was prepared by reacting $CoCl_2.6H_2O$ with hexadecylamine and triphenylphosphite in 1-octadecene at 300 °C under argon atmosphere to give a black precipitate which was separated by centrifugation to afford nano-Co_2P which is then dispersed on hydrotalcite support (**Scheme 7**).

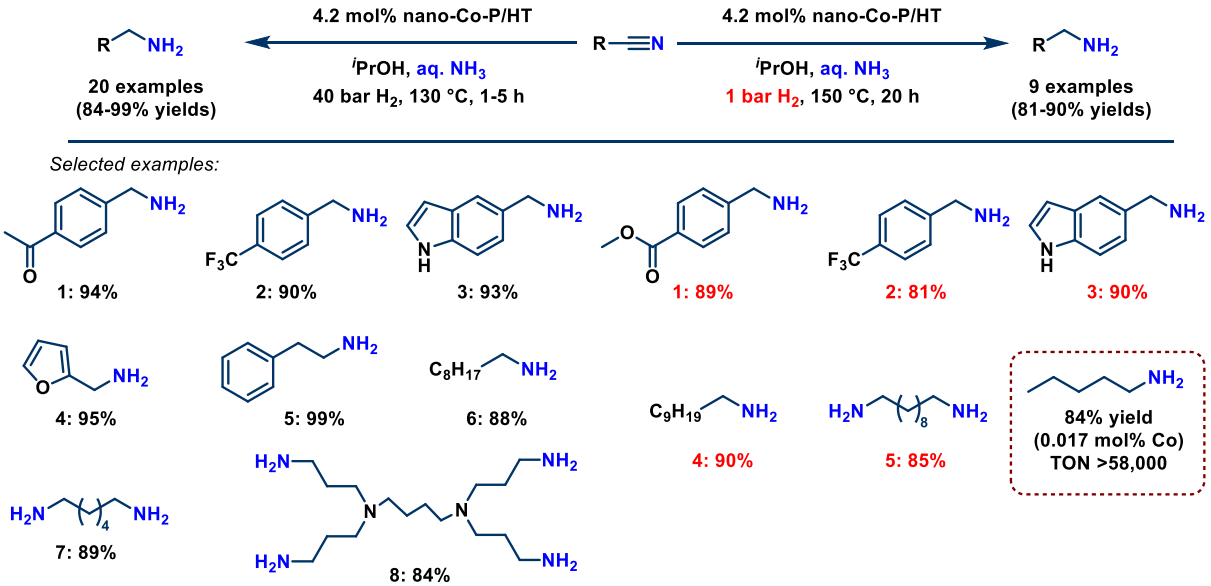

Scheme 7. *Nano-Co-P/HT catalyzed hydrogenation of nitriles.*

This new class of cobalt phosphide (nano-Co_2P) supported on hydrotalcite (nano-Co_2P/HT) has unique air-stable metallic nature which showed excellent activity and selectivity towards hydrogenation of different nitriles including di- and tetra-nitriles even at atmospheric H_2 pressure (1 bar). Upon scaling up, the catalyst showed high TON of 58000 for the

hydrogenation of valeronitrile (**Scheme 7**). TEM, HRTEM, SAED, STEM, EDX analysis of catalyst revealed rod-like structure with average size 20 × 9 nm (length × width) in hexagonal phase as dicobalt phosphide (Co_2P), consisting of cobalt and phosphorous distributed homogeneously with atomic ratio of 2:1 (Co:P). TEM of used catalyst has similar rod-like structure as fresh one which supports the high durability of catalyst even after 7 runs.

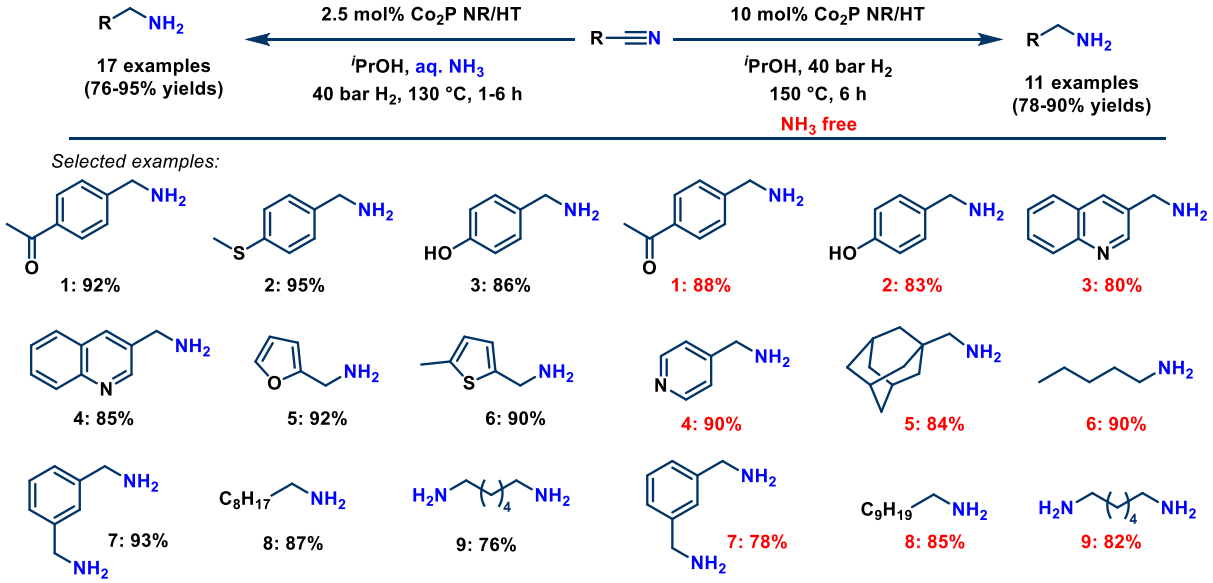

Scheme 8. *Co_2P NR/HT catalyzed hydrogenation of nitriles.*

Later in 2021, the same group[38g] reported an improved Co_2P nano-alloy on hydrotalcite (Co_2P NR/HT) which is twofold active than previously reported nano-Co-P/HT. Apart from air stability, the high activity of Co_2P NR/HT allowed hydrogenation of nitriles under mild condition (at 1 bar H_2) with broad substrate scope including N-, O-, and S-containing hetero-nitriles outperforming previous nano-Co-P/HT. Also, by increasing catalyst loading the reaction can be performed in absence of ammonia to synthesize primary amines (**Scheme 8**). Co_2P NR/HT prepared from $Co(acac)_2$ has a rod like morphology of Co_2P which is different from nano-Co_2P prepared using $CoCl_2$ indicating the effect of cobalt source on the morphology of nanoalloy. By DFT calculations the high activity attributed to back donation of d-electrons from Co to π*-antibonding orbital of nitrile group. Finally, the catalyst was recovered and reused for five cycles without any significant loss of catalytic activity.

From a sustainable point of view, the ideal catalyst system for nitriles hydrogenation should be based on iron because of its abundance, inexpensiveness, and low-toxicity.[17] Indeed, in the past decade utilizing sophisticated/synthetically demanding PNP-pincer ligands,[20a-b] it was possible to generate active iron complexes to hydrogenate nitriles. In contrast, heterogeneous catalysts show improved stability and can be easily reused.[21d] Unfortunately, creating analogous active iron centers on a surface was not possible, yet. In 2021, we developed the first general Fe-based heterogeneous catalyst for the hydrogenation

of nitriles to primary amines. These results are discussed in this thesis (Section 3, Chapter 3.1).

1.4 Catalytic reductive aminations

Catalytic reductive aminations constitute as a powerful method for the synthesis of amines from carbonyl compounds, which are widely used in industries and research labs.[31,39] Through this methodology different kinds of amines can be synthesized and functionalized in a convenient and cost-effective manner.[21e,31,39]

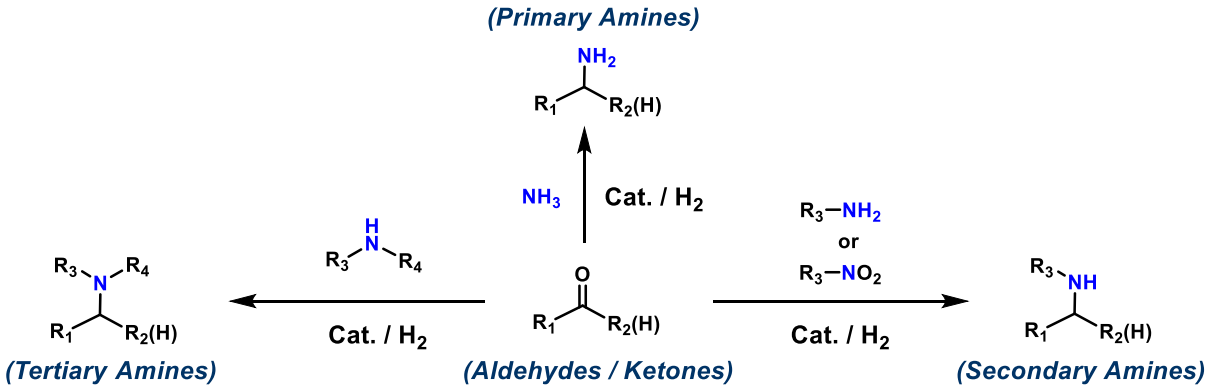

Scheme 9. *Catalytic reductive aminations for the synthesis of amines.*

In general, aldehydes or ketones react with ammonia, primary, secondary amines, or nitro compounds to give the corresponding imines as intermediates, which in presence hydrogen using suitable catalysts are reduced to the corresponding amines (**Scheme 9**). Molecular hydrogen as a reductant is highly preferred as it produces only water as byproduct and is inexpensive.[31a-b,39a-c,g-h]

1.5 General reaction mechanism and challenges associated with reductive aminations

In this method, primary, secondary, and tertiary amines can be selectively prepared or functionalized using suitable catalysts. Often these reactions suffer from lack of selectivity and reduction of carbonyl compounds to corresponding alcohols.[39a,40] Reductive amination of carbonyl compounds with ammonia to form primary amines is more challenging as catalyst deactivation associated with use of ammonia and drastic conditions required for ammonia activation.[31,39a,40]

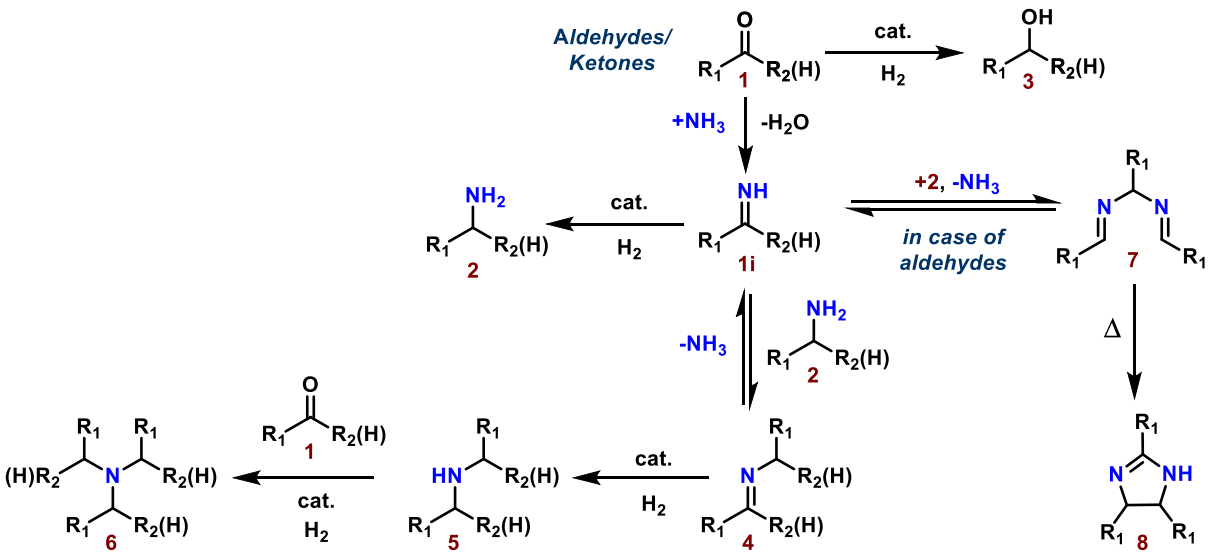

Scheme 10. General reaction mechanism in reductive amination with ammonia.

As shown in **Scheme 10** first, the carbonyl compound **1** condenses with ammonia to form primary imine **1i** as intermediate. In presence of suitable catalysts and hydrogen **1i** is reduced to the desired primary amine **2**. Direct reduction of carbonyl compounds **1** to corresponding alcohol **3** can occur if the catalyst is less selective towards imine **1i** reduction. If the imine **1i** hydrogenation does not proceed fast, this increases the concentration of imine in the system which can lead to side reactions. Secondary imine **4** is formed by condensation of primary amine **2** with carbonyl compound **1** or intermediate imine **1i**. This formed secondary imine **4** can be reduced to secondary amine **5**, which can react again with carbonyl compound **1** to form tertiary amine **6**. In case of aldehydes, primary imine **1i** can also trimerize to form **7**, which undergo thermal cyclization to form imidazole derivatives **8**.

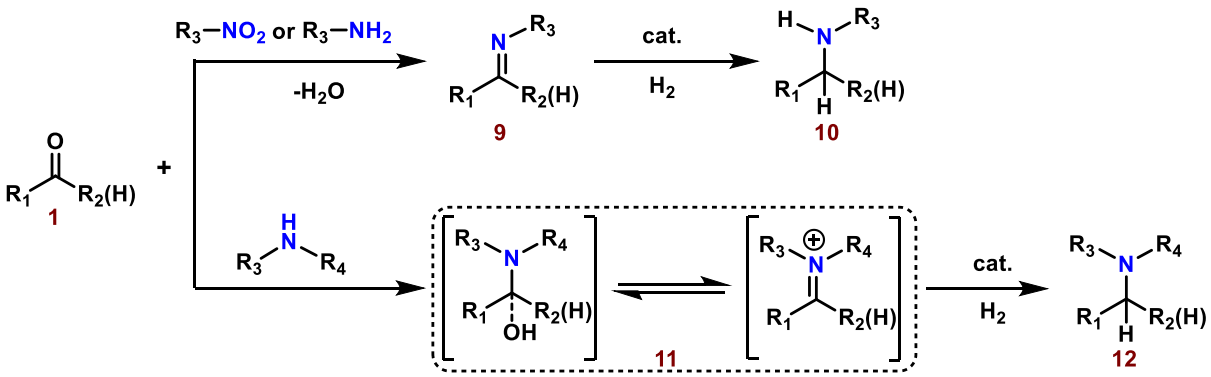

Scheme 11. General reaction mechanism in reductive amination with amines.

Likewise, anilines can condense with carbonyl compound to form secondary imines **9** which are hydrogenated in presence of catalyst to form secondary amines **10** (**Scheme 11**). Even nitroarenes can be used for the synthesis of secondary amines.[31,39a,40] Here, the nitroarene reduced *in situ* to aniline which undergoes reductive amination to form secondary amine **10**. For tertiary amines, the condensation of carbonyl compounds with secondary

amines proceeds *via* corresponding enamine or iminium ion **11** as intermediate, which is further hydrogenated in presence of catalyst to tertiary amines **12**.

Despite of all these challenges, in homogeneous catalysis usually the catalyst tends to deactivate when using ammonia due to formation of Werner type complexes.[40c] To overcome these challenges precious metal-based catalysts were used.[41] Hence, development of base-metal homogeneous catalyst is still interesting. As heterogeneous materials some non-noble metal-based ones have been developed (*e.g.,* Raney Ni, Co-, Ni-, Fe-based).[31,42] Below we will discuss the previous reports on catalytic reductive amination for the synthesis of primary amines with cobalt and iron based homogeneous catalysts (Section 1.6) and catalytic reductive amination for the synthesis of amines from HMF with cobalt based heterogeneous materials (Section 1.7).

1.6 Homogeneous cobalt catalyzed synthesis of primary amines

The development of homogeneous catalysts for the reductive amination of carbonyl compounds with ammonia is more challenging and less explored. The formation of stable Werner-type complexes of transition metals with ammonia is a major issue which leads to deactivation of catalyst.[40c] Thus, only few metal-complexes systems are known for the synthesis primary amines from carbonyl compounds in presence of NH_3 and H_2, which are mainly based on precious metals like Rh,[41a-b] Ru,[41d-e] and Ir.[41c]

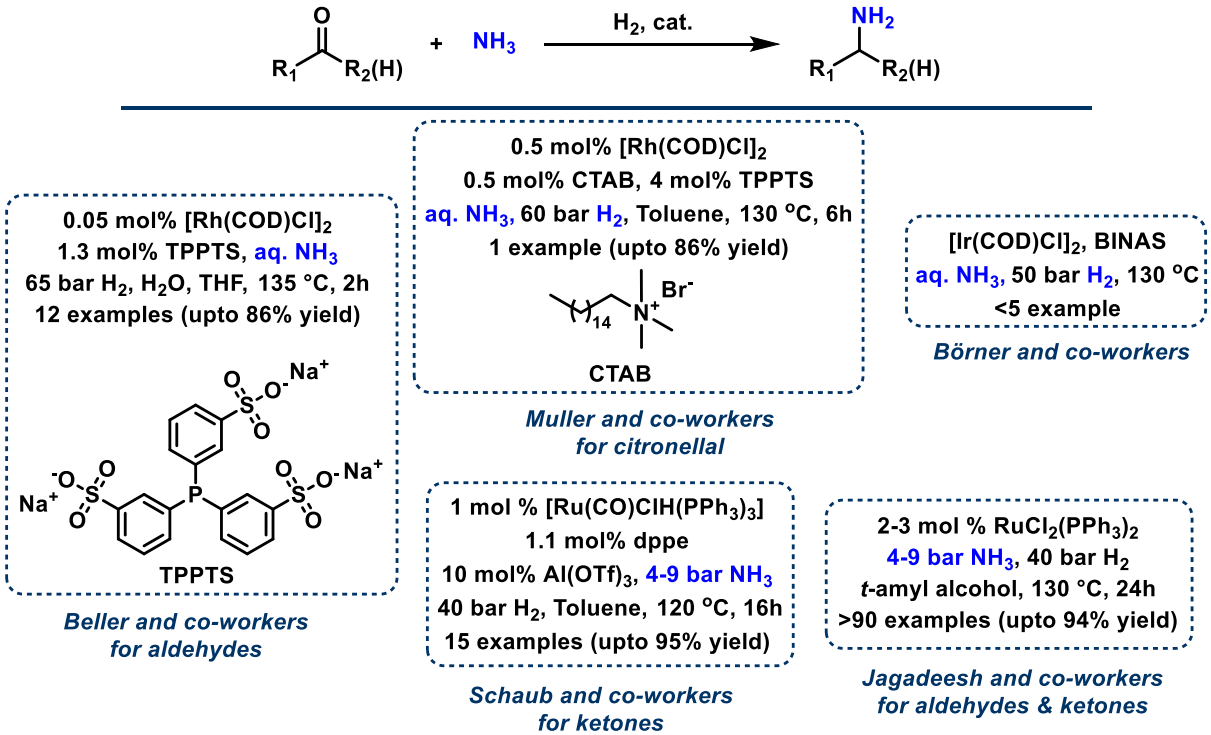

Scheme 12. *Precious metal catalyzed reductive amination of carbonyl compounds with ammonia.*

For Rh & Ir, Beller and co-workers[41a] developed the first homogeneous catalyst based on $[Rh(COD)Cl]_2$-TPPTS for the reductive amination of aldehydes with NH_3 and H_2 (**Scheme**

12). This catalyst system worked well for aromatic aldehydes (>95%) compared to aliphatic aldehydes (<40%). In 2015, Muller and co-workers[41b] showed synthesis of citronellylamine from citronellal using $[Rh(COD)Cl]_2$-TPPTS catalyst in a biphasic solvent system using phase transfer catalyst (CTBA). Börner and co-workers[41c] reported a patent where $Rh[(dppb)(COD)]BF_4$, and $[Rh(COD)Cl]_2$-BINAS including $[Ir(COD)Cl]_2$-BINAS systems were used for the synthesis of primary amines.

For Ru, in 2016 Schaub and co-workers[41d] reported $[Ru(CO)ClH(PPh_3)_3]$-dppe catalyst for the synthesis of branched primary amines from ketones in presence $Al(OTf)_3$ as additives, the authors demonstrated 15 examples upto 95% yield. Later in 2018, our group[41e] reported a simple commercially available $RuCl_2(PPh_3)_2$ catalyst for the efficient reductive amination of aldehydes and ketones with ammonia without any additives. Here, we demonstrated >90 examples with up to 94% yield and under industrially viable conditions.

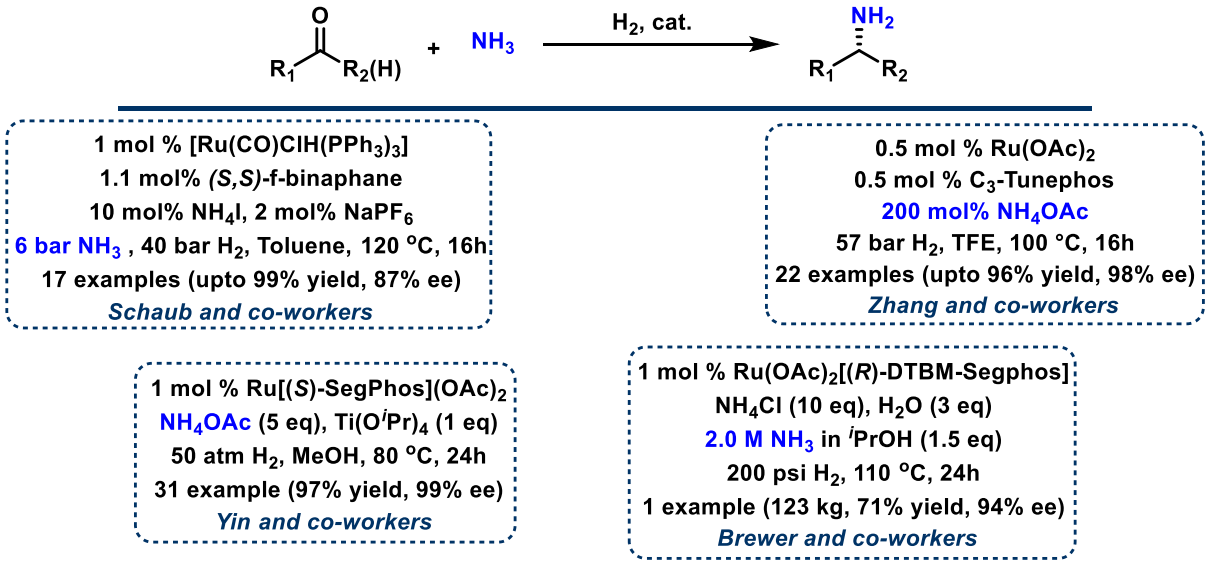

Scheme 13. *Asymmetric reductive amination for the synthesis of chiral primary amines.*

Apart from these catalysts for reductive aminations, few Ru[43] catalysts were also reported for asymmetric reductive amination of branched ketones for the synthesis of chiral primary amines (**Scheme 13**). Till 2019, there was no homogeneous base-metal catalyst developed for this challenging reaction. Our group developed first base-metal catalyst based on cobalt-triphos system for reductive amination of various aldehydes and ketones, these results are discussed in this thesis (Section 3 and Chapter 3.2).

1.7 Heterogeneous cobalt-based catalyst for reductive amination of HMF

Development of heterogeneous methodology for preparation of fuels and chemicals from biomass-based feedstock has gained substantial attention, due to their renewable nature, meets green chemistry metrics and can reduce environmental issues caused by rapid depletion of fossil fuels.[44] In this respect, development of cost-effective methodologies for the valorization of biomass and related compounds to platform chemicals for developing novel chemicals is of central importance.[44]

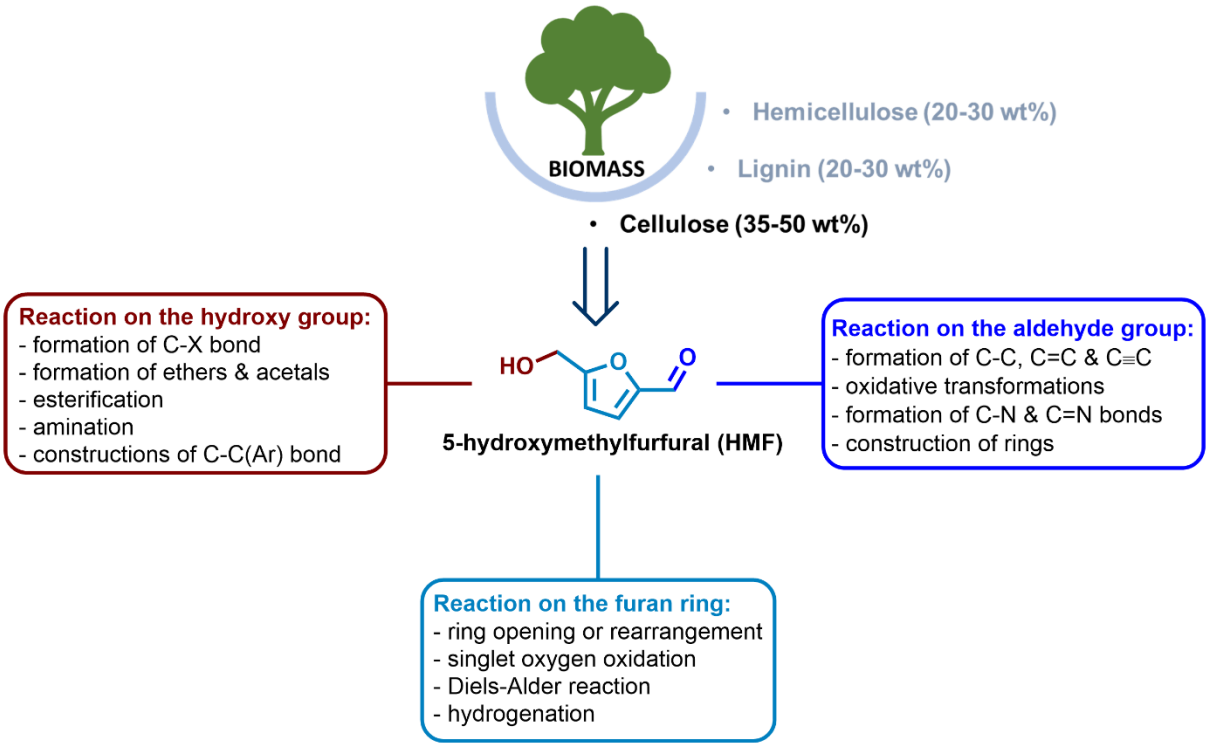

Figure 5. *Overview of HMF and its functionalization.*

The crude biomass predominantly consists of cellulose (35-50%), hemicellulose (20-30%), and lignin (20-30%). These three biopolymers transformed into small organic intermediates called platform chemicals.[45] Among these platform chemicals, 5-hydroxymethylfurfural appears to be rich building block and can be directly produced from C-6 sugars.[45] HMF has an aldehyde group at C-2 position, a hydroxymethyl group at C-5 position, including a reactive furan ring, these functional groups offer a wide range of possibility for late-stage functionalization and chemical transformation for value-added chemicals, fuels, and polymers (**Figure 5**).[45f] Among these latter products *N*-substituted furfuryl amines represents an important class of compounds due to their biological activities such as antimuscarinic agent, carcinogenesis inhibitors, calcium antagonistic activity, and cholinergic agent.[44d-f,46a-c] Also, application in surfactants, polymers, agrochemicals.[44d,f,46d] Catalytic reductive amination of aldehyde group in HMF with an amine source (ammonia, primary or secondary amines) and molecular hydrogen is an effective method to synthesize these *N*-substituted chemicals.[44d-f] In

this respect, few heterogeneous catalysts are reported majorly based on noble metals like Rh,[47a] Pt,[47b] Pd,[47c-d] Ru,[47e-g] and Au.[47h] With respect to base-metal heterogeneous catalysts, Raney-Ni,[48a] Raney-Co,[48g] Ni,[48d-f] Cu, [48b-c] and Co[48h] based ones are known. Below we discuss the previous reports on catalytic reductive amination of HMF for the synthesis of primary amines with cobalt based heterogeneous catalysts.

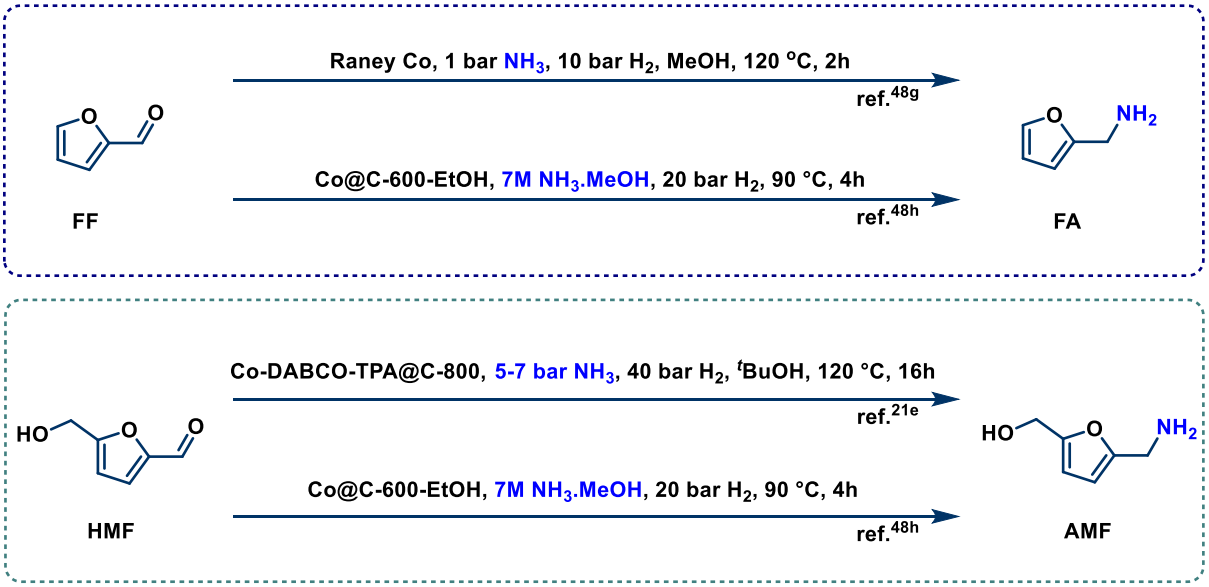

Scheme 14. *Heterogeneous Co-catalyzed reductive amination of FF and HMF with ammonia.*

Despite many reports in base metal category, not much development has been done with Co-based catalysts for reductive amination of HMF and related furfural. In 2017, our group[21e] reported MOF-derived graphitic shell encapsulated Co-NPs for reductive aminations of aldehydes and ketone in presence of ammonia, here we have demonstrated the application of this Co-NPs in synthesis of primary amines from HMF and related compounds (**Scheme 14**). Later, in 2019 Wei and co-workers[48g] studied the activity of commercially available catalyst like Rh/C, Pt/C, Pd/C, Ru/C, Raney Ni, and Raney Co in reductive amination of furfural with ammonia. Among these, Raney Co found to be more active for the synthesis of furfuryl amine in 98.8% yield. By studying the reaction mechanism and catalytic pathways, the high activity of Raney Co attributed to faster hydrogenolysis of the Schiff base intermediate and using ammonia in the system greatly promoted hydrogenolysis. The catalyst recycled for 8 times without any significant loss of activity (**Scheme 14**). Recently, Ma and co-workers[48h] reported environmentally friendly method for the synthesis of Co-NPs supported on carbonaceous matrix by using cobalt acetate, citric acid in water or ethanol and successive pyrolysis at 600 °C. Under optimal conditions the active Co@C-600-EtOH catalyst can facilitate reductive amination of HMF, FF, and related biomass-derived aldehyde compounds (>24 examples) in good to excellent yields (**Scheme 14**). TEM/mapping, XRD, XPS, and *in situ* FTIR revealed the catalyst contains metallic Co-NPs uniformly dispersed on carbonaceous matrix, due to

sponge-like structures no aggregation was observed, and these NPs encapsulated with multilayers of graphene. The reaction pathways revealed metallic-Co activates carbonyl group and promotes imine formation, while the acid sites on the particle hydrogenates imine. The catalyst can be reused up to eight times obtaining 88% yield. In this thesis, we discuss the development of MOF-based Co-catalyst for reductive amination of HMF at mild condition with H_2 and NH_3 or amines. These results are discussed in this thesis (Section 3 and Chapter 3.3).

1.8 Catalytic hydrogenation of pyridines and other *N*-heteroarenes

The catalytic hydrogenation of *N*-heteroarenes has not lost its importance as the corresponding saturated amines immensely used for the synthesis of biologically active building blocks and key intermediates in the manufacture of pharmaceuticals, agrochemicals, and other fine chemicals.[49] Nitrogen containing compounds are the central structural components of pharmaceuticals (**Figure 6**).[49a-c]

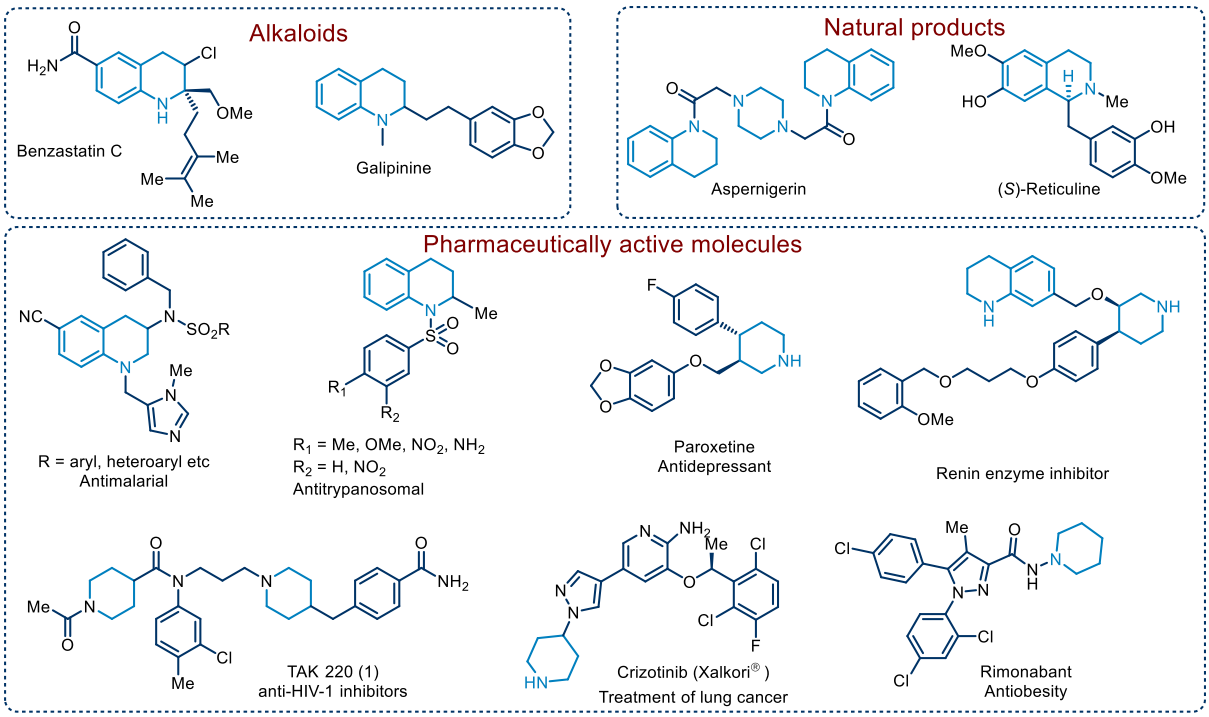

Figure 6. *Piperazine and tetrahydro(iso)quinoline in life-sciences.*

In a report of 2014, U.S. FDA approved drugs reveals that 59% of unique small-molecule drugs contain a nitrogen heterocycle.[49b] Particularly, piperidine is used as one of the most common building blocks in organic synthesis.[49a-b] Among the different methods to prepare piperidine derivatives, hydrogenation of easily accessible pyridines is more efficient.[50] Although some homogeneous protocols (Rh,[51] Ir[52]) have been reported for this reaction, as cost effective and sustainable point heterogeneous systems are desired. However, this reaction is challenging as the catalyst is often poisoned by the coordination of the metal with the ring nitrogen of pyridine or piperidine.[53] In 1928, Adams reported successful catalytic

hydrogenation of pyridines with PtO_2 using HCl in the system.[54] The formation of pyridine salt can block the coordination of the nitrogen to metal center thereby avoiding catalyst deactivation. Other catalysts were reported based on precious metals like (Rh NPs, Rh/C, Pt/C, RuO_2, Pd/C)[50] and in most cases addition of acids was needed to avoid poisoning. For such reactions, development of low cost and less toxic earth-abundant 3d metals continues to be primary goal. Till now only a cobalt-based heterogeneous catalyst is known for the hydrogenation of pyridines which works under drastic conditions limiting its applicability (160 °C, 60 bar H_2).[55] On the other hand, several non-noble heterogeneous catalysts based on Raney Ni,[56a] Ni,[56b] Fe,[56c-d] and Co[57] have been reported for the hydrogenation of (iso) quinolines and related heterocycles. In this thesis, we discuss previous reports of heterogeneous catalysts based on iron and cobalt for the hydrogenation of pyridines and other *N*-heteroarenes.

1.9 Iron catalyzed hydrogenation of quinolines and *N*-heteroarenes

In 1987, Stapp and Shaw first demonstrated the use of iron(III) oxide for the hydrogenation of 2-methylquinoline at 300 °C (**Scheme 15**).[56c]

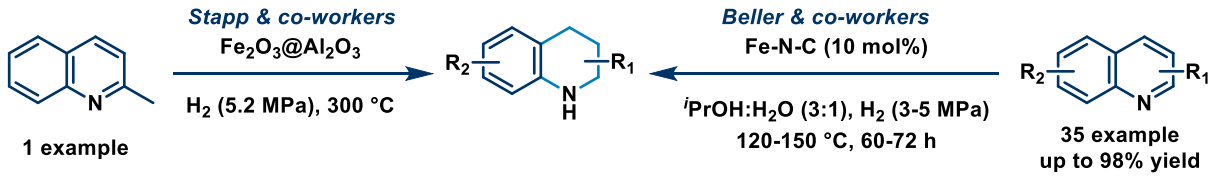

Scheme 15. *Iron catalyzed hydrogenation of quinolines.*

Later, in 2018 Beller and co-workers[56d] showed complexation of iron(II) acetate and *N*-aryliminopyridines, supported on carbon and successive pyrolysis gives iron NPs consisting of Fe^0, Fe_3C, and FeN_x in *N*-doped carbon matrix. This Fe-N-C catalyst could selectively hydrogenate of quinolines and isoquinolines, even in the presence of functional groups, such as halogens, esters, nitriles, and amides (**Scheme 15**). This methodology was showcased in the synthesis of natural products and pharmaceutical compounds.

1.10 Cobalt catalyzed hydrogenation of pyridines and *N*-heteroarenes

In 2018, Chen *et al.*[55] reported first base metal catalyst for the hydrogenation of pyridines based on Co-metal. Simple impregnation of cobalt acetate, melamine on TiO_2 and subsequent pyrolysis at 800 °C resulted in Co-NPs supported TiO_2 with large amount of nitrogen-modified TiN and oxidized Ti-N-O structure. Under optimal condition the catalyst hydrogenated numerous substituted pyridines without any acid additives with good activity and selectivity up to 98% with water as solvent. The catalyst can be recycled up to 5 times up to 92% yield without much decrease in activity and synthesis of bioactive compounds (*Desoxypipradrol* and *Isosolenopsin A*) were showcased (**Scheme 16**).

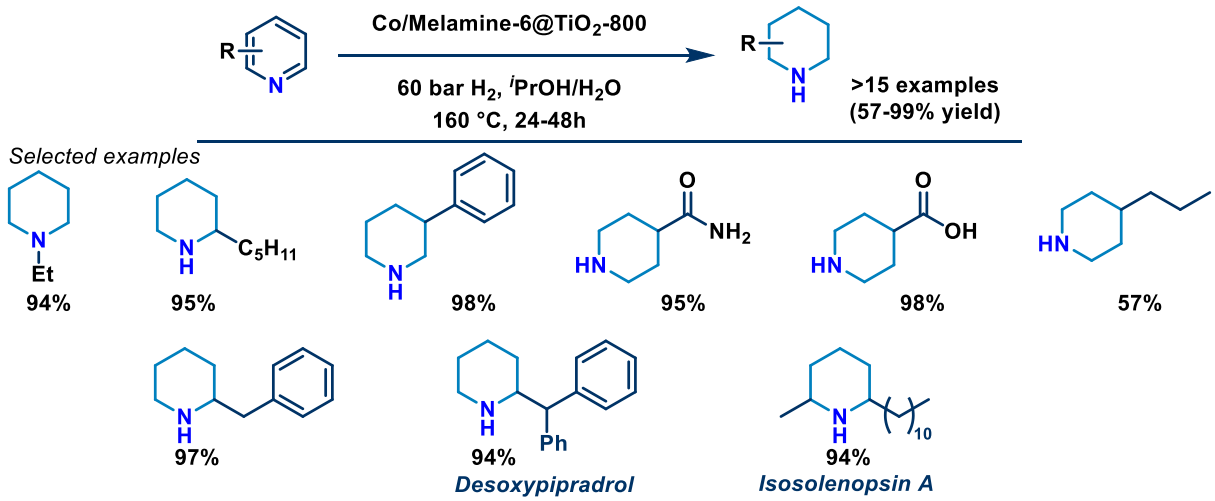

Scheme 16. *Co-Melamine catalyzed hydrogenation of pyridines.*

After this no base metal catalyst were reported for this challenging transformation. In 2020, our group developed MOF-based Co-catalyst for this reaction and these results are discussed in this thesis (Section 3 and Chapter 3.4).

Previously, many Co-based heterogeneous materials have been developed for the hydrogenation of quinoline is listed below (**Table 1**)[57] and very few catalysts are extensively studied for the synthesis of tetrahydro quinolines (Entry 1, 6, 10, 11, 14). With these catalysts many functionalized and structurally diverse tetrahydroquinolines were synthesized with up to 98% yields. All these catalysts use relatively high temperature and hydrogen pressure, development of catalyst which works at milder condition is always desired. As an extended scope hydrogenation of quinoline was also performed with our Co-catalyst (Section 3 and Chapter 3.4).

Table 1. *Co-catalyzed hydrogenation of quinoline.*

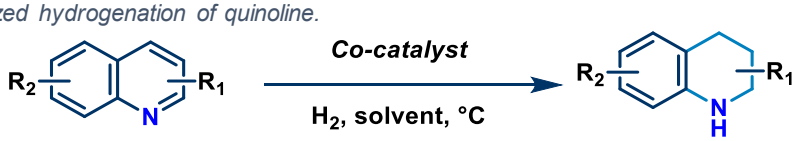

Entry	Catalyst	H_2 (bar)	Temp. (°C)	Solvent	Yields (%)	*e.g.,*	*et al.* [57]
1	Co_3O_4-Co/NGr@α-Al_2O_3	20-30	120-140	Toluene	49-97	32	*Chen (2015)*[a]
2	Zr-MTBC-CoH	40	80-100	Toluene	72-99	7	*Ji (2016)*[b]
3	CoO_x@CN	30	110-140	MeOH	77-99	9	*Wei (2016)*[c]
4	Co@NGC-800	40	120	^{i}PrOH	82	1	*Li (2017)*[d]
5	Ti_8-BDC-CoH	50	160	Neat	78-100	4	*Ji (2018)*[e]
6	Co-Mo-S-0.83	12-30	120-150	Toluene	50-98	23	*Sorribes (2018)*[f]
7	Co-SA/AC@N-CNTs-L	20	100	Ethanol	96-99	9	*Gong (2019)*[g]

8	Co-Phen@C	35	120	Toluene	71-98	11	*Garima (2019)*[h]
9	Co/AlN	40	100-140	^{i}PrOH	70-99	11	*He (2020)*[i]
10	$CoCl_2$ + $NaBH_4$	20-30	130-150	H_2O	57-99	24	*Hervochon (2020)*[j]
11	Co@C	20	80-100	^{i}PrOH	83-99	20	*Zhang (2020)*[k]
12	Co-L/Carrier	100	100-150	MeOH	79-99	11	*Asaula (2021)*[l]
13	CoW@C NPs	8	100	Toluene	85-98	11	*Puche (2021)*[m]
14	$Co(OAc)_2.4H_2O$ & Zn	30	70-150	H_2O	50-99	24	*Timelthaler (2022)*[n]

2. Objectives of this work

The development of new catalysts and their applications play crucial roles in organic synthesis to produce all kinds of chemicals needed for our daily life products including many molecules used in life sciences. Thus, not surprisingly around 90% of all chemical products in industry are made via catalysis. Among the various catalytic reactions, catalytic hydrogenations are widely used and allow for the cost-effective and sustainable production of fine and bulk chemicals as well as pharmaceuticals, agrochemicals, and other daily life products. In this context, specifically catalytic hydrogenations applied for the synthesis of amines are of prime importance because the resulting products are highly valued compounds, finding interesting applications in chemistry, medicine, biology, material sciences, and energy technologies. In particular, catalytic hydrogenation of nitroarenes and nitriles as well as reductive aminations can be applied for the synthesis of all kinds of amines. Hence, the primary goal of this work was to develop earth abundant Fe- and Co-based nanoparticles and molecularly defined catalysts for hydrogenations and reductive amination reactions to prepare different kinds of amines. Here, main objectives were a) to develop 3d-metal catalysts for the hydrogenation of nitriles to amines and b) to prepare and apply both homogeneous and heterogeneous 3d metal catalysts for reductive aminations. In this respect, specifically the hydrogenation of renewables was interesting, too.

3. Summary of this work

This section includes summary of the research work on the development of Fe- and Co-based heterogeneous and homogenous (Co) catalysts for hydrogenation and reductive amination reactions.

3.1 Silica-supported Fe/Fe–O nanoparticles for the catalytic hydrogenation of nitriles to amines in the presence of aluminium additives

The hydrogenation of nitriles to amines represents an important and largely used industrial processes because the resulting products constitute important precursors and central intermediates in chemical, pharmaceutical, agrochemical and material industries.[27-28] The state-of-the-art catalysts for nitrile hydrogenation in industry continue to be Raney-Ni,[35d] and copper chromite,[35h] which require drastic conditions and suffer from toxicity issues. To overcome these issues alternative nickel- and cobalt- based heterogeneous catalysts have been reported in recent years.[37-38] Despite of these catalytic systems, from a sustainable and cost-effective point of view, iron-based heterogeneous catalysts are highly desired.[17] Surprisingly, until 2021 no Fe-based heterogenous catalysts have been reported for the hydrogenation of nitriles. Noteworthy, very recently, we reported supported Fe-based nanoparticles for the nitrile hydrogenation. This Fe-catalyst consisting of iron/iron oxide (Fe/Fe-O@SiO_2) cores shell particle supported on silica. In a typical procedure, these nanoparticles have been prepared by pyrolysis of iron acetate on commercial silica (Aerosil-SiO_2) at 800 °C under reductive (H_2) conditions (**Figure 7**).

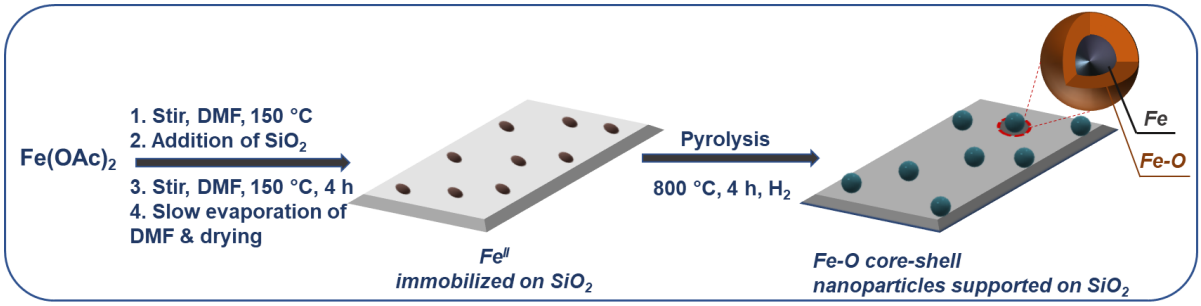

Figure 7. *Preparation of Fe/Fe-O core-shell structured nanoparticles.*

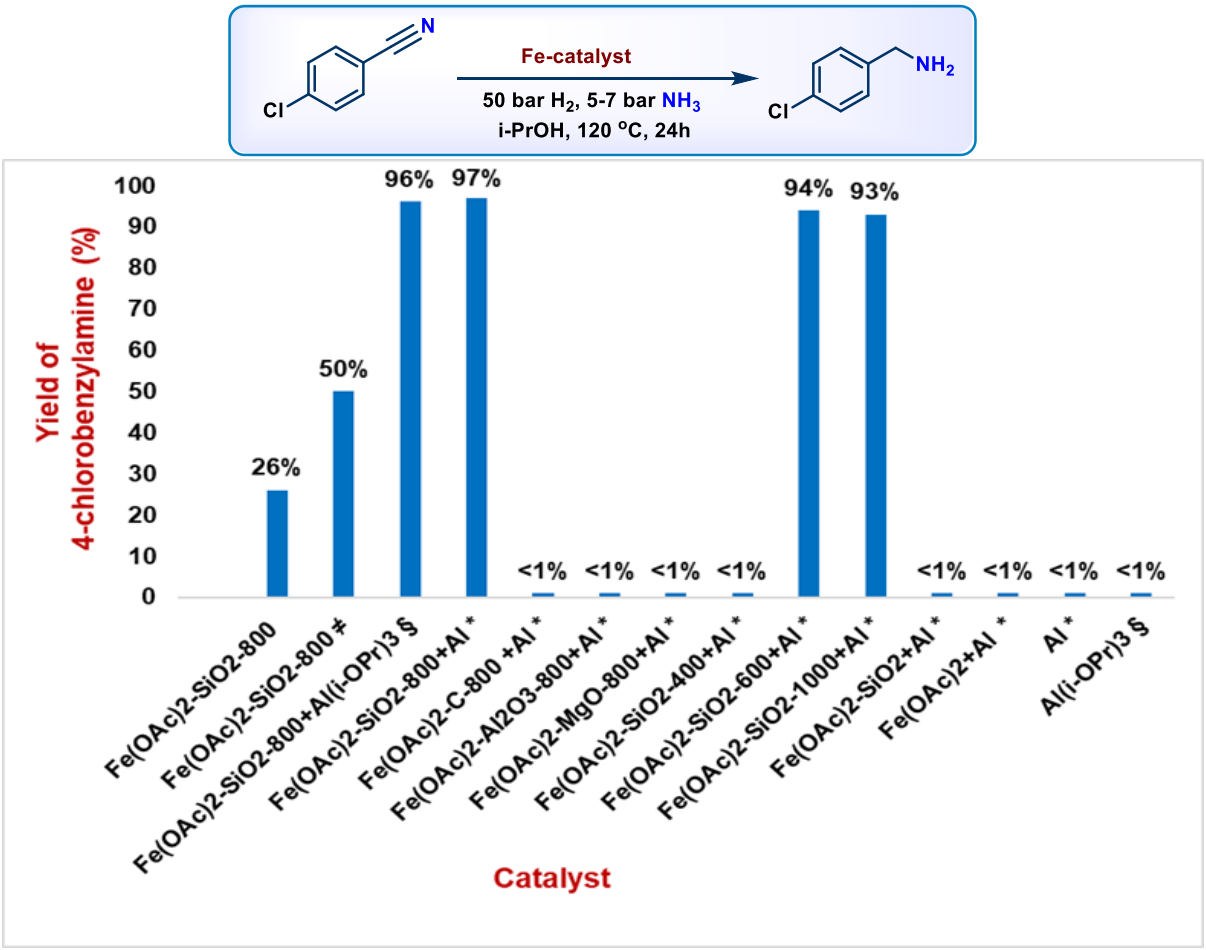

Scheme 17. *Iron-catalyzed hydrogenation of 4-chlorobenzonitrile: Activity of different catalysts.*

We started initial optimization with Fe-catalysts prepared on different supports (Vulcan XC72R carbon, SiO_2, γ-Al_2O_3, and MgO) for the hydrogenation of 4-chlorobenzonitrile **1** to 4-chlorobenzylamine **2**, not only to identify an active catalyst system, but also a selective one (**Scheme 17**). Among these, Fe-catalysts ($Fe(OAc)_2$-SiO_2-800) supported on SiO_2 (8.5 mol%) showed some activity (26% yield of **2**) and high selectivity (>90%) for the formation of desired primary amine. Upon increasing catalyst loading up to 12.8 mol% the product yield increased up to 50%, while maintaining the selectivity (>90%). Studying the influence of different acidic and basic additives, we found the positive effect on reactivity with Lewis acidic additives. Gratifyingly, in the presence of Al-foil or aluminum triisopropoxide (Al(*i*-OPr)$_3$) the yield for 4-chlorobenzylamine **2** dramatically increased to 96-97%.

The crucial role of aluminium additives was explained by monitoring reaction course in presence and absence of Al-foil and Al(*i*-OPr)$_3$ (**Scheme 18**). Surprisingly, in presence and absence of Al-foil the reactions needed a significant pre-activation time (9 h) to start. In the presence of Al(*i*-OPr)$_3$ this pre-activation is drastically reduced (3 h). We found in presence of ammonia, Al-foil is completely dissolved in the solvent (iso-propanol) and forms an active Lewis acid co-catalyst similar as in Al(*i*-OPr)$_3$ case, which activates the nitrile group.

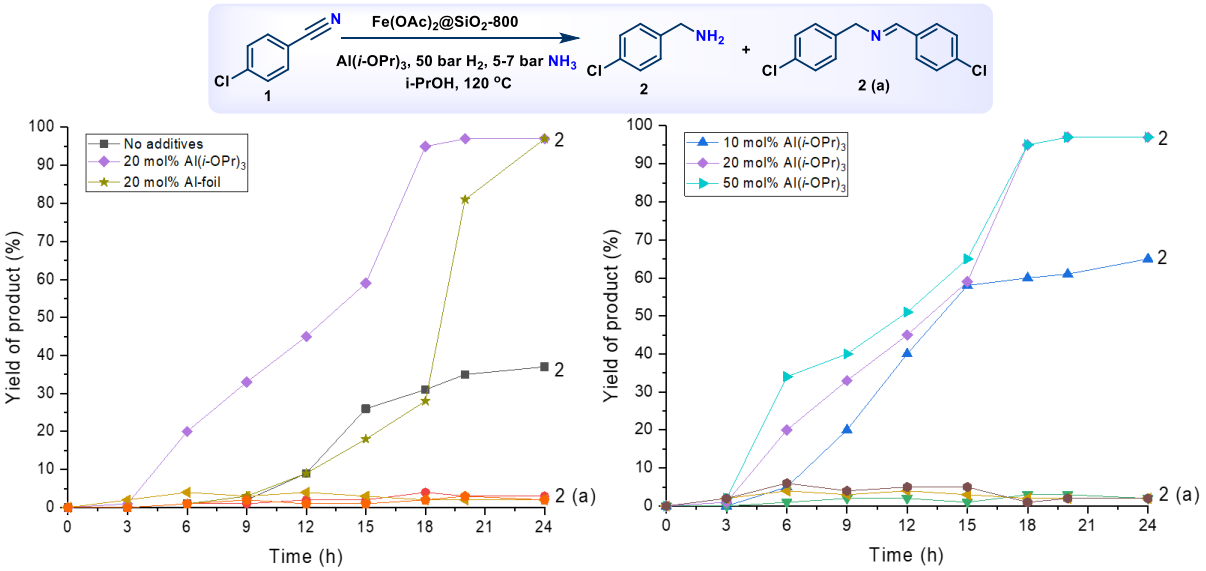

Scheme 18. *Reaction course in presence and absence of Al(i-OPr)3, Al-foil.*

We performed detailed characterization of the most active, $Fe(OAc)_2$-SiO_2-800 catalyst using TEM, HRTEM, STEM, EDX, XPS, XRD, EPR and Mössbauer spectroscopy allowed to explore the chemical and structural model of the Fe/Fe-O@SiO_2 catalyst being composed of SiO_2 matrix, fayalite interface (Fe_2SiO_4) and α-Fe/amorphous-Fe_2O_3 core-shell nanoparticles with globular and rod-shape morphologies of diameter ranging from 10 to 30 nm and length up to 100 nm growing from the silica matrix and, they are covered by an ultrathin iron oxide layer with the thickness of a few nm (**Figure 8**).

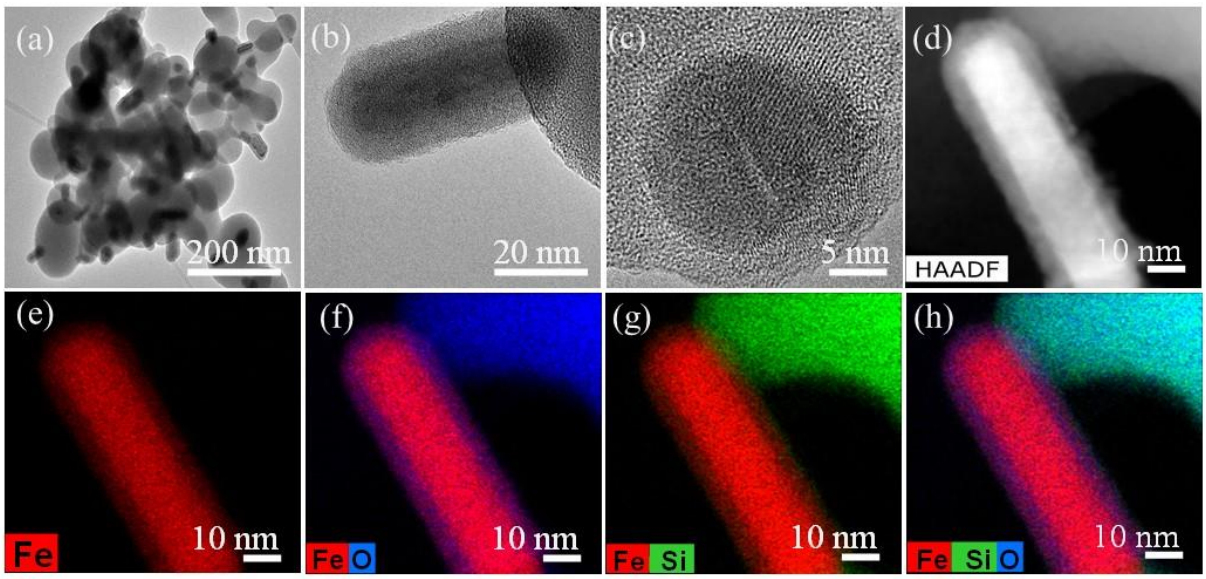

Figure 8. *TEM and HRTEM imaging for Fe/Fe-O@SiO_2.*
(a and b) TEM images. (c) HRTEM image (d) HAADF-STEM image and the corresponding elemental mapping of (e) iron (red), (f) iron/oxygen (red/blue), (g) iron/silica (red/green), (h) iron /silicon/oxygen (red/ green/blue).

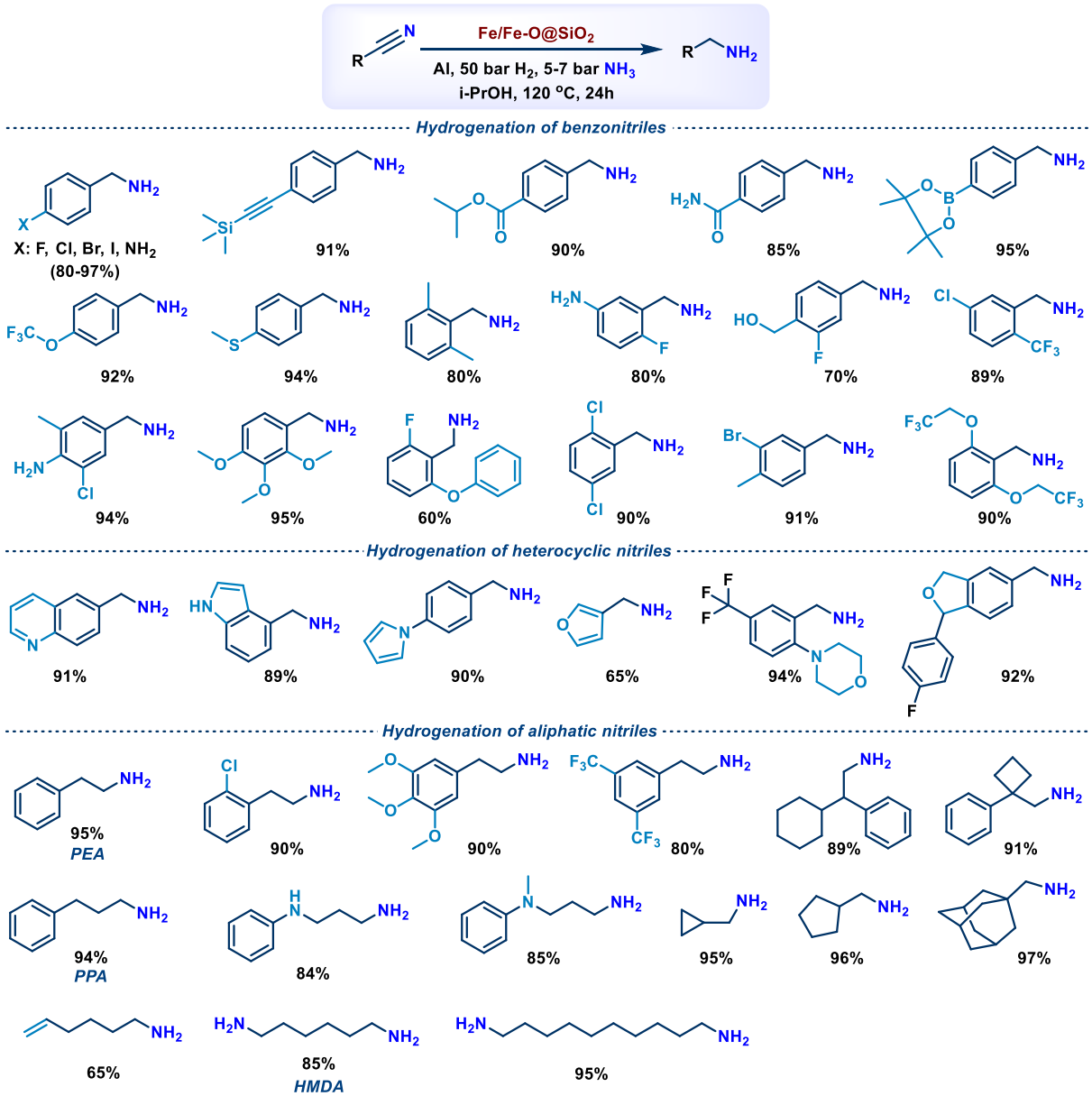

Scheme 19. *Selected examples of iron catalyzed hydrogenation of nitriles with Al-foil.*

Using this Fe-catalyst in combination with Al-foil or Al(*i*-OPr)$_3$ in presence of ammonia and molecular hydrogen >85 functionalized, structurally challenging, aromatic, heterocyclic and aliphatic including fatty nitriles were hydrogenated to corresponding primary amines under scalable and industrially viable conditions (**Scheme 19**). Halogen- and functional groups containing nitriles were selectively hydrogenated. As a result, alkene, alkyne, ester, boronic ester, amide, thio-ether groups are well tolerated. In addition, heterocyclic nitriles containing quinoline, indole, pyrrole, furan, morpholine, and benzofuran motifs gave good to excellent yields (65-94%). Further, the challenging aliphatic including nitriles were also successfully hydrogenated too (**Scheme 19**).

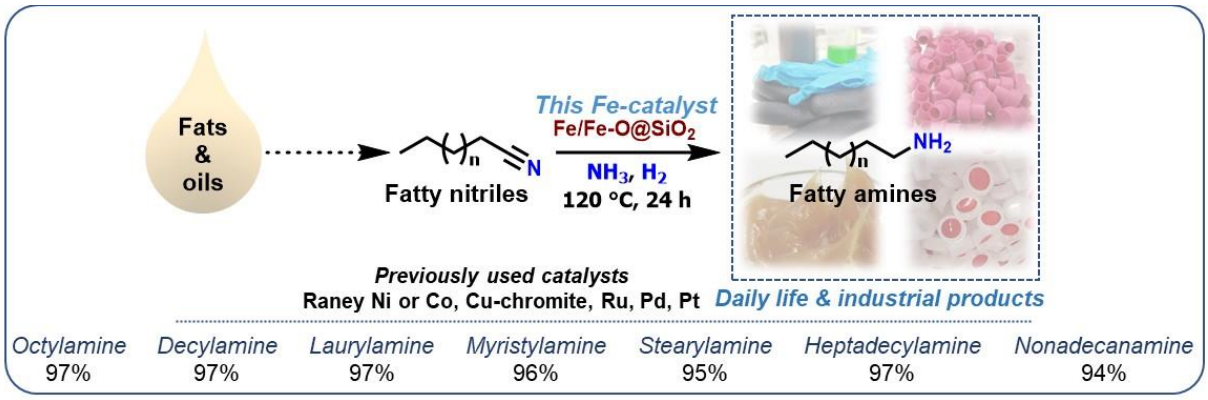

Figure 9. *Synthesis of fatty amines.*

The hydrogenation fatty nitriles are of central importance due to their wide application of resulting amines. Hydrogenation of fatty nitriles to primary amines majorly relies on Raney-Ni, Raney-Co and copper chromite or Pd, Ru and Pt based catalysts.[36] Delightfully, our Fe-catalyst could hydrogenate seven different fatty nitriles to fatty amines in excellent yields up to 97% (**Figure 9**). Finally, synthetic utility and practicability of this Fe-based hydrogenation protocol have been demonstrated by scaling up of both catalyst preparation and (up to 12g) and synthesis of amine (up to 20g).

3.2 Homogeneous cobalt-catalyzed reductive amination for synthesis of functionalized primary amines

Reductive amination of carbonyl compounds with ammonia is an efficient method for the synthesis of linear and branched primary amines.[31,41-43] For this reaction the development homogeneous catalysts are challenging due to the deactivation of the metal complex by forming Werner-type complex. Nevertheless, Rh, Ir, and Ru-complexes known to catalyze reductive amination of carbonyl compounds with ammonia and molecular hydrogen to prepare primary amines.[41,43] To the best of our knowledge no 3d-metal complexes have been reported for this reaction until 2019. Noteworthy, we report a specific combination of cobalt salt and bis(diphenylphosphinoethyl)phenylphosphine (linear triphos) for the reductive amination of broad carbonyl compounds with ammonia in presence of molecular hydrogen to produce corresponding primary amines. The resulting primary amines serve as key precursors and central intermediates to produce advanced chemicals, pharmaceuticals, agrochemicals, biomolecules, and materials.[27]

To find the suitable 3d-metal based complex, we tested *in situ* metal complexes based on Fe, Mn, Co salts and phosphorus ligands for the reductive amination of 4-methylbenzaldehyde with ammonia as the benchmark reaction. Privileged ligands (**L1**-**L8**) with strong coordinating property to metal center were selected to avoid the formation of Werner-type ammonia complexes. Mn-(**L1**-**L7**) and Fe-(**L1**-**L7**) systems were inactive (**Table 2**), while

Co-(**L1**-**L7**) systems exhibited varying activities. Among these, the ones based on linear- and tripodal-triphos ligands (Co-**L7** and Co-**L8**) gave desired primary amine in 96% and 93% yield, respectively (**Table 2**). Applying Co-**L7** the optimal results were obtained using 3 mol% of $Co(BF_4)_2$•$6H_2O$ and 4 mol% of **L7** at 40 bar of hydrogen, 5 bar of ammonia at 100 °C.

Table 2. *Reductive amination of 4-methylbenzaldehyde with in situ generated metal-phosphine complexes.*

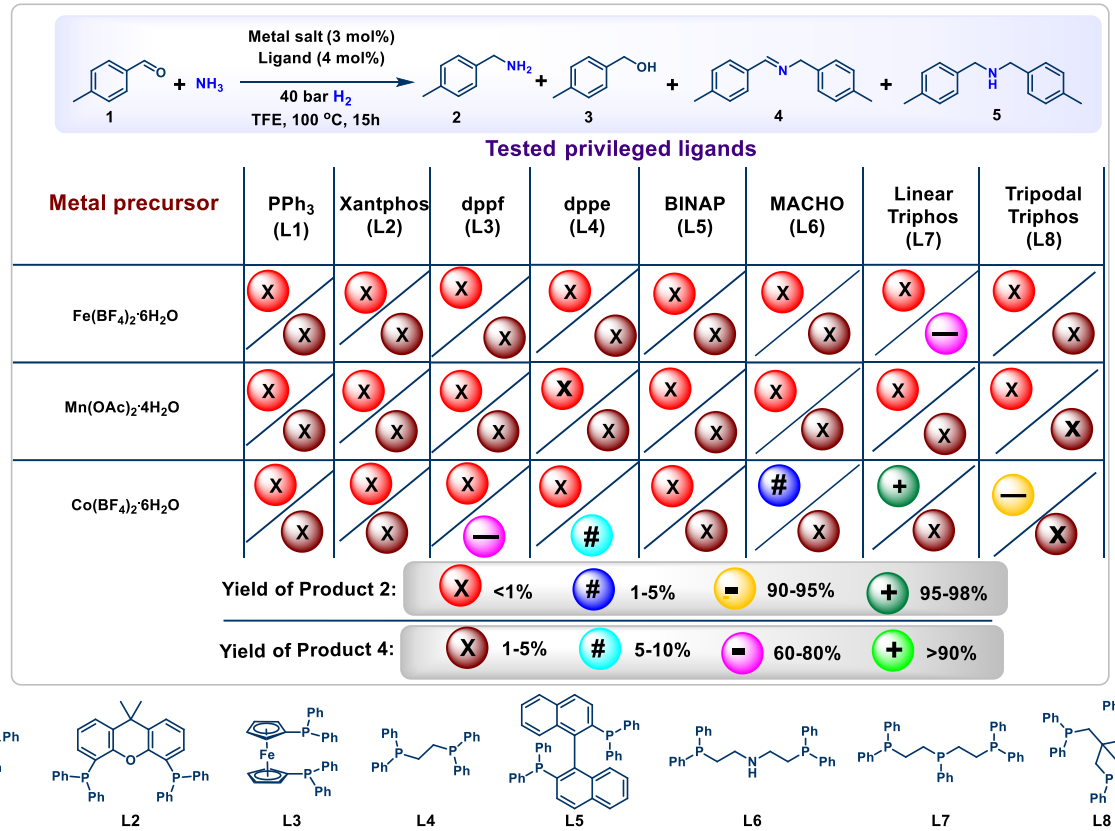

Reaction conditions: *0.5 mmol 4-methylbenzaldehyde, 3 mol% metal salt, 4 mol% ligand, 5 bar NH_3, 40 bar H_2, 2 mL TFE, 100 °C, 15 h, GC yields using n-hexadecane as standard.*

Under the optimized conditions, Co-L7 enabled for the reductive amination of various functionalized and structurally diverse aromatic, aliphatic and heterocyclic carbonyl compounds with ammonia to produce corresponding linear and branched primary amines in good to excellent yields in presence of molecular. As an application in late-stage functionalization of life science and bio-active molecules, amination of drugs such as Nabumetone, Pentoxifylline and Azaperone including steroid derivatives of Estrone and Stanolone were performed too (**Scheme 20**).

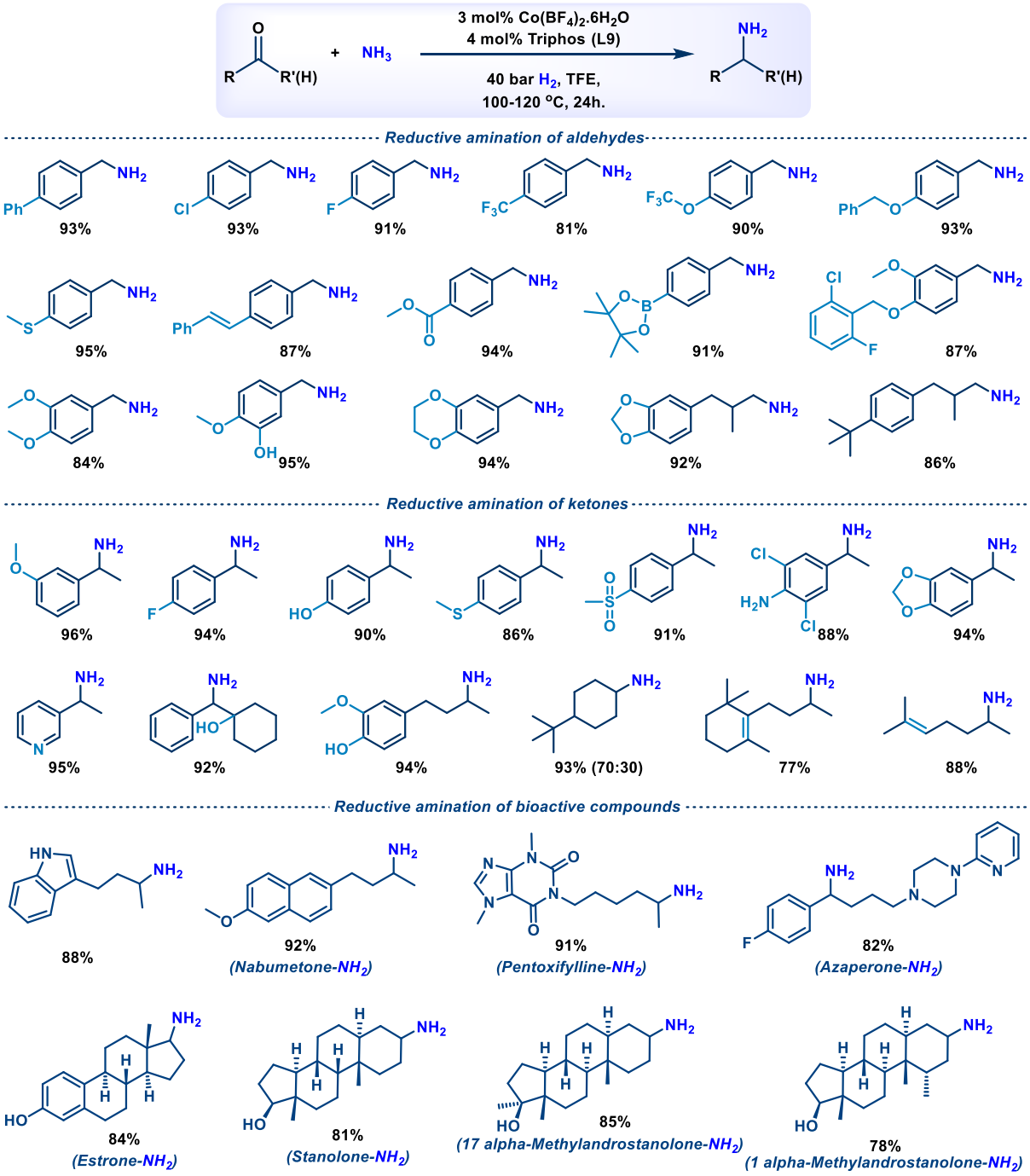

Scheme 20. *Selected examples of Co-triphos catalyzed reductive amination of carbonyl compounds with NH_3 and H_2.*

The molecularly defined Co-**L7** (complex **A**) was also prepared and tested in the model reaction and found that this defined catalyst also exhibits the similar activity and selectivity to that of *in situ* system. The single crystal analysis of complex **A** revealed that Co center was coordinated with two phosphine ligands (1:2 ratio of Co:**L7**), in which one ligand coordinates *via* three phosphorus atoms and the second ligand via two phosphorus atoms to cobalt (II) species with two tetrafluoroborates as counter ions (**Scheme 21**). Complex crystallized without exclusion of air gave partially oxidized cobalt-complex (complex **B**) which is inactive and indicates a major deactivation of the catalyst by oxidation of phosphine-to-phosphine oxide.

The first step is the dissociation of one **L7** ligand from the cationic complex **A** $[(L7)_2Co^{II}]^{2+}$ and formation of mono-cationic hydride $[L7CoH]^+$ (**I**) species in presence of ammonia and H_2. In absence of ammonia, no hydrogenation of carbonyl group to the corresponding alcohol occurred. Next, the primary imine formed from **1** and ammonia generates complex **II**. Based on our previous work and DFT calculations, we propose first substrate coordination followed by beta hydride addition. Finally, hydrogenolysis with H_2 to give primary amine and regeneration of catalytically active species **I** (**Scheme 21**).

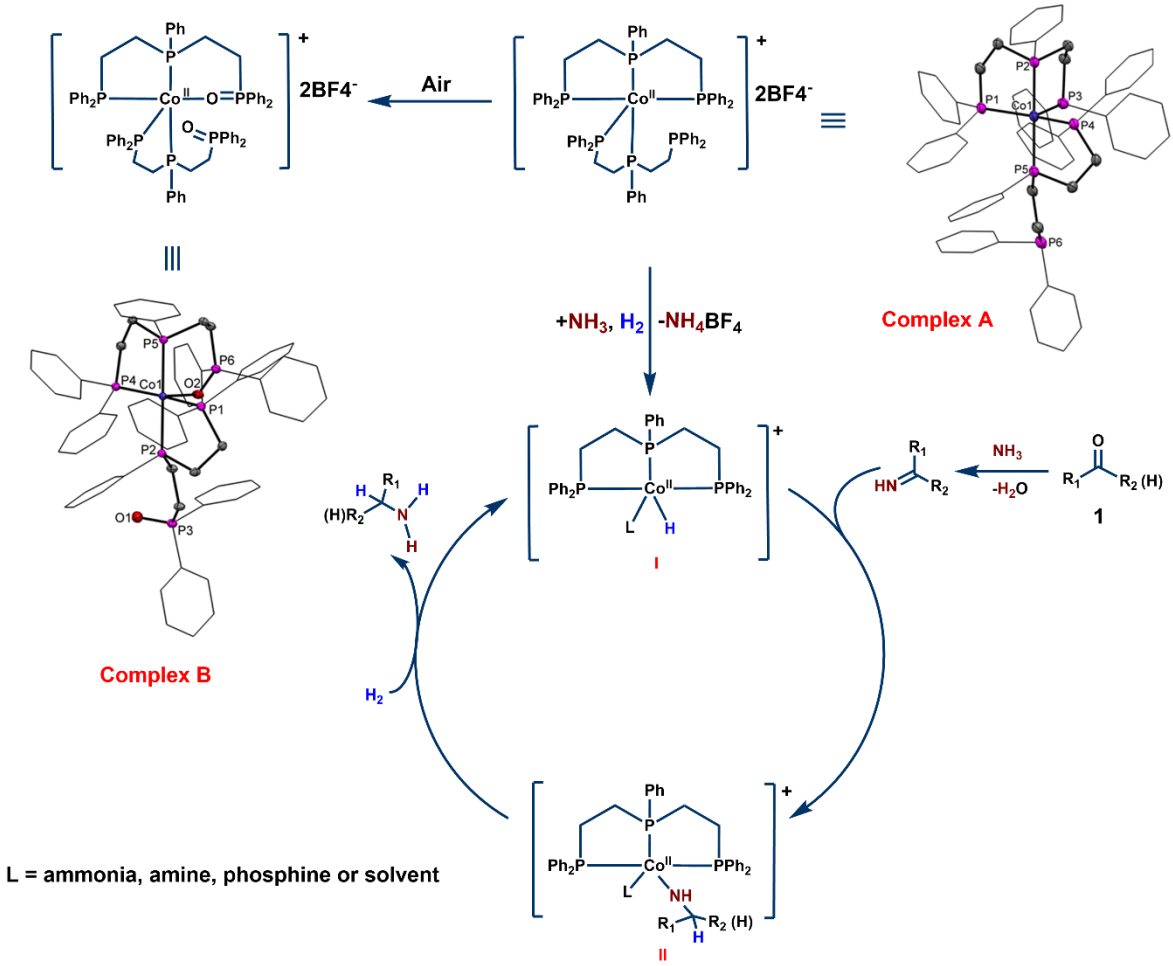

Scheme 21. *Proposed reaction mechanism for the Co-triphos catalyzed reductive amination.*

To support proposed mechanism, B3PW91 DFT computations for the hydrogenation of phenylmethanimine (Ph-CH=NH) generated from benzaldehyde and NH_3 (**Figure 10**) has been performed. The mono-cationic complex $[L7CoH]^+$ (**I**) in solvation has *fac* and *mer* conformations under equilibrium, we computed both catalytic cycles and found that ***mer*-I** is more stable than ***fac*-I** by 33 kJ/mol, while ***fac*-I** based catalytic cycle has lower apparent barrier than that of ***mer*-I** (108 vs. 140 kJ/mol). Based on Curtin–Hammett principle, the ***fac*-I** based catalytic cycle is more preferred kinetically. Starting from the ***mer*-I**, the coordination of Ph−CH=NH to form ***fac*-II-LP** is endergonic by 14 kJ/mol, and the formation of π-coordinated ***fac*-II-π** is endergonic by 72 kJ/mol. The Gibbs free energy barrier of Ph−CH=NH insertion into ***fac*-I** is 71 kJ/mol. The formation of intermediate ***fac*-III** with agostic interaction is endergonic

by 50 kJ/mol. In the second step, H_2 coordination to form ***fac*-IV** is endergonic by 71 kJ/mol. The metathesis step has Gibbs free energy barrier of 108 kJ/mol for ***fac*-IV**. The formation of ***fac*-V** is exergonic by 40 kJ/mol. The release of amine from complex ***fac*-V** with the regeneration of ***mer*-I** is exergonic 59 kJ/mol. The transition state of H_2 metathesis represents the highest point on the Gibbs free energy surface and is the rate-determining transition state; and the apparent Gibbs free energy barrier is 108 kJ/mol from ***mer*-I** (**Figure 10**). Based on our reaction conditions (100-120 °C, 40 bar H_2 and 15-24 h reaction time), the barrier is reasonable. This catalytic cycle is similar with that proposed by Hanson and Jones.

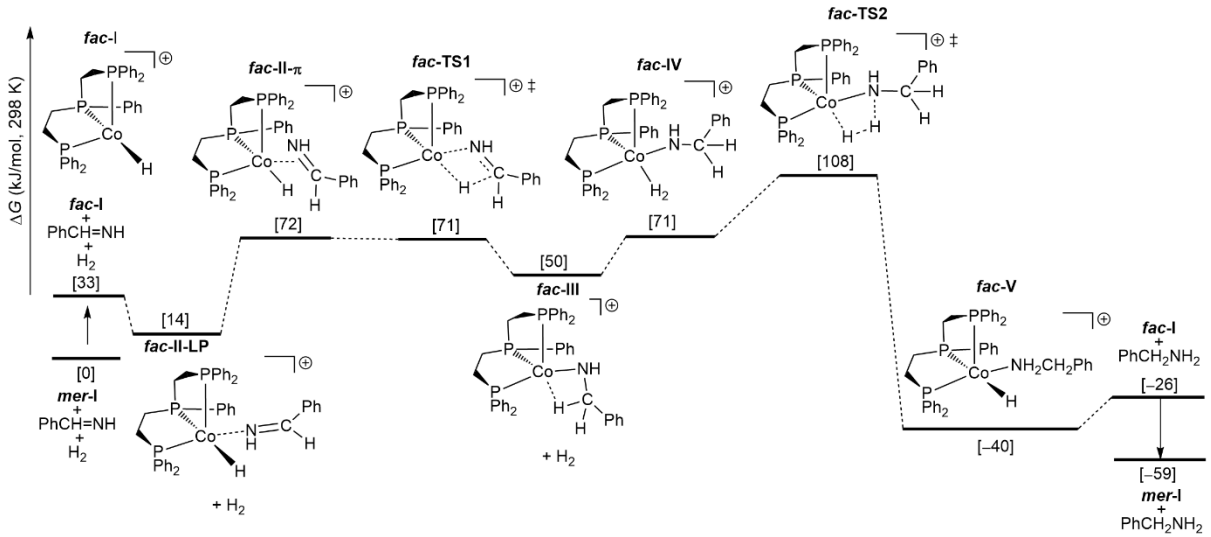

Figure 10. *Gibbs free energy surface for Ph−CH=NH hydrogenation in TFE solvation.*

3.3 Reductive amination, hydrogenation and hydrodeoxygenation of 5-hydroxymethylfurfural using silica-supported cobalt-nanoparticles

Development of efficient methods for the valorization of biomass and related compounds to value added products constitute as an important goal of chemical research.[44] Among the major platform chemicals, HMF listed as top 10 renewable chemicals by U.S. Department of Energy.[45d] Different catalytic reactions such as hydrogenations, hydrodeoxygenations, oxidations, and aminations are applied to valorize HMF and produce value-added chemicals, fuels, and polymers.[45-46] Using reductive aminations, the aldehyde group of HMF can be converted to bio-based primary, secondary, and tertiary amines including *N*-methylamines.[45-46] These furan-based amines are applied for the synthesis of diuretics, antihypertensives, antiseptic agents, and as intermediate in manufacture of polymers, fibers, as well as perfumes.[46] Herein, we report MOF-derived Co-NPs for efficient and selective reusable reductive amination and hydrogenation catalysts for the valorization of HMF under mild conditions. To prepare optimal catalyst, first, $Co(NO_3)_2.6H_2O$, terephthalic acid, and piperazine were mixed in DMF and stirred at 150 °C to generate cobalt-terephthalic-piperazine MOF. Next, to this mixture, Aerosil silica as support was added and continued the stirring at 150 °C for 4 h. After slow evaporation of DMF and drying, cobalt-terephthalic acid-piperazine MOF template on silica was obtained. Finally, this Co-MOF-SiO_2 templated material was pyrolyzed at 800 °C under argon to obtain silica supported cobalt nanoparticles (Co-terephthalic-piperazine@SiO_2-800; **Figure 11**).

Figure 11. *Preparation of Co-terephthalic-piperazine@SiO_2-800 catalyst.*

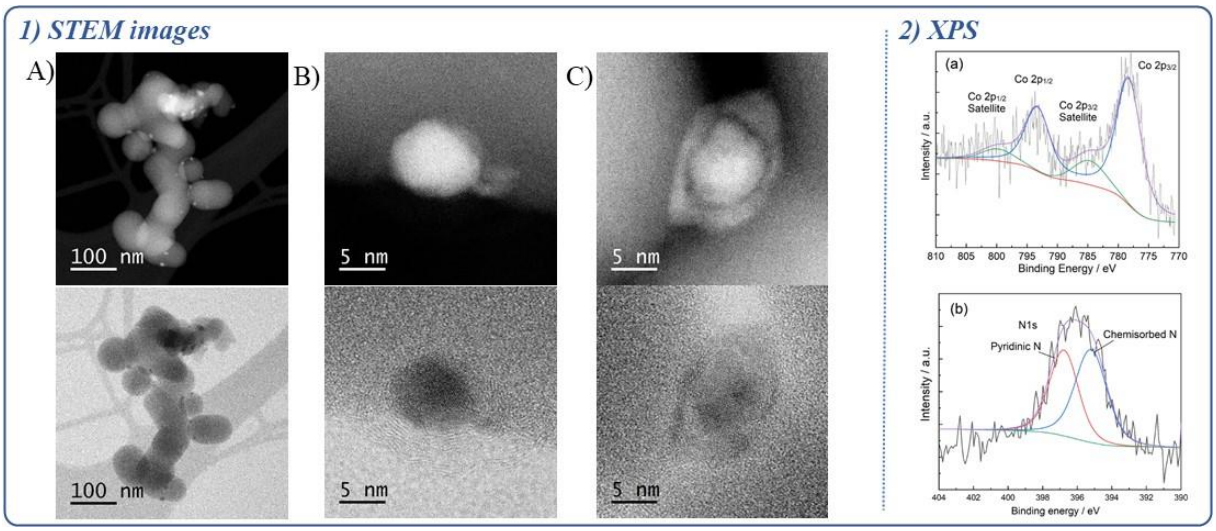

Figure 12. *Characterization of Co-terephthalic-piperazine@SiO_2-800 catalyst.*
1) STEM images of Co-terephthalic acid-piperazine@SiO_2-800 catalyst. Top row HAADF images and bottom row corresponding ABF images. (A) Distribution of cobalt nanoparticles, (B) metallic Co nanoparticles surrounded by graphitic layers. (C) Co-oxide particle without carbon shell. 2) XP spectra of the (a) Co2p and (b) N1s of Co- catalyst.

The best catalytic material was characterized using STEM, EDXS, XPS, XRD techniques, which showed both metallic and oxidic cobalt particles. The metallic cobalt-particles are 5-15 nm in size (**Figure 12**. 2A) and surrounded by graphitic shells (**Figure 12**. 2B). Oxidic cobalt particles are presented without surrounded by graphitic shells instead are in-between states like metal core particles fully or partially surrounded by Co oxide (**Figure 12**. 2C). The Co2p XP spectra (**Figure 12**. 3a) contains two main peaks at 778.44 and 793.47 eV correspond to $Co2p_{3/2}$ and $Co2p_{1/2}$, which are assigned to cobalt in metallic form. Other, two small satellite peaks at 785.26 and 800.11 eV represent the presence of some high spin Co^{2+} mixed up with the peaks of metallic Co. Weak satellite peaks might be due to presence of Co_3O_4 where mixed Co(II) and Co(III) are present. Next, N1s narrow scan spectra (**Figure 12**. 3b) predicts two types of N with peaks centered at 395.20 and 396.8 eV. Such a significant downfield shift of both types of nitrogen represents electron density rich N atoms. The peak at 395.20 eV can be attributed to chemisorbed N and at 396.8 eV might be pyridinic N.

First, reductive amination HMF with ammonia in presence of molecular hydrogen to produce 5-(aminomethyl)-2-furanmethanol (AMF **2**) (**Table 3**) using Co-terephthalic-piperazine@SiO_2-800 was performed. In general, this reaction is challenging and non-selective as often results in the formation of side-products such as over alkylated products (secondary imine and secondary amine) or corresponding alcohol as the reduced product **3**. Nevertheless, this catalyst showed high activity and selectivity and obtained 94% of AMF, the desired product (**Table 3**, Entry 3 & 4).

Table 3. *Cobalt-catalyzed reductive amination of HMF using NH_3 and H_2.*

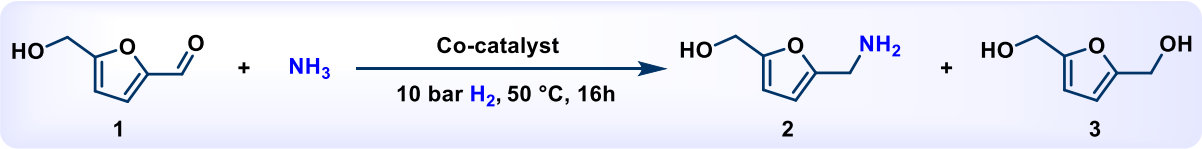

Entry	Catalyst	Solvent	Conv. (%)	Yield (%)	
				2	3
1[a]	Co-terephthalic acid-piperazine@SiO_2-800	MeOH	>99	80	15
2[a]	Co-terephthalic acid-piperazine@SiO2-800	EtOH	>99	89	4
3[a]	Co-terephthalic acid-piperazine@SiO_2-800	H_2O	>99	94	1
4[b]	Co-terephthalic acid-piperazine@SiO_2-800	H_2O	>99	94	1
5[c]	Co-terephthalic acid-piperazine@SiO_2-800	H_2O	90	80	-
6[b]	Co-terephthalic acid-piperazine@SiO_2-400	H_2O	50	-	-
7[b]	Co-terephthalic acid-piperazine@SiO_2-600	H_2O	85	70	-
8[b]	Co-terephthalic acid-piperazine@SiO_2-1000	H_2O	>99	88	6

Reaction conditions: *0.5 mmol HMF, 5 bar NH_3, 25 mg catalyst (5 mol% Co), 10 bar H_2, 3 ml solvent, 50 °C, 16 h. [b] same as [a] with 0.1 mL aq.NH_3 (33 wt% of NH_3 in water). [c] same as [b] with 15 mg catalyst (3 mol% Co). All yields are determined by GC using DMAc as standard. In entry 6, 45% secondary imine was observed. In entry 7, 12% secondary imine was observed.*

Next, we continued the reductive amination of HMF with primary, secondary amines including N-methylamines and obtained corresponding furan-based amines in up to 95% yield (**Scheme 22**). In addition, interesting heterocyclic compounds-based furan-benzimidazole, -benzothiazole, and -oxazolidine were produced by reacting HMF with *ortho*-substituted hetero-anilines. Thus, this Co-based amination protocol makes use of renewable feedstock not only for the synthesis of amines, but also for accessing heterocycles (**Scheme 22**).

In addition to reductive aminations, hydrogenation and hydrodeoxygenation of HMF also been demonstrated. With our Co-catalyst HMF can be selectively hydrogenated to produce 2,5-bis(hydroxymethyl)furan (BHMF) in high yields at 70 °C with 15 bar hydrogen (**Scheme 22**). This heterocyclic diol used as key precursor to produce polyurethane foams and polyesters. Upon increasing the catalyst loading, temperature and pressure (6 mol% Co, 100 °C and 30 bar H_2), the HMF underwent hydrodeoxygenation to provide 5-methylfuran-2-yl)methanol (MFM, **Scheme 22**). Finally, recycling and stability studies were performed, and the catalyst can be conveniently recycled and reused 4 times without much significant loss in catalytic activity, but in 5th run yield of product is decreased. In catalyst stability runs for half conversion at 10 h, the catalyst was stable up to 3rd run later decrease in activity was observed.

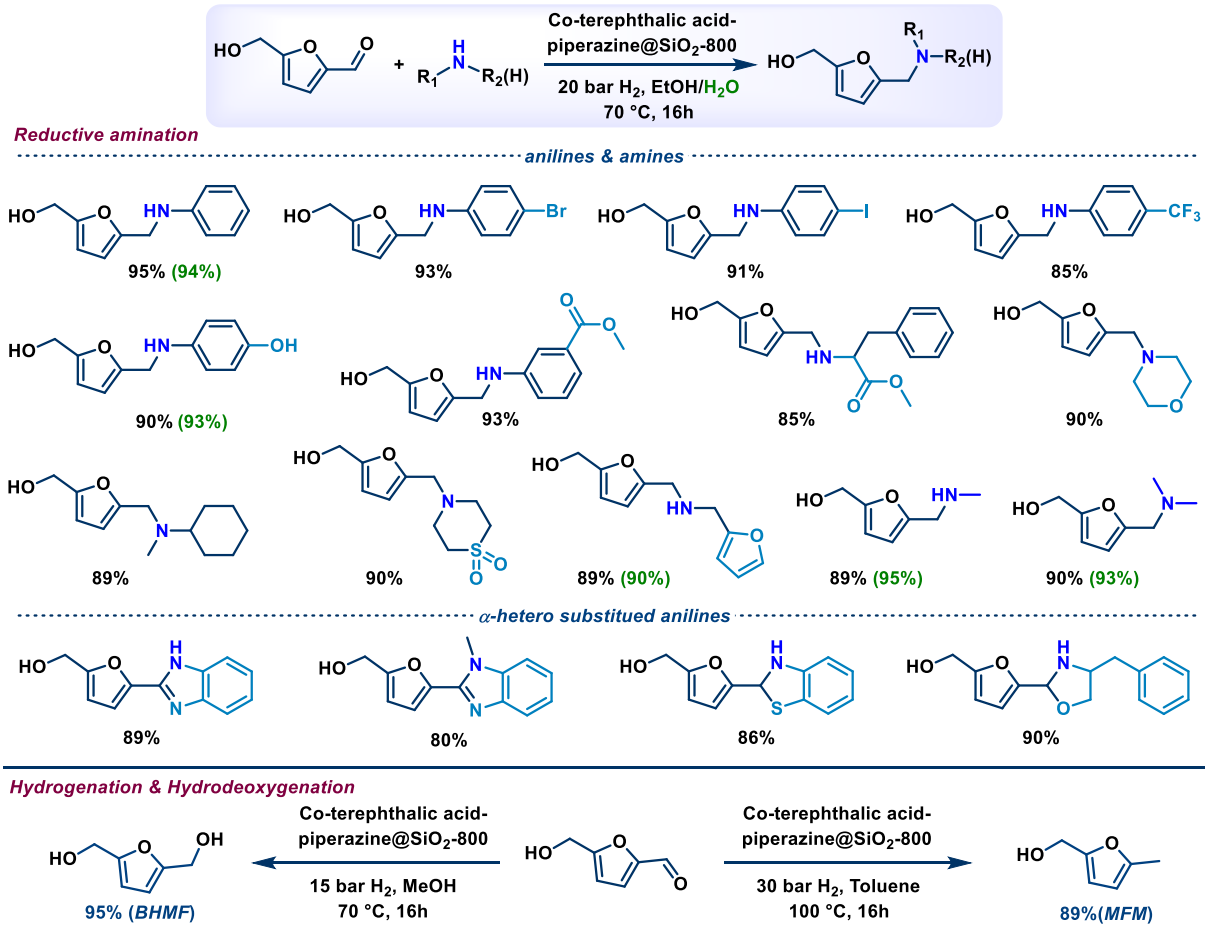

Scheme 22. *Selected examples of Co-catalyzed reductive amination, hydrogenation, and hydrodeoxygenation of HMF.*

3.4 A general catalyst based on cobalt core–shell nanoparticles for the hydrogenation of *N*-heteroarenes including pyridines

The catalytic hydrogenation of pyridines, quinolines and other *N*-heteroarenes offers a straightforward approach for the synthesis of aliphatic cyclic amines.[50-57] Piperidines and 1,2,3,4-tetrahydroquinolines are major building blocks for pharmaceuticals, agrochemicals, biomolecules, and natural products.[49] The hydrogenation of pyridines is particularly challenging due to the catalyst deactivation by the interaction of nitrogen moiety of pyridine and pieridine with the metal active centers.[53] In this respect, development of active and stable heterogeneous catalysts for the hydrogenation of pyridines is of central importance. Regarding potential heterogeneous catalysts supported nanoparticles are of prime importance due to their tunable activities and selectivities in addition to their easy recycling and reusability. In our previous works we noticed that compared thermal or chemical reduction of simple metal salts on heterogeneous supports, the template synthesis of metal complexes MOFs in in organic supports and subsequent pyrolysis produces more active and selective nanoparticles-based catalysts. Advantageously, a plethora of inexpensive and stable organic ligands/linkers are commercially available to prepare these metal complexes or MOFs, which can be used as potential precursors to synthesize diverse nanomaterials. As an example, we reported the use of cobalt-MOFs obtained from di-, tri- or tetracarboxylic acids, as appropriate precursors for the preparation of silica supported Co/Co_3O_4 core-shell nanoparticles. The optimal material was obtained by the pyrolysis of in situ generated Co- pyromellitic acid MOF on SiO_2 at 800 °C under argon (**Scheme 23**).

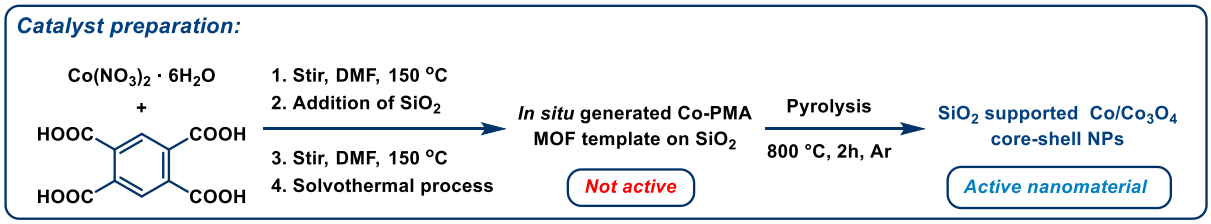

Scheme 23. *Preparation of Co-pyromellitic acid@SiO_2-800 catalyst.*

All the new materials prepared were tested for the hydrogenation of nicotinamide as the benchmark reactions (**Table 4**). The catalyst prepared using benzoic acid gave completely inactive material, while other di-, tri-, and tetra-carboxylic acids gave active catalysts (**Table 4**; Entries 1-4). Among thee, the one prepared form Co-pyromellitic acid (Co-pyromellitic acid@SiO_2-800), exhibited best activity and obtained 97% yield of desired product, nipecotamide (**2**, **Table 4**; Entries 4). Homogeneous system (**Table 4**; Entries 8-9) and pyrolyzed cobalt(II) nitrate on silica as well as non-pyrolyzed Co-pyromellitic acid on silica showed no activity (**Table 4**; Entries 5-6).

Table 4. *Cobalt-catalyzed hydrogenation of nicotinamide and catalyst preparation.*

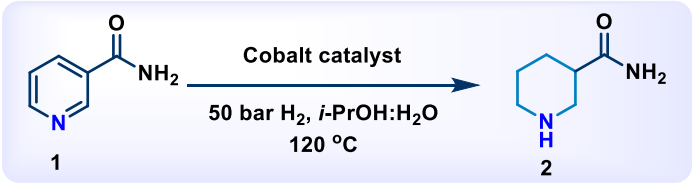

ENTRY	CATALYST	CONV. (%)	YIELD (%)
1	Co-benzoic acid@SiO_2-800	<3	<2
2	Co-terephthalic acid @SiO_2-800	65	63
3	Co- trimesic acid @SiO_2-800	75	73
4	Co-pyromellitic acid@SiO_2	>99	97
5	Co$(NO_3)_2$@SiO_2-800	<2	<1
6	Co-pyromellitic acid@SiO_2 (unpyrolyzed)	<2	<1
7	Co$(NO_3)_2$@SiO_2 (unpyrolyzed)	-	-
8	Co$(NO_3)_2{\cdot}6H_2O$ + pyromellitic acid (Homo)	-	-
9	Co$(NO_3)_2{\cdot}6H_2O$ (Homo)	-	-

Reaction conditions: *0.5 mmol nicotinamide, 40 mg catalyst (7.5 mol% Co), 50 bar H_2, 3 mL solvent (^{i}PrOH:H_2O; 2:1), 120 °C, 24h. Yields were determined by GC using n-hexadecane as standard.*

With the active catalyst in hand, a series of substituted (electron donating, withdrawing) and functionalized (amide, ester) pyridines were hydrogenated to corresponding piperidines in good to excellent yields (83-97%) (**Scheme 24**). Also, quinolines were semi-hydrogenated under relatively mild condition at 70 °C with 10 bar H_2 and produced tetrahydroquinolines in up to 97% yield. Here, functional groups like halides, hydroxyl, ether, ester were well tolerated. In addition, quinoline moiety in tocopherol derivative was also selectively semi-hydrogenated without effecting other structure. Other *N*-heteroarenes such as quinoxaline, indole, imidazo[1,2-a]pyridine, 1,5-naphthyridine, acridines, and phenanthroline were also successfully hydrogenated to give partially reduced products with 97% yields (**Scheme 24**). The optimal catalyst was also tested for the reverse dehydrogenation process. As a result, 2-methyl-1,2,3,4-tetrahydroquinoline underwent dehydrogenation and yielded 93% of 2-methylquinoline, which is of interest in the context of LOHC technologies (**Scheme 24**).

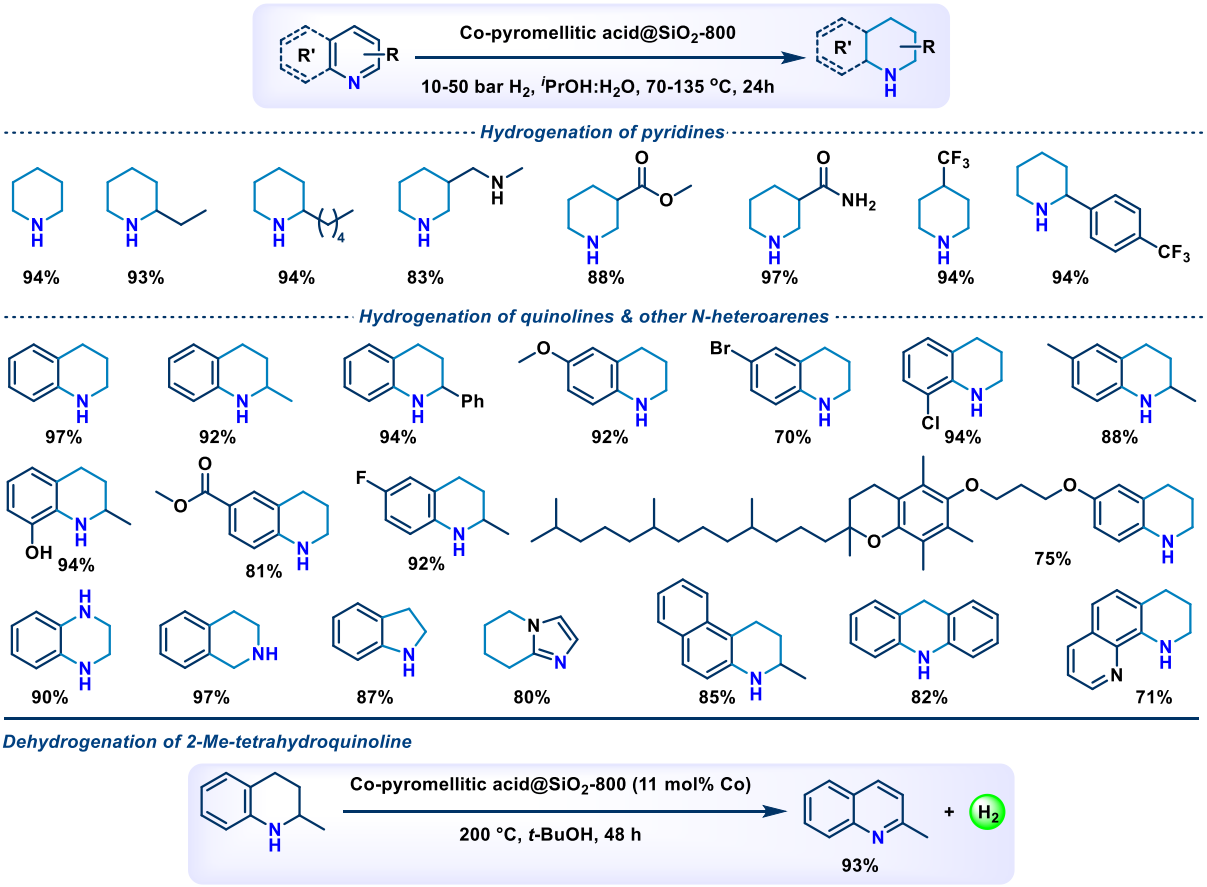

Scheme 24. *Selected examples of Co-catalyzed hydrogenation of N-heteroarenes and dehydrogenation of 2-methyltetrahydroquinoline.*

The optimal catalyst Co-pyromellitic acid@SiO_2-800 was characterized using STEM, XRD, XPS and BET techniques. STEM analysis revealed the formation of metallic Co and different oxidic-Co NPs with 10-20 nm in sizes (**Figure 13**). Most of these particles are of core-shell structure with metallic Co as core covered with oxidic shell (**Figure 13**, B and C), which is also confirmed with elemental mapping (**Figure 13**, D and E). XRD showed the presence of both metallic and oxidic cobalt phases (Co and Co_3O_4). XPS confirmed the presence of mixed oxidation for Co ($Co2p_{3/2}$ in Co(0): 778.49 eV; Co^{2+}: 779.92 eV), the presence of strong satellite peaks at 786.43 eV and 802.20 eV are indicative for multiple oxidized Co species as satellite peaks arise due to spin-spin interactions of different Co-species.

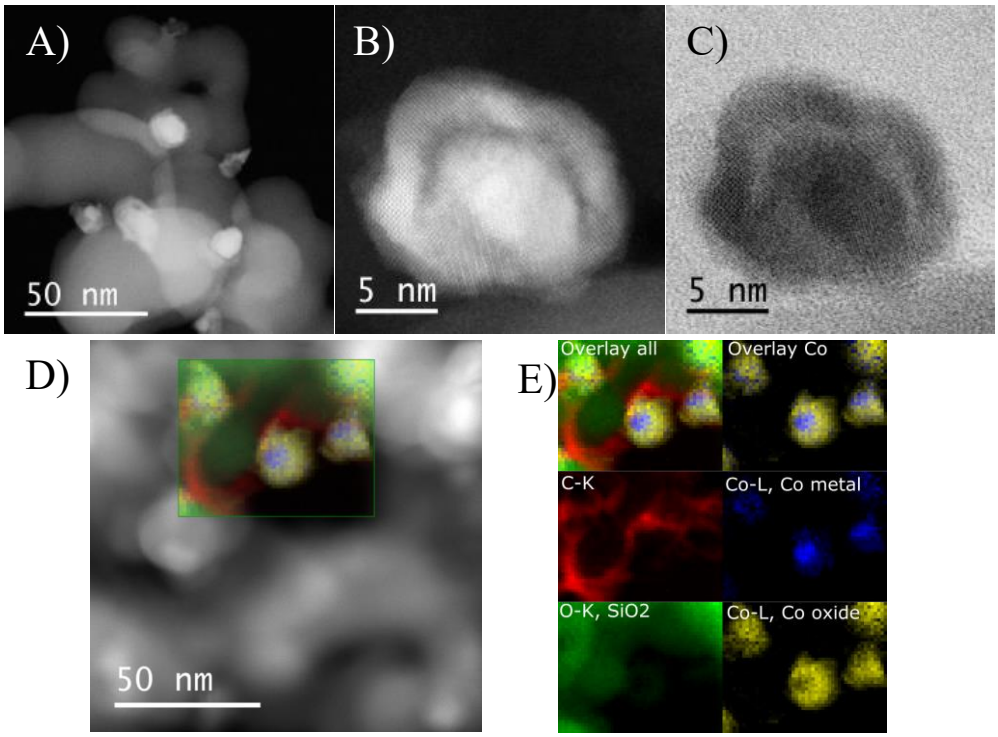

Figure 13. *Characterization of Co-pyromellitic acid@SiO_2-800 catalyst. STEM-HAADF (A, B) and -ABF (C) images. STEM-ADF (D) overlaid with false color elemental map showing the distribution of C, O and maps of the different oxidation states of Co, with the single-color elemental maps (E).*

Finally, Co-pyromellitic acid@SiO_2-800 was conveniently recycled and reused for 7 runs without significant loss in the activity or selectivity (**Figure 14**). STEM analysis of catalyst samples after one and seven reuses showed a partial re-dispersion of cobalt into a thin layer of Co-oxide on the surface of the support progressing with the number of uses.

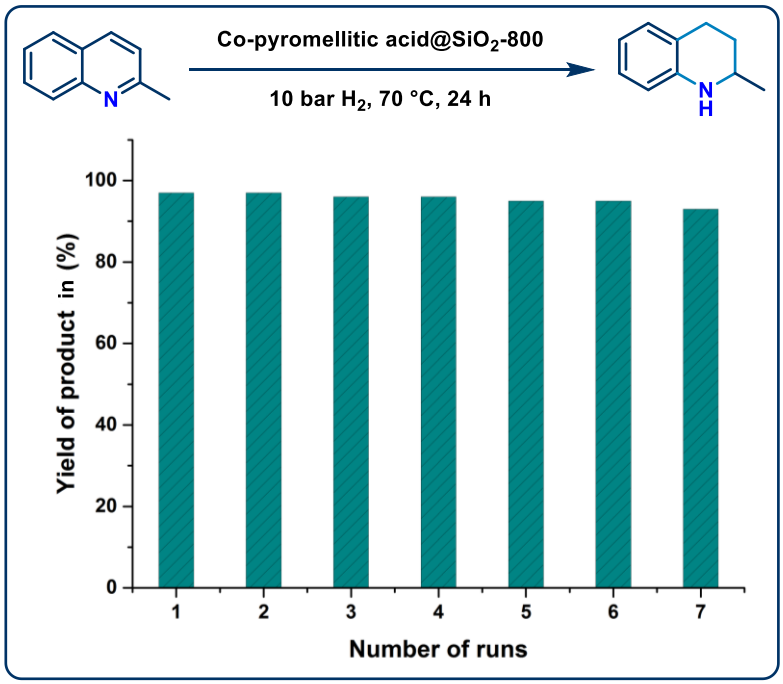

Figure 14. *Catalyst recycling for the hydrogenation of 2-methyl quinoline.*
Reaction conditions: *1.4 gram 2-methyl quinoline (10 mmol), 1 g of Co-pyromellitic acid@SiO_2-800 (9 mol % Co), 10 bar H_2, 15 mL t-BuOH, 120 °C, 24 h.*

4. References

1. K. C. Nicolaou, *Proc. R. Soc. A*, 2014, **470**, 20130690.
2. E. J. Corey and X-M. Cheng, *The logic of chemical synthesis*, Wiley, New York, 1989.
3. K. C. Nicolaou, *Angew. Chem. Int. Ed.,* 2013, **52**, 131-146.
4. K. C. Nicolaou and T. Montagnon, *Molecules that changed the world*, Wiley-VCH, Germany, 2008.
5. F. Wöhler, *Ann. Phys.,* 1828, **88**, 253-256.
6. E. J. Corey, B. Czakó and L. Kürti, *Molecules and medicine,* Wiley, Weinheim, Germany, 2007.
7. K. C. Nicolaou and C. Nilewski, *Organic synthesis* in *Discoveries in modern science: exploration, invention, technology* (Ed: J. Trefil), Macmillan Reference USA, Woodbridge, 2014.
8. A. McKillop and K. W. Young, *Organic synthesis using supported reagents-part I & part II*, *Synthesis*, pp. 401–422, 481–500, 1979.
9. P. Laszlo, *Preparative chemistry using supported reagents*, Academic Press, San Diego, Calif, USA, 1987.
10. R. A. Sheldon, I. W. C. E. Arends and U. Hanefeld, *Green chemistry and catalysis*, Wiley-VCH Verlag, 2007.
11. R. A. van Santen, *Catalysis in perspective: Historic review*. In M. Beller, A. Renken, and R. A. van Santen (Ed.), *Catalysis: From principles to applications,* Wiley-VCH Verlag, 2012.
12. (a) M. Beller and C. Bolm, in *Transition metals for organic synthesis,* Wiley-VCH: New York, 2008. (b) G. V. Smith and F. Notheisz, in *Heterogeneous catalysis in organic chemistry*, Academic Press, San Diego, pp. xiii-xv, 1999. (c) E.-i. Negishi, *Angew. Chem. Int. Ed.*, 2011, **50**, 6738-6764.
13. (a) Statista. *https://www.statista.com/statistics/302081/revenue-of-global-chemical-industry*. (b) K. P. de Jong, *Synthesis of solid catalysts*, Wiley, pp-111–134, 2009.
14. *All Nobel Prizes in Chemistry*. https://www.nobelprize.org/prizes/lists/all-nobel-prizes-in-chemistry/.
15. B. Cornils and W. A. Herrmann, *Applied homogeneous catalysis with organometallic compounds*, Wiley-VCH, Weinheim, 1996.

16. Metals Price: https://www.mining.com/markets/; https://www.metalary.com/; https://www.chemicool.com/elements/;

17. (a) C. Bolm, J. Legros, J. Le Paih and L. Zani, *Chem. Rev.*, 2004, **104**, 6217-6254. (b) B. Plietker, *Iron catalysis in organic chemistry,* Wiley-VCH, 2008. (c) S. Enthaler, K. Junge and M. Beller, *Angew. Chem. Int. Ed.,* 2008, **47**, 3317–3321. (d) C. Bolm, *Nat. Chem.,* 2009, **1**, 420. (e) I. Bauer and H.-J. Knölker, *Chem. Rev.*, 2015, **115**, 3170-3387. (f) L. C. Misal Castro, H. Li, J.-B. Sortais and C. Darcel, *Green Chem.*, 2015, **17**, 2283-2303. (g) D. Wei and C. Darcel, *Chem. Rev.*, 2019, **119**, 2550-2610.

18. (a) P. Chirik and R. Morris, *Acc. Chem. Res.*, 2015, **48**, 2495-2495. (b) J. Maes, E. A. Mitchell and B. U. W. Maes, in *Green and sustainable medicinal chemistry: Methods, tools and strategies for the 21st century pharmaceutical Industry*, The Royal Society of Chemistry, pp. 192-202, 2016. (c) D. Wang and D. Astruc, *Chem. Soc. Rev.*, 2017, **46**, 816-854. (d) W. Liu, B. Sahoo, K. Junge and M. Beller, *Acc. Chem. Res.*, 2018, **51**, 1858-1869. (e) L. Alig, M. Fritz and S. Schneider, *Chem. Rev.*, 2019, **119**, 2681-2751. (f) D. Formenti, F. Ferretti, F. K. Scharnagl and M. Beller, *Chem. Rev.*, 2019, **119**, 2611-2680. (g) P. Gandeepan, T. Müller, D. Zell, G. Cera, S. Warratz and L. Ackermann, *Chem. Rev.*, 2019, **119**, 2192-2452. (h) K. Junge, V. Papa and M. Beller, *Chem. Eur. J.*, 2019, **25**, 122-143. (i) R. M. Bullock, J. G. Chen, L. Gagliardi, P. J. Chirik, O. K. Farha, C. H. Hendon, C. W. Jones, J. A. Keith, J. Klosin, S. D. Minteer, R. H. Morris, A. T. Radosevich, T. B. Rauchfuss, N. A. Strotman, A. Vojvodic, T. R. Ward, J. Y. Yang and Y. Surendranath, *Science*, 2020, **369**, eabc3183. (j) N. Kaplaneris and L. Ackermann, *Beilstein J. Org. Chem.*, 2022, **18**, 86–88.

19. (a) E. Peris and R. H. Crabtree, *Chem. Soc. Rev.,* 2018, **47**, 1959-1968. (b) M. E. O'Reilly and A. S. Veige, *Chem. Soc. Rev.,* 2014, **43**, 6325-6369. (c) D. Morales-Morales and C. M. Jensen, *The chemistry of pincer compounds*, Elsevier Science, Amsterdam, 2007.

20. (a) C. Bornschein, S. Werkmeister, B. Wendt, H. Jiao, E. Alberico, W. Baumann, H. Junge, K. Junge and M. Beller, *Nat commun.*, 2014, **5**, 4111. (b) S. Chakraborty, G. Leitus and D. Milstein, 2016, **52**, 1812-1815. (c) K. Junge, K. Schröder and M. Beller, *Chem. Commun.*, 2011, **47**, 4849-4859.

21. (a) T. Zambelli, J. Wintterlin, J. Trost and G. Ertl, *Science*, 1996, **273**, 1688-1690. (b) J. K. Nørskov, T. Bligaard, B. Hvolbæk, F. Abild-Pedersen, I. Chorkendorff and C. H. Christensen, *Chem. Soc. Rev.*, 2008, **37**, 2163-2171. (c) A. Corma, *Science*, 2006, **313**, 332-334. (d) R. V. Jagadeesh, A.-E. Surkus, H. Junge, M.-M. Pohl, J. Radnik, J. Rabeah, H. Huan, V. Schünemann, A. Brückner and M. Beller, *Science*, 2013, **342**,

1073-1076. (e) R. V. Jagadeesh, K. Murugesan, A. S. Alshammari, H. Neumann, M.-M. Pohl, J. Radnik and M. Beller, *Science*, 2017, **358**, 326-332. (f) L. Liu and A. Corma, *Chem. Rev.*, 2018, **118**, 4981-5079. (g) C. Vogt and B. M. Weckhuysen, *Nat. Rev. Chem.*, 2022, **6**, 89-111.

22. (a) J. G. de Vries and C. J. Elsevier, *Handbook of Homogeneous Hydrogenation*, Wiley-VCH, New York, 2007. (b) S. Nishimura, *Handbook of Heterogeneous Catalytic Hydrogenation for Organic Synthesis,* Wiley, New York, 2001. (c) P. A. Chaloner, M. A. Esteruelas, F. Joo, L. Oro, *Homogeneous Hydrogenation*, Kluwer Academic publisher, Dordrecht, 1994. (d) A. M. Smith, R. Whyman, *Chem. rev.* 2014, **114**, 5477-5510.

23. (a) P. Sabatier and J. B. Senderens, Comptes Rendus Hebdomadaires des séances de l'Académie des sciences, 1897, **124**, 616–618 and 1358–1361. b) https://www.nobelprize.org/prizes/chemistry/1912/sabatier/lecture/

24. (a) J. A. Osborn, F. H. Jardine, J. F. Young and G. Wilkinson, *J. Chem. Soc. A.,* 1966, 1711-1732. (b) https://www.nobelprize.org/prizes/chemistry/1973/wilkinson/facts/

25. (a) C. Bosch, *Process of producing ammonia,* U.S. Patent 990,191, (2 March 1908). (b) https://www.nobelprize.org/prizes/chemistry/1931/bosch/facts/

26. P. N. Rylander, *Catalytic hydrogenation over Platinum metals*, Academic Press, New York, 1967.

27. (a) S. A. Lawrence, *Amines: Synthesis, properties and applications*, Cambridge University Press, 2004. (b) A. Ricci, *Amino group chemistry: From synthesis to the life sciences*, Wiley-VCH, 2008. (c) A. Ricci, *Modern amination method*, Wiley-VCH Verlag, Weinheim, New York, 2000. (d) *Top 200 Pharmaceuticals by Retail Sales in 2020*. https://njardarson.lab.arizona.edu/sites/njardarson.lab.arizona.edu/files/Top%20200%20Pharmaceuticals%20By%20Retail%20Sales%202020V3.pdf. (e) S. D. Roughley and A. M. Jordan, *J. Med. Chem*., 2011, **54**, 3451-3479. (f) C. Joyce, W. F. Smyth, V. N. Ramachandran, E. O'Kane, D. J. Coulter, *J. Pharm. Biomed. Anal.,* 2004, **36**, 465-476. (g) F. Shi and X. Cui, *Catalytic amination for N-alkyl amine synthesis*, Academic Press, 2018. (h) W. R. Meindl, E. V. Angerer, H. Schoenenberger and G. Ruckdeschel, *Med. Chem.,* 1984, **27**, 1111-1118. (i). V. Froidevaux, C. Negrell, S. Caillol, J.-P. Pascault, B. Boutevin, *Chem. Rev.,* 2016, **116**, 14181-14224.

28. Amine market: (a) https://www.mordorintelligence.com/industry-reports/aminesmarket; (b) https://www.grandviewresearch.com/industry-analysis/amines-industry.

29. A. Ricci and L. Bernardi, *Methodologies in amine synthesis,* Wiley-VCH, Weinheim, 2021.

30. Nitrile hydrogenation: (a) C. De Bellefon and P. Fouilloux, *Catal. Rev.*, 1994, **36**, 459-506. (b) J. A. Garduño and J. J. García, *ACS Catal.*, 2020, **10**, 8012-8022. (c) S. Werkmeister, K. Junge and M. Beller, *Org. Process Res. Dev.*, 2014, **18**, 289-302. (d) D. M. Sharma and B. Punji, *Chem Asian J.*, 2020, **15**, 690-708.

31. Reductive amination: (a) K. Murugesan, T. Senthamarai, V. G. Chandrashekhar, K. Natte, P. C. J. Kamer, M. Beller and R. V. Jagadeesh, *Chem. Soc. Rev.*, 2020, **49**, 6273-6328. (b) T. Irrgang and R. Kempe, *Chem. Rev.*, 2020, **120**, 9583-9674. (c) O. I. Afanasyev, E. Kuchuk, D. L. Usanov and D. Chusov, *Chem. Rev.*, 2019, **119**, 11857-11911. (d) M. A. Sprung, *Chem. Rev.*, 1940, **26**, 297-338. (e) T. Yasukawa, R. Masuda and S. Kobayashi, *Nat. Catal.*, 2019, **2**, 1088-1092.

32. C-N: (a) P. Ruiz-Castillo and S. L. Buchwald, *Chem. Rev.*, 2016, **116**, 12564-12649. (b) J. L. Klinkenberg and J. F. Hartwig, *Angew. Chem. Int. Ed.,* 2011, **50**, 86–95.

33. Hydroamination: (a) A. Trowbridge, S. M. Walton and M. J. Gaunt, *Chemical reviews*, 2020, **120**, 2613-2692. (b) J. Gui, C.-M. Pan, Y. Jin, T. Qin, J. C. Lo, B. J. Lee, S. H. Spergel, M. E. Mertzman, W. J. Pitts, T. E. L. Cruz, M. A. Schmidt, N. Darvatkar, S. R. Natarajan and P. S. Baran, *Science*, 2015, **348**, 886-891. (c) S. Streiff and F. Jérôme, *Chem. Soc. Rev.*, 2021, **50**, 1512-1521. (d) T. E. Müller and M. Beller, *Chem. Rev.,* 1998, **98**, 675-704.

34. Alcohol amination: (a) T. Yan, B. L. Feringa and K. Barta, *Nat. Commun*, 2014, **5**, 5602. (b) T. Irrgang and R. Kempe, *Chem. Rev.*, 2019, **119**, 2524-2549. (c) S. Imm, L. Neubert, H. Neumann and M. Beller, *Angew. Chem. Int. Ed*., 2010, **49**, 8126–8129.

35. (a) P. Sabatier and J.B. Sanderens, *C. R. Hebd. Séances Acad. Sci.,* 1905, **140**, 482–484. (b) C. Paal and J. Gerum, *Ber. Dtsch. Chem. Ges.,* 1909, **42**, 1553-1560. (c) V.J. Braun, G. Blessing and F. Zobel, *Ber. Dtsch. Chem. Ges. A*, 1923, **56**, 1988-2001. (d) M. Raney, US Patent 1563587A, 1925. (e) W. H. Carothers and G. A. Jones, *J. Am. Chem. Soc.,* 1925, **47**, 3051-3057. (f) L. Faucouneau, *Bull. Soc. Chim. Fr.*, 1937, **4**, 63. (g) G. Dupont and P. Piganiol, *Bull. Soc. chim. Fr.,* 1939, **6**, 322. (h) B. V. Aller, *J. Appl. Chem.,* 2007, **7**, 130–134. (i) H. Adkins, *Reactions of hydrogen with organic compounds over copper-chromium oxide and nickel catalysts*, Univ. Wisconsin Press, Madison, p. 53, 1937.

36. (a) M. A. Freifelder, *J. Am. Chem. Soc.,* 1960, **82**, 2386–2389. (b) L. K. Freidlin and T. A. Sladkova, *Russ. Chem. Rev.,* 1964, **33**, 319–330. (c) C. Barnett, *Ind. Eng. Chem. Prod. Res. Dev.,* 1969, **8**, 145–149. (d) C. De Bellefon and P. Fouilloux, *Catal. Rev.*,

1994, **36**, 459-506. (e) Y. M. López-De Jesús, C. E. Johnson, J. R. Monnier and C. T. Williams, *Top. Catal.,* 2010, **53**, 1132–1137. (f) K. Lévay and L. Hegedűs, *Curr. Org. Chem.,* 2019, **23**, 1881–1900. (g) M. Yoshimura, A. Komatsu, M. Niimura, Y. Takagi, T. Takahashi, S. Ueda, T. Ichikawa, Y. Kobayashi, H. Okami, T. Hattori, Y. Sawama, Y. Monguchi and H. Sajiki, *Adv. Synth. Catal.*, 2018, **360**, 1726-1732. (h) Y. Liu, S. He, Z. Quan, H. Cai, Y. Zhao and B. Wang, *Green Chem.*, 2019, **21**, 830-838. (i) H. Wang, Q. Luo, W. Liu, Y. Lin, Q. Guan, X. Zheng, H. Pan, J. Zhu, Z. Sun, S. Wei, J. Yang and J. Lu, *Nat. commun.,* 2019, **10**, 4998.

37. Supported Ni NPs: (a) P. Ryabchuk, G. Agostini, M.-M. Pohl, H. Lund, A. Agapova, H. Junge, K. Junge and M. Beller, *Sci. Adv.,* 2018, **4**, eaat0761. (b) Y. Zhang, H. Yang, Q. Chi and Z. Zhang, *ChemSusChem*, 2019, **12**, 1246-1255. (c) J. Wang, Q. Tang, S. Jin, Y. Wang, Z. Yuan, Q. Chi and Z. Zhang, *New J. Chem.*, 2020, **44**, 549-555.

38. Supported Co NPs: (a) F. Chen, C. Topf, J. Radnik, C. Kreyenschulte, H. Lund, M. Schneider, A.-E. Surkus, L. He, K. Junge and M. Beller, *J. Am. Chem. Soc.*, 2016, **138**, 8781-8788. (b) P. Ji, K. Manna, Z. Lin, X. Feng, A. Urban, Y. Song and W. Lin, *J. Am. Chem. Soc.*, 2017, **139**, 7004-7011. (c) R. Ferraccioli, D. Borovika, A.-E. Surkus, C. Kreyenschulte, C. Topf and M. Beller, *Catl. Sci. Technol.*, 2018, **8**, 499-507. (d) K. Murugesan, T. Senthamarai, M. Sohail, A. S. Alshammari, M.-M. Pohl, M. Beller and R. V. Jagadeesh, *Chem. Sci.*, 2018, **9**, 8553-8560. (e) D. Formenti, R. Mocci, H. Atia, S. Dastgir, M. Anwar, S. Bachmann, M. Scalone, K. Junge and M. Beller, *Chem. Eur. J.*, 2020, **26**, 15589-15595. (f) T. Mitsudome, M. Sheng, A. Nakata, J. Yamasaki, T. Mizugaki and K. Jitsukawa, *Chem. Sci.*, 2020, **11**, 6682-6689. (g) M. Sheng, S. Yamaguchi, A. Nakata, S. Yamazoe, K. Nakajima, J. Yamasaki, T. Mizugaki and T. Mitsudome, *ACS Sustainable Chem. Eng.*, 2021, **9**, 11238-11246.

39. (a) S. Gomez, J. A. Peters and T. Maschmeyer, *Adv. Synth. Catal*., 2002, **344**, 1037-1057. (b) H. Alinezhad, H. Yavari and F. Salehian, *Curr. Org. Chem*., 2015, **19**, 1021-1049. (c) T. C. Nugenta and M. El-Shazlya, *Adv. Synth. Catal.,* 2010, **352**, 753-819. (d) V. N. Wakchaure, J. Zhou, S. Hoffmann and B. List, *Angew. Chem. Int. Ed*., 2010, **49**, 4612-4614. (e) D. Chusov and B. List, *Angew. Chem. Int. Ed.,* 2014, **53**, 5199-5201. (f) K. Natte, H. H. Neumann, R.V. Jagadeesh and M. Beller, *Nat. commun.*, 2017, **8**, 1344. (g) R. V. Jagadeesh, T. Stemmler, A.-E. Surkus, H. Junge, J. Junge and M. Beller, *Nat. Protoc*., 2015, **10**, 548-557. (h) https://reagents.acsgcipr.org/reagent-guides/reductive-amination/list-of-reagents/hydrogen-metal-catalysts-precious-and-base-metal.

40. (a) Chapter 436: Mignonac reaction in *Comprehensive organic name reactions and reagents*, (Ed: Z. Wang), Part 2, Wiley, 2009. (b) G. Mignonac, *Compt. Rend.*, 1921,

172, 223. (c) J. L. Klinkenberg, and J. F. Hartwig, *Angew. Chem. Int. Ed.,* 2011, **50**, 86–95.

41. Primary Amine: (a) T. Gross, A. M. Seayad, M. Ahmad and M. Beller, *Org. Lett.,* 2002, **4**, 2055-2058. (b) A. Behr, A. Wintzer, C. Lübke and M. Müller, *J. Mol. Catal. A: Chem.,* 2015, **404-405**, 74-82. (c) T. Riermeier, K.-J. Haack, U. Dingerdissen, A. Börner, A.V. Tararov and R. Kadyrov, Weniger. *US 6,884,887 B1*, 2005. (d) J. Gallardo-Donaire, M. Ernst, O. Trapp and T. Schaub, *Adv. Synth. Catal*., 2016, **358**, 358-363. (e) T. Senthamarai, K. Murugesan, J. Schneidewind, N. V. Kalevaru, W. Baumann, H. Neumann, P. C. J. Kamer, M. Beller and R. V. Jagadeesh, *Nat. Commun*., 2018, **9**, 4123.

42. (a) G. Hahn, P. Kunnas, N. de Jonge and R. Kempe, *Nat. Catal.,* 2018, **2**, 71–77. (b). J. Liu, Y. Song and L. Ma, *Chem. Asian J.,* 2021, **16**, 2371-2391. (c) P. Yang, L. H. Lim, P. Chuanprasit, H. Hirao and J. Zhou, *Angew. Chem. Int. Ed.,* 2016, **55**, 12083-12087. (d) R. J. Kalbasi, O. Mazaheri, *Catal. Commun.*, 2015, **69**, 86-91.

43. Chiral Primary Amine: (a) J. Gallardo-Donaire, M. Hermsen. Wysocki, M. Ernst, F. Rominger, O. Trapp, A. Stephen, L. Hashmi, A. Schaefer, P. Comba, T. Schaub, *J. Am. Chem. Soc*., 2018, **140**, 355–361. (b) X. Tan, S. Gao, W. Zeng, S. Xin, Q. Yin and X. Zhang, *J. Am. Chem. Soc*., 2018, **140**, 2024-2027. (c) L. a. Hu, Y. Zhang, Q.-W. Zhang, Q. Yin and X. Zhang, *Angew. Chem. Int. Ed*., 2020, **59**, 5321-5325. (d) A. C. Brewer, J. C. Ruble, H. G. Vandeveer, S. A. Frank and C. R. Nevill, *Org. Process Res. Dev.*, 2021, **25**, 576-582.

44. (a) A. Corma, S. Iborra and A. Velty, *Chem. Rev.,* 2007, **107**, 2411–2502. (b) M. Besson, P. Gallezot and C. Pinel, *Chem. Rev.,* 2014, **114**, 1827–1870. (c) K. Natte, A. Narani, V. Goyal, N. Sarki and R. V. Jagadeesh, *Adv. Synth. Catal.,* 2020, **362**, 5143–5169. (d) V. Froidevaux, C. Negrell, S. Caillol, J.-P. Pascault and B. Boutevin, *Chem. Rev.,* 2016, **116**, 14181–14224. (e) M. Pelckmans, T. Renders, S. V. de Vyver and B. F. Sels, *Green Chem.,* 2017, **19**, 5303–5331. (f) J. He, L. Chen, S. Liu, K. Song, S. Yang and A. Riisager, *Green Chem.,* 2020, **22**, 6714–6747. (g) Z. Zhang, J. Song and B. Han, *Chem. Rev.,* 2017, **117**, 6834–6880. (h) K. Barta and P. C. Ford, *Acc. Chem. Res.,* 2014, **47**, 1503–1512. (i) R. Rinaldi, R. Jastrzebski, M. T. Clough, J. Ralph, M. Kennema, P. C. A. Bruijnincx and B. M. Weckhuysen, *Angew. Chem. Int. Ed.,* 2016, **55**, 8164–8215. (j) R. Mariscal, P. Maireles-Torres, M. Ojeda, I. Sádaba and M. López Granados, *Energy Environ. Sci.* 2016, **9**, 1144–1189. (k) S. U. Raut and P. R. Bhagat, *Fuel,* 2021, **303**, 121154. (l) Y. Yang, Y. Wang, S. Li, X. Shen, B. Chen, H. Liu and B. Han, *Green Chem.,* 2020, **22**, 4937-4942. (m) A. Dunbabin, F. Subrizi, J. M. Ward, T. D. Sheppard and H. C. Hailes, *Green Chem.,* 2017, **19**, 397-404. (n) J. B. Binder and

R. T. Raines, *J. Am. Chem. Soc.,* 2009, **131**, 1979-1985. (o) Y. Román-Leshkov, J. N. Chheda and J. A. Dumesic, *Science,* 2006, **312**, 1933-1937. (p) H. Chang, I. Bajaj, A. H. Motagamwala, A. Somasundaram, G. W. Huber, C. T. Maravelias, J. A. Dumesic, *Green Chem.,* 2021, **23**, 3277-3288.

45. (a) R.-J. Van Putten, J. C. van der Waal, E. de Jong, C. B. Rasrendra, H. J. Heeres and J. G. De Vries, *Chem. Rev.,* 2013, **113**, 1499–1597. (b) J. G. de Vries in *Heterocyclic Chemistry in the 21st Century: A Tribute to Alan Katritzky, Advances in Heterocyclic Chemistry, Vol. 121* (Eds.: E. F. V. Scriven, C. A. Ramsden), Chapter 8: Green Syntheses of Heterocycles of Industrial Importance. 5-Hydroxymethylfurfural as a Platform Chemical, Academic Press (Elsevier), Cambridge, MA, pp. 247–293, 2017. (c) J. J. Bozell and G. R. Petersen, *Green Chem.,* 2010, **12**, 539–554. (d) T. Werpy and G. Petersen in *Top Value-Added Chemicals from Biomass: Volume I – Results of Screening for Potential Candidates from Sugars and Synthesis Gas.* United States: N. p., **2004**. (e) A. A. Rosatella, S. P. Simeonov, R. F. M. Frade and C. A. Afonso, *Green Chem.,* 2011, **13**, 754–793. (f) F. Weigang, V. Charlie, Q. Yves and P. Florence, *Curr. Org. Synth.,* 2019, **16**, 583–614. (g) S. P. Teong, G. Yi and Y. Zhang, *Green Chem.*, 2014, **16**, 2015-2026.

46. (a) W. Chen, Y. Jiang, Y. Sun, Y. Wang, Z. Li, X. Wang, X. Zeng, S. Liu and L. Lin, *J. Biobased Mater. Bioenergy,* 2016, **10**, 378–384. (b) A. Feriani, G. Gaviraghi, G. Toson, M. Mor, A. Barbieri, E. Grana, C. Boselli, M. Guarneri, D. Simoni and S. Manfredini, *J. Med. Chem.,* 1994, **37**, 4278–4287. (c) M.-S. Michael, B. J. Price, B. John and W. John, US Pat, 4279911, 1981. (d) M.-L. Yang, Y.-X. Wu, Y. Liu, J.-J. Qiu and C.-M. Liu, *Polym. Chem.,* 2019, **10**, 6217–6226.

47. Nobel Metals: (a) M. Chatterjee, T. Ishizaka and H. Kawanami, *Green Chem.,* 2016, **18**, 487–496. (b) A. L. Nuzhdin, P. A. Simonov, G. A. Bukhtiyarova, I. V. Eltsov, V. I. Bukhtiyarov, *J. Mol. Catal.,* 2021, **499**, 111297. (c) V. V. Karve, D. T. Sun, O. Trukhina, S. Yang, E. Oveisi, J. Luterbacher, W. L. Queen, *Green Chem.,* 2020, **22**, 368–378. (d) A. García-Ortiz, J. D. Vidal, M. J. Climent, P. Concepción, A. Corma, S. Iborra, *ACS Sustainable Chem. Eng.,* 2019, **7**, 6243–6250. (e) Z. Xu, P. Yan, W. Xu, S. Jia, Z. Xia, B. Chung and Z. C. Zhang, *RSC Adv.,* 2014, **4**, 59083–59087. (f) D. Deng, Y. Kita, K. Kamata, M. Hara, *ACS Sustainable Chem. Eng.,* 2019, **7**, 4692–4698. (g) C. Dong, H. Wang, H. Du, J. Peng, Y. Cai, S. Guo, J. Zhang, C. Samart, M. Ding, *J. Mol. Catal.,* 2020, **482**, 110755. (h) M.-M. Zhu, L. Tao, Q. Zhang, J. Dong, Y.-M. Liu, H.-Y. He, Y. Cao, *Green Chem.,* 2017, **19**, 3880–3887.

48. (a) Z. Wei, Y. Cheng, K. Zhou, Y. Zeng, E. Yao, Q. Li, Y. Liu, Y. Sun, *ChemSusChem* 2021, **14**, 2308–2312. (b) A. L. Nuzhdin, M. V. Bukhtiyarova, V. I. Bukhtiyarov,

Molecules, 2020, **25**, 4771. (c) H. Yuan, B. T. Kusema, Z. Yan, S. Streiff, F. Shi, *RSC Adv.,* 2019, **9**, 38877–38881. (d) H. Yuan, J P. Li, F. Su, Z. Yan, B. T. Kusema, S. Streiff, Y. Huang, M. PeraTitus, F. Shi, *ACS Omega* 2019, **4**, 2510–2516. (e) W. Chen, Y. Sun, J. Du, Z. Si, X. Tang, X. Zeng, L. Lin, S. Liu, T. Lei, *J. Chem. Technol. Biotechnol.,* 2018, **93**, 3028–3034. (f) G. Chieffi, M. Braun, D. Esposito, *ChemSusChem,* 2015, **8**, 3590–3594. (g) K. Zhou, B. Chen, X. Zhou, S. Kang, Y. Xu and J. Wei, *ChemCatChem*, 2019, **11**, 5562-5569. (h) X. Zhuang, J. Liu, S. Zhong and L. Ma, *Green Chem.,* 2022, **24**, 271-284.

49. (a) V. Sridharan, P. A. Suryavanshi and J. C. Menéndez, *Chem. Rev.*, 2011, **111**, 7157-7259. (b) E. Vitaku, D. T. Smith and J. T. Njardarson, *J. Med. Chem.*, 2014, **57**, 10257-10274. (c) S. Källström and R. Leino, *Bioorg. Med. Chem.*, 2008, **16**, 601-635. (d) A. O'Byrne and P. Evans, *Tetrahedron*, 2008, **64**, 8067-8072. (e) A. Gualandi and D. Savoia, *RSC Adv.,* 2016, **6**, 18419-18451. (f) Z. Wei, F. Shao and J. Wang, *Chin. J. Chem*., 2019, **40**, 980-1002. (g) J. D. Scott and R. M. Williams, *Chem. Rev.*, 2002, **102**, 1669-1730. (h) A. R. Katritzky, S. Rachwal and B. Rachwal, *Tetrahedron*, 1996, **52**, 15031-15070. (i) R. J. Pagliero, S. Lusvarghi, A. B. Pierini, R. Brun and M. R. Mazzieri, *Bioorg. Med. Chem.*, 2010, **18**, 142-150. (j) J.-P. Liou, Z.-Y. Wu, C.-C. Kuo, C.-Y. Chang, P.-Y. Lu, C.-M. Chen, H.-P. Hsieh and J.-Y. Chang, *J. Med. Chem.*, 2008, **51**, 4351-4355. (k) J. Balint, G. Egri, E. Fogassy, Z. Bçcskei, K. Simon, A. Gajary and A. Friesz, *Tetrahedron: Asymmetry*, 1999, **10**, 1079-1087.

50. (a) M. P. Wiesenfeldt, Z. Nairoukh, T. Dalton and F. Glorius, *Angew. Chem. Int. Ed.*, 2019, 58, 10460-10476. (b) Z. Nairoukh, M. Wollenburg, C. Schlepphorst, K. Bergander and F. Glorius, *Nat. Chem.*, 2019, **11**, 264-270. (c) T. Mahdi, J. N. del Castillo and D. W. Stephan, *Organometallics*, 2013, **32**, 1971-1978. (d) Y. Liu and H. Du, *J. Am. Chem. Soc.*, 2013, **135**, 12968-12971. (e) W.-J. Tang, J. Tan, L.-J. Xu, K.-H. Lam, Q.-H. Fan and A. S. C. Chan, *Adv. Synth. Catal.*, 2010, **352**, 1055-1062. (f) X.-B. Wang, W. Zeng and Y.-G. Zhou, *Tetrahedron Lett.*, 2008, **49**, 4922-4924. (g) M. Studer, C. Wedemeyer-Exl, F. Spindler and H.-U. Blaser, *Monatsh. Chem.*, 2000, **131**, 1335-1343.

51. (a) E. Baralt, S. J. Smith, J. Hurwitz, I. T. Horvath and R. H. Fish, *J. Am. Chem. Soc.*, 1992, **114**, 5187-5196. (b) M. Studer, C. Wedemeyer-Exl, F. Spindler and H.-U. Blaser, *Monatsh. Chem.*, 2000, **131**, 1335-1343.

52. (a) X.-B. Wang, W. Zeng and Y.-G. Zhou, *Tetrahedron Lett.* 2008, **49**, 4922-4924. (b) W.-J. Tang, J. Tan, L.-J. Xu, K.-H. Lam, Q.-H. Fan and A. S. C. Chan, *Adv. Synth. Catal.*, 2010, **352**, 1055-1062.

53. (a) D.-S. Wang, Q.-A. Chen, S.-M. Lu and Y.-G. Zhou, *Chem. Rev.,* 2012, **112**, 2557-2590. (b) Y.-G. Zhou, *Acc. Chem. Res.*, 2007, **40**, 1357-1366.

54. T. S. Hamilton and R. Adams, *J. Am. Chem. Soc.*, 1928, **50**, 2260-2263.

55. F. Chen, W. Li, B. Sahoo, C. Kreyenschulte, G. Agostini, H. Lund, K. Junge and M. Beller, *Angew. Chem. Int. Ed.*, 2018, **57**, 14488-14492.

56. Examples for Raney Ni, Ni, Fe-catalyzed (iso)quinoline hydrogenation: (a) W. M. Czaplik, J.-M. Neudçrfl and A. J. von Wangelin, *Green Chem.,* 2007, **9**, 1163-1165. (b) C. Liu, Z. Rong, Z. Sun, Y. Wang, W. Du, Y. Wang and L. Lu, *RSC Adv.*, 2013, **3**, 23984-23988. (c) J. E. Shaw and P. R. Stapp, *J. Heterocyclic Chem.*, 1987, **24**, 1477-1483. (d) B. Sahoo, C. Kreyenschulte, G. Agostini, H. Lund, S. Bachmann, M. Scalone, K. Junge and M. Beller, *Chem. Sci.*, 2018, **9**, 8134-8141.

57. Co-catalyzed *N*-arene hydrogenation: (a) F. Chen, A.-E. Surkus, L. He, M.-M. Pohl, J. Radnik, C. Topf, K. Junge and M. Beller, *J. Am. Chem. Soc.*, 2015, **137**, 11718-11724. (b) P. Ji, K. Manna, Z. Lin, A. Urban, F. X. Greene, G. Lan and W. Lin, *J. Am. Chem. Soc.*, 2016, **138**, 12234-1224. (c) Z. Wei, Y. Chen, J. Wang, D. Su, M. Tang, S. Mao and Y. Wang, *ACS Catal.*, 2016, **6**, 5816-5822. (d) J. Li, G. Liu, X. Long, G. Gao, J. Wu and F. Li, *Journal of Catalysis*, 2017, **355**, 53-62. (e) P. Ji, Y. Song, T. Drake, S. S. Veroneau, Z. Lin, X. Pan and W. Lin, *J. Am. Chem. Soc.*, 2018, **140**, 433-440. (f) I. Sorribes, L. Liu, A. Doménech-Carbó and A. Corma, *ACS Catal.*, 2018, **8**, 4545-4557. (g) W. Gong, Q. Yuan, C. Chen, Y. Lv, Y. Lin, C. Liang, G. Wang, H. Zhang and H. Zhao, *Adv. Mater.*, 2019, **31**, 1906051. (h) G. Jaiswal, M. Subaramanian, M. K. Sahoo and E. Balaraman, *ChemCatChem*, 2019, **11**, 2449-2457. (i) Z.-H. He, Y.-C. Sun, K. Wang, Z.-Y. Wang, P.-P. Guo, C.-S. Jiang, M.-Q. Yao, Z.-H. Li and Z.-T. Liu, *Mol. Catal.*, 2020, **496**, 111192. (j) J. Hervochon, V. Dorcet, K. Junge, M. Beller and C. Fischmeister, *Catal. Sci. Technol.*, 2020, **10**, 4820-4826. (k) S. Zhang, J. Gan, Z. Xia, X. Chen, Y. Zou, X. Duan and Y. Qu, *Chem*, 2020, **6**, 2994-3006. (l) V. M. Asaula, V. V. Buryanov, B. Y. Solod, D. M. Tryus, O. O. Pariiska, I. E. Kotenko, Y. M. Volovenko, D. M. Volochnyuk, S. V. Ryabukhin and S. V. Kolotilov, *Eur. J. Org. Chem.*, 2021, **2021**, 6616-6625. (m) M. Puche, L. Liu, P. Concepción, I. Sorribes and A. Corma, *ACS Catal.*, 2021, **11**, 8197-8210. (n) D. Timelthaler and C. Topf, *Synthesis*, 2022, **54**, 629-642.

Publications

5. Contribution to the publications

This chapter includes selected publications of this thesis work. Further publications are available in chapter 6

5.1 Silica-supported Fe/Fe–O nanoparticles for the catalytic hydrogenation of nitriles to amines in the presence of aluminium additives

Vishwas G. Chandrashekhar[1], Thirusangumurugan Senthamarai[1], Ravishankar G. Kadam[2], Ondřej Malina[2], Josef Kašlík[2], Radek Zbořil[2,3], Manoj B. Gawande[2,4], Rajenahally V. Jagadeesh[1] and Matthias Beller[1]

Nat Catal, 2022, **5,** 20-29.

Author contributions:

In this paper, I developed the catalyst, designed, and optimized experimental conditions, investigation of substrate scope, mechanistic studies and co-wrote the paper. My contribution as the first author of this paper is approximately 75%.

Signature of the student

(Vishwas G. Chandrashekhar)

Signature of the supervisor

(Prof. Dr. Matthias Beller)

5.2 Homogeneous cobalt-catalyzed reductive amination for synthesis of functionalized primary amines

Kathiravan Murugesan[1], Zhihong Wei[1], Vishwas G. Chandrashekhar[1], Helfried Neumann[1], Anke Spannenberg[1], Haijun Jiao[1], Matthias Beller[1]* & Rajenahally V. Jagadeesh[1]*

Nat Commun, 2019, **10,** 5443.

Author contributions:

In this paper, I was involved in development of catalyst, investigation of substrate scope along with isolation of products, reproduced the results and writing the manuscript. My contribution as a co-author in this paper is approximately 35%.

Signature of the student

(Vishwas G. Chandrashekhar)

Signature of the supervisor

(Prof. Dr. Matthias Beller)

5.3 Reductive amination, hydrogenation and hydrodeoxygenation of 5-hydroxymethylfurfural using silica-supported cobalt-nanoparticles

Vishwas G. Chandrashekhar,[a] Kishore Natte,[b] Asma M. Alenad,[c] Ahmad S. Alshammari,[d] Carsten Kreyenschulte,[a] and Rajenahally V. Jagadeesh*[a]

ChemCatChem, 2021, **13,** 1-10.

Author contributions:

In this paper, I designed the catalyst and optimized experimental conditions, investigated substrate scope, and co-wrote the paper. My contribution as the first author of this paper is approximately 80%.

Signature of the student

(Vishwas G. Chandrashekhar)

Signature of the supervisor

(Prof. Dr. Matthias Beller)

5.4 A general catalyst based on cobalt core–shell nanoparticles for the hydrogenation of *N*-heteroarenes including pyridines

Kathiravan Murugesan, Vishwas G. Chandrashekhar, Carsten Kreyenschulte, Matthias Beller,* and Rajenahally V. Jagadeesh*

Angew. Chem. Int. Ed., 2020, **59,** 17408-17412.

Author contributions:

In this paper, I involved in development of catalyst, optimized experimental conditions, performed substrate scope and isolation of reported compounds, and co-wrote the paper. My contribution as the first author of this paper is approximately 50%.

Signature of the student

(Vishwas G. Chandrashekhar)

Signature of the supervisor

(Prof. Dr. Matthias Beller)

ARTICLES
https://doi.org/10.1038/s41929-021-00722-x

nature catalysis

Check for updates

OPEN

Silica-supported Fe/Fe–O nanoparticles for the catalytic hydrogenation of nitriles to amines in the presence of aluminium additives

Vishwas G. Chandrashekhar[1], Thirusangumurugan Senthamarai[1], Ravishankar G. Kadam[2], Ondřej Malina[2], Josef Kašlík[2], Radek Zbořil[2,3]✉, Manoj B. Gawande[2,4]✉, Rajenahally V. Jagadeesh[1]✉ and Matthias Beller[1]✉

The hydrogenation of nitriles to amines represents an important and frequently used industrial process due to the broad applicability of the resulting products in chemistry and life sciences. Despite the existing portfolio of catalysts reported for the hydrogenation of nitriles, the development of iron-based heterogeneous catalysts for this process is still a challenge. Here, we show that the impregnation and pyrolysis of iron(II) acetate on commercial silica produces a reusable Fe/Fe–O@SiO_2 catalyst with a well-defined structure comprising the fayalite phase at the Si–Fe interface and α-Fe nanoparticles, covered by an ultrathin amorphous iron(III) oxide layer, growing from the silica matrix. These Fe/Fe–O core–shell nanoparticles, in the presence of catalytic amounts of aluminium additives, promote the hydrogenation of all kinds of nitriles, including structurally challenging and functionally diverse aromatic, heterocyclic, aliphatic and fatty nitriles, to produce primary amines under scalable and industrially viable conditions.

Catalysis plays a decisive role in many basic and applied chemical processes and is involved in the industrial production of more than 90% of fine and bulk chemicals as well as polymeric materials and many other everyday products[1–5]. In addition, the synthesis of bioactive compounds for life sciences and the success of sustainable energy technologies, including green fuels, depend on efficient catalytic processes[1–5]. Indeed, the success of organic synthesis in the last 100 years relied to a large extent on the discovery and application of suitable catalysts[1–5]. In this respect, specifically, the development of practical and cost-efficient hydrogenation strategies constitutes a key achievement of the last century[6]. Nowadays, a plethora of molecularly defined metal complexes as well as heterogeneous materials are frequently applied for the selective hydrogenation of alkynes[7,8], olefins[7,9,10], carbonyl compounds[11,12], nitroarenes[13,14] as well as (hetero)arenes[7,15–17]. Among these hydrogenation reactions, the transformation of nitriles to primary amines is particularly valuable because the latter products are privileged compounds in chemistry, medicine and biology[18–22]. In general, primary amines constitute important precursors and central intermediates in the chemical, pharmaceutical, agrochemical and materials industries[18–22]. After the original discovery of benzonitrile hydrogenation in the presence of nickel in 1905 (ref. [23]), many catalysts were developed for this and related reactions (Fig. 1)[24–42]. These achievements were mainly possible due to the design of precious metal systems, which allow reactions to be performed at low temperature and pressure[24,30,31,33–38]. However, despite their tremendous success, their limited availability and higher price constitute major drawbacks. Thus, state-of-the-art catalysts for nitrile hydrogenation in industry continue to be Raney nickel[26,27,31,33] and copper chromite[29], which demand harsh conditions and suffer from toxicity issues. To solve these problems, alternative nickel- and cobalt-based heterogeneous catalysts have been reported in recent years[35,39–41].

From a sustainability point of view, iron would be an ideal catalyst system for nitrile hydrogenation because of its abundance (at 4.7% it is the second-most abundant metal in the earth crust), low price and low toxicity[14,17,42–44]. Indeed, in the last decade, using sophisticated/synthetically demanding PNP pincer ligands, active iron complexes have been developed to hydrogenate nitriles[44]. In general, however, these metal complexes are less stable and difficult to use. In contrast, heterogeneous catalysts show improved stability and can be easily reused[14,17,22,45–47]. Unfortunately, to the best of our knowledge, analogous supported active iron centres for the hydrogenation of nitriles have not been created yet.

Here, we report a stable and convenient iron-based nanocatalyst obtained by the pyrolysis of iron acetate on commercial silica that shows excellent activity and selectivity for the hydrogenation of a large number of nitriles to produce primary amines in the presence of catalytic amounts of aluminium additives.

Results

Synthesis and characterization of Fe-based nanocatalysts. In the last decade, the excellent catalytic performance of carbon-encapsulated core–shell 3*d* metal nanoparticles has been demonstrated in a variety of hydrogenation reactions[14,16,17,22,39,40,46]. These catalysts were prepared by the immobilization and pyrolysis of metal complexes or metal organic frameworks on inorganic supports (for example, carbon, SiO_2 and Al_2O_3)[14,16,17,22,39,40,46]. In this context, we developed activated Fe_2O_3 nanoparticles, surrounded by

[1]Leibniz-Institut für Katalyse e.V., Rostock, Germany. [2]Regional Centre of Advanced Technologies and Materials, Czech Advanced Technology and Research Institute, Palacky University Olomouc, Olomouc, Czech Republic. [3]Nanotechnology Centre, Centre of Energy and Environmental Technologies, VŠB–Technical University of Ostrava, Ostrava-Poruba, Czech Republic. [4]Department of Industrial and Engineering Chemistry, Institute of Chemical Technology Mumbai-Marathwada Campus, Jalna, Maharashtra, India. ✉e-mail: radek.zboril@upol.cz; mb.gawande@marj.ictmumbai.edu.in; jagadeesh.rajenahally@catalysis.de; matthias.beller@catalysis.de

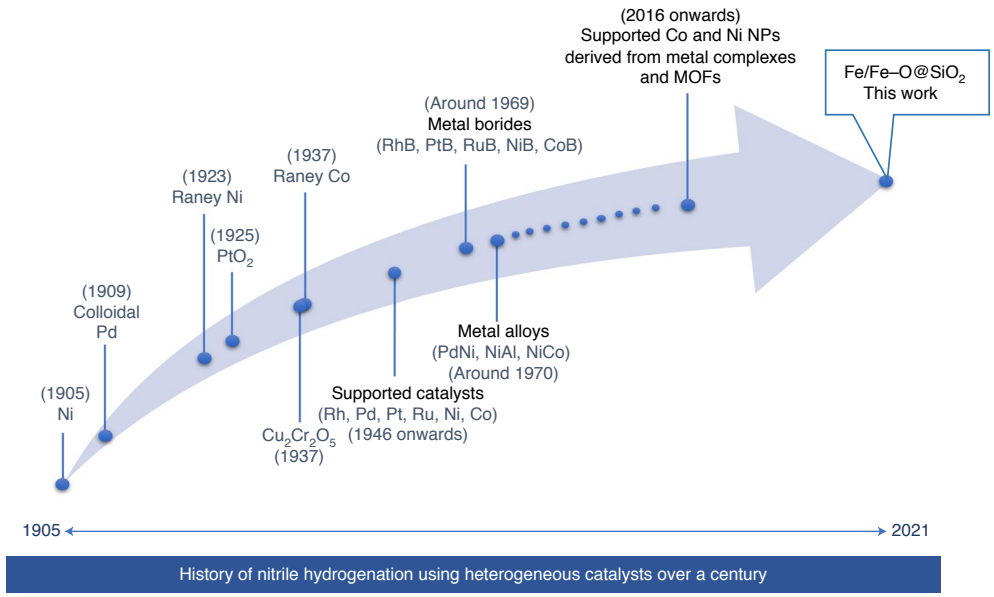

Fig. 1 | Historical overview of heterogeneous nitrile hydrogenation catalysts. The hydrogenation of nitriles using heterogeneous catalysts has a long history that covers more than a century.

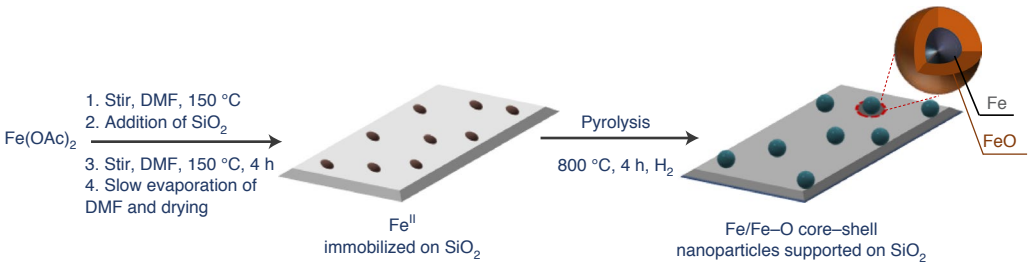

Fig. 2 | Catalyst preparation. Synthesis of Fe/Fe–O core–shell nanoparticles by the impregnation and pyrolysis of iron(II) acetate on SiO_2. DMF, *N*,*N*-dimethylformamide.

nitrogen-doped graphene, as selective catalysts for the hydrogenation of nitroarenes to anilines[14]. In addition, supported Fe-based nanoparticles have also been found active for the hydrogenation of quinolines[17]. However, these and related Fe materials showed no activity for more challenging substrates, including nitriles (Supplementary Table 1, entries 1 and 2). To identify potential iron-based heterogeneous catalysts for nitrile hydrogenation, we prepared a series of iron nanoparticles supported on various supports. Specifically, commercially available neutral, acidic and basic inorganic supports, for example, Vulcan XC72R carbon powder, Aerosil silica (SiO_2), γ-Al_2O_3 and MgO, were impregnated with iron(II) acetate. Subsequently, these materials were pyrolysed at 800 °C under reductive (H_2) conditions. A schematic illustration of the synthetic procedure with the SiO_2 support is presented in Fig. 2. Hereafter, these materials are denoted as $Fe(OAc)_2$-support-*x*, where *x* denotes the pyrolysis temperature.

As a benchmark reaction, the hydrogenation of 4-chlorobenzonitrile (**1**) to 4-chlorobenzylamine (**2**) was chosen (Fig. 3), not only to identify an active catalyst system, but also a selective one. Notably, **1** easily undergoes reductive dehalogenation in the presence of many known hydrogenation catalysts. To our surprise, during initial control experiments, we observed some activity (26% yield of **2**) and high selectivity (>90%) for the primary amine in the presence of $Fe(OAc)_2$-SiO_2-800 (Fig. 3). To improve the conversion and yield, we varied the reaction conditions (temperature, solvent, catalyst loading) and investigated the influence of additives (Supplementary Tables 1–3). Applying higher catalyst loadings (up to 12.8 mol%), the product yield increased up to 50%, and the selectivity for the primary amine remained very good. Gratifyingly, in the presence of aluminium triisopropoxide, the yield of 4-chlorobenzylamine (**2**) dramatically increased to 96%. Following this excellent result, several other metal alkoxides, aluminium compounds as well as Lewis acids and bases were tested as additives (Supplementary Table 2). Surprisingly, only a few additives, for example, *p*-toluenesulfonic acid, showed a positive effect on the reaction, while most, for example, bases, had a negative impact. Optimal results, with an almost quantitative yield of **2**, were achieved in the presence of inexpensive aluminium foil (Fig. 3 and Supplementary Fig. 1). In this case, the aluminium foil completely dissolved in the solvent (isopropanol), which explains the similar positive effect of aluminium foil and aluminium triisopropoxide. Control experiments proved that this dissolution only takes place in the presence of ammonia (Supplementary Table 4). To elucidate the crucial role of aluminium additives, we performed kinetic investigations of the model reaction in the absence and presence of aluminium foil and aluminium triisopropoxide (Supplementary Figs. 2 and 3). Surprisingly, all the reactions needed a preactivation time (3–9 h) to start. Only in the presence of aluminium triisopropoxide was this preactivation drastically reduced. Based on these results and the testing of the different additives, we assume that both aluminium

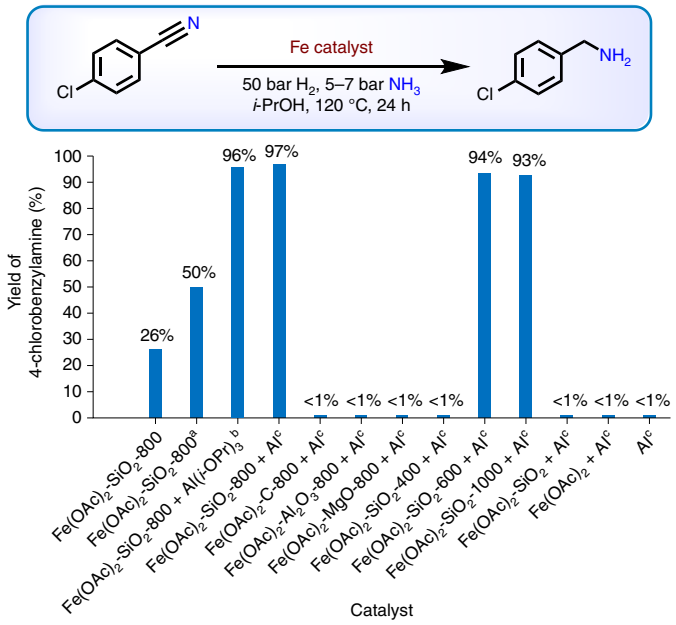

Fig. 3 | Evaluation of Fe catalysts. Hydrogenation of 4-chlorobenzonitrile. Reaction conditions: 0.5 mmol 4-chlorobenzonitrile, 40 mg catalyst (8.5 mol% Fe), 50 bar H_2, 5–7 bar NH_3, 3 ml *i*-PrOH, 120 °C, 24 h. Gas chromatography (GC) yields are given using *n*-hexadecane as standard. [a]With 60 mg catalyst. [b]With 20 mol% Al(*i*-OPr)$_3$. [c]With 20 mol% (3 mg) Al foil.

triisopropoxide and aluminium foil are converted under the reaction conditions to an active Lewis acid co-catalyst that activates the nitrile group. These Lewis acidic centres can probably also be generated on the silica support close to the nanoparticles by reaction with Si–OH sites on the surface. Notably, catalytic (substoichiometric) amounts (20 mol%) of the aluminium additives were sufficient to achieve improved yields.

Under the optimized conditions, other supported catalysts, such as Fe(OAc)$_2$-C-800, Fe(OAc)$_2$-Al_2O_3-800 and Fe(OAc)$_2$-MgO-800 (Supplementary Figs. 4–6), did not show any activity (Fig. 3). In these samples we did not observe needle-like well-developed α-Fe nanoparticles growing from the matrix, as we did in the case of the optimal catalyst, Fe(OAc)$_2$-SiO_2-800. In contrast, the iron nanoparticles were highly aggregated and/or encapsulated within the matrix (Supplementary Figs. 4–6). Similarly, Fe(OAc)$_2$ on SiO_2 pyrolysed at 400 °C (Fe(OAc)$_2$-SiO_2-400) was completely inactive (Fig. 3). This is explained by a not fully developed active Fe nanostructure at low pyrolysis temperature, which is evident from the powder X-ray diffraction (PXRD) pattern (Supplementary Fig. 7) and transmission electron microscopy (TEM) image (Supplementary Fig. 8) of the Fe(OAc)$_2$-SiO_2-400 sample. By contrast, Fe(OAc)$_2$-SiO_2-600 and Fe(OAc)$_2$-SiO_2-1,000 exhibited comparable activities to that of Fe(OAc)$_2$-SiO_2-800, providing 93 and 94% yields of the desired product, respectively. This correlates well with the similar size and well-developed core–shell structure of the Fe(OAc)$_2$-SiO_2-600 and Fe(OAc)$_2$-SiO_2-1,000 samples (see the TEM images in Supplementary Figs. 9 and 10) compared with Fe(OAc)$_2$-SiO_2-800 (Fig. 4c). As expected, iron(II) acetate, unpyrolysed Fe(OAc)$_2$-SiO_2 and Al additives alone were completely inactive in the reaction (Fig. 3). Additionally, we prepared control samples, including pure amorphous Fe_2O_3 nanoparticles (NPs), fayalite (Fe_2SiO_4) NPs and matrix-free Fe–Fe_2O_3 core–shell NPs with a very thin oxidic shell (Supplementary Figs. 11–13), and investigated their performance in the model reaction. Notably, the fayalite and Fe_2O_3 NPs were completely inactive, whereas the Fe–Fe_2O_3 core–shell NPs gave 30% yield (Supplementary Table 5, entries 1–3). This confirmed the crucial role of the Fe–Fe_2O_3 core–shell superstructure in triggering the catalytic process. We believe that the active material involves Fe centres and/or the Fe–O atomic interface[48]. The high activity of the catalyst incorporating the SiO_2 matrix (Fe(OAc)$_2$-SiO_2-800) strongly indicates that the matrix regulates the size of the iron oxide crystallites[49,50]. Indeed, it has already been reported that the Cu–O–SiO_x interface in a silica-supported copper (Cu@SiO_2) catalyst plays a key role in H_2 dissociation to form Cu–$H^{\delta-}$ and SiO–$H^{\delta+}$ species[51]. Thus, we believe that the silica in Fe(OAc)$_2$-SiO_2-800 would contribute to the catalytic activity by forming such an active metal–support (Fe–O–SiO_x) interface.

Next, we conducted a detailed characterization of the most active catalyst Fe(OAc)$_2$-SiO_2-800. TEM analysis revealed the formation of core–shell structures with globular and rod-shape morphologies, with the needle diameters ranging from 10 to 30 nm and lengths up to 100 nm (Fig. 4a–c). Energy-dispersive X-ray spectroscopy (EDS) of this material showed the presence of Si, O and Fe elements (Supplementary Fig. 14). The high-resolution TEM image (HRTEM; Fig. 4d) confirms that the metallic part of the catalyst is composed of an α-Fe core growing from the SiO_2 matrix. Indeed, the high-angle annular dark-field scanning transmission electron microscopy (HAADF-STEM) and elemental mapping images clearly verify that the Fe core nanoparticles are growing from the SiO_2 matrix and are covered by a layer of ultrathin iron oxide with a thickness of a few nanometres (Fig. 4f–i). Based on this assignment, the most active Fe(OAc)$_2$-SiO_2-800 catalyst is abbreviated to Fe/Fe–O@SiO_2 in the following text. A representative HAADF-STEM image of a globular particle and typical depth profile plot showing the intensity distribution of the Si, O and Fe elements at various distances from the surface are shown in Fig. 5a,b, respectively. The depth profiles confirm that the thickness of the oxidic Fe-O shell is less than 5 nm. Clearly, the catalyst surface is composed of iron nanoparticles, which grow from the SiO_2 matrix, stabilized by an extremely thin iron oxide shell.

Furthermore, we performed very detailed chemical mapping with a focus on the iron-containing surface components that are responsible for the catalytic activity. All the identified Fe-bearing surface-active phase was composed of Fe nanoparticles covered with a very thin shell of iron oxide, irrespective of the size and morphology (globular, needle-like) of the Fe NPs (Supplementary Fig. 15).

To identify the chemical and structural character of the catalyst, we analysed the Fe/Fe–O@SiO_2 sample by PXRD, Mössbauer spectroscopy, X-ray photoelectron spectroscopy (XPS) and electron paramagnetic resonance (EPR) spectroscopy. The PXRD pattern of Fe/Fe–O@SiO_2 (Supplementary Fig. 16) shows strong metallic α-Fe reflections at $2\theta = 52.33$, 77.16 and 99.60°, corresponding to crystalline facets of the Fe (110), (200) and (211) planes, respectively (Joint Committee on Powder Diffraction Standards (JCPDS) card number 04-012-6482). Thus, α-Fe is the dominant crystalline phase involved in the catalyst superstructure. The low-crystalline SiO_2 matrix is represented by a broad peak at $2\theta \approx 26°$, indicating the presence of poorly crystalline cristobalite (JCPDS card number 04-008-7643). The ultrathin iron oxide layer is, in accord with expectation, not identifiable in the PXRD pattern due to its mostly amorphous nature. However, detailed PXRD analysis clearly showed additional low-intensity diffraction peaks corresponding to fayalite (Fe_2SiO_4, JCPDS card number 04-002-3681) and crystalline silicon (Si(0), JCPDS card number 04-014-8844). In summary, PXRD provided a complex picture of the high-temperature chemistry of the Fe–Si–O system.

These observations are in line with the XPS analysis, which confirmed the presence of just Fe, Si and O elements in the survey spectrum (Supplementary Fig. 17a). The high-resolution O1*s* spectrum of Fe/Fe–O@SiO_2 (Supplementary Fig. 17b) identifies peaks

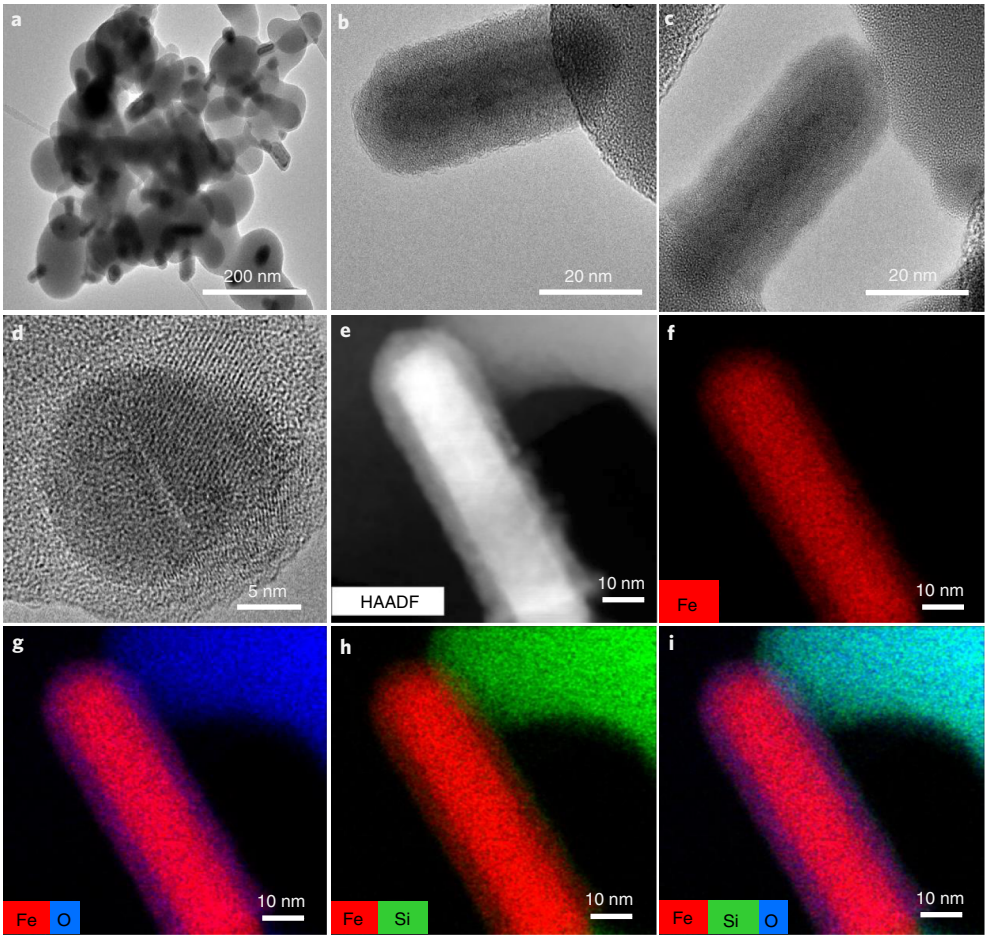

Fig. 4 | TEM and HRTEM imaging of Fe(OAc)$_2$-SiO$_2$-800. a–i, TEM (**a**–**c**), HRTEM (**d**) and HAADF-STEM (**e**) images and elemental mapping of iron (**f**), iron and oxygen (**g**), iron and silicon (**h**), and iron, silicon and oxygen (**i**) for the Fe(OAc)$_2$-SiO$_2$-800 catalyst.

at 530.72 and 533.14 eV, corresponding to Fe–O and Si–O bonds, respectively. Most importantly, the high-resolution Fe2*p* spectrum (Supplementary Fig. 17d) reveals Fe $2p_{3/2}$ peaks at 710.27 and 712.73 eV, and Fe$2p_{1/2}$ peaks at 723.37 and 725.83 eV, which can be ascribed to Fe^{3+} species[52], along with two satellite peaks at 717.41 and 730.51 eV. This is strong proof that the amorphous iron oxide phase covering the Fe(0) core corresponds to amorphous Fe_2O_3. The formation of iron(III) oxide was confirmed by the hyperfine parameters derived from room-temperature Mössbauer spectroscopy (Fig. 5c). The ^{57}Fe Mössbauer spectrum of the sample shows a dominant sextet (68% of the relative spectrum area) and two doublet components. According to the Mössbauer hyperfine parameters, the sextet with zero isomer shift and a hyperfine field of 32.9 T can be unambiguously assigned to ferromagnetic α-Fe. The doublet with high isomer shift (1.18 mm s^{-1}) and quadrupole splitting (2.64 mm s^{-1}) clearly belongs to Fe(II) ions in the fayalite structure formed at the Si–Fe interface[53], in perfect agreement with the results of the PXRD measurements. Finally, the doublet with an isomer shift of 0.35 mm s^{-1} is typical of high-spin Fe(III) in amorphous iron(III) oxide with disordered symmetry of the iron environment, as proved by the relatively high quadrupole splitting (1.31 mm s^{-1})[54]. It is worth mentioning that possible traces of Fe(III) ions usually involved in the fayalite structure would overlap the doublet of the iron(III) oxide phase. Finally, the EPR spectrum of Fe/Fe–O@SiO_2 shows broad anisotropic signals with *g* factor values of $g_x = 2.72$, $g_y = 2.04$ and $g_z = 1.8$ ($g_{ave} = 2.19$) at 77 K (Fig. 5d), which indicates the presence of ferromagnetic particles corresponding to Fe(0) with distinct size and morphology. In summary, HRTEM, HAADF-STEM, XPS, PXRD, EPR and Mössbauer spectroscopy allowed us to explore the chemical and structural character of the Fe/Fe–O@SiO_2 catalyst, being composed of a SiO_2 matrix, a fayalite interface (Fe_2SiO_4) and α-Fe–amorphous Fe_2O_3 core–shell nanoparticles growing from the silica matrix and representing the surface-active phase participating in the catalytic process. The EPR and Mössbauer data confirm the ferromagnetic character of the sample, predetermining the catalyst for simple magnetic separation.

Hydrogenation of benzonitriles and heterocyclic nitriles. With an active Fe-based catalyst (Fe/Fe–O@SiO_2) in hand, we demonstrated its general applicability for the selective hydrogenation of all kinds of nitriles. Although in most of the reactions aluminium foil was used as an inexpensive additive, experiments performed for comparison in the presence of aluminium triisopropoxide gave similar product yields. First, we carried out the hydrogenation of a series of aromatic nitriles (Fig. 6). Simple benzonitriles as well as substituted ones bearing aromatic or alkyl groups gave the corresponding primary amines in yields of up to 96% (Fig. 6, products **3**–**7**). For the general applicability of any new catalyst, its chemoselectivity is an important aspect. Thus, from a synthetic point of view, it is important to note that this iron-based catalyst system is highly selective for the hydrogenation of the nitrile group in functionalized and multisubstituted substrates. As an example, amino-substituted and halogenated benzylic amines were prepared, which are versatile intermediates in organic synthesis as well as for pharmaceuticals and agrochemicals. Such products, including the more sensitive 4-iodobenzylamine, were easily produced from the corresponding

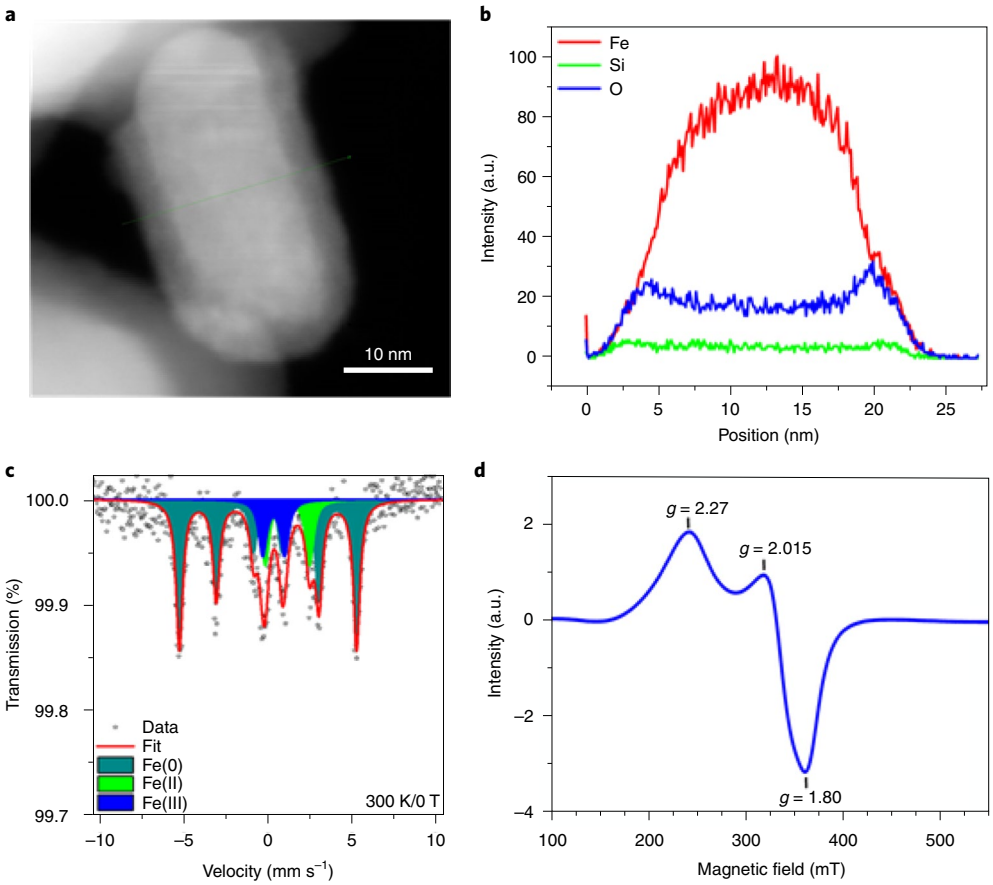

Fig. 5 | Spectral data for Fe/Fe–O@SiO_2. a–d, HAADF-STEM image (**a**), depth profiles showing the intensity distribution of Fe, Si and O (**b**), Mössbauer spectrum recorded at 300 K (**c**) and EPR spectrum (X-band 9.090 GHz) recorded at 77 K (**d**).

benzonitriles in yields of up to 97% (Fig. 6, products **8**–**16**). In addition, trifluoromethyl-substituted benzylamines were obtained in yields of 94 and 95% (Fig. 6, products **17** and **18**, respectively). We were also pleased to find that the nitrile group was also selectively hydrogenated in the presence of the more challenging C≡C, ester, boronic ester, amide, ether, trifluoromethoxy and thioether groups (Fig. 6, products **19**–**30**). Furthermore, when multisubstituted nitriles were subjected to hydrogenation, reduction of the CN group again took place highly selectively towards the corresponding benzylic amines in yields of up to 95% (Fig. 6, products **31**–**46**).

Heterocyclic amines constitute versatile intermediates in the pharmaceutical and agrochemical industries. In this respect, the selective hydrogenation of cyano-substituted heterocycles, for example, quinolines, indoles, pyrroles, benzodioxoles, benzodioxanes, furans, morpholines and phthalanes, is of particular interest. The corresponding heterocyclic amines were obtained (except for 3-cyanofuran) in yields of 85–94% (Fig. 6).

Hydrogenation of aliphatic nitriles. Compared with aromatic nitriles, the hydrogenation of aliphatic nitriles is in general more challenging. Importantly, Fe/Fe–O@SiO_2 exhibited high activity and selectivity for these substrates, including dinitriles, under identical conditions (Fig. 7). Initially, several benzylic cyanides were hydrogenated to the corresponding primary amines in excellent yields (Fig. 7, products **57**–**72**). Interestingly, the 2-arylethylamino motif is a common scaffold in many central nervous system-active compounds. Here, a variety of substituted derivatives were smoothly hydrogenated and furnished the corresponding primary amines in yields of up to 98% (Fig. 7, products **57**–**68**). Phenylpropylamines are another important class of pharmaceutically relevant amines. For example, the parent compound (phenylpropylamine) is used in the synthesis of carboxypeptidase B-type enzyme inhibitors, muscarinic receptor antagonists and potential anticancer agents. Here, it was prepared in 94% yield from the corresponding nitrile (Fig. 7, product **69**).

Although 3-(arylamino)propanenitriles are prepared in a straightforward manner from anilines and acrylonitrile, the hydrogenation of such substrates is difficult because retro-Michael additions can occur. However, this class of compounds was smoothly hydrogenated under our conditions to give the respective primary amines in good yields of up to 85% (Fig. 7, products **70**–**72**). Finally, a selection of aliphatic nitriles was tested. Gratifyingly, Fe/Fe–O@SiO_2 also showed good-to-excellent activity and selectivity for these demanding substrates (Fig. 7, products **73**–**78**). Particularly interesting is the selective reduction of 5-hexenenitrile (Fig. 7, product **78**). Notably, hexamethylenediamine (**79**), the key feedstock for the production of nylon 66, was prepared in 85% yield by direct hydrogenation of adiponitrile. Similarly, other diamines were obtained in 90–95% yield (Fig. 7, products **80** and **81**).

Synthesis of fatty nitriles. With a worldwide production of fatty amines of >800,000 tons yr^{-1}, the hydrogenation of fatty nitriles constitutes an important industrial application[55]. Fatty amines are valuable oleochemicals mainly used to produce fabric softeners, flotation agents, emulsifiers, corrosion inhibitors and lubricating additives[55].

Until today, the industrial hydrogenation of fatty nitriles to amines has relied on well-established Raney Ni or Co catalysts as well as copper chromite[55]. These materials have considerable toxicity issues for biological systems. Hence, alternative Ru-, Pd- and

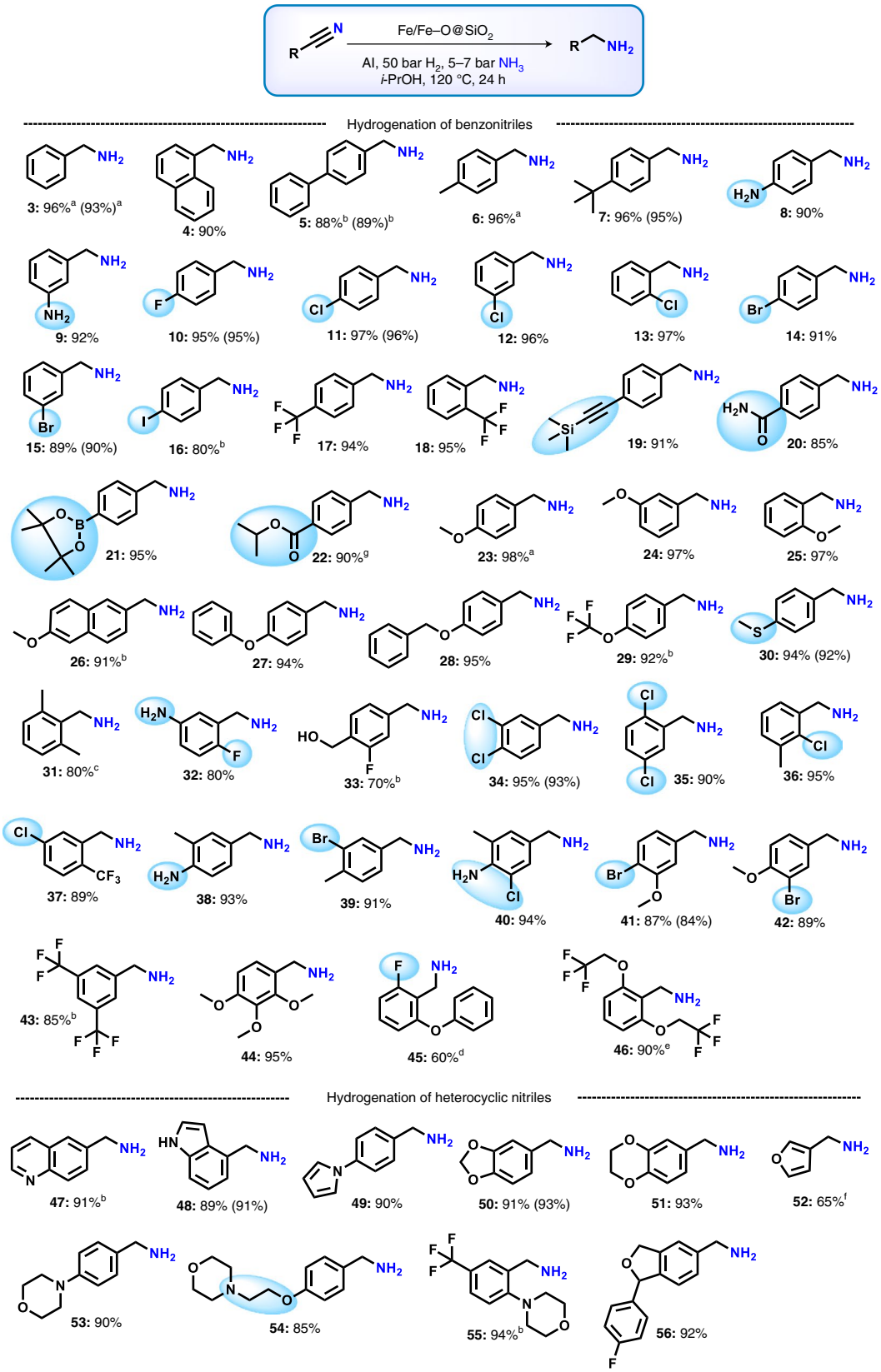

Fig. 6 | Substrate scope. Hydrogenation of (hetero)aromatic nitriles. Reaction conditions: 0.5 mmol nitrile, 40 mg Fe/Fe–O@SiO_2 (8.5 mol% Fe), 3 mg Al foil (20 mol%), 5–7 bar NH_3, 50 bar H_2, 3 ml *i*-PrOH, 120 °C, 24 h. Isolated yields are given. [a]Yields were determined by GC using *n*-hexadecane as standard. [b]With 50 mg Fe/Fe–O@SiO_2. [c]With 50 mg Fe/Fe–O@SiO_2 and 5 mg Al foil. [d]At 135 °C. [e]With 60 mg Fe/Fe–O@SiO_2 and 5 mg Al foil. [f]With 50 mg Fe/Fe–O@SiO_2 at 135 °C. [g]Methyl 4-cyanobenzoate was used as substrate. Transesterification product with *i*-PrOH. Yields in parentheses refer to the reaction performed in the presence of 20 mol% Al(*i*-OPr)$_3$. Products were isolated as free amines and converted to their hydrochloride salts for NMR and high-resolution mass spectrometry (HRMS) analysis.

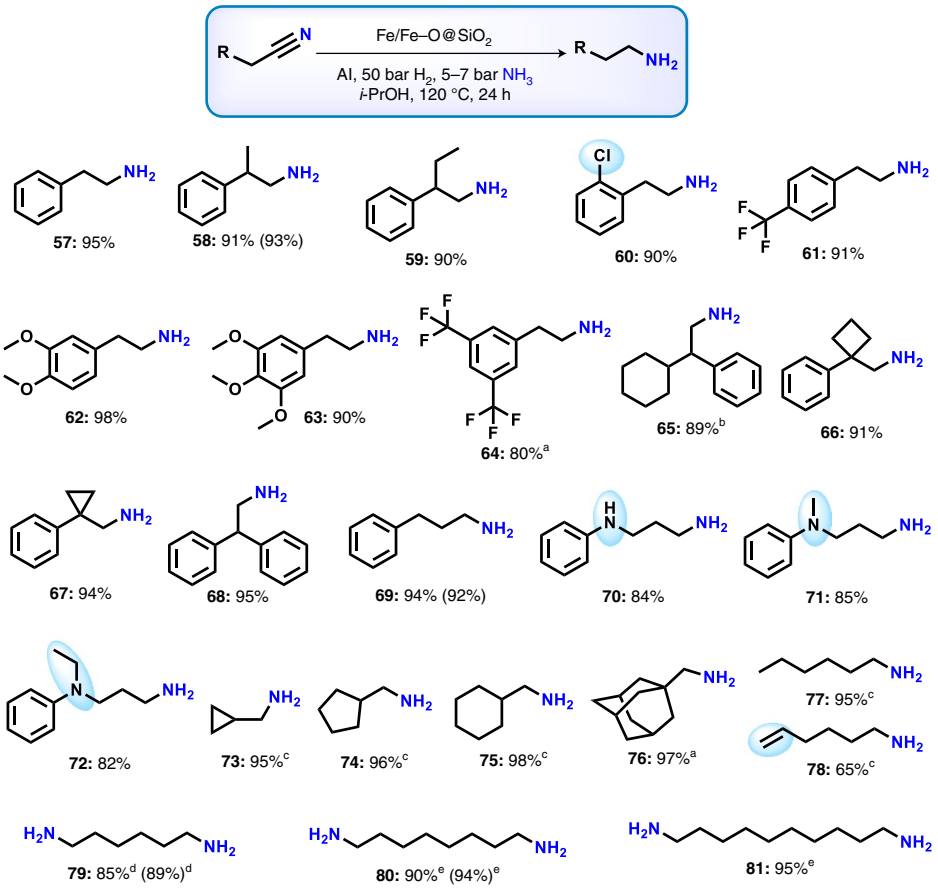

Fig. 7 | Substrate scope. Hydrogenation of aliphatic nitriles. Reaction conditions: 0.5 mmol nitrile, 40 mg Fe/Fe-O@SiO_2 (8.5 mol% Fe), 3 mg Al foil (20 mol%), 5–7 bar NH_3, 50 bar H_2, 3 ml *i*-PrOH, 120 °C, 24 h. Isolated yields are given. [a]With 50 mg Fe/Fe-O@SiO_2. [b]At 135 °C. [c]Yields were determined by GC using *n*-hexadecane as standard. [d]With 80 mg Fe/Fe-O@SiO_2 and 6 mg Al foil at 135 °C. [e]With 80 mg Fe/Fe-O@SiO_2 and 6 mg Al foil at 120 °C. Yields in parentheses refer to the reaction performed in the presence of 20 mol% Al(*i*-OPr)$_3$. Products were isolated as free amines and converted to their hydrochloride salts for NMR and HRMS analysis.

Pt-based catalysts were developed[55]. Unfortunately, none of these systems is commercially viable due to the high price of the precious metals. Gratifyingly, our catalyst is capable of hydrogenating fatty nitriles in a highly selective manner. As a result, seven different fatty amines were prepared in excellent yields of 95–97% (Fig. 8, products **82**–**88**).

To further prove the synthetic utility and practicability of our Fe catalyst, we scaled up both the catalyst preparation (up to 12 g; Supplementary Table 6) and the nitrile hydrogenation protocol (up to 20 g). Regardless of the scale of preparation (1–12 g), all the Fe materials exhibited similar activity and selectivity (Supplementary Table 7). Next, the catalytic hydrogenation reactions of four selected aromatic and aliphatic nitriles were performed using quantities of up to 20 g nitrile. Again, similar conversions and yields were obtained to those achieved with small-scale reactions using up to 100 mg nitrile (Supplementary Fig. 18).

Finally, catalyst recycling was investigated at full and half conversions, which is an important aspect for any heterogeneous catalyst. Indeed, the Fe/Fe–O@SiO_2 catalyst could be reused up to the fourth run. After that, a decrease in the product yield was observed. Recycling tests performed at half conversion for 14 h showed a drop in activity from the third run onward (Supplementary Fig. 19).

Conclusions

We have presented here the development of a heterogeneous iron-based catalyst for the hydrogenation of nitriles. Key to success was the use of silica-supported Fe nanoparticles covered with an ultrathin shell of amorphous iron(III) oxide (Fe/Fe–O@SiO_2). These core–shell nanoparticles were prepared by simple impregnation of iron(II) acetate on commercial silica and subsequent pyrolysis under reductive conditions. The low cost and environmentally friendly character of the catalyst, easy recycling as well as upscaling of the synthetic process represent key advantages and make the material attractive for many applications. Importantly, the developed silica-supported Fe/Fe–O core–shell material exhibited high chemoselectivity for the reduction of functionalized and structurally diverse aromatic, heterocyclic and aliphatic nitriles, including industrially relevant fatty nitriles, to produce the corresponding primary amines in good-to-excellent yields. Aluminium alkoxide species generated in situ from aluminium foil or aluminium triisopropoxide proved to be important for the co-catalytic activation of the nitrile substrate.

Methods

General considerations. All nitriles were obtained commercially from various chemical companies. Before using, the purity of all the nitriles was checked. Iron(II) acetate (99.99%, cat no. 517933-25G) was obtained from Sigma Aldrich. Silica (Aerosil OX-50) was obtained from Evonik. Carbon powder (VULCAN XC72R, with code XVC72R) was obtained from Cabot Corporation. γ-Al_2O_3 and MgO were obtained from Sigma-Aldrich. Al foil was obtained from Sigma-Aldrich (Mini Bin, HS23534A). For comparison purposes, Al foil used for food covering was also purchased from a local store (Kaufland, ALUFOLIE; ICP). The percentage of aluminium in Al-foil was determined by inductively coupled plasma (ICP) and it was found to be 99.97%. DMF was obtained from Acros Chemicals. Pyrolysis experiments were carried out in a Lenton tube furnace.

PXRD patterns were measured at room temperature with an Aeris diffractometer (PANalytical) in Bragg–Brentano geometry equipped with

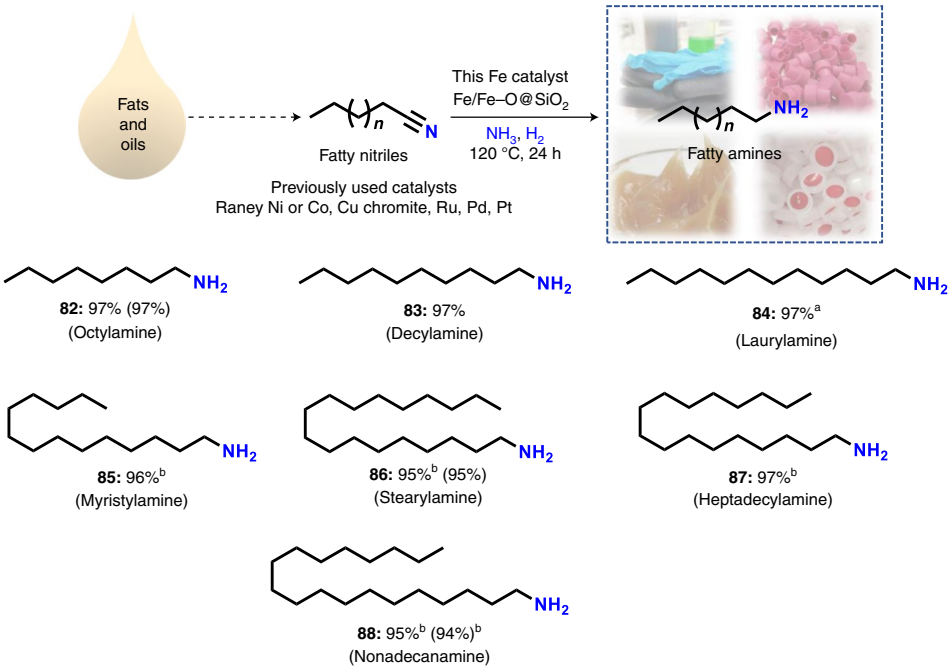

Fig. 8 | Substrate scope. Synthesis of fatty amines. Reaction conditions: 0.5 mmol nitrile, 40 mg Fe/Fe-O@SiO_2 (8.5 mol% Fe), 3 mg Al foil (20 mol%), 5–7 bar NH_3, 50 bar H_2, 3 ml *i*-PrOH, 120 °C, 24 h. Isolated yields are given. [a]At 135 °C. [b]With 50 mg Fe/Fe-O@SiO_2. Yields in parentheses refer to the reaction performed in the presence of 20 mol% Al(*i*-OPr)$_3$. Products were isolated as free amines and converted to their hydrochloride salts for NMR and HRMS analysis.

an iron-filtered Co Kα radiation source (40 kV, 15 mA, $\lambda = 0.1789$ nm) and PIXcell detector. Some samples were measured employing an X'PertPRO MPD diffractometer (PANalytical) in Bragg–Brentano geometry equipped with a Co Kα radiation source (40 kV, 30 mA, $\lambda = 0.1789$ nm), programmable divergence, diffracted beam anti-scatter slits and X'Celerator detector. The angular range of measurement was 5–105° 2θ (Fe/Fe–O@SiO_2 was measured in the range 10–105° 2θ) with a step size of 0.022 and 0.033° for Aeris and X'Pert PRO MPD diffractometers, respectively. The crystalline phases in the experimental PXRD patterns were identified using the X'Pert High Score Plus software[56] in conjunction with the PDF-4+[57] and ICSD[58] databases. The commercially available silicon standard reference material SRM 640 was used to evaluate the line positions.

Low-resolution TEM imaging of the catalyst morphology was carried out with a JEOL microscope equipped with a LaB6 emission gun, operating at 160 kV. HRTEM images were obtained with a TITAN 60-300 HRTEM microscope equipped with an X-FEG-type emission gun, operating at 80 kV. This microscope was equipped with a Cs image corrector and a HAADF-STEM instrument. The point resolution was 0.06 nm in TEM mode. Elemental mapping was performed by STEM-EDS with an acquisition time of 20 min. For the HRTEM analysis, the powder samples were dispersed in ethanol and ultrasonicated for 5 min. One drop of this solution was placed on a copper grid supporting a holey carbon film.

The XPS surface investigation was performed on a PHI 5000 VersaProbe II XPS system (Physical Electronics) with a monochromatic Al Kα source (15 kV, 50 W) and photon energy of 1,486.7 eV. Dual beam charge compensation was used for all measurements. All spectra were recorded in a vacuum of 1.3×10^{-7} Pa at 21 °C. A 200-µm-diameter spot was analysed for each sample. The survey spectra were measured with a pass energy of 187.850 eV and an electronvolt step of 0.8 eV, whereas the high-resolution spectra were recorded with a pass energy of 23.500 eV and an electronvolt step of 0.2 eV. The spectra were evaluated with the MultiPak software (ULVAC-PHI). All binding energies are referenced to the C1*s* carbon peak at 284.80 eV.

The transmission ^{57}Fe Mössbauer spectra were collected employing a Mössbauer MS96 spectrometer operating in constant acceleration mode and equipped with a 40 mCi 57Co(Rh) source. The Mössbauer spectra were fitted with the MossWinn software. The isomer shifts are referenced to α-Fe at room temperature. EPR spectra were recorded on a JEOL JES-X-320 spectrometer, operating at the X-band frequency (~9.14 GHz) at 77 K, and equipped with a JEOL ES 13060DVT5 variable-temperature control apparatus.

All catalytic experiments were carried out in 300 or 100 ml autoclaves (PARR Instrument). To avoid unspecific reactions, all catalytic reactions were carried out either in glass vials, which were placed inside the autoclave, or in autoclaves fitted with a glass/Teflon vessel.

GC and GC-mass spectrometry (GC–MS) were performed on an Agilent Technologies 6890N instrument. GC conversions and yields were determined by GC using flame ionization detection (FID) on an Agilent 6890N chromatograph equipped with Agilent HP-5MS 30m column (250 mm × 0.25 µm). The mass was determined by GC-MS using Agilent 6890N chromatograph equipped with Agilent HP-5MS 30m column (250 mm × 0.25 µm) and Agilent 5973N Mass Selective Detector (MSD).

^{1}H and ^{13}C NMR spectra were recorded on Bruker ARX 300 and ARX 400 spectrometers using [D_6]DMSO and $CDCl_3$ solvents.

Preparation of Fe/Fe–O@SiO_2 on the 1.5 g scale. A magnetic stirring bar and 280.33 mg Fe(OAc)$_2$ were transferred to a 50- ml round-bottomed flask and 30 ml DMF was added. The reaction mixture was stirred at 50 °C to dissolve the iron acetate. To this solution, 1.2 g SiO_2 (Aerosil OX 50) was added, followed by 10 ml DMF. Next, a reflux condenser was fitted to the round-bottomed flask containing the reaction mixture, which was then placed in an aluminium block preheated at 150 °C and stirred for 4 h. Next, the reflux condenser was removed and the round-bottomed flask containing the reaction products was allowed to stand without stirring or closing for 20 h at 150 °C for the slow evaporation of DMF. After evaporation of the solvent and ensuring complete drying, the solid material was cooled to room temperature and ground to a fine powder. This powder was pyrolysed at a defined temperature (400, 600, 800 or 1,000 °C) for 4 h in a tubular furnace under the flow of 20% H_2/N_2 (ramp: 5 °C min^{-1}, total flow: 31 h^{-1}) and then cooled to room temperature.

Elemental analysis of Fe/Fe–O@SiO_2 by ICP and CHN analysis revealed the following (wt%) distribution: Fe = 6.09%; Si = 37.73%; C = 0.11%; H = 0.41%. The Brunauer–Emmett–Teller surface area was measured to be 46.04 m^2 g^{-1}.

The same procedure was employed for the preparation of Fe(OAc)$_2$-C-800, Fe(OAc)$_2$-γ-Al_2O_3-800 and Fe(OAc)$_2$-MgO-800.

Preparation of Fe/Fe–O@SiO_2 on 6 and 12 g batches. The same procedure was used for the preparation of Fe/Fe–O@SiO_2 (Fe(OAc)$_2$-SiO_2-800) on the 6 and 12 g scale with a slight modification of the pyrolysis procedure, as described in Supplementary Table 6.

General procedure for the hydrogenation of nitriles. A magnetic stirring bar and 0.5 mmol of the corresponding nitrile were transferred to a 7-ml glass vial and then 3 ml *i*-PrOH was added. Next, 40 mg Fe/Fe–O@SiO_2 (8.5 mol% Fe) and 3 mg Al foil (the Al foil was cut into small pieces and used in the reactions) or 20.42 mg Al(*i*-OPr)$_3$ (20 mol%) were added and the vial was fitted with a septum, cap and needle. Then, the reaction vials were placed in a 300-ml autoclave (eight vials containing different substrates at a time). The autoclave was closed, flushed twice with 20 bar hydrogen and then pressurized with 5–7 bar ammonia gas and 50 bar hydrogen. The autoclave was placed in an aluminium block preheated at 133 °C and the reactions were allowed to proceed for the required time under stirring.

During the reactions, the inside temperature of the autoclave was measured to be 120 °C, and this temperature was considered to be the reaction temperature. After completion of the hydrogenation reactions, the autoclave was cooled to room temperature. The remaining ammonia and hydrogen were discharged and the vials containing the reaction products were removed from the autoclave. The solid catalyst was filtered and washed thoroughly with ethyl acetate. The reaction products were analysed by GC–MS. The corresponding primary amines were purified by column chromatography (silica, methanol–dichloromethane). The amines were converted to their respective hydrochloride salt and characterized by GC–MS and NMR analysis. To convert the amines to the hydrochloride salts, 1–2 ml methanolic HCl (0.5 M HCl in methanol) was added to the ethyl acetate solution of the respective amine and the mixture stirred at room temperature for 4–5 h. Then, the solvent was removed and the resulting hydrochloride salt was dried under high vacuum. For selected amines, the yields were determined by GC using the following procedure. After completing the reaction, *n*-hexadecane (100 µl) was added as standard to the reaction vials and the reaction products were diluted with ethyl acetate followed by filtration using a plug of silica and then analysed by GC.

Gram-scale reactions. A magnetic stirring bar and the corresponding nitrile were transferred to a glass-fitted 300-ml Parr autoclave and 15–50 ml *i*-PrOH was added. Next, the required amount of catalyst (Fe/Fe–O@SiO_2, 8.5–10 mol%) and Al foil (20 mol%; the Al foil was cut into small pieces and used in the reactions) were added. Then, the autoclave was closed, flushed twice with 20 bar hydrogen and then pressurized with 5–7 bar NH_3 followed by 50 bar hydrogen. The autoclave was placed in an aluminium block preheated at 133–147 °C (placed 30 min before counting the reaction time to achieve the reaction temperature) and the reactions were stirred for 24 h. During the reactions, the inside temperature of the autoclave was measured to be 120–135 °C. After completion of the reactions, the autoclave was cooled to room temperature. The remaining ammonia and hydrogen were discharged, and the reaction products were removed from the autoclave. The solid catalyst was filtered and washed thoroughly with methanol and ethyl acetate. The reaction products were analysed by GC–MS and the corresponding products were purified by column chromatography (silica, dichloromethane–methanol) and characterized by NMR and GC–MS analysis.

Catalyst recycling. A magnetic stirring bar and 10 mmol benzonitrile were transferred to a 100-ml autoclave and then 20 ml *i*-PrOH was added. Next, 900 mg catalyst (Fe/Fe–O@SiO_2) and 408.50 mg Al(i-OPr)$_3$ were added. The autoclave was closed, flushed with 20 bar hydrogen and then pressurized with 5–7 bar NH_3 and 50 bar H_2. The autoclave was placed in a preheated aluminium block at 130 °C and the reactions were stirred for the required time. During the reactions, the inside temperature of the autoclave was measured to be 120 °C. After completion of the reactions, the autoclave was cooled to room temperature. The remaining ammonia and hydrogen were then discharged, and the reaction products were removed from the autoclave. Next, 250 µl *n*-hexadecane was added as standard to the reaction products. The catalyst was separated by filtration and the filtrate containing the reaction products was subjected to GC analysis to determine the yield of benzylamine. The separated catalyst was washed with ethyl acetate, dried under vacuum and used without further purification or reactivation for the next run.

Data availability

All data are available from the authors upon reasonable request.

Received: 31 March 2021; Accepted: 10 November 2021;
Published online: 30 December 2021

References

1. Beller, M. & Bolm, C. *Transition Metals for Organic Synthesis* (Wiley-VCH, 2008).
2. Negishi, E.-I. Magical power of transition metals: past, present, and future (Nobel lecture). *Angew. Chem. Int. Ed.* **50**, 6738–6764 (2011).
3. Hagen, J.*Industrial Catalysis: A Practical Approach* (Wiley-VCH, 2006).
4. Catlow, C. R., Davidson, M., Hardacre, C. & Hutchings, G. J. Catalysis making the world a better place. *Philos. Trans. R. Soc. A* **374**, 20150089 (2016).
5. Busacca, C. A., Fandrick, D. R., Song, J. J. & Senanayake, C. H. The growing impact of catalysis in the pharmaceutical industry. *Adv. Synth. Catal.* **353**, 1825–1864 (2011).
6. Rylander, P. N.*Catalytic Hydrogenation in Organic Syntheses* (Academic Press, 1979).
7. Alonso, D. A. et al. in *Science of Synthesis: Water in Organic Synthesis* (ed. Kobayashi, S.) 95–119 (Thieme, 2012); https://doi.org/10.1055/sos-SD-206-00075
8. Oger, C., Balas, L., Durand, T. & Galano, J.-M. Are alkyne reductions chemo-, regio-, and stereoselective enough to provide pure (*Z*)-olefins in polyfunctionalized bioactive molecules? *Chem. Rev.* **113**, 1313–1350 (2013).
9. Massaro, L., Zheng, J., Margarita, C. & Andersson, P. G. Enantioconvergent and enantiodivergent catalytic hydrogenation of isomeric olefins. *Chem. Soc. Rev.* **49**, 2504–2522 (2020).
10. Chirik, P. J. Iron- and cobalt-catalyzed alkene hydrogenation: catalysis with both redox-active and strong field ligands. *Acc. Chem. Res.* **48**, 1687–1695 (2015).
11. Magano, J. & Dunetz, J. R. Large-scale carbonyl reductions in the pharmaceutical industry. *Org. Process Res. Dev.* **16**, 1156–1184 (2012).
12. Zhong, R., Wie, Z., Zhang, W., Liu, S. & Liu, Q. A practical and stereoselective *in situ* NHC-cobalt catalytic system for hydrogenation of ketones and aldehydes. *Chem* **5**, 1552–1566 (2019).
13. Formenti, D., Ferretti, F., Scharnagl, F. K. & Beller, M. Reduction of nitro compounds using 3d-non-noble metal catalysts. *Chem. Rev.* **119**, 2611–2680 (2019).
14. Jagadeesh, R. V. et al. Nanoscale Fe_2O_3-based catalysts for selective hydrogenation of nitroarenes to anilines. *Science* **342**, 1073–1076 (2013).
15. Wiesenfeldt, M. P., Nairoukh, Z., Dalton, T. & Glorius, F. Selective arene hydrogenation for direct access to saturated carbo- and heterocycles. *Angew. Chem. Int. Ed.* **58**, 10460–10476 (2019).
16. Murugesan, K. et al. Cobalt-nanoparticles catalyzed efficient and selective hydrogenation of aromatic hydrocarbons. *ACS Catal.* **9**, 8581–8591 (2019).
17. Sahoo, B. et al. A robust iron catalyst for the selective hydrogenation of substituted (iso)quinolones. *Chem. Sci.* **9**, 8134–8141 (2018).
18. Lawrence, S. A. *Amines: Synthesis, Properties and Applications* (Cambridge Univ. Press, 2004).
19. Ricci, A. *Amino Group Chemistry: From Synthesis to the Life Sciences* (Wiley-VCH, 2008).
20. Qureshi, M. H. *Top 200 Pharmaceuticals by Retails Sales in 2020* (University of Arizona, 2020); https://njardarson.lab.arizona.edu/sites/njardarson.lab.arizona.edu/files/Top%20200%20Pharmaceuticals%20By%20Retail%20Sales%202020V3.pdf
21. Murugesan, K. et al. Catalytic reductive aminations using molecular hydrogen for synthesis of different kinds of amines. *Chem. Soc. Rev.* **49**, 6273–6328 (2020).
22. Hahn, G., Kunnas, P., de Jonge, N. & Kempe, R. General synthesis of primary amines via reductive amination employing a reusable nickel catalyst. *Nat. Catal.* **2**, 71–77 (2019).
23. Sabatier, P. & Senderens, J. B. Application aux nitriles de la methode d'hydrogenation directe par catalyse: synthese d'amines primaires, secondaires et tertiaires. *C. R. Hebd. Séances Acad. Sci.* **140**, 482–484 (1905).
24. Paal, C. & Gerum, J. Über katalytische Wirkungen kolloidaler Metalle der Platingruppe. VI. Reduktionskatalysen mit kolloidalem Palladium. *Ber. Dtsch. Chem. Ges.* **42**, 1553–1560 (1909).
25. Braun, V. J., Blessing, G. & Zobel, F. Katalytische hydrierungen unter Druck bei Gegenwart von nickelsalzen. VI.: nitrile. *Ber. Dtsch. Chem. Ges. A* **56**, 1988–2001 (1923).
26. Raney, M. Method of preparing catalytic material. US patent 1563587A (1925).
27. Carothers, W. H. & Jones, G. A. The preparation of some primary amines by the catalytic reduction of nitriles. *J. Am. Chem. Soc.* **47**, 3051–3057 (1925).
28. Aller, B. V. Raney cobalt hydrogenation catalysts. I. The preparation of the catalyst. *J. Appl. Chem.* **7**, 130–134 (2007).
29. Adkins, H. *Reactions of Hydrogen with Organic Compounds Over Copper-Chromium Oxide and Nickel Catalysts* 53 (Univ. Wisconsin Press, 1937).
30. Freifelder, M. A low pressure process for the reduction of nitriles. Use of rhodium catalyst. *J. Am. Chem. Soc.* **82**, 2386–2389 (1960).
31. Freidlin, L. K. & Sladkova, T. A. Catalytic reduction of dinitriles. *Russ. Chem. Rev.* **33**, 319–330 (1964).
32. Barnett, C. Hydrogenation of aliphatic nitriles over transition metal borides. *Ind. Eng. Chem. Prod. Res. Dev.* **8**, 145–149 (1969).
33. de Bellefon, C. & Fouilloux, P. Homogeneous and heterogeneous hydrogenation of nitriles in a liquid phase: chemical, mechanistic, and catalytic aspects. *Catal. Rev.* **36**, 459–506 (1994).
34. López-De Jesús, Y. M., Johnson, C. E., Monnier, J. R. & Williams, C. T. Selective hydrogenation of benzonitrile by alumina-supported Ir–Pd catalysts. *Top. Catal.* **53**, 1132–1137 (2010).
35. Lévay, K. & Hegedűs, L. Recent achievements in the hydrogenation of nitriles catalyzed by transitional metals. *Curr. Org. Chem.* **23**, 1881–1900 (2019).
36. Yoshimura, M. et al. Selective synthesis of primary amines from nitriles under hydrogenation conditions. *Adv. Synth. Catal.* **360**, 1726–1732 (2018).
37. Liu, Y. et al. Mild palladium-catalysed highly efficient hydrogenation of C≡N, C–NO_2, and C=O bonds using H_2 of 1 atm in H_2O. *Green Chem.* **21**, 830–838 (2019).
38. Wang, H. et al. Quasi Pd_1Ni single-atom surface alloy catalyst enables hydrogenation of nitriles to secondary amines. *Nat. Commun.* **10**, 4998 (2019).
39. Ryabchuk, P. et al. Intermetallic nickel silicide nanocatalyst—a non-noble metal–based general hydrogenation catalyst. *Sci. Adv.* **4**, eaat0761 (2018).

40. Murugesan, K. et al. Cobalt-based nanoparticles prepared from MOF–carbon templates as efficient hydrogenation catalysts. *Chem. Sci.* **9**, 8553–8560 (2018).
41. Mitsudome, T., Sheng, M., Nakata, A., Mizugaki, T. & Jitsukawa, K. A cobalt phosphide catalyst for the hydrogenation of nitriles. *Chem. Sci.* **11**, 6682–6689 (2020).
42. Enthaler, S., Junge, K. & Beller, M. Sustainable metal catalysis with iron: from rust to a rising star. *Angew. Chem. Int. Ed.* **47**, 3317–3321 (2008).
43. Plietker, B. *Catalysis in Organic Chemistry: Reactions and Applications* (Wiley-VCH, 2008).
44. Bornschein, C. et al. Mild and selective hydrogenation of aromatic and aliphatic (di)nitriles with a well-defined iron pincer complex. *Nat. Commun.* **5**, 4111 (2014).
45. Liu, L. & Corma, A. Metal catalysts for heterogeneous catalysis: from single atoms to nanoclusters and nanoparticles. *Chem. Rev.* **118**, 4981–5079 (2018).
46. Jagadeesh, R. V. et al. MOF-derived cobalt nanoparticles catalyze a general synthesis of amines. *Science* **358**, 326–332 (2017).
47. Yang, X.-F. et al. Single-atom catalysts: a new frontier in heterogeneous catalysis. *Acc. Chem. Res.* **46**, 1740–1748 (2013).
48. Zhang, J. et al. Tuning polarity of Cu-O bond in heterogeneous Cu catalyst to promote additive-free hydroboration of alkynes. *Chem* **6**, 725–737 (2020).
49. Bukur, D. B. et al. Binder/support effects on the activity and selectivity of iron catalysts in the Fischer-Tropsch synthesis. *Ind. Eng. Chem. Res.* **29**, 1588–1599 (1990).
50. Suo, H. et al. Chemical and structural effects of silica in iron-based Fischer–Tropsch synthesis catalysts. *J. Catal.* **286**, 111–123 (2012).
51. Xu, C. et al. Interfacing with silica boosts the catalysis of copper. *Nat. Commun.* **9**, 3367 (2018).
52. Dhavale, V. M., Singh, S. K., Nadeema, A., Gaikwad, S. S. & Kurungot, S. Nanocrystalline Fe–Fe_2O_3 particle-deposited N-doped graphene as an activity-modulated Pt-free electrocatalyst for oxygen reduction reaction. *Nanoscale* **7**, 20117–20125 (2015).
53. Qafoku, O. et al. Fayalite dissolution and siderite formation in water-saturated supercritical CO_2. *Chem. Geol.* **332–333**, 124–135 (2012).
54. Machala, L., Zboril, R. & Gedanken, A. Amorphous iron(III) oxide—a review. *J. Phys. Chem. B* **111**, 4003–4018 (2007).
55. Hinzmann, A. & Gröger, H. Selective hydrogenation of fatty nitriles to primary fatty amines: catalyst evaluation and optimization starting from octanenitrile. *Eur. J. Lipid Sci. Technol.* **122**, 1900163 (2020).
56. X'Pert High Score Plus version 4.8 (4.8.0.25518) (Malvern Panalytical B.V., 2018).
57. PDF-4+ database (ICDD, 2021).
58. ICSD database version 4.5.0 (build 20200929-1047) (FIZ Karlsruhe GmbH, 2021).

Acknowledgements

We acknowledge the European Research Council (EU project 670986-NoNaCat) and the State of Mecklenburg-Vorpommern for financial and general support. We thank the analytical team of the Leibniz-Institut für Katalyse for their excellent service. We thank O. Tomanec, M. Petr, I. Medřík and G. Zoppellaro (all from Palacky University Olomouc) for TEM, XPS and EPR measurements and control sample synthesis. The authors from Palacky University acknowledge the support of the Operational Program Research, Development and Education - European Regional Development Fund (project no. CZ.02.1.01/0.0/0.0/16_019/0000754) and the ERDF project 'Development of pre-applied research in nanotechnology and biotechnology' (project no. CZ.02.1.01/0.0/0.0/17_048/0007323) of the Ministry of Education, Youth and Sports of the Czech Republic. R.Z. acknowledges support from the Czech Science Foundation (project no. 19-27454X).

Author contributions

R.V.J. and M.B. supervised the project. V.G.C., R.V.J. and M.B. planned and developed the project. V.G.C. developed and prepared the catalytic materials and performed the catalytic experiments. T.S. assisted in the catalyst preparation and catalytic experiments and also reproduced the results. R.G.K., J.K., O.M., M.B.G. and R.Z. characterized the catalysts. R.V.J., V.G.C. and M.B. wrote the paper with contributions from M.B.G., R.G.K. and R.Z.

Competing interests

The authors declare no competing interests.

Additional information

Supplementary information The online version contains supplementary material available at https://doi.org/10.1038/s41929-021-00722-x.

Correspondence and requests for materials should be addressed to Radek Zbořil, Manoj B. Gawande, Rajenahally V. Jagadeesh or Matthias Beller.

Peer review information *Nature Catalysis* thanks Bhalchandra Bhanage, Hironao Sajiki and Dingsheng Wang for their contribution to the peer review of this work.

nature COMMUNICATIONS

ARTICLE

https://doi.org/10.1038/s41467-019-13351-7 OPEN

Homogeneous cobalt-catalyzed reductive amination for synthesis of functionalized primary amines

Kathiravan Murugesan[1], Zhihong Wei[1], Vishwas G. Chandrashekhar[1], Helfried Neumann[1], Anke Spannenberg[1], Haijun Jiao[1], Matthias Beller[1*] & Rajenahally V. Jagadeesh[1*]

The development of earth abundant 3d metal-based catalysts continues to be an important goal of chemical research. In particular, the design of base metal complexes for reductive amination to produce primary amines remains as challenging. Here, we report the combination of cobalt and linear-triphos (bis(2-diphenylphosphinoethyl)phenylphosphine) as the molecularly-defined non-noble metal catalyst for the synthesis of linear and branched benzylic, heterocyclic and aliphatic primary amines from carbonyl compounds, gaseous ammonia and hydrogen in good to excellent yields. Noteworthy, this cobalt catalyst exhibits high selectivity and as a result the -NH_2 moiety is introduced in functionalized and structurally diverse molecules. An inner-sphere mechanism on the basis of the mono-cationic $[triphos\text{-}CoH]^+$ complex as active catalyst is proposed and supported with density functional theory computation on the doublet state potential free energy surface and H_2 metathesis is found as the rate-determining step.

[1] Leibniz-Institut für Katalyse e.V. an der Universität Rostock, Albert-Einstein Str. 29a, Rostock D-18059, Germany. *email: matthias.beller@catalysis.de; jagadeesh.rajenahally@catalysis.de

Catalysis constitutes an indispensable tool for controlling all kinds of chemical transformations[1–11]. Although catalysts are routinely employed in industrial production of fine and bulk chemicals as well as for exhaust gas decomposition in environmental technologies and enzymatic processes, there is a constant need for better and improved catalytic systems[1–11]. With respect to organometallic catalysts, their activity and selectivity are controlled to a large extent by the nature of the metal and the adjacent ligands[1,2,8–11]. In this regard, precious metals were generally believed to be crucial components[12–23]. Indeed, organometallic complexes based on palladium (coupling reactions)[12–14], ruthenium (metathesis)[15,16], rhodium (hydrogenations and hydroformylations)[17–19], platinum (hydrosilylations)[20,21], and iridium (hydrogenations)[22,23] have revolutionized organic synthesis. Key for their success is the use of a broad variety of complexes based on certain privileged ligands[24,25]. However, the limited availability (10^{-7}–10^{-6}% proportion of weight in the Earth's crust) and consequently the higher price as well as the toxicity of some derivatives of these metals[26,27] have spurred interest towards the development of alternative earth abundant metal catalysts. Hence in recent years, 3d-metal complexes have been successfully developed for a variety of reactions including hydrogenation of carboxylic acids, esters, ketones, nitriles and olefins[28–37]. Nevertheless, more challenging reactions such as reductive amination with ammonia and hydrogen to access primary amines were scarcely explored[38–44]. In general, applying molecularly defined catalysts this transformation suffers from low selectivity to the desired product due to side reactions such as over-alkylation or reduction to the corresponding alcohols[38–44]. In addition, catalyst deactivation by ammonia constitutes another problem[45]. Thus, to the best of our knowledge no defined homogeneous catalysts based on available 3d-metals are known for this transformation and only a few Rh-, Ir-, and Ru-complexes have been reported to catalyze amination of carbonyl compounds with ammonia and molecular hydrogen[38–44]. Thus, in the past reductive aminations are mainly relied on heterogeneous catalysts of precious metals[38,39,46–50] or Raney nickel[38,39,50,51]. However, the latter material is limited in its application due to selectivity, stability and handling problems. Notably in 2017, we reported specific supported cobalt nanoparticles derived from metal organic frameworks, which proved to be general reductive amination catalysts[52]. In addition, very recently, Kempe[53] and our group[54] disclosed nickel materials. Despite these notable advancements, the development of related homogeneous non-noble metal catalysts remains interesting because of the inherent advantage regarding activity—in principle, all the individual metal centers can be active here. Furthermore, compared to homogeneous catalysts the upscaling of advanced heterogeneous materials possesses additional challenges.

Here, we report that the specific combination of cobalt and bis (diphenylphosphinoethyl)phenylphosphine (so-called linear triphos) allows the reductive amination of broad variety of aldehydes and ketones with ammonia in presence of molecular hydrogen, and this enables the synthesis of a series of functionalized and structurally diverse linear and branched benzylic, heterocyclic and aliphatic amines. The resulting primary amines serve as key precursors and central intermediates for the production of advanced chemicals, pharmaceuticals, agrochemicals, biomolecules, and materials[55–57]. Our present work is complementary to the known syntheses of primary benzylic and aliphatic amines by direct catalytic amination of alcohols[58–61] and hydroamination using ammonia[45,62–64].

Results

Catalyst and reaction design. We started our investigations to identify potentially active non-noble metal complexes based on iron, manganese and cobalt for the reaction of 4-methylbenzaldehyde with ammonia and molecular hydrogen. In general, the presence of strongly coordinating anions (e.g., halides) is inferior for hydrogen catalysis. Hence, Fe $(BF_4)_2$•$6H_2O$ and $Co(BF_4)_2$•$6H_2O$ were employed as metal salts. In case of manganese, the corresponding tetrafluoroborate salt is not commercially available, therefore the inexpensive manganese(II) acetate was used. To avoid the formation of well-known Werner-type ammonia complexes, selected privileged phosphine ligands (**L1**-**L8**) with strong coordination to the metal center were chosen (Table 1). Testing the in situ generated respective Fe-phosphorus complexes, all ligands produced inactive catalysts except for **L7**. This Fe-**L7** system showed some activity and gave the secondary imine as the main product. However, no 4-methylbenzylamine was observed. In case of manganese, none of the ligands led to an active catalyst. Conversely, Co-complexes based on linear- and tripodal-triphos ligands (Co-**L7** and Co-**L8**) produced the desired primary amine in 96 and 93% yield, respectively. Next applying Co-**L7**, important reaction parameters such as catalyst concentration, temperature and pressure of hydrogen were tested (Supplementary Table 1, entries 2–5). Optimal results for the synthesis of 4-methylbenzylamine were achieved with a combination of 3 mol% of $Co(BF_4)_2$•$6H_2O$ and 4 mol% of **L7** at 40 bar of hydrogen, 5 bar of ammonia and 100 °C. Variation of different solvents revealed the importance of alcohols, with 2,2,2-trifluoroethanol (TFE) as the best one (Supplementary Table 2). Notably, this 3d-metal catalyst system allows performing reductive aminations with ammonia under milder reaction conditions compared to all previously reported precious metal complexes[40–44].

To know the structure of the in situ-formed cobalt-triphos complex (C-**L7**) and to understand its mode of reactivity, the molecularly defined Co-**L7** complex **A** was prepared (Methods). Surprisingly, the single crystal analysis of complex **A** revealed the coordination of two phosphine ligands (1:2 ratio of Co:**L7**) to the Co center, in which one ligand coordinates via three phosphorus atoms and the second ligand via two phosphorus atoms (Supplementary methods, complex **A**). Performing the crystallization attempts without vigorous exclusion of air gave the partially oxidized phosphine ligand, which forms cobalt complex **B**. Both complexes **A** and **B** were observed as cobalt (II) species consisting of a complex dication and two tetrafluoroborates. Comparing these two defined complexes in the benchmark reaction, complex **A** exhibited similar activity and selectivity to that of the in situ generated Co-triphos system, while **B** is much less active and produced only 70% of the corresponding secondary imine **4** as the sole product (Supplementary Table 1, entries 8–9). This indicates a major deactivation of the catalyst by oxidation of phosphine to phosphine oxide. poisoning experiments were performed. As expected, adding Hg or 50 mol%PPh_3 to the reaction under standard conditions did not affect the activity or selectivity of complex **A** (Supplementary Table 4).

Synthesis of linear primary amines from aldehydes. After having identified the active homogeneous cobalt catalyst system $[L7CoH]^+$, we explored its general applicability for the preparation of primary amines.

As shown in Fig. 1, substituted, functionalized and structurally diverse aldehydes underwent amination to produce linear primary amines in good to excellent yields at 100–120 °C. Substrates containing either electron-donating or electron-withdrawing groups were successfully reacted and gave the desired products. The tested halogenated aldehydes were well tolerated and produced corresponding amines without significant dehalogenations (<5%) (Fig. 1, products **12**–**15** and

Table 1 Reductive amination of 4-methylbenzaldehyde with in situ generated complexes.

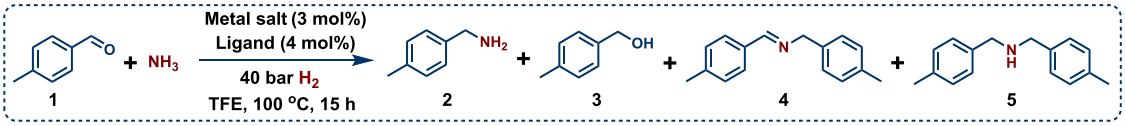

Tested privileged ligands

Metal precursor	PPh_3 (L1)	Xantphos (L2)	dppf (L3)	dppe (L4)	BINAP (L5)	MACHO (L6)	Linear Triphos (L7)	Tripodal Triphos (L8)
$Fe(BF_4)_2{\cdot}6H_2O$	X / X	X / X	X / X	X / X	X / X	X / X	X / —	X / X
$Mn(OAc)_2{\cdot}4H_2O$	X / X	X / X	X / X	X / X	X / X	X / X	X / X	X / X
$Co(BF_4)_2{\cdot}6H_2O$	X / X	X / X	X / —	X / #	X / X	# / X	+ / X	— / X

Yield of Product 2: X <1% # 1-5% — 90-95% + 95-98%

Yield of Product 4: X 1-5% # 5-10% — 60-80% + >90%

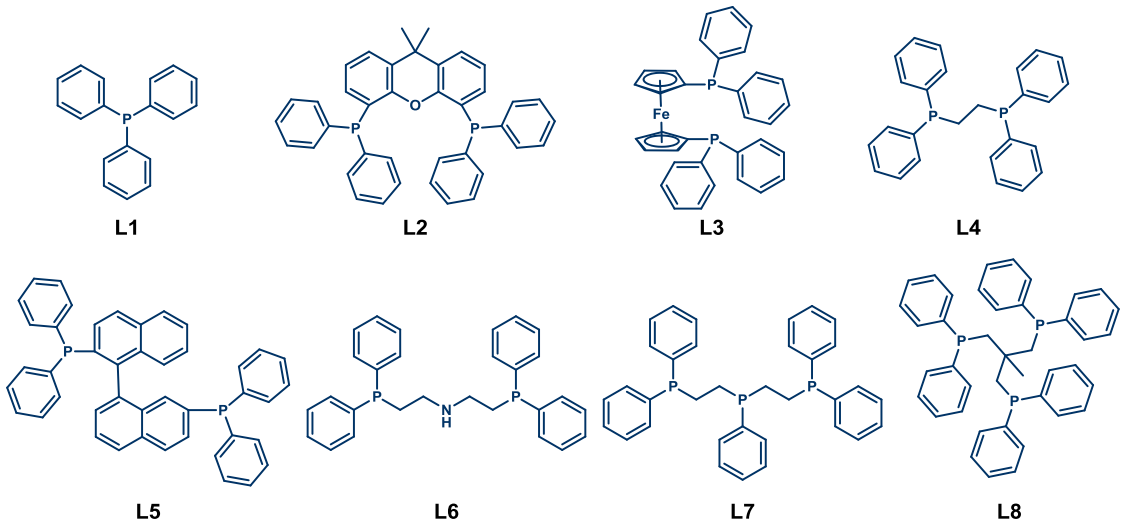

Reaction conditions: [a]0.5 mmol 4-methylbenzaldehyde, 3 mol% metal salt, 4 mol% ligand, 5 bar NH_3, 40 bar H_2, 2 mL TFE, 100 °C, 15 h, GC yields using n-hexadecane as standard.

21). For any catalyst applicable in organic synthesis as well as drug discovery, achieving a high degree of chemoselectivity is important, yet challenging. To showcase this aspect, reductive aminations of various functionalized aldehyde were performed. Reducible groups such as C–C double bonds and esters remained untouched. In addition, thioethers and boronic ester groups are well tolerated (Fig. 1; products **22**–**25**). Primary amines of 3,4-methylenedioxy and benzo-1,4-dioxane, which represent versatile motifs in many drugs and natural products, were prepared in up to 96 % yield (products **26**–**28**). Finally, also aliphatic aldehydes produced the corresponding amines (Fig. 1, products **28**–**30**).

Synthesis of branched primary amines from ketones. Compared to aldehydes, amination of ketones is more challenging, because the hydrogenation of the sterically hindered imine is more difficult. Nevertheless, this Co-triphos catalyst system is active and selective for the reductive amination of ketones, too (Figs. 2, 3). As a result, 30 ketones were efficiently aminated to produce branched primary amines in high yields. Substrates bearing easily coordinating groups to the metal such as $–NH_2$, –OH and phenolic groups as well as pyridines gave 90–95% yield of corresponding amines (Fig. 2; products **35**–**36** and **40**–**43**). Further aliphatic ketones smoothly gave the branched amines in up to 93% yield (Fig. 2; products **48**–**52**).

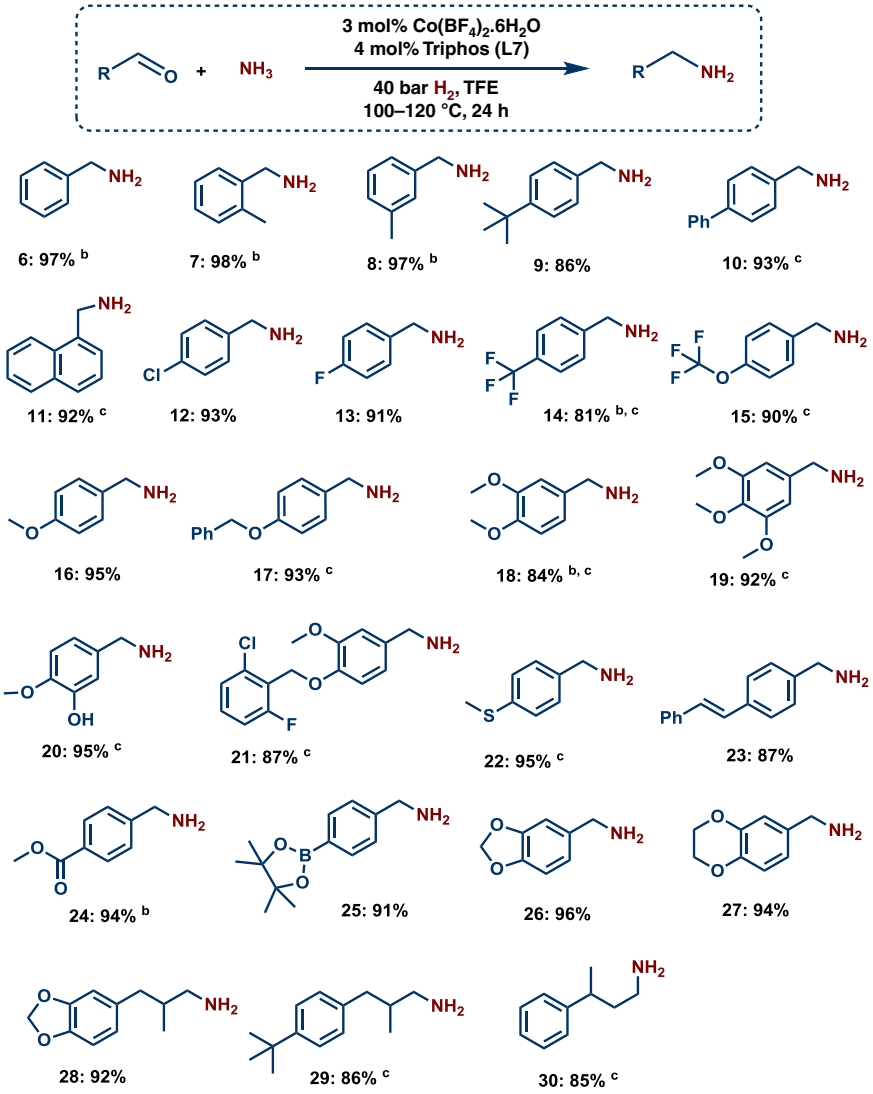

Fig. 1 Cobalt-triphos catalyzed synthesis of primary amines from aldehydes. Reaction conditions: [a]0.5 mmol aldehyde, 3 mol% $Co(BF_4)_2.6H_2O$, 4 mol% triphos (**L7**), 5–7 bar NH_3, 40 bar H_2, 2 mL degassed TFE, 100 °C, 24 h. [b]GC yields using n-hexadecane as standard. [c]Same as 'a' at 120 °C. Isolated as free amines and converted to hydrochloride salts. Corresponding hydrochloride salts were subjected to NMR analysis.

Amination of life science molecules and steroid-derivatives. For any potential catalyst, its utility for the refinement of complex molecules is of central importance. In order to prove the general applicability of our catalytic system, we performed the amination of structurally complex ketones, including existing drug and steroid-based molecules (Fig. 3). Gratifyingly, cobalt-triphos is highly efficient and selective for the amination of drugs such as Nabumetone, Pentoxifylline, and Azaperone as well as Estrone and Stanolone-based steroid derivatives (Fig. 3). This methodology offers many opportunities for late stage functionalization of life science and bioactive molecules.

Discussion

Since $Co^{II}(BF_4)_2$•$6H_2O$ is the most active cobalt salt for the reductive amination of 4-methylbenzaldehyde (Supplementary Table 3), the mono-cationic hydride $[L7CoH]^+$ (**I**) complex is proposed as the active catalyst along the catalytic cycle (Fig. 4) on the basis of our results as well as those of the previously reported cobalt/phosphine-catalyzed hydrogenation reactions[31,65–68], Starting from the cationic complex **A** $[(L7)_2Co^{II}]^{2+}$, the first step is the dissociation of one L7 ligand and the formation of the active cobalt hydride catalyst $[L7CoH]^+$ (**I**) in the presence of ammonia and H_2. Without ammonia present, no hydrogenation of 4-methylbenzaldehyde to the corresponding alcohol occurred (Supplementary Table 1, entries 6–7).Next, the primary imine formed from **1** and ammonia generates complex **II**. In agreement with previous work using ruthenium complexes and based on our DFT calculations, we propose first substrate coordination and then beta hydride addition. Finally, coordination of H_2 followed by hydrogenolysis releases the primary amine and regenerates catalytically active species **I**.

To understand the detailed mechanism, we carried out B3PW91 density functional theory computations for the hydrogenation of phenylmethanimine (Ph-CH = NH) generated from benzaldehyde and NH_3. In our calculations we used the real-size complexes and substrate and calculated the catalytic cycle in the gas phase as well as in a solution of 2,2,2-trifluoroethanol (dielectric constant = 26.69) without and with van de Waals dispersion correction. All these data are listed in Supplementary Information. The potential energy surfaces show the same trend and shape but differ quantitatively. In the gas phase and in a solution, the apparent barriers are close (96 vs. 108 kJ/mol), while that in a solution with dispersion correction is highly

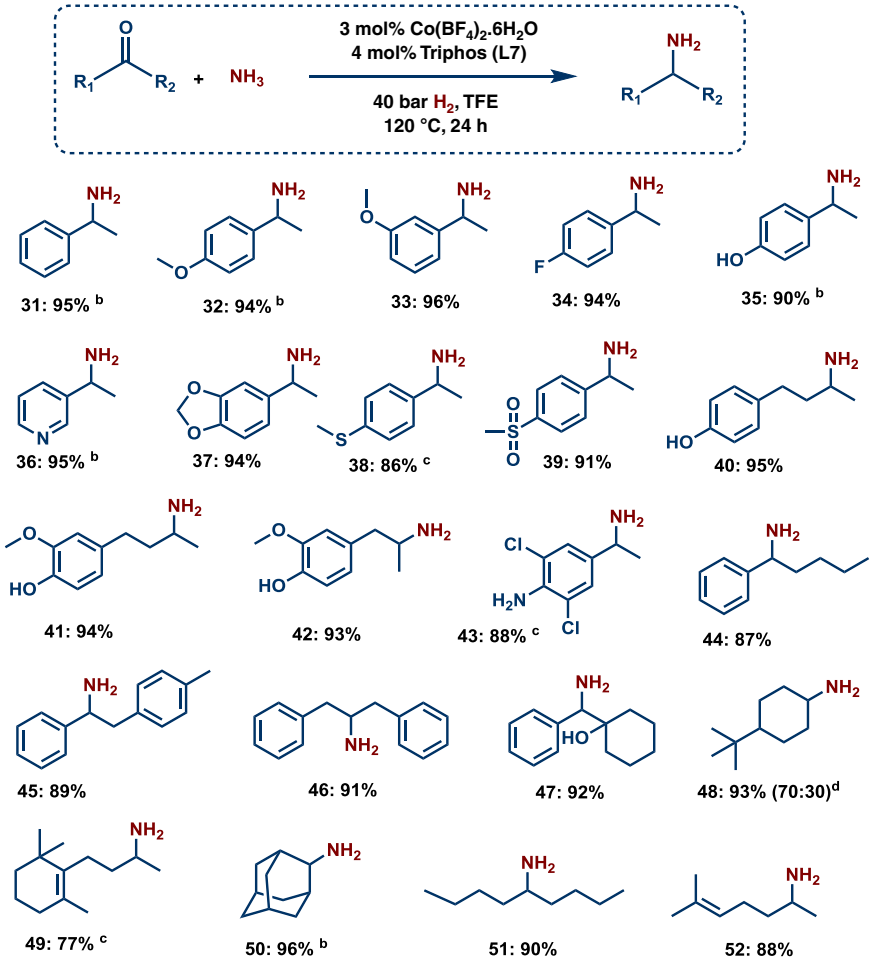

Fig. 2 Synthesis of primary amines from ketones using cobalt-triphos catalyst. Reaction conditions: [a]0.5 mmol ketone, 3 mol% $Co(BF_4)_2{\cdot}6H_2O$, 4 mol% triphos (**L7**), 5–7 bar NH_3, 40 bar H_2, 2 mL degassed TFE, 120 °C, 24 h. [b]GC yields using n-hexadecane as standard. [c]Same as '**a**' with 50 bar H_2. [d]Diastereomeric ratio. Isolated as free amines and converted to hydrochloride salts. Corresponding hydrochloride salts were subjected to NMR analysis.

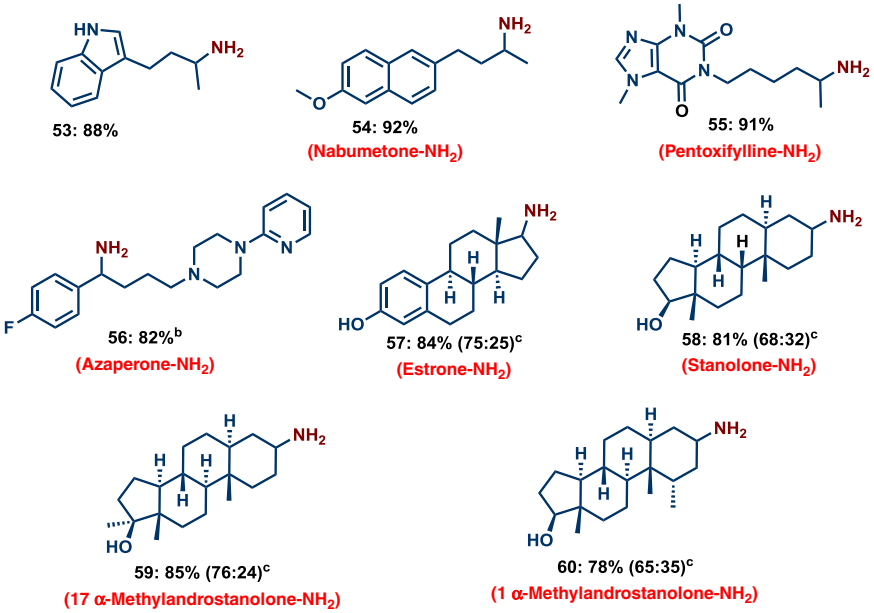

Fig. 3 Co-catalyzed amination of bioactive compounds. Reaction conditions: [a]0.5 mmol substrate, 3 mol% $Co(BF_4)_2{\cdot}6H_2O$, 4 mol% triphos (**L7**), 5–7 bar NH_3, 40 bar H_2, 2 mL degassed TFE, 120 °C, 24 h. [b]Same as 'a' with 50 bar H_2. [c]Diastereomeric ratio. Isolated as free amines and converted to hydrochloride salts. Corresponding hydrochloride salts were subjected to NMR analysis.

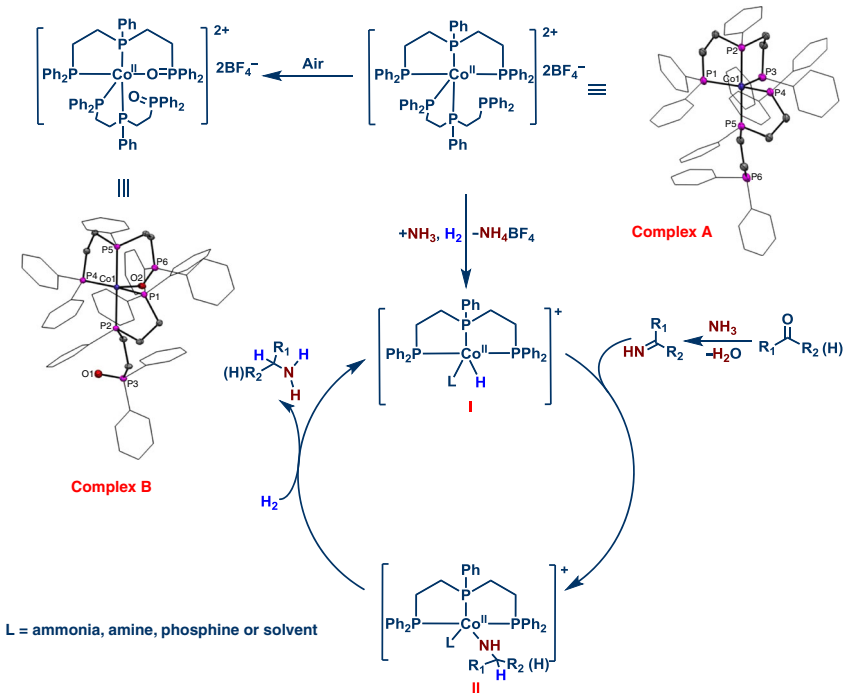

Fig. 4 Proposed reaction mechanism for the Co-triphos catalysed reductive amination. Molecular structure of the cation of complexes A and B. Displacement ellipsoids are drawn at the 30% probability level; phenyl rings are shown as wireframe; hydrogen atoms are omitted for clarity.

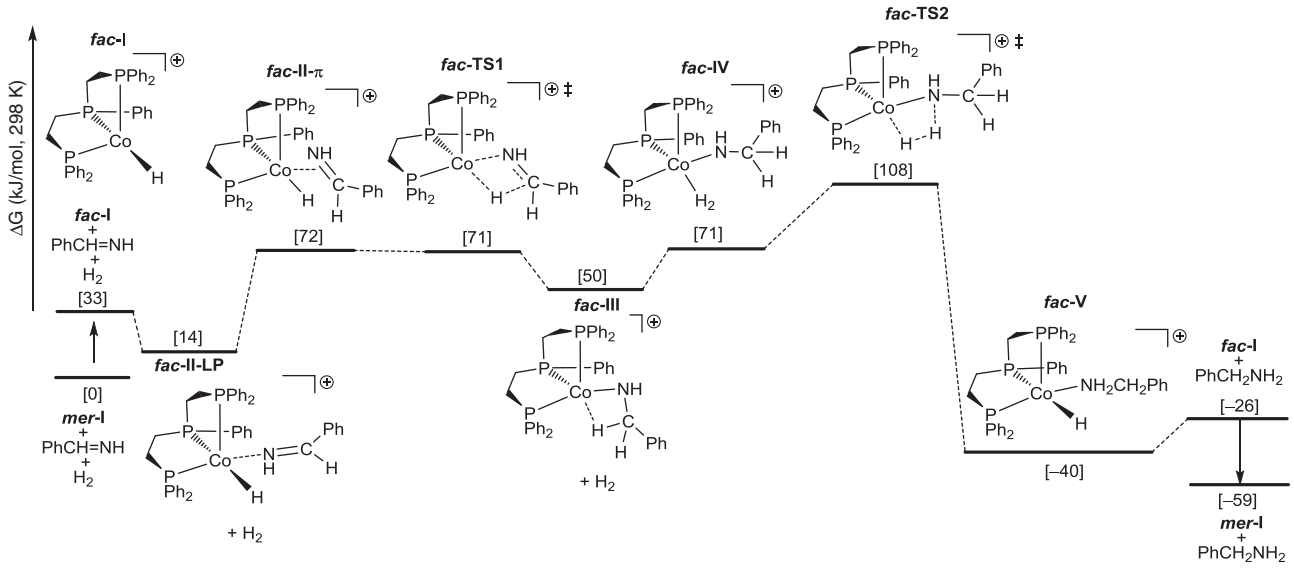

Fig. 5 Gibbs free energy surface for Ph−CH=NH hydrogenation in TFE solvation. Ph−CH=NH hydrogenation by using mono-cationic $[triphos\text{-}CoH]^+$ as active catalyst.

underestimated (29 kJ/mol). In addition to the mono-cationic catalyst $[L7CoH]^+$, we included the di-cationic catalyst $[L7Co]^{2+}$, and the apparent barriers are much too high (128 kJ/mol in the gas phase and 212 kJ/mol in a solution, 122 kJ/mol in a solution with dispersion correction, Supplementary Figs. 8–10) and this catalytic cycle can be discarded. We therefore discussed our results of the mono-cationic complex $[L7CoH]^+$ (**I**) in solvation. Since complex **I** has *fac* and *mer* conformations under equilibrium, we computed both catalytic cycles and found that ***mer*-I** is more stable than ***fac*-I** by 33 kJ/mol, while ***fac*-I** based catalytic cycle has lower apparent barrier than that of ***mer*-I** (108 vs. 140 kJ/mol, Supplementary Fig. 6). On the basis of Curtin–Hammett principle, the ***fac*-I** based catalytic cycle is more preferred kinetically (Fig. 5). Starting from the ***mer*-I**, the coordination of Ph −CH = NH to form ***fac*-II-LP** is endergonic by 14 kJ/mol, and the formation of π-coordinated ***fac*-II-π** is endergonic by 72 kJ/mol. The Gibbs free energy barrier of Ph−CH = NH insertion into ***fac*-I** is 71 kJ/mol. The formation of intermediate ***fac*-III** with agostic interaction is endergonic by 50 kJ/mol. In the second step, H_2 coordination to form ***fac*-IV** is endergonic by 71 kJ/mol. The metathesis step has Gibbs free energy barrier of 108 kJ/mol for ***fac*-IV**. The formation of ***fac*-V** is exergonic by 40 kJ/mol. The release of amine from complex ***fac*-V** with the regeneration of ***mer*-I** is exergonic 59 kJ/mol. The transition state of H_2

metathesis represents the highest point on the Gibbs free energy surface and is the rate-determining transition state; and the apparent Gibbs free energy barrier is 108 kJ/mol from ***mer*-I**. On the basis of our reaction conditions (100–120 °C, 40 bar H_2 and 15–24 h reaction time), the barrier is reasonable. This catalytic cycle is similar with that proposed by Hanson and Jones. It is noted that the result with GD3BJ correction (Supplementary Figs. 9 and 12) has extremely low apparent barrier (29 kJ/mol).

In conclusion, we demonstrate that reductive aminations for the preparation of primary amines can be easily performed using non-noble metal-based homogeneous catalysts. Key to success for this achievement is the use of a specific metal ligand system (cobalt-triphos), which enables the synthesis of a broad variety of linear and branched benzylic, heterocyclic, and aliphatic amines starting from inexpensive and easily accessible carbonyl compounds, gaseous ammonia and hydrogen. Remarkably, this cobalt-triphos system works under milder reaction conditions compared to the previously reported precious homogeneous catalysts for reductive amination with ammonia. Isolation of an active pre-catalyst revealed the fast oxidation of phosphine moiety as a potential deactivation pathway of the catalyst. Density functional theory computations verified the proposed inner-sphere mechanism with the H_2 metathesis step as the rate-determining step.

Methods

General considerations. Unless specified, all substrates were obtained commercially from various chemical companies and their purity has been checked before use. Unless otherwise stated, all commercial reagents were used as received without purification. All catalytic reactions were carried out in 300 mL and 100 mL autoclaves (PARR Instrument Company). In order to avoid unspecific reactions, catalytic reactions were carried out either in glass vials, which were placed inside the autoclave, or glass/Teflon vessel fitted autoclaves. GC conversion and yields were determined by GC-FID, HP6890 with FID detector, column HP530 m × 250 mm × 0.25 µm. ^{1}H, ^{13}C, ^{19}F NMR data were recorded on a Bruker ARX 300 and Bruker ARX 400 spectrometers using DMSO-d_6, CD_3OD and $CDCl_3$ solvents. HRMS data were recorded on (1) ESI-HRMS: HPLC System 1200 /ESI-TOF-MS 6210 (Agilent).

X-ray crystal structure analysis of Complex **A** and Complex **B**: Data were collected on a Bruker Kappa APEX II Duo diffractometer. The structures were solved by direct methods (SHELXS-97: Sheldrick, G. M. *Acta Cryst*. **2008**, *A*64, 112.) and refined by full-matrix least-squares procedures on F^2 (SHELXL-2014: Sheldrick, G. M. *Acta Cryst*. **2015**, *C*71, 3.). XP (Bruker AXS) and Mercury (Macrae, C. F., Edgington, P. R., McCabe, P., Pidcock, E., Shields, G. P., Taylor, R., Towler, M., van de Streek, J. *J. Appl. Cryst*. **2006**, *39*, 453.) were used for graphical representations.

Synthesis of cobalt (II) complexes A and B. In 100 mL dried schlenk tube, 340.63 mg of $Co(BF_4)_2.6H_2O$ (1.0 mmol) was stirred in 40 mL of THF (dry and degassed) for 5 min under argon to dissolve metal salt completely to give pink colored solution. Then, 535.55 mg of triphos ((phenylphosphanediyl) bis(ethane-2,1-diyl)) bis (diphenylphosphane) (1.0 mmol) was added to the solution of metal precursor. Upon adding the ligand, the pink colored catalyst precursor solution was turned to brown colored solution. To this, another 20 mL of THF (dry and degassed) was added and stirring was continued for 2 h at RT. In 10 min of stirring time, the ligand was completely dissolved. After 1 h of stirring, the brown color solid was started to form along with some brown color crystal type material. After the completion of the reaction, the reaction mixture was stored at −30 °C for overnight. The THF solution was removed by using syringe and the complex formed was washed with 10 mL of THF (dry and degassed). Further, it was washed with dry and degassed hexane (2 × 10 mL) and then dried under high vacuum for 6 h, to get a brown color solid in 48–50% yield. The dark brown crystals were observed along with brown solid. These crystals were separated carefully and recrystallized with dry and degassed ethanol under argon. The crystals obtained were suitable for X-ray analysis. The oxide species of complex **B** (yellow crystals) were formed during the crystallization, when we carried out in normal solvent without dry and degas.

General procedure for synthesis of primary amines. The magnetic stirring bar and $Co(BF_4)_2.6H_2O$ (3 mol%) and linear triphos ((phenylphosphanediyl)bis (ethane-2,1-diyl))bis(diphenylphosphane) (4 mol%) were transferred to 8 mL glass vial and then 2 mL degassed (degassed under argon for 15 minutes before adding) trifluoroethanol (TFE) solvent was added. The colorless solution turned in to pale yellow first and then finally to brown color by stirring under argon for 15 min. Then, 0.5 mmol corresponding carbonyl compound was added to the reaction vial. The vial was fitted with septum, cap, and needle. The reaction vials (8 vials with different substrates at a time) were placed into a 300 mL autoclave. The autoclave was flushed with hydrogen twice at 30 bar pressure and then it was pressurized with 5–7 bar ammonia gas and 40 bar hydrogen. The autoclave was placed into an aluminum block preheated at 130 °C (placed 30 minutes before counting the reaction time in ordered to attain reaction temperature) and the reactions were stirred for a required time. During the reaction, the inside temperature of the autoclave was measured to be 120 °C and this temperature was used as the reaction temperature. After the completion of the reactions, the autoclave was cooled to room temperature. The remaining ammonia and hydrogen were discharged and the vials containing reaction products were removed from the autoclave. The reaction mixture was filtered off and washed thoroughly with ethyl acetate. The reaction products were analyzed by GC-MS. The crude product was purified by flash column chromatography. The corresponding primary amines were converted to their respective hydrochloride salt and characterized by NMR and GC-MS analysis. For converting into hydrochloride salt of amine, 1–2 mL methanolic HCl (0.5 M HCl in methanol) was added to the ether solution of respective amine and stirred at room temperature for 4–5 h. Then, the solvent was removed and the resulted hydrochloride salt of amine is dried under high vacuum. The yields were determined by GC for the selected amines: After completion of the reaction, n-hexadecane (100 µL) as standard was added to the reaction vials and the reaction products were diluted with ethyl acetate followed by filtration using a plug of silica and then analyzed by GC.

Note: Dry and degassed solvent should necessary for this transformation to achieve high yield and reactivity. Similarly, dry ligand and metal salts have been employed. And also well-defined complex-A is more active than in situ prepared system and Complex-A should be stored at −30 °C for maintaining its stability for a longer time.

Computational methods and models. All calculations were carried out with Gaussian 09 program[69]. Geometry optimization was carried out in gas phase at the B3PW91[70] level with the TZVP[71] basis set. All optimized structures were further characterized either as energy minimums without imaginary frequencies or transition states with only one imaginary frequency by frequency calculations, which provided zero-point vibrational energies and thermodynamic corrections to enthalpy and Gibbs free energy at 298.15 K under 1 atmosphere. On the basis of B3PW91/TZVP geometries in gas phase, two types single-point energies were calculated, one including solvation effect of 2,2,2-trifluoroethanol (TFE) as solvent (dielectric constant $\varepsilon = 26.69$[72]) based on solute electron density (SMD) at the B3PW91/Def2-TZVP[73] level (B3PW91-SMD) and one including solvation[73] and van der Waals dispersion[74] correction for the effect of phenyl substitution (B3PW91-SMD-D3). The Gibbs free energies were further corrected to standard state in solution with a standard concentration of 1 mol/L ($p = 24.5$ atm) from standard state in gas phase ($p = 1$ atm). Both mono-cationic hydride $[L7CoH]^+$ (L7 = triphos) and di-cationic $[L7Co(H)_2]^{2+}$ complexes are proposed as potential active catalysts (Table 1).

Data availability

The data that support the findings of this study are available from the corresponding authors (M.B. and R.V.J.) upon reasonable request. The X-ray crystallographic coordinates for structures reported in this study have been deposited at the Cambridge Crystallographic Data Centre (CCDC), under deposition numbers CCDC 1897492-1897493. These data can be obtained free of charge from The Cambridge Crystallographic Data Centre via www.ccdc.cam.ac.uk/data_request/cif.

Received: 30 April 2019; Accepted: 4 November 2019;
Published online: 29 November 2019

References

1. Beller, M. & Bolm, C. *Transition Metals for Organic Synthesis* (Wiley-VCH, NewYork, 2008).
2. Negishi, E.-i Magical power of transition metals: past, present, and future (Nobel lecture). *Angew. Chem. Int. Ed.* **50**, 6738–6764 (2011).
3. Smith, G. V., Notheisz, F. *Heterogeneous Catalysis in Organic Chemistry* (Academic Press, San Diego, 1999).
4. Ertl, G., Knözinger, H., Weitkamp, J. *Environmental Catalysis* (WILEY-VCH, 2008).
5. Drauz, K., Gröger, H., May, O. *Enzyme Catalysis in Organic Synthesis* (Wiley-VCH, 2012).
6. Boersma, A. J., Megens, R. P., Feringa, B. L. & Roelfes, G. DNA-based asymmetric catalysis. *Chem. Soc. Rev.* **39**, 2083–2092 (2010).
7. James, T., van Gemmeren, M. & List, B. Development and applications of disulfonimides in enantioselective organocatalysis. *Chem. Rev.* **115**, 9388–9409 (2015).

8. Leeuwen, P. W. N. M. V. *Homogeneous Catalysis: Understanding the Art* (Kluwer Academic Publishers, Boston, 2004).
9. Cornils, B. & Herrmann, W. A. *Applied homogeneous Catalysis with Organometallic Compounds* (Wiley-VCH, Weinheim, 1996).
10. Alig, L., Fritz, M. & Schneider, S. First-row transition metal (de)hydrogenation catalysis based on functional pincer ligands. *Chem. Rev.* **119**, 2681–2751 (2019).
11. O'Reilly, M. E. & Veige, A. S. Trianionic pincer and pincer-type metal complexes and catalysts. *Chem. Soc. Rev.* **43**, 6325–6369 (2014).
12. de Meijere, A. & Diederich, F. *Metal-Catalyzed Cross-Coupling Reactions* (Wiley-VCH, ed. 2, Weinheim, 2004).
13. Ruiz-Castillo, P. & Buchwald, S. L. Applications of palladium-catalyzed C–N cross-coupling reactions. *Chem. Rev.* **116**, 12564–12649 (2016).
14. Hartwig, J. F. Evolution of a fourth generation catalyst for the amination and thioetherification of aryl halides. *Acc. Chem. Res.* **41**, 1534–1544 (2008).
15. Alcaide, B., Almendros, P. & Luna, A. Grubbs' ruthenium-carbenes beyond the metathesis reaction: less conventional non-metathetic utility. *Chem. Rev.* **109**, 3817–3858 (2009).
16. Ogba, O. M., Warner, N. C., O'Leary, D. J. & Grubbs, R. H. Recent advances in ruthenium-based olefin metathesis. *Chem. Soc. Rev.* **47**, 4510–4544 (2018).
17. Franke, R., Selent, D. & Börner, A. Applied hydroformylation. *Chem. Rev.* **112**, 5675–5732 (2012).
18. Leeuwen, P. W. N. M. V. & Claver, C. *Rhodium Catalyzed Hydroformylation* (Springer Netherlands, 2002).
19. Etayo, P. & Vidal-Ferran, A. Rhodium-catalysed asymmetric hydrogenation as a valuable synthetic tool for the preparation of chiral drugs. *Chem. Soc. Rev.* **42**, 728–754 (2013).
20. Troegel, D. & Stohrer, J. Recent advances and actual challenges in late transition metal catalyzed hydrosilylation of olefins from an industrial point of view. *Coord. Chem. Rev.* **255**, 1440–1459 (2011).
21. Marciniec, B., Maciejewski, H., Pietraszuk, C., Pawluc, P. *Hydrosilylation: A Comprehensive Review on Recent Advances* (Springer: London, 2009).
22. Roseblade, S. J. & Pfaltz, A. Iridium-catalyzed asymmetric hydrogenation of olefins. *Acc. Chem. Res.* **40**, 1402–1411 (2007).
23. Hopmann, K. H. & Bayer, A. Enantioselective imine hydrogenation with iridium-catalysts: reactions, mechanisms and stereocontrol. *Coord. Chem. Rev.* **268**, 59–82 (2014).
24. Zhou, Q.-L. *Privileged Chiral Ligands and Catalysts* (Wiley-VCH, Weinheim, 2011).
25. Privileged ligands. https://www.sigmaaldrich.com/content/dam/sigmaaldrich/docs/Aldrich/Brochure/al_chemfile_v6_n8.pdf (2006).
26. Precious metals management (pmm). www.platinum.matthey.com. (2019).
27. Metals market prices, forecasts & analysis. www.metalprices.com. (2019).
28. Gebbink, R. J. M. K. & Moret, M.-E. *Non-Noble Metal Catalysis Molecular Approaches and Reactions* (Wiley-VCH, 2019).
29. Beller, M. Introduction: first row metals and catalysis. *Chem. Rev.* **119**, 2089–2089 (2019).
30. Irrgang, T. & Kempe, R. 3d-Metal catalyzed N- and C-alkylation reactions via borrowing hydrogen or hydrogen autotransfer. *Chem. Rev.* **119**, 2524–2549 (2019).
31. Korstanje, T. J., van der Vlugt, Ivar, Elsevier, J. & de Bruin, C. J. B. Hydrogenation of carboxylic acids with a homogeneous cobalt catalyst. *Science* **350**, 298–302 (2015).
32. Ai, W., Zhong, R., Liu, X. & Liu, Q. Hydride transfer reactions catalyzed by cobalt complexes. *Chem. Rev.* **119**, 2876–2953 (2019).
33. Jerphagnon, T., Pizzuti, M. G., Minnaard, A. J. & Feringa, B. L. Recent advances in enantioselective copper-catalyzed 1,4-addition. *Chem. Soc. Rev.* **38**, 1039–1075 (2009).
34. Wei, D. & Darcel, C. Iron catalysis in reduction and hydrometalation reactions. *Chem. Rev.* **119**, 2550–2610 (2019).
35. Liu, W., Sahoo, B., Junge, K. & Beller, M. Cobalt complexes as an emerging class of catalysts for homogeneous hydrogenations. *Acc. Chem. Res.* **51**, 1858–1869 (2018).
36. Cahiez, G. & Moyeux, A. Cobalt-catalyzed cross-coupling reactions. *Chem. Rev.* **110**, 1435–1462 (2010). 51.
37. Chirik, P. & Morris, R. Getting down to earth: the renaissance of catalysis with abundant metals. *Acc. Chem. Res.* **48**, 2495–2495 (2015).
38. Gomez, S., Peters, J. A. & Maschmeyer, T. The reductive amination of aldehydes and ketones and the hydrogenation of nitriles: mechanistic aspects and selectivity control. *Adv. Synth. Catal.* **344**, 1037–1057 (2002).
39. Alinezhad, H., Yavari, H. & Salehian, F. Recent advances in reductive amination catalysis and its applications. *Curr. Org. Chem.* **19**, 1021–1049 (2015).
40. Gross, T., Seayad, A. M., Ahmad, M. & Beller, M. Synthesis of primary amines: first homogeneously catalyzed reductive amination with ammonia. *Org. Lett.* **4**, 2055–2058 (2002).
41. Gallardo-Donaire, J., Ernst, M., Trapp, O. & Schaub, T. Direct synthesis of primary amines via ruthenium-catalysed amination of ketones with ammonia and hydrogen. *Adv. Synth. Catal.* **358**, 358–363 (2016).
42. Gallardo-Donaire, J. et al. Direct asymmetric ruthenium-catalyzed reductive amination of alkyl–aryl ketones with ammonia and hydrogen. *J. Am. Chm. Soc.* **140**, 355–361 (2018).
43. Senthamarai, T. et al. Simple ruthenium-catalyzed reductive amination enables the synthesis of a broad range of primary amines. *Nat. Commun.* **9**, 4123 (2018).
44. Tan, X. et al. Asymmetric synthesis of chiral primary amines by ruthenium-catalyzed direct reductive amination of alkyl aryl ketones with ammonium salts and molecular H2. *J. Am. Chm. Soc.* **140**, 2024–2027 (2018).
45. Klinkenberg, J. L. & Hartwig, J. F. Catalytic organometallic reactions of ammonia. *Angew. Chem., Int. Ed.* **50**, 86–95 (2011).
46. Nakamura, Y., Kon, K., Touchy, A. S., Shimizu, K.-i & Ueda, W. Selective synthesis of primary amines by reductive amination of ketones with ammonia over supported Pt catalysts. *ChemCatChem* **7**, 921–924 (2015).
47. Liang, G. et al. Production of Primary Amines by Reductive Amination of Biomass-Derived Aldehydes/Ketones. *Angew. Chem. Int. Ed.* **56**, 3050–3054 (2017).
48. Komanoya, T., Kinemura, T., Kita, Y., Kamata, Y. K. & Hara, M. Electronic Effect of Ruthenium Nanoparticles on Efficient Reductive Amination of Carbonyl Compounds. *J. Am. Chem. Soc.* **139**, 11493–11499 (2017).
49. Chatterjee, M., Ishizaka, T. & Kawanami, H. Reductive amination of furfural to furfurylamine using aqueous ammonia solution and molecular hydrogen: an environmentally friendly approach. *Green. Chem.* **18**, 487–496 (2016).
50. Reductive amination review. https://erowid.org/archive/rhodium/chemistry/reductive.amination.html (2004).
51. Hintermann, L. Mignonac Reaction in Comprehensive Organic Name Reactions and Reagents (Wiley, 2010).
52. Jagadeesh, R. V. et al. MOF-derived cobalt nanoparticles catalyze a general synthesis of amines. *Science* **358**, 326–332 (2017).
53. Hahn, G., Kunnas, P., de Jonge, N. & Kempe, R. General synthesis of primary amines via reductive amination employing a reusable nickel catalyst. *Nat. Catal.* **2**, 71–77 (2019).
54. Murugesan, K., Beller, M. & Jagadeesh, R. V. Reusable nickel nanoparticles-catalyzed reductive amination for selective synthesis of primary amines. *Angew. Chem. Int. Ed.* **58**, 5064–5068 (2019).
55. Lawrence, S. A. *Amines: Synthesis, Properties and Applications* (Cambridge University Press, 2004).
56. Ricci, A. *Amino Group Chemistry: From Synthesis to the Life Sciences* (Wiley-VCH, 2008).
57. Smith, D. T., Delost, M. D., Qureshi, H. & Njarðarson, J. T. Top 200 Pharmaceutical Products by Retail Sales in 2016. https://njardarson.lab.arizona.edu/sites/njardarson.lab.arizona.edu/files/2016Top200PharmaceuticalRetailSalesPosterLowResV3_0.pdf (2017).
58. Gunanathan, C. & Milstein, D. Selective synthesis of primary amines directly from alcohols and ammonia. *Angew. Chem. Int. Ed.* **47**, 8661–8664 (2008).
59. Imm, S., Bähn, S., Neubert, L., Neumann, H. & Beller, M. An efficient and general synthesis of primary amines by ruthenium-catalyzed amination of secondary alcohols with ammonia. *Angew. Chem., Int. Ed.* **49**, 8126–8129 (2010).
60. Pingen, D., Müller, C. & Vogt, D. Direct amination of secondary alcohols using ammonia. *Angew. Chem., Int. Ed.* **49**, 8130–8133 (2010).
61. Bähn, S. et al. The catalytic amination of alcohols. *ChemCatChem* **3**, 1853–1864 (2011).
62. Müller, T. E. & Beller, M. Metal-initiated amination of alkenes and alkynes. *Chem. Rev.* **98**, 675–704 (1998).
63. Pohlki, F. & Doye, S. The catalytic hydroamination of alkynes. *Chem. Soc. Rev.* **32**, 104–114 (2003).
64. Müller, T. E., Hultzsch, K. C., Yus, M., Foubelo, F. & Tada, M. Hydroamination: direct addition of amines to alkenes and alkynes. *Chem. Rev.* **108**, 3795–3892 (2008).
65. Ma, X. & Lei, M. Mechanistic insights into the directed hydrogenation of hydroxylated alkene catalyzed by bis(phosphine)cobalt dialkyl complexes. *J. Org. Chem.* **82**, 2703–2712 (2017).
66. Yuwen, J., Chakraborty, S., Brennessel, W. W. & Jones, W. D. Additive-free cobalt-catalyzed hydrogenation of esters to alcohols. *ACS Catal.* **7**, 3735–3740 (2017).
67. Zhang, G., Scott, B. L. & Hanson, S. K. Mild and homogeneous cobalt-catalyzed hydrogenation of C-C, C-O, and C-N bonds. *Angew. Chem. Int. Ed.* **51**, 12102–12106 (2012).
68. Zhang, G., Vasudevan, K. V., Scott, B. L. & Hanson, S. K. Understanding the mechanisms of cobalt-catalyzed hydrogenation and dehydrogenation reactions. *J. Am. Chem. Soc.* **135**, 8668–8681 (2013).
69. Frisch, M. J. et al. *Gaussian software, version 09 revision D01.* (Gaussian Inc.: Wallingford, CT, USA, 2009).
70. Becke, A. D. Density-functional thermochemistry. III. The role of exact exchange. *J. Chem. Phys.* **98**, 5648–5652 (1993).

71. Schäfer, A., Huber, C. & Ahlrichs, R. Fully optimized contracted Gaussian basis sets of triple zeta valence quality for atoms Li to Kr. *J. Chem. Phys.* **100**, 5829–5835 (1994).
72. Wohlfarth, C. *Static Dielectric Constants of Pure Liquids and Binary Liquid Mixtures* 17 (Springer, 2015).
73. Marenich, A. V., Cramer, C. J. & Truhlar, D. G. Universal solvation model based on solute electron density and on a continuum model of the solvent defined by the bulk dielectric constant and atomic surface tensions. *J. Phys. Chem. B* **113**, 6378–6396 (2009).
74. Grimme, S., Ehrlich, S. & Goerigk, L. Effect of the damping function in dispersion corrected density functional theory. *J. Comput. Chem.* **32**, 1456–1465 (2011).

Acknowledgements

We gratefully acknowledge the support of the European Research Council (ERC), the Federal Ministry of Education and Research (BMBF), the State of Mecklenburg-Vorpommern and the Leibniz Association (Leibniz Competition, SAW-2016-LIKAT-1). We thank the analytical staff of the Leibniz-Institute for Catalysis, Rostock, for their excellent service. All data are available in the supplementary information.

Author contributions

K.M., R.V.J. and M.B. planned and developed the project. K.M., R.V.J., V.G.C., H.N. and M.B. designed the experiments. K.M. and V.G.C. performed catalytic experiments. Z.W. and H.J. carried out DFT calculations. A.S. performed X-ray crystallography analysis. K.M., R.V.J., M.B., H.N., Z.W. and H.J. wrote the manuscript. R.V.J. and M.B. supervised the project.

Competing interests

The authors declare no competing interests.

Additional information

Supplementary information is available for this paper at https://doi.org/10.1038/s41467-019-13351-7.

Correspondence and requests for materials should be addressed to M.B. or R.V.J.

Peer review information *Nature Communications* thanks Kuo-Wei Huang, Basker Sundararaju and the other, anonymous, reviewer(s) for their contribution to the peer review of this work. Peer reviewer reports are available.

Reprints and permission information is available at http://www.nature.com/reprints

Publisher's note Springer Nature remains neutral with regard to jurisdictional claims in published maps and institutional affiliations.

Reductive Amination, Hydrogenation and Hydrodeoxygenation of 5-Hydroxymethylfurfural using Silica-supported Cobalt- Nanoparticles

Vishwas G. Chandrashekhar,[a] Kishore Natte,[b] Asma M. Alenad,[c] Ahmad S. Alshammari,[d] Carsten Kreyenschulte,[a] and Rajenahally V. Jagadeesh*[a]

Efficient and selective conversion of renewable feedstocks to essential chemicals and fuels applying green and sustainable catalytic processes is of central importance and attracts scientific interest. Among different biomass-based feedstocks, 5-hydroxymethylfurfural (HMF) represents valuable platform compound widely used for the synthesis of valuable chemicals, fuels, and polymers. Here we report cobalt nanoparticles catalyzed reductive amination, hydrogenation and hydrodeoxygenation of HMF to produce furan based primary, secondary and tertiary amines including N-methylamines as well as 2,5-bis (hydroxymethyl)furan, (5-methylfuran-2-yl)methanol and selected N-, O-, and S-containing heterocycles. Key to success for this HMF valorization is the use of reusable silica supported cobalt-based nanoparticles, which have been prepared by the immobilization and pyrolysis of Co-terephthalic acid-piperazine MOF template on silica.

Introduction

The valorization of renewable resource, especially biomass and its based compounds to produce value-added chemicals and fuels as well as pharmaceutically relevant compounds in more efficient and sustainable manner continues to be an important goal of chemical research.[1–19] In this regard the development of resourceful and cost-effective catalytic methodologies to convert biomass and its derived feedstock to essential products is of central importance.[1–19] Among sugar derived feedstocks, 5-hydroxymethylfurfural (HMF) represents highly valuable platform compound,[20–25] which has been listed as the top 10 renewable chemicals by the U.S. Department of Energy.[22–23] Notably, HMF serves as renewable feedstock to produce value-added chemicals, fuels, and polymers.[20–35] In order to valorize HMF, different reactions such as catalytic hydrogenations, hydrodeoxygenations, oxidations, and aminations have been applied.[20–35,44–59] Applying these processes, a variety of compounds for example, 2,5-bis(hydroxymethyl)furan, 2,5-dimethylfuran, 2,5-dimethyltetrahydrofuran, hexanediols, levulinic acid, furan-2,5-dicarboxylic acid, alkanes, and bio-based amines could be accessed from HMF.[20–21,24–35]

Amines are indispensable compounds widely used in chemical, pharmaceuticals agrochemical and material industries.[36–39] Among these, bio-based amines represent renewable compounds, which serve as key and intermediates for the synthesis of advanced chemicals, pharmaceuticals, and materials.[4–6] To produce these products, especially furan-based amines, HMF serves as the key starting material, which can be converted to primary, secondary, and tertiary amines including N-methylamines.[11,33–35] These furan- based amines are used in the synthesis of bioactive molecules such as antihypertensives, diuretics, and antiseptic agents.[40–42] In addition, they also employed as intermediates in the manufacture of polymers, fibers and perfumes.[4,6,43] To prepare furan-based amines, catalytic reductive amination of HMF using molecular hydrogen constitute convenient methodology in which aldehyde group of HMF can be reacted with ammonia, primary and secondary amines to access different kinds of amines.[4–6,44–59] To perform reductive amination of HMF in more selective and efficient manner, the use of suitable catalyst systems is crucial. Regarding catalysts for this transformation, more frequently precious metal-based homogeneous,[44] and heterogeneous[45–59] systems based on, Rh,[45] Pt,[46] Pd,[47–48] Ru,[44,49–50] and Au[51] were used. With respect to non-noble metal heterogeneous catalysts, Raney Ni,[52] Co,[53] Cu,[54–55] and Ni[56–58] based ones are known to catalyze the reductive amination of HMF. Despite these achievements the development of earth abundant metal-based catalysts, which should work in more efficient and selective manner under mild conditions, is still desired for reductive amination of HMF to produce biobased amines. In particular, nanoparticles-

[a] V. G. Chandrashekhar, Dr. C. Kreyenschulte, Prof. Dr. R. V. Jagadeesh
Leibniz-Institut für Katalyse e.V
Albert-Einstein-Straße 29A,
18059 Rostock, Germany
E-mail: jagadeesh.rajenahally@catalysis.de
[b] Dr. K. Natte
Chemical and Material Science Division
CSIR - Indian Institute of Petroleum
Haridwar road, Mohkampur,
Dehradun 248005 India
[c] Dr. A. M. Alenad
Chemistry Department, College of Science
Jouf University
P.O. Box: 2014, Sakaka, Kingdom of Saudi Arabia.
[d] Dr. A. S. Alshammari
King Abdulaziz City for Science and Technology
P.O. Box 6086, Riyadh 1442, Kingdom of Saudi Arabia.

Supporting information for this article is available on the WWW under https://doi.org/10.1002/cctc.202101234

based catalysts are more appropriate due to their unique advantages such as stability, easy recycling and tunable activities and selectivities.[39,60–65] In addition to the synthesis of bio-based amines, catalytic hydrogenation and hydrodeoxygenation of HMF constitute pivotal processes to produce valuable products and fuels such as 2,5-bis(hydroxymethyl)furan, 5-methylfurfuryl alcohol, 2,5-dimethylfuran, alcohols, diols, and alkanes.[28–31]

Here we report the preparation of silica supported cobalt-based nanoparticles as efficient, selective and reusable reductive amination and hydrogenation catalysts for the valorization of HMF under mild conditions (Scheme 1). These nanoparticles have been prepared by the immobilization and pyrolysis of cobalt-terephthalic acid-piperazine MOF template on silica under argon at 800 °C. Applying these cobalt nanoparticles, reductive amination of HMF with ammonia, anilines, benzylic and aliphatic amines was performed to prepare furan based, primary amines, secondary and tertiary amines as well as N-methylamines in good to excellent yields (Scheme 1). The synthetic applicability of this Co-reductive amination protocol has been showcased for the synthesis of furan-benzimidazole, furan-2,3-dihydrobenzothiazole, and furan-oxazolidine based heterocycles (Scheme 1). In addition, hydrogenation and hydrodeoxygenation of HMF were also carried out to produce 2,5-bis(hydroxymethyl)furan and 5-methylfurfuryl alcohol (Scheme 1).

Results and Discussion

Preparation of Co-nanoparticles based catalysts

For the preparation of successful nanoparticles-based catalysts, the use of suitable precursor and appropriate methodology considered as curial aspects.[39,62–63]

Regarding potential precursors, compared to simple metal salts, metal complexes or metal organic formworks are more promising, which can be easily immobilized and pyrolyzed on heterogeneous supports to create active and selective nanostructured catalysts for organic synthesis.[39,62–65] Based on this concept, to prepare desired supported cobalt-nanoparticles, first we generated cobalt-based MOF *in situ* and immobilized on silica and subsequently pyrolyzed this templated material under argon.[63–65] In a typical procedure, $Co(NO_3)_2 \cdot 6H_2O$ terephthalic acid piperazine were mixed in DMF and stirred at 150 °C to generate cobalt- terephthalic-piperazine MOF. To this generated MOF in DMF, silica was added and continued the stirring at 150 °C. After slow evaporation of DMF and drying cobalt-terephthalic acid-piperazine MOF templated on silica (Co-terephthalic acid-piperazine@SiO_2) was formed. Finally, this MOF-SiO_2 templated material was pyrolyzed at 800 °C under argon to obtain silica supported cobalt nanoparticles (Co-terephthalic acid-piperazine@SiO_2-800; Figure 1). The same produce was applied to prepare other materials, pyrolyzed at different temperatures (400, 600, 1000 °C).

Reductive amination of HMF with NH_3: Evaluation of activity and selectivity of Co-nanocatalysts

The prepared new material, Co-terephthalic acid-piperazine@-SiO_2-800, was tested for its activity in the reductive amination of HMF 1 with ammonia in presence of molecular hydrogen to produce 5-(aminomethyl)-2-furanmethanol, AMF 2 (Table 1). This bifunctional compound, 2 (AMF) constitute as an important precursor and key intermediate to produce advanced compounds, since it contains primary amine and alcohol, groups which can be functionalized further.[25] In general, reductive amination of HMF to obtain selectively the corresponding primary amine is challenging. This reaction is often non-selective and results in the formation of side-products such as

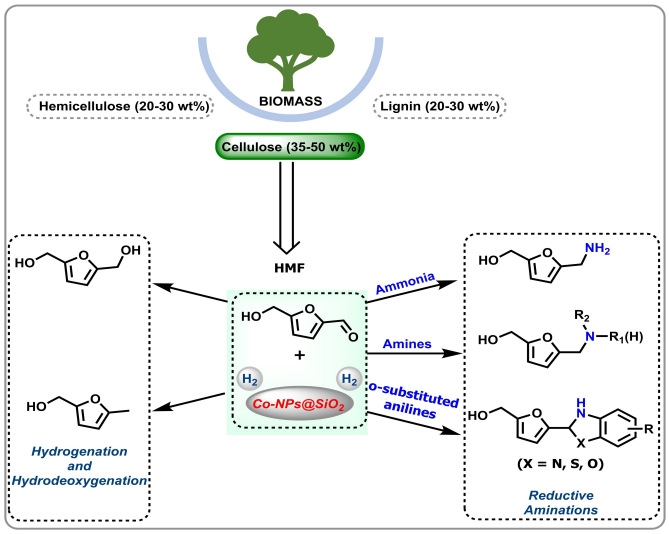

Scheme 1. Co-nanoparticles catalyzed valorization of HMF.

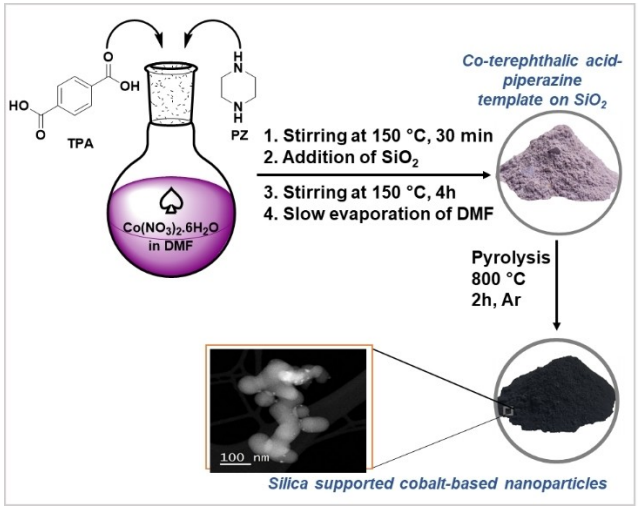

Figure 1. preparation of cobalt-based nanoparticles by the pyrolysis of Co-terephthalic-piperazine MOF template on silica.

Table 1. Cobalt-catalyzed reductive amination of HMF using ammonia in presence of molecular hydrogen.

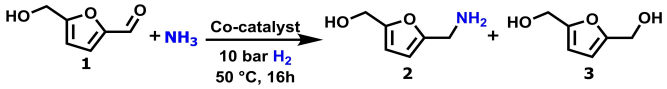

Entry	Catalyst	Solvent	Conv. (%)	Yield (%)	
				2	3
1[a]	Co-terephthalic acid-piperazine@SiO_2-800	MeOH	>99	80	15
2[a]	Co-terephthalic acid-piperazine@SiO2-800	EtOH	>99	89	4
3[a]	Co-terephthalic acid-piperazine@SiO_2-800	H_2O	>99	94	1
4[b]	Co-terephthalic acid-piperazine@SiO_2-800	H_2O	>99	94	1
5[c]	Co-terephthalic acid-piperazine@SiO_2-800	H_2O	>99	94	1
6[d]	Co-terephthalic acid-piperazine@SiO_2-800	H_2O	90	80	–
7[b]	Co-terephthalic acid-piperazine@SiO_2-400	H_2O	50	–	–
8[b]	Co-terephthalic acid-piperazine@SiO_2-600	H_2O	85	70	–
9[b]	Co-terephthalic acid-piperazine@SiO_2-1000	H_2O	>99	88	6
10[b]	Co-nitrate@ SiO_2-800	H_2O	10	6	–
11[b]	Co-terephthalic acid-piperazine@SiO_2	H_2O	–	–	–
12[b]	Co-terephthalic acid-piperazine	H_2O	–	–	–
13[b]	$Co(NO_3)_2 \cdot 6H_2O$	H_2O	–	–	–

Reaction conditions: [a] 0.5 mmol HMF, 5 bar NH3, 25 mg catalyst (5 mol% Co), 10 bar H2, 3 ml solvent, 50 °C, 16 h. [b] same as [a] with 0.1 mL aq.NH3 (33 wt% of NH3 in water) instead of NH3 (gas). [c] same as [b] with 35 mg catalyst (7 mol% Co). [d] same as [b] with 15 mg catalyst (3 mol% Co). All yields are determined by GC using DMAc as standard. In entry 7, 45% of corresponding secondary imine was observed. In entry 8, 12% of corresponding secondary imine was observed.

over alkylated products (secondary imine 4 and secondary amine 5) or corresponding alcohol as the reduced product 3 (Scheme 2).

In the beginning, HMF was reacted with 5 bar of NH_3 and 10 bar of H_2 in the presence 25 mg (5 mol% Co) of Co-terephthalic acid-piperazine@SiO_2-800 catalyst in methanol as solvent at 50 °C (Table 1, entry 1). Under this reaction conditions, 80% of the desired product **2**, was obtained (Table 1, entry 1). Under same conditions, next reaction was performed in ethanol and water (Table 1, entries 2–3). Among these, water was found to be the best and gave 94% of the targeted product **2**. Interestingly, a similar result was obtained using 0.1 mL of aq.NH_3 (33 wt%) instead of gaseous NH_3 (Table 1, entry 4). By increasing the amount of catalyst to 35 mg (7 mol% Co), same results were obtained that of 25 mg catalyst (Table 1, entry 5). However, by decreasing the amount of catalyst to 15 mg (3 mol%), both conversion (90%) of **1** and yield (80%) of **2** were decreased (Table 1, entry 6).

Further to know the effect of temperature on the formation of active material, Co-terephthalic acid-piperazine@SiO_2 was pyrolyzed at different temperatures (400, 600 and 1000 °C) and tested their activities and selectivities in the model reaction. The material pyrolyzed at 400 °C (Co-terephthalic acid-piperazine@SiO_2-400) showed less activity and selectivity and gave corresponding secondary imine **4** as the products without the formation of **2** (Table 1, entry 7). The material pyrolyzed at 600 °C (Co-terephthalic acid-piperazine@SiO_2-600) exhibited moderate activity and produced 70% of **2** and 12% of corresponding secondary imine **4** (Table 1, entry 8). On the other hand, catalyst pyrolyzed at 1000 °C (Co-terephthalic acid-piperazine@SiO_2-1000) displayed good activity and provided 88% of **2** (Table 1, entry 9). In contrast, material prepared using simple cobalt nitrate without MOF (cobalt nitrate@SiO_2-800) exhibited very less activity and gave 6% of **2** (Table S7, entry 10). The unpyrolyzed material (Co-terephthalic acid-piperazine @SiO_2) and MOF (Co-terephthalic acid-piperazine), as well as catalysts under homogeneous conditions are all completely inactive (Table 1, entries 11–13).

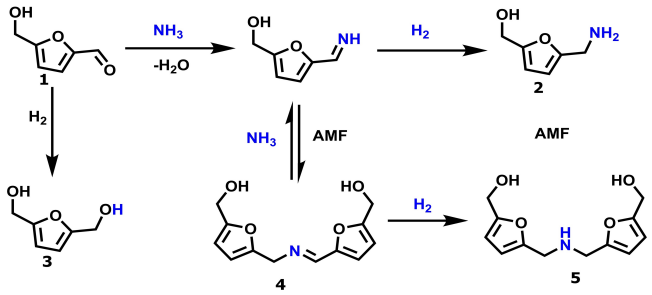

Scheme 2. Reductive amination of HMF with ammonia: Desired and side products

Characterization of Co-based catalyst

The most active catalyst, Co-terephthalic acid-piperazine@SiO_2-800 was characterized using X-ray powder diffraction (XRD), scanning transmission electron microscopy (STEM), energy-dispersive X-ray spectroscopy (EDXS), X-ray photoelectron spectroscopy (XPS). XRD patterns of Co-terephthalic acid-piperazine@SiO_2-800, displayed the presence of both metallic and oxidic cobalt particles (Figure S1). In contrast, the very less active material, cobalt-nitrte@SiO_2-800, contained mainly oxidic cobalt particles. Aberration corrected STEM analysis of Co-terephthalic acid-piperazine@SiO_2-800 catalyst revealed the formation of metallic cobalt-particles of about 5 to 15 nm in

diameter (Figure 2A). Usually, these Co-particles are surrounded by graphitic shells (Figure 2B, S2).

In addition, oxidic cobalt particles of comparable sizes are also present as are in-between states like metal core particles fully or partially surrounded by Co oxide (Figure 2C, S2). The oxide phase is not covered by graphitic shells. As morphology of Co metal and Co oxide particles is often quite similar and a potential carbon coverage of particles only identifiable at particles sitting close to the edge of the support due to contrast reasons, it is not possible to determine the ratio between the metal and the oxide Co phase by STEM.

To know the states of cobalt and nitrogen at the surface of the catalyst, XPS analysis of Co-terephthalic acid-piperazine@-SiO_2-800 was conducted (Figure 3). Figure 3a, shows the high resolution Co2p spectra in which the two main peaks at 778.44 and 793.47 eV correspond to Co2p3/2 and Co2p1/2, respectively. These peak positions can be assigned to the dominant presence of cobalt in metallic form. Other, two small satellite peaks at 785.26 and 800.11 eV represent the presence of some high spin Co^{2+} mixed up with the peaks of metallic Co. Weak satellite peaks might be due to presence of Co_3O_4 where mixed Co(II) and Co(III) are present.[66–67] Next, N1s narrow scan spectra (Figure 3b) predicts two types of N with peaks centred at

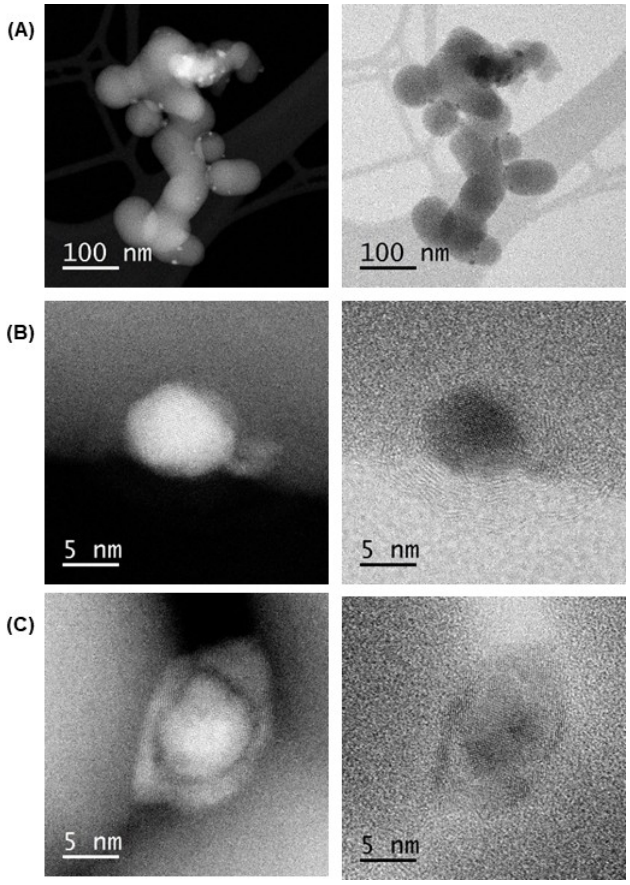

Figure 2. STEM images of Co-terephthalic acid-piperazine@SiO_2-800 catalyst. Left column HAADF images and right column corresponding ABF images. (A) Distribution of cobalt nanoparticles, (B) metallic Co nanoparticles surrounded by graphitic layers. (C) Co-oxide particle without carbon shell.

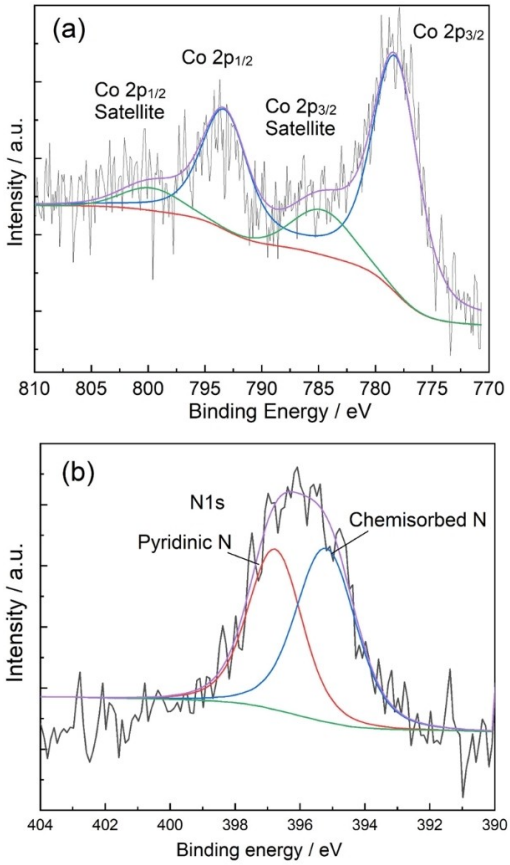

Figure 3. XP spectra of the (A) Co2p and (B) N1s of Co-terephthalic acid-piperazine@SiO_2-800 catalyst

395.20 and 396.8 eV. Such a significant downfield shift of both types of nitrogen represents electron density rich N atoms. This prominent download shift in N1s binding energy is caused if N-atoms are present on the substitutional sites replacing O bound to metal or doped in the graphitic carbon. The peak at 395.20 eV can be attributed to chemisorbed N and at 396.8 eV might be pyridinic N.[68]

BET surface areas of Co-terephthalic acid-piperazine@SiO_2-800 and cobalt-nitrte@SiO_2-800 were found to be 85.587 m^2/g and 39.722 m^2/g, which revealed that the most active catalyst has more surface area (Figure S5–S6). Hereafter we represent the most active catalyst, Co-terephthalic acid-piperazine@SiO_2-800 catalyst as Co–Co_3O_4@SiO_2.

Co-nanoparticles catalyzed reductive amination of HMF with amines

After having performed the synthesis of AMF 2, we carried out the reductive amination of HMF with different amines (Scheme 3). Interestingly, HMF underwent reductive amination with primary, secondary amines as well as mono N-methyl and N,N-dimethyl amines and provided corresponding furan-based amines in excellent yields up to 95%. Aniline and 4-methyl

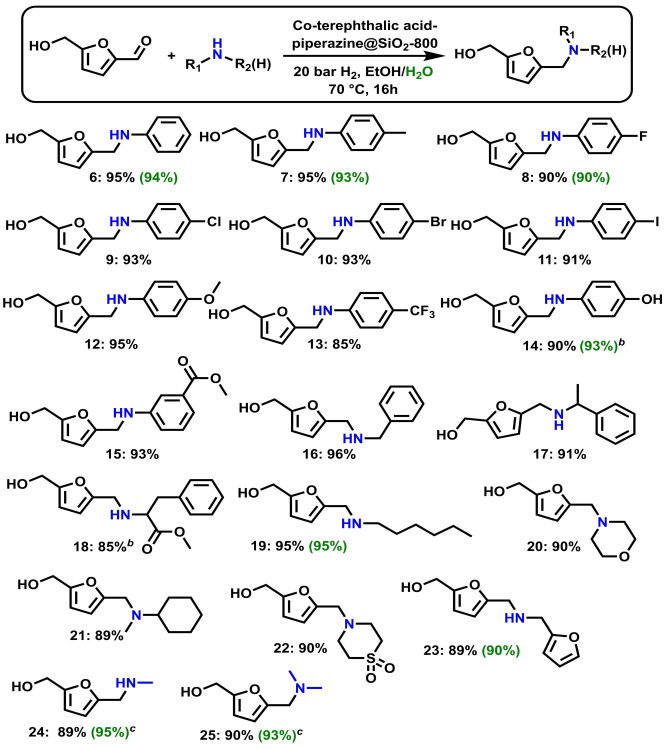

Scheme 3. Co-catalyzed reductive amination of HMF with different amines. Reaction conditions: [a] 0.5 mmol HMF, 0.5 mmol amines, 25 mg Co-terephthalic acid-piperazine@SiO_2-800 (5 mol% Co), 20 bar H_2, 3 ml solvent (EtOH or H_2O), 70 °C, 16 h. [b] same as [a] at 80 °C. [c] same as [a] using 0.1 mL methyl or dimethyl amine solution (12 M in Ethanol) at 50 °C. Yields given parenthesis in green colour refer to the reactions conducted in water. All isolated yields.

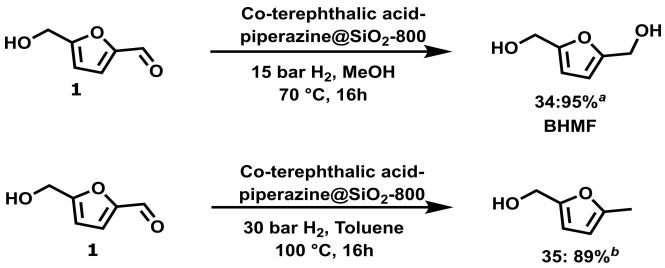

Scheme 4. Co-catalyzed hydrogenation/hydrodeoxygenation of HMF. Reaction conditions: [a] 0.5 mmol HMF, 25 mg catalyst (5 mol% Co), 15 bar H_2, 3 ml MeOH, 70 °C, 16 h. Isolated yield. [b] 0.5 mmol HMF, 30 mg catalyst (≈6 mol% Co), 30 bar H_2, 3 ml Toluene, 100 °C, 16 h. GC Yield.

aniline were reacted with HMF and afforded the corresponding secondary amine in up to 95% (Scheme 3, products 6–7). Notably, HMF and halogenated anilines (–F, –Cl, –Br, and –I) were smoothly reacted without being dehalogenation and offered corresponding products in up to 93% yield (scheme 3, products 8–11). Due to the versatility of reactivity of halogen atoms, these furan-based halogenated compounds could serve as special starting materials or intermediates for the synthesis of different products. HMF was smoothly aminated with anilines containing $–OCH_3$, OH, $–COOCH_3$ and $–CF_3$ groups and produced functionalized furan-based amines in 85–95% yields. (Scheme S5 products 12–15).

Next, benzylic and arylaphatic primary amines were N-alkylated with HMF and gave corresponding secondary amines (Scheme 3, products 16–18). In addition, aliphatic primary amine such as N-hexane amine was also reacted smoothly and gave 95% of (5-((hexylamino)methyl)furan-2-yl)methanol (product 19). As an example of secondary amine, morpholine, N-methylcyclohexanamine, and thiomorpholine 1,1-dioxide were reacted with HMF and obtained corresponding tertiary amines in up to 90% yield (Scheme 4; products 20–22). These kind of furan-morpholine derived products could be interesting for drug discovery. Interestingly, furfuryl amine, which is produced form another renewable feedstock furfural was also N-alkylated with HMF and provided (5-(((furan-2-ylmethyl)amino)methyl) furan-2-yl)methanol as di-furan based amine (Product 23) Finally, both mono N-methyl and N,N-dimethyl amines, which are important bulk chemicals, were also efficiently reacted with HMF and produced corresponding furan-based N-methylated products (Products 21–22). In general N-methylated amines represent an important class of amines and these functionalities found in a number of drugs and biomolecules, that play significant roles in the function of these life Science molecules.[39]

Synthesis of heterocyclic compounds using Co-nanoparticles

Heterocyclic compounds are an important class of products widely used in organic synthesis and drug discovery.[69] Noteworthy, many pharmaceuticals and natural products contain heterocyclic motifs, which play vital roles in their activities.[69] Based on the importance of heterocyclic compounds, their synthesis starting from renewable feedstocks applying cost-effective and green methods is of central importance.

In this regard, we applied our Co-based reductive amination protocol for the synthesis of *N*, *S* and *O*- containing heterocycle starting from HMF and different amines (Table 2). Furan-benzimidazole based heterocyclic compounds (Table 2, 27–29) were selectively prepared by the Co-catalyzed reductive amination of HMF with *o*-phenylenediamine, and *N*-methyl-*o*-phenylenediamine, respectively. Next, 2-aminothiophenol was reacted with HMF and gave furan-dihydrobenzothiazole based products in 86% yield (Product 31). Further, HMF and phenylalaninol reacted and gave Furan-oxazolidine based heterocyclic compounds (Product 33).

Co-catalyzed hydrogenation/hydrodeoxygenation of HMF

In addition to reductive aminations, the applicability of our Co-nanoparticles has also been demonstrated for the hydrogenation/hydrodeoxygenation of HMF. As shown in Scheme 4, HMF can be selectively hydrogenated to produce 2,5-bis (hydroxymethyl)furan (BHMF) in high yields (Product 34) at 70 °C with 15 bar hydrogen. This heterocyclic diol **34** serves as the key precursor to produce polyurethane foams and

Table 2. synthesis of heterocyclic compounds from HMF and amines using Co-nanoparticles.

Entry	HMF	Amine	Heterocyclic product	Yield (%)
1	1	26	27	89%
2	1	28	29	80%
3	1	30	31	86%
4	1	32	33	90%

Reaction conditions: [a] 0.5 mmol HMF, 0.5 mmol amines, 25 mg Co-terephthalic acid-piperazine@SiO_2-800 (5 mol% Co), 10 bar H_2, 3 ml EtOH, 50 °C, 16 h. All isolated yields.

polyesters.[70–71] On increasing the temperature and pressure (100 °C and 30 bar H_2), the HMF underwent hydrodeoxygenation to provide 5-methylfuran-2-yl)methanol (Product 35).

Finally, the recycling, reusability, and stability studies of Co–Co_3O_4@SiO_2 were performed for the reductive amination of HMF with mono N-methylamine at two different conditions (Figure 4). For 16 h of reaction time, the catalyst recycled and reused up to 4 times. Up to 4th run there is not much significant loss in either activity or selectivity, but in the 5th run the yield of product is decreased. To know the catalyst stability the recycling was carried for half conversion at 10 h of reaction time and found that the catalyst is stable up to 3rd run and afterwards the decrease in the activity was observed.

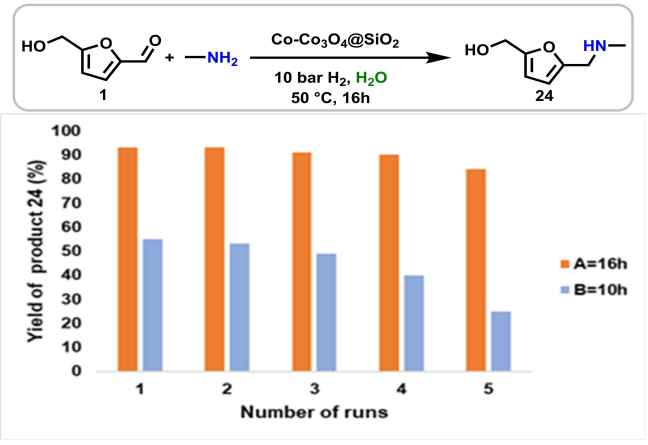

Figure 4. Recycling of Co-terephthalic acid-piperazine@SiO_2-800 for the N-methylation of HMF. Reaction conditions: Condition A: 2 mmol HMF, 0.4 mL N-methyl amine (12 M in EtOH), 100 mg catalyst (5 mol% Co), 10 bar H_2, 10 ml H_2O, 50 °C, 16 h. Condition B: Same as 'A' at 10 h. Yields were determined by GC.

Conclusion

We successfully prepared and applied silica supported cobalt-based nanoparticles as general reductive amination and hydrogenation catalysts to valorize HMF in an efficient and selective manner. The optimal Co-nanoparticles-based catalyst has been synthesized by the immobilization and pyrolysis of Co-terephthalic acid-piperazine MOF on aerosil silica at 800 °C for 2 h under argon. Using these nanoparticles, we performed the reductive amination of HMF with ammonia, anilines, benzylic, arylaphatic and aliphatic amines as well as N-methylamines to produce furan-based primary, secondary, and tertiary amines including N-methylated products. The applicability of this Co-catalyzed amination methodology is showcased for the preparation of selected *N*-, *O*-, and *S*- containing heterocycles. In addition, this Co-catalyst was also used for the hydrogenation and hydrodeoxygenation activity for HMF to produce 2,5-bis (hydroxymethyl)furan, (5-methylfuran-2-yl)methanol.

Experimental Section

Materials and methods

All substrates were obtained commercially from various chemical companies. Cobalt(II) nitrate hexahydrate (Alfa Aesar; cat no. 36418-100G), piperazine anhydrous (PZ; TCI, ≥98%; cat no. P0446). Terephthalic acid (Aldrich; cat no. 185361-100G; 98%). Silica (Aerosil OX-50) was obtained from Evonik. N,N-dimethylformamide (DMF) was obtained from Across chemicals. Pyrolysis experiments were carried out in Nytech-Qex oven. Before using, purity of all the substrates has been checked by GC-MS.

XRD powder pattern were recorded either on a Panalytical X'Pert diffractometer equipped with a Xcelerator detector or on a Panalytical Empyrean diffractometer equipped with a PIXcel 3D detector system. Both were used with automatic divergence slits and Cu kα1/α2 radiation (40 kV, 40 mA; λ = 0.015406 nm, 0.0154443 nm). Cu beta-radiation was excluded by using nickel filter foil. Peak positions and profile were fitted with Pseudo-Voigt function using the HighScore Plus software package (Panalytical). Phase identification was done by using the PDF-2 database of the International Center of Diffraction Data (ICDD).

The STEM measurements were performed at 200 kV with a probe aberration-corrected JEM-ARM200F (JEOL, Corrector: CEOS). The microscope is equipped with a JED-2300 (JEOL) energy-dispersive x-ray-spectrometer (EDXS). The aberration corrected STEM imaging were performed with High-Angle Annular Dark Field (HAADF) and Annular Bright Field (ABF) detectors simultaneously. The solid samples were dry deposited without any pretreatment on a holey carbon supported Cu-grid (mesh 300) and transferred to the microscope.

XPS (X-ray Photoelectron Spectroscopy) data was obtained with a VG ESCALAB220iXL (ThermoScientific) with monochromatic Al Kα (1486.6 eV) radiation. The electron binding energies EB were obtained without charge compensation. For quantitative analysis the peaks were deconvoluted with Gaussian-Lorentzian curves, the peak area was divided by a sensitivity factor obtained from the element specific Scofield factor and the transmission function of the spectrometer. CasaXPS was used for XPS peak deconvolution.

BET surface areas (BET-SA) of the catalysts were determined on NOVA 4200e instrument by N_2-physisorption at −196 °C. Prior to the measurements, the known amount of catalyst was evacuated for 2 h at 220 °C to remove physically adsorbed water. GC and GC-MS were recorded on Agilent 6890 N instrument. GC conversion and yields were determined by GC-FID, HP6890 with FID detector, column HP530 m × 250 mm × 0.25 μm. 1H and 13C NMR data were recorded on a Bruker ARX 300 and Bruker ARX 400 spectrometers using DMSO-d6, CD_3OD and $CDCl_3$ solvents.

Procedure for the preparation of Co-terephthalic acid-piperazine@SiO_2-800 catalyst

In a 50 mL round bottomed flask, 444.5 mg of cobalt (II) nitrate hexahydrate and 395.2 mg of piperazine were stirred in 20 mL of N,N-dimethylformamide (DMF) at 150 °C for 5 minutes. To this mixture, 761.1 mg of terephthalic acid, which was already dissolved (by heating) in 10 mL DMF was added. Next, the round bottomed flask containing the reaction mixture was fixed with reflux condenser and was placed into an aluminum block preheated at 150 °C and stirred for 20–30 minutes. Then, 1.2 g of silica (Aerosil-OX-50) was added followed by the addition of 10 mL DMF and the reaction mixture was stirred again at 150 °C for 4–5 h. Then after, the reflux condenser was removed and the round bottomed flask containing reaction product was allowed to stand without stirring and closing for 20 h at 150 °C to slowly evaporate DMF and to grow MOF template on carbon. After the evaporation of the solvent and ensuring the complete drying, the material was cooled to room temperature and grinded to give a fine powder. The powdered material was pyrolyzed at 800 °C for 2 hours under an argon atmosphere and then cooled to room temperature after pyrolysis.

Elemental analysis (Wt%) of Co-terephthalic acid-piperazine@SiO_2-800: Co = 6.27%, C = 16.98%, H = 0.10%, Si = 32.59% N = 0.81%.

Procedure for the reductive amination of HMF with NH_3

A magnetic stirring bar and 0.5 mmol HMF were transferred to 4 mL glass vial and then 2.5 mL H_2O and 0.4 mL aq. NH_3 (33 wt%) was added. Then, 25 mg of catalyst (Co-terephthalic acid-piperazine@SiO_2-800; 5 mol% Co) was added and the vial was fitted with septum, cap, and needle. The reaction vial was placed into a 50 mL autoclave. The autoclave was flushed with hydrogen twice at 20 bar pressure and then it was pressurized with 10 bar H_2. The autoclave was placed into an aluminium block preheated at 55 °C (placed 30 minutes before counting the reaction time in ordered to attain reaction temperature) and the reactions were stirred for 16 h. During the reaction, the inside temperature of the autoclave was measured to be 50 °C and this temperature was used as the reaction temperature. After the completion of the reactions, the autoclave was cooled to room temperature. The remaining H_2 were discharged and the vial containing reaction product was removed from the autoclave. The solid catalyst was filtered off and washed thoroughly with ethanol. The reaction products were analysed by GC-MS. The corresponding primary amines were purified by column chromatography. The same procedure was followed using 5–7 bar ammonia gas instead of aq. NH_3.

General procedure for the reductive amination of HMF with anilines/amines

The magnetic stirring bar and 0.5 mmol HMF was transferred to 7 mL glass vial and then 3 mL EtOH/H_2O, 0.5 mmol corresponding aniline/amine was added. Then, 25 mg of catalyst (Co-terephthalic acid-piperazine@SiO_2-800; 5 mol% Co) was added and the vial was fitted with septum, cap and needle. The reaction vials (8 vials with different amines at a time) were placed into a 300 mL autoclave. The autoclave was flushed with H_2 twice at 20 bar pressure and then it was pressurized with 20 bar hydrogen. The autoclave was placed into an aluminium block preheated at 76 °C (placed 30 minutes before counting the reaction time in ordered to attain reaction temperature) and the reactions were stirred for 16 h. During the reaction, the inside temperature of the autoclave was measured to be 70 °C and this temperature was used as the reaction temperature. After the completion of the reactions, the autoclave was cooled to room temperature. The remaining H_2 were discharged and the vials containing reaction products were removed from the autoclave. The solid catalyst was filtered off and washed thoroughly with ethanol. The reaction products were analyzed by GC-MS. The corresponding products were purified by column chromatography and isolated as semi-solid materials. The resulted amines were characterized by NMR and HR-MS spectral analysis.

Procedure for the hydrogenation of HMF

A magnetic stirring bar and 0.5 mmol HMF was transferred to 4 mL glass vial and then 3 mL MeOH added. Then, 25 mg of catalyst (Co-terephthalic acid-piperazine@SiO_2-800; 5 mol% Co) was added and the vial was fitted with septum, cap and needle. The reaction vial was placed into a 50 mL autoclave. The autoclave was flushed with hydrogen twice at 20 bar pressure and then it was pressurized with 15 bar H_2. The autoclave was placed into an aluminium block preheated at 76 °C (placed 30 minutes before counting the reaction time in ordered to attain reaction temperature) and the reactions were stirred for 16 h. During the reaction, the inside temperature of the autoclave was measured to be 70 °C and this temperature was used as the reaction temperature. After the completion of the reactions, the autoclave was cooled to room temperature. The remaining H_2 were discharged and the vial containing reaction product was removed from the autoclave. The solid catalyst was filtered off and washed thoroughly with methanol. The reaction products were analyzed by GC-MS and NMR without any purification.

Procedure for the hydrodeoxygenation of HMF

A magnetic stirring bar and 0.5 mmol HMF was transferred to 4 mL glass vial and then 3 mL Toluene added. Then, 30 mg of catalyst (Co-terephthalic acid-piperazine@SiO_2-800; 6 mol% Co) was added and the vial was fitted with septum, cap and needle. The reaction vial was placed into a 50 mL autoclave. The autoclave was flushed with hydrogen twice at 20 bar pressure and then it was pressurized with 30 bar H_2. The autoclave was placed into an aluminium block preheated at 110 °C (placed 30 minutes before counting the reaction time in ordered to attain reaction temperature) and the reactions were stirred for 16 h. During the reaction, the inside temperature of the autoclave was measured to be 100 °C and this temperature was used as the reaction temperature. After the completion of the reactions, the autoclave was cooled to room temperature. The remaining H_2 were discharged and the vial containing reaction product was removed from the autoclave. After completion of the reaction, dimethylacetamide (46 μL) as standard was added to the reaction vial followed by filtration using plug of silica and then analyzed by GC.

Procedure for recycling the catalyst

A magnetic stirring bar and 2 mmol of HMF were transferred to a 50 mL autoclave fitted with a glass vessel and then 10 mL H_2O,

0.4 mL methylamine (12 M in EtOH) was added. Then, 100 mg of catalyst (Co-terephthalic acid-piperazine@SiO_2-800) was added. The autoclave was flushed with 20 bar hydrogen and then it was pressurized with 10 bar H_2. The autoclave was placed into a pre-heated aluminium block at 55 °C and the reactions were stirred for 16 h. During the reaction, the inside temperature of the autoclave was measured to be 50 °C. After the completion of the reactions, the autoclave was cooled to room temperature. The remaining hydrogen was discharged, and the reaction products were removed from the autoclave. To the reaction products, 100 μL dimethylacetamide as standard was added. The catalyst was separated from the reaction mass through filtration and the reaction product was subjected to GC analysis for determining the yield of product. The filtered catalyst was washed thoroughly with ethanol, acetone and dried at 130 °C overnight.

Acknowledgements

We gratefully acknowledge the Deputyship for Research & Innovation, Ministry of Education in Saudi Arabia for funding this work through the project number "375213500". We thank the State of Mecklenburg-Vorpommern and LIKAT for general support. We are thankful to the analytical team of the Leibniz-Institut für Katalyse e.V. for their excellent service. Open Access funding enabled and organized by Projekt DEAL.

Conflict of Interest

The authors declare no conflict of interest.

Keywords: 5-Hydroxymethylfurfural · Co-nanoparticles · reductive amination · hydrogenation · hydrodeoxygenation · bio-based amines

[1] A. Corma, S. Iborra, A. Velty, *Chem. Rev.* **2007**, *107*, 2411–2502.
[2] M. Besson, P. Gallezot, C. Pinel, *Chem. Rev.* **2014**, *114*, 1827–1870.
[3] K. Natte, A. Narani, V. Goyal, N. Sarki, R. V. Jagadeesh, *Adv. Synth. Catal.* **2020**, *362*, 5143–5169.
[4] V. Froidevaux, C. Negrell, S. Caillol, J.-P. Pascault, B. Boutevin, *Chem. Rev.* **2016**, *116*, 14181–14224.
[5] M. Pelckmans, T. Renders, S. V. de Vyver, B. F. Sels, *Green Chem.* **2017**, *19*, 5303–5331.
[6] J. He, L. Chen, S. Liu, K. Song, S. Yang, A. Riisager, *Green Chem.* **2020**, *22*, 6714–6747.
[7] Z. Zhang, J. Song, B. Han, *Chem. Rev.* **2017**, *117*, 6834–6880.
[8] a) K. Barta, P. C. Ford, *Acc. Chem. Res.* **2014**, *47*, 1503–1512; b) R. Rinaldi, R. Jastrzebski, M. T. Clough, J. Ralph, M. Kennema, P. C. A. Bruijnincx, B. M Weckhuysen, *Angew. Chem. Int. Ed.* **2016**, *55*, 8164–8215; *Angew. Chem.* **2016**, *128*, 8296–8354.
[9] a) R. Mariscal, P. Maireles-Torres, M. Ojeda, I. Sádaba, M. López Granados, *Energy Environ. Sci.* **2016**, *9*, 1144–1189; b) S. U. Raut, P. R. Bhagat, *Fuel* **2021**, *303*, 121154.
[10] Y. Yang, Y. Wang, S. Li, X. Shen, B. Chen, H. Liu, B. Han, *Green Chem.* **2020**, *22*, 4937–4942.
[11] A. Dunbabin, F. Subrizi, J. M. Ward, T. D. Sheppard, H. C. Hailes, *Green Chem.* **2017**, *19*, 397–404.
[12] J. B. Binder, R. T. Raines, *J. Am. Chem. Soc.* **2009**, *131*, 1979–1985.
[13] Y. Román-Leshkov, J. N. Chheda, J. A. Dumesic, *Science* **2006**, *312*, 1933–1937.
[14] H. Chang, I. Bajaj, A. H. Motagamwala, A. Somasundaram, G. W. Huber, C. T. Maravelias, J. A. Dumesic, *Green Chem.* **2021**, *23*, 3277–3288.
[15] R. M. Abdilla-Santes, W. Guo, P. C. A. Bruijnincx, J. Yue, P. J. Deuss, H. J. Heeres, *ChemSusChem* **2019**, *12*, 4304–4312.
[16] B. Saha, M. M. Abu-Omar, *Green Chem.* **2014**, *16*, 24–38.
[17] S. P. Teong, G. Yi, Y. Zhang, *Green Chem.* **2014**, *16*, 2015–2026.
[18] P. J. Deuss, K. Barta, J. G. de Vries, *Catal. Sci. Technol.* **2014**, *4*, 1174–1196.
[19] R. A. Sheldon, *Phil. Trans. R. Soc. A* **2020**, *378*, 20190274.
[20] R.-J. Van Putten, J. C. van der Waal, E. de Jong, C. B. Rasrendra, H. J. Heeres, J. G. De Vries, *Chem. Rev.* **2013**, *113*, 1499–1597.
[21] J. G. de Vries in *Heterocyclic Chemistry in the 21st Century: A Tribute to Alan Katritzky, Advances in Heterocyclic Chemistry, Vol. 121* (Eds.: E. F. V. Scriven, C. A. Ramsden), Chapter 8: Green Syntheses of Heterocycles of Industrial Importance. 5-Hydroxymethylfurfural as a Platform Chemical, Academic Press (Elsevier), Cambridge, MA, **2017**, pp. 247–293.
[22] J. J. Bozell, G. R. Petersen, *Green Chem.* **2010**, *12*, 539–554.
[23] T. Werpy, G. Petersen in *Top Value-Added Chemicals from Biomass: Volume I – Results of Screening for Potential Candidates from Sugars and Synthesis Gas.* United States: N. p., **2004**.
[24] A. A. Rosatella, S. P. Simeonov, R. F. M. Frade, C. A. Afonso, *Green Chem.* **2011**, *13*, 754–793.
[25] F. Weigang, V. Charlie, Q. Yves, P. Florence, *Curr. Org. Synth.* **2019**, *16*, 583–614.
[26] L. Hu, L. Lin, Z. Wu, S. Zhou, S. Liu, *Renew. Sust. Energ. Rev.* **2017**, *74*, 230–257.
[27] A. Lancien, R. Wojcieszak, E. Cuvelier, M. Duban, P. Dhulster, S. Paul, F. Dumeignil, R. Froidevaux, E. Heuson, *ChemCatChem* **2021**, *13*, 247–259.
[28] a) J. Long, Y. Xu, W. Zhao, H. Li, S. Yang, *Front. Chem.* **2019**, *7*, 529; b) T. Schwob, P. Kunnas, N. D. Jonge, C. Papp, H.-P. Steinrück, R. Kempe, *Sci. Adv.* **2019**, *5*, eaav3680.
[29] X. Kong, Y. Zhu, Z. Fang, J. A. Kozinski, I. S. Butler, L. Xu, H. Song, X. Wei, *Green Chem.* **2018**, *20*, 3657–3682.
[30] a) C. Xu, E. Paone, D. Rodríguez-Padrón, R. Luque, F. Mauriello, *Chem. Soc. Rev.* **2020**, *49*, 4273–4306; b) S. Li, M. Dong, J. Yang, X. Cheng, X. Shen, S. Liu, Z.-Q. Wang, X.-Q. Gong, H. Liu, B. Han, *Nat. Commun.* **2021**, *12*, 584.
[31] S. Kim, E. E. Kwon, Y. T. Kim, S. Jung, H. J. Kim, G. W. Huber, J. Lee, *Green Chem.* **2019**, *21*, 3715–3743.
[32] a) A. Salazar, P. Hünemörder, J. Rabeah, A. Quade, R. V. Jagadeesh, E. Mejia, *ACS Sustainable Chem. Eng.* **2019**, *7*, 12061–12068; b) S. Verma, M. N. Nadagouda, R. S. Varma, *Sci. Rep.* **2017**, *7*, 13596.
[33] D. L. J. Pinheiro, M. Nielsen, *Catalysts* **2021**, *11*, 558.
[34] G. Liang, A. Wang, L. Li, G. Xu, N. Yan, T. Zhang, *Angew. Chem. Int. Ed.* **2017**, *56*, 3050–3054; *Angew. Chem.* **2017**, *129*, 3096–3100.
[35] J. J. Roylance, K.-S. Choi, *Green Chem.* **2016**, *18*, 5412–5417.
[36] K. Murugesan, T. Senthamarai, V. G. Chandrashekhar, K. Natte, P. C. J. Kamer, M. Beller, R. V. Jagadeesh, *Chem. Soc. Rev.* **2020**, *49*, 6273–6328.
[37] a) T. Irrgang, R. Kempe, *Chem. Rev.* **2020**, *120*, 9583–9674; b) O. I. Afanasyev, E. Kuchuk, D. L. Usanov, D. Chusov, *Chem. Rev.* **2019**, *119*, 11857–11911.
[38] a) S. A. Lawrence in *Amines: Synthesis, Properties and Applications*, Cambridge University Press, **2004**; b) A. Ricci in *Amino Group Chemistry: From Synthesis to the Life Sciences*, Wiley-VCH, **2008**; c) https://njardarson.lab.arizona.edu/sites/njardarson.lab.arizona.edu/files/Top%20200%20Pharmaceuticals%20By%20Retail%20Sales%202020V3.pdf.
[39] R. V. Jagadeesh, K. Murugesan, A. S. Alshammari, H. Neumann, M–M. Pohl, J. Radnik, M. Beller, *Science* **2017**, *358*, 326–332.
[40] W. Chen, Y. Jiang, Y. Sun, Y. Wang, Z. Li, X. Wang, X. Zeng, S. Liu, L. Lin, *J. Biobased Mater. Bioenergy* **2016**, *10*, 378–384.
[41] A. Feriani, G. Gaviraghi, G. Toson, M. Mor, A. Barbieri, E. Grana, C. Boselli, M. Guarneri, D. Simoni, S. Manfredini, *J. Med. Chem.* **1994**, *37*, 4278–4287.
[42] M.-S. Michael, B. J. Price, B. John, W. John, US Pat, 4279911, 1981.
[43] M.-L. Yang, Y.-X. Wu, Y. Liu, J.-J. Qiu, C.-M. Liu, *Polym. Chem.* **2019**, *10*, 6217–6226.
[44] Z. Xu, P. Yan, W. Xu, S. Jia, Z. Xia, B. Chung, Z. C. Zhang, *RSC Adv.* **2014**, *4*, 59083–59087.
[45] M. Chatterjee, T. Ishizaka, H. Kawanami, *Green Chem.* **2016**, *18*, 487–496.
[46] A. L. Nuzhdin, P. A. Simonov, G. A. Bukhtiyarova, I. V. Eltsov, V. I. Bukhtiyarov, *J. Mol. Catal.* **2021**, *499*, 111297.
[47] V. V. Karve, D. T. Sun, O. Trukhina, S. Yang, E. Oveisi, J. Luterbacher, W. L. Queen, *Green Chem.* **2020**, *22*, 368–378.
[48] A. García-Ortiz, J. D. Vidal, M. J. Climent, P. Concepción, A. Corma, S. Iborra, *ACS Sustainable Chem. Eng.* **2019**, *7*, 6243–6250.
[49] D. Deng, Y. Kita, K. Kamata, M. Hara, *ACS Sustainable Chem. Eng.* **2019**, *7*, 4692–4698.

[50] C. Dong, H. Wang, H. Du, J. Peng, Y. Cai, S. Guo, J. Zhang, C. Samart, M. Ding, *J. Mol. Catal.* **2020**, *482*, 110755.
[51] M.-M. Zhu, L. Tao, Q. Zhang, J. Dong, Y.-M. Liu, H.-Y. He, Y. Cao, *Green Chem.* **2017**, *19*, 3880–3887.
[52] Z. Wei, Y. Cheng, K. Zhou, Y. Zeng, E. Yao, Q. Li, Y. Liu, Y. Sun, *ChemSusChem* **2021**, *14*, 2308–2312.
[53] a) H. Qi, J. Yang, F. Liu, L. Zhang, J. Yang, X. Liu, L. Li, Y. Su, Y. Liu, R. Hao, A. Wang, T. Zhang, *Nat. Commun.* **2021**, *12*, 3295; b) M. Elfinger, T. Schönauer, S. L. J. Thomä, R. Stäglich, M. Drechsler, M. Zobel, J. Senker, R. Kempe, *ChemSusChem* **2021**, *14*, 2360–2366; c) T. Schwob, R. Kempe, *Angew. Chem. Int. Ed.* **2016**, *55*, 15175–15179; *Angew. Chem.* **2016**, *128*, 15400–15404.
[54] A. L. Nuzhdin, M. V. Bukhtiyarova, V. I. Bukhtiyarov, *Molecules* **2020**, *25*, 4771.
[55] H. Yuan, B. T. Kusema, Z. Yan, S. Streiff, F. Shi, *RSC Adv.* **2019**, *9*, 38877–38881.
[56] H. Yuan, J–P. Li, F. Su, Z. Yan, B. T. Kusema, S. Streiff, Y. Huang, M. Pera-Titus, F. Shi, *ACS Omega* **2019**, *4*, 2510–2516.
[57] W. Chen, Y. Sun, J. Du, Z. Si, X. Tang, X. Zeng, L. Lin, S. Liu, T. Lei, *J. Chem. Technol. Biotechnol.* **2018**, *93*, 3028–3034.
[58] G. Chieffi, M. Braun, D. Esposito, *ChemSusChem* **2015**, *8*, 3590–3594.
[59] H. Ishikawa, M. Sheng, A. Nakata, K. Nakajima, S. Yamazoe, J. Yamasaki, S. Yamaguchi, T. Mizugaki, T. Mitsudome, *ACS Catal.* **2021**, *11*, 750–757.
[60] a) L. Liu, A. Corma, *Chem. Rev.* **2018**, *118*, 4981–5079; b) M. B. Gawande, P. S. Branco, R. S. Varma, *Chem. Soc. Rev.* **2013**, *42*, 3371–3393.
[61] a) K. J. Lee, J. H. Lee, S. Jeoung, H. R. Moon, *Acc. Chem. Res.* **2017**, *50*, 2684–2692; b) K. Shen, X. Chen, J. Chen, Y. Li, *ACS Catal.* **2016**, *6*, 5887–5903.
[62] G. Hahn, P. Kunnas, N. de Jonge, R. Kempe, *Nat. Catal.* **2019**, *2*, 71–77.
[63] R. V. Jagadeesh, A.-E. Surkus, H. Junge, M.-M. Pohl, J. Radnik, J. Rabeah, H. Huan, V. Schünemann, A. Brückner, M. Beller, *Science* **2013**, *342*, 1073–1076.
[64] K. Murugesan, T. Senthamarai, A. S. Alshammari, R. M. Altamimi, C. Kreyenschulte, M.-M. Pohl, H. Lund, R. V. Jagadeesh, M. Beller, *ACS Catal.* **2019**, *9*, 8581–8591.
[65] K. Murugesan, V. G. Chandrashekhar, C. Kreyenschulte, M. Beller, R. V. Jagadeesh, *Angew. Chem. Int. Ed.* **2020**, *59*, 17408–17412; *Angew. Chem.* **2020**, *132*, 17561–17565.
[66] A. Amri, X. F. Duan, C.-Y. Yin, Z.-T. Jiang, M. M. Rahman, T. Pryor, *Appl. Surf. Sci.* **2013**, *275*, 127–135.
[67] P. Lazar, R. Mach, M. Otyepka, *J. Phys. Chem. C* **2019**, *123*, 10695–10702.
[68] Y. Nosaka, M. Matsushita, J. Nishino, A. Y. Nosaka, *Sci. Technol. Adv. Mater.* **2005**, *6*, 143–148.
[69] A. P. Taylor, R. P. Robinson, Y. M. Fobian, D. C. Blakemore, L. H. Jones, O. Fadeyi, *Org. Biomol. Chem.* **2016**, *14*, 6611–6637.
[70] A. Gandini, M. N. Belgacem, *Prog. Polym. Sci.* **1997**, *22*, 1203–1379.
[71] C. Moreau, M. N. Belgacem, A. Gandini, *Top. Catal.* **2004**, *27*, 11–30.

Manuscript received: August 20, 2021
Revised manuscript received: October 28, 2021
Accepted manuscript online: October 29, 2021
Version of record online: ■■, ■■■

FULL PAPERS

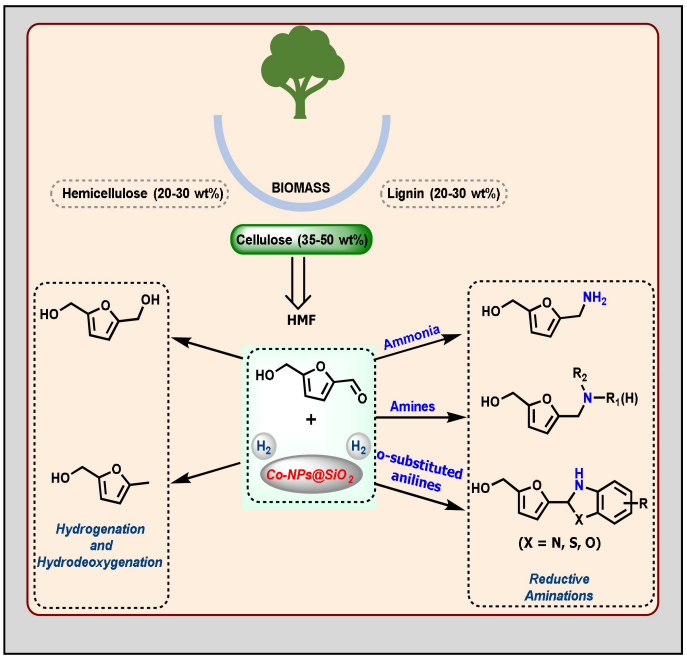

*V. G. Chandrashekhar, Dr. K. Natte, Dr. A. M. Alenad, Dr. A. S. Alshammari, Dr. C. Kreyenschulte, Prof. Dr. R. V. Jagadeesh**

Valorization of HMF by cobalt-nanoparticles catalyzed reductive amination, hydrogenation and hydrodeoxygenation processes produce bio-based amines and heterocycles as well as 2,5-bis(hydroxymethyl)furan, (5-methylfuran-2-yl)methanol.

How to cite: *Angew. Chem. Int. Ed.* **2020**, *59*, 17408–17412
International Edition: doi.org/10.1002/anie.202004674
German Edition: doi.org/10.1002/ange.202004674

Nanoparticle Catalysts

A General Catalyst Based on Cobalt Core–Shell Nanoparticles for the Hydrogenation of N-Heteroarenes Including Pyridines

Kathiravan Murugesan, Vishwas G. Chandrashekhar, Carsten Kreyenschulte, Matthias Beller, and Rajenahally V. Jagadeesh**

In memory of Professors B. S. Sheshadri and S. M. Mayanna, former Chairmen of the Chemistry Department, Bangalore University, India

Abstract: *Herein, we report the synthesis of specific silica-supported Co/Co_3O_4 core–shell based nanoparticles prepared by template synthesis of cobalt-pyromellitic acid on silica and subsequent pyrolysis. The optimal catalyst material allows for general and selective hydrogenation of pyridines, quinolines, and other heteroarenes including acridine, phenanthroline, naphthyridine, quinoxaline, imidazo[1,2-a]pyridine, and indole under comparably mild reaction conditions. In addition, recycling of these Co nanoparticles and their ability for dehydrogenation catalysis are showcased.*

The catalytic hydrogenation of N-heteroarenes represents an atom-efficient methodology to access aliphatic cyclic amines, which are of interest for basic organic synthesis, drug discovery, material sciences, and alternative energy technologies.[1] In particular, piperidines and 1,2,3,4-tetrahydroquinolines are integral parts of pharmaceuticals, agrochemicals, biomolecules, and natural products.[1a,c,g] For these products, the catalytic hydrogenation of pyridines[2,3] and quinolines[3n,4–7] offers a straightforward approach compared to typically applied multistep procedures.[1a,c] However, catalyst deactivation might occur easily due to the interaction of nitrogen moiety of substrates or products with the supported metal centers.[8] In this respect, the hydrogenation of pyridines is known to be particularly challenging. Hence, this reaction mainly relies on precious-metal-based catalysts.[2a,-b,e–g,3e,n] In addition, a cobalt-based heterogeneous catalyst is known; however, it requires drastic conditions limiting its applicability (160 °C, 60 bar H_2).[3o] On the other hand, for the facile hydrogenation of quinolones and related N-heteroarenes, several non-noble homogeneous[5] and heterogeneous[7] catalysts based on Fe,[7a] Co,[7b–e,h] Ni,[7f] and Mn[7i] have been successfully developed complementary to state-of-the-art precious metal catalysts.[6] Despite these achievements, still the development of a general and selective non-noble metal based catalyst for the hydrogenation of N-heteroarenes including pyridines under milder reaction conditions continues to be of scientific interest and is challenging.

The preparation of active supported nanoparticles depends strongly on the use of appropriate precursors and optimized preparation techniques. Compared to the thermal or chemical reduction of simple metal salts,[9] the template synthesis of metal–organic frameworks (MOFs) or coordination polymers (CPs) on a solid support and subsequent pyrolysis offers an alternative approach, which has become highly attractive in recent years.[10] Advantageously, a plethora of relatively inexpensive and stable organic ligands are commercially available to prepare MOFs or CPs, which can be used as precursors to synthesize diverse nanomaterials. As an example, we[10d,i] and others[10e–h] reported the use of cobalt MOFs and CPs, obtained from diamines and di- or tetracarboxylic acids, as appropriate precursors for the preparation of supported nanoparticles for redox reactions. Based on this work, herein we report the preparation of silica-supported Co/Co_3O_4 core–shell nanoparticles by immobilization and pyrolysis of cobalt-pyromellitic acid template on commercial silica (Figure 1). Catalytic investigations revealed the superiority of these novel supported nanoparticles for the hydrogenation of pyridines, quinolines, and other different N-heteroarenes.

Aromatic carboxylic acids are key building blocks for the formation of MOFs and metal-containing coordination polymers (MCPs).[11] Based on their use, new innovative materials have been introduced in the past two decades, which showed interesting performances, especially in separation technologies.[11] In contrast, relatively few applications of such materials have been demonstrated in modern catalysis, despite significant efforts.[10d,i,e–h] On the other hand, it has been demonstrated that pyrolysis of MOFs or MCPs can lead to stable supported nanoparticles with unique structures. For example, the pyrolysis of cobalt-MOF on carbon and silica led

Figure 1. Preparation of cobalt nanoparticles by pyrolysis of Co-carboxylic acid templates on SiO_2.

[*] Dr. K. Murugesan, V. G. Chandrashekhar, Dr. C. Kreyenschulte, Prof. Dr. M. Beller, Dr. R. V. Jagadeesh
Leibniz-Institut für Katalyse e. V.
Albert-Einstein-Str. 29a, 18059 Rostock (Germany)
E-mail: matthias.beller@catalysis.de
jagadeesh.rajenahally@catalysis.de
Supporting information and the ORCID identification number(s) for the author(s) of this article can be found under: https://doi.org/10.1002/anie.202004674.

to general reductive amination and arene hydrogenation catalysts.[10d,i]

Based on this and related work,[10d,i] we became interested in studying the behavior of supported cobalt nanoparticles prepared from cobalt salts of different carboxylic acids. For this purpose, a cobalt salt was mixed with a set of four model carboxylic acids, which have been used as common organic linkers for the preparation of MOFs. Specifically, benzoic acid, terephthalic acid, trimesic acid (1,3,5-benzenetricarboxylic acid), or pyromellitic acid (1,2,4,5-benzenetetracarboxylic acid) were stirred with cobalt(II) nitrate hexahydrate in DMF at 150 °C.[10i] To these in situ generated materials, Aerosil silica was added and the whole mixture was stirred again at the same temperature for another 4–5 h. After slow evaporation of the solvent, followed by drying, the templated materials (Co-carboxylic acid@SiO_2) were obtained as colored solids. Subsequent pyrolysis at 800 °C under argon for 2 h led to different cobalt nanoparticles supported on silica (Figure 1).

All the materials were tested for liquid-phase hydrogenation of nicotinamide (**1**) at 120 °C and 50 bar of hydrogen. This benchmark reaction was chosen due to the difficult nature of hydrogenation of pyridines (vide supra) and the intrinsic chemoselectivity problem. Moreover, due to the biochemical relevance of nicotinamide as part of coenzymes, its catalytic hydrogenation is also considered to be interesting.

Among the prepared materials, the cobalt-pyromellitic acid on silica at 800 °C constitutes the most active and selective catalyst (Co-pyromellitic acid@SiO_2-800), which allowed for the complete hydrogenation of nicotinamide (**1**) and produced the desired product, nipecotamide (**2**) in 97 % yield. Notably, there is strong influence on catalysis depending on the carboxylic acid linker used. Benzoic acid resulted in a completely inactive material, while other di-, tri-, and tetracarboxylic acids gave active catalysts (Table 1, entries 1–4). Comparison experiments in the presence of simple cobalt(II) nitrate or a mixture of it and pyromellitic acid were carried out and showed that both are inactive, too. Similarly, nonpyrolyzed and pyrolyzed cobalt(II) nitrate on silica as well as nonpyrolyzed Co-pyromellitic acid on silica were also not active (Table 1, entries 6–8).

Table 1: Hydrogenation of nicotinamide: activity of different cobalt catalysts.

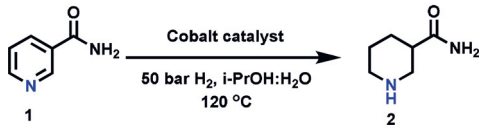

Entry	Catalyst	Conv. [%]	Yield [%]
1[a]	Co-benzoic acid@SiO_2-800	< 3	< 2
2[a]	Co-terephthalic acid @SiO_2-800	65	63
3[a]	Co- trimesic acid @SiO_2-800	75	73
4[a]	Co-pyromellitic acid@SiO_2	> 99	97
5[a]	$Co(NO_3)_2$@SiO_2-800	< 2	< 1
6[a]	Co-pyromellitic acid@SiO_2	< 2	< 1
7[a]	$Co(NO_3)_2$@SiO_2	–	–
8[b]	$Co(NO_3)_2 \cdot 6H_2O$ + pyromellitic acid	–	–
9[b]	$Co(NO_3)_2 \cdot 6H_2O$	–	–

Reaction conditions: [a] 0.5 mmol nicotinamide, weight of catalyst corresponds to 40 mg catalyst (7.5 mol% Co), 50 bar H_2, 3 mL solvent (i-PrOH: H_2O; 2:1), 120 °C, 24 h. Yields were determined by GC using *n*-hexadecane as standard. [b] 0.5 mmol substrate, 7.5 mol% Co-$(NO_3)_2 \cdot 6H_2O$, 7.5 mol% of pyromellitic acid, 50 bar H_2, 3 mL solvent (i-PrOH:H_2O; 2:1), 120 °C, 24 h yields were determined by GC using *n*-hexadecane standard.

To understand the superior activity of Co-pyromellitic acid@SiO_2-800, detailed structural characterization of this material was performed using X-ray powder diffraction (XRD), scanning transmission electron microscopy (STEM), X-ray photoelectron spectroscopy (XPS), and Brunauer–Emmett–Teller (BET) techniques.[10i] XRD analysis of Co-pyromellitic acid@SiO_2-800 showed the presence of both metallic and oxidic cobalt phases (Co and Co_3O_4) (Figure S1). In the case of $Co(NO_3)_2$@SiO_2-800, only the presence of the oxidic cobalt phase was observed (Figure S2).

STEM analysis of the most active catalyst also revealed the formation of particles consisting of metallic Co and different Co oxides (Co_3O_4) with sizes in the range of about 10–20 nm (Figure 2 and Figures S3 and S4). Many of these particles are of core–shell structure, where the core consists of metallic Co with an oxide shell as indicated by HAADF (Figure 2, center and right). The oxide shells and purely oxide particles are usually polycrystalline. Next, XPS analysis of the most active catalyst was performed to identify the nature of cobalt species at the surface of the material. More specifically, deconvolution of Co 2p peaks confirmed the presence of mixed oxidation for Co (Co 2p3/2 in Co^0: 778.49 eV; Co^{2+}: 779.92 eV) (Figure S9). Although a peak for Co^{3+} could not be deconvoluted, the presence of strong satellite peaks at 786.43 eV and 802.20 eV is indicative for multiple oxidized Co species, as satellite peaks arise due to spin–spin interactions of different Co species.[12]

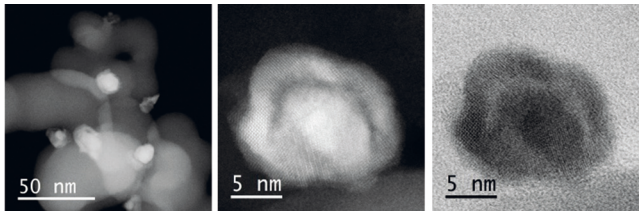

Figure 2. STEM-HAADF (left and center) and -ABF (right) images of Co-pyromellitic acid @SiO_2-800 catalyst.

With a successful catalyst for the hydrogenation of nicotinamide in hand, we explored its applicability for different N-heteroarenes. As shown in Schemes 1–3, a series of substituted and functionalized pyridines and quinolines as well as other heteroarenes underwent complete or partial hydrogenation to produce cycle aliphatic derivatives in good to excellent yields.

Noteworthy, simple pyridine was efficiently hydrogenated and produced the parent piperidine in excellent yield (product **5**). Substituted pyridines with both electron-donating and -withdrawing groups were hydrogenated to give the corresponding products in up to 94 % yields (Scheme 1). Interestingly, the catalyst system preferentially reduces the N-heteroarene ring in the presence of other reducible groups such as amide and ester (products **2**, **3**, **9**). Similarly, the presence of substituted arene rings is tolerated (products **10**–**12**).

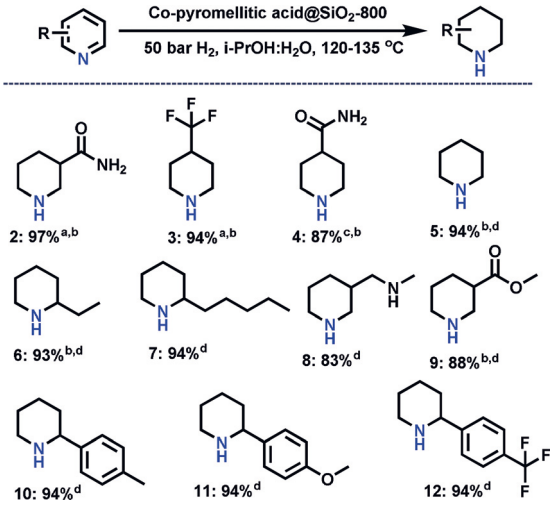

Scheme 1. Hydrogenation of pyridines catalyzed by Co-pyromellitic acid@SiO_2-800.[a] Reaction conditions: [a] 0.5 mmol substrate, 40 mg catalyst (7.5 mol% Co), 50 bar H_2, 3 mL (i-PrOH:H_2O; 2:1), 120 °C, 24 h, yields of isolated products. [b] Yields were determined by GC using *n*-hexadecane standard. [c] Same conditions as [a] but with 50 mg catalyst. [d] Same conditions as [a] but with 60 mg catalyst at 135 °C for 48 h.

Next, we applied this cobalt catalyst for the hydrogenation of quinolines (Scheme 2). As a result, nine quinolines were hydrogenated under comparably mild conditions (70 °C, 10 bar of hydrogen) and 1,2,3,4-tetrahydroquinolines were produced in up to 97% yield (products **13**, **15**, **17**, **19**, **21**, **22**, **24**, **25**, and **28**). Here, sensitive substituents (Br, Cl) and functional groups such as hydroxyl, ether, and ester groups were well tolerated (products **19**, **24**–**29**). Notably, some of the terahydroquinolines presented in Scheme 2 serve as precursors/intermediates for the preparation of bioactive molecules. Specifically, the preparation of products **14**, **16**, **18**, **20** and **29** resulted in 5-HT3 receptor antagonist, antitrypanosomal drug, tubulin polymerization inhibitor, flumequine, and tocopherol derivatives.

Following the hydrogenation of pyridines and quinolines, the reduction of other N-heteroarenes such as quinoxaline, indole, imidazo[1,2-*a*]pyridine, 1,5-naphthyridine, acridines, and phenanthroline was performed (Scheme 3). Again, in all these cases the N-heteroarene rings were selectively reduced and the corresponding partially reduced products were obtained in up to 97% yield.

To prove the synthetic utility and practicability of the general hydrogenation procedure, several reactions were completed on 0.5–1 g scale (Figure S11). In addition, this catalyst can be conveniently recycled and reused up to six times without significant loss in the activity or selectivity (Figure S12). STEM analysis of catalyst samples after one and seven reuses showed a partial re-dispersion of cobalt into a thin layer of Co-oxide on the surface of the support progressing with the number of uses (Figures S5–S8).

Finally, the optimal catalyst was also tested for the reverse dehydrogenation process. Because of the microreversibility of the individual catalytic steps, such a transformation should be also possible. Indeed, in presence of Co-pyromellitic acid@-

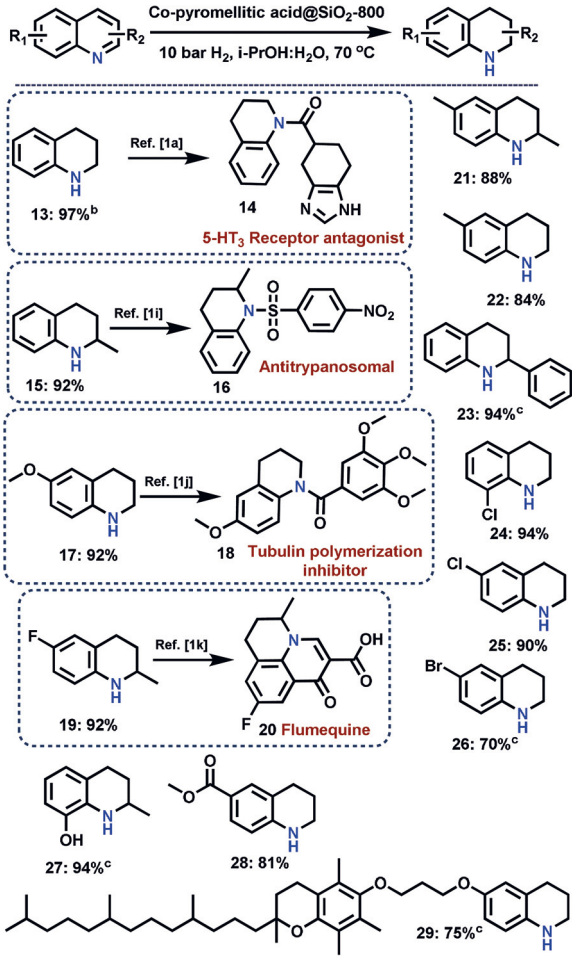

Scheme 2. Synthesis of tetrahydroquinolines catalyzed by Co-pyromellitic acid@SiO_2-800. Reaction conditions: [a] 0.5 mmol substrate, 50 mg Co-pyromellitic acid @SiO_2-800, (9 mol% Co), 10 bar H_2, 3 mL (i-PrOH:H_2O; 2:1), 70 °C, 24 h, yields of isolated products. [b] Yields were determined by GC using *n*-hexadecane standard. [c] Same conditions as [a] but at 120 °C with 30 bar H_2.

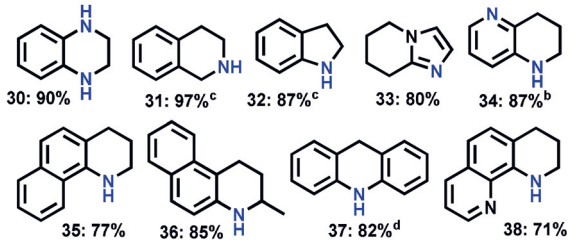

Scheme 3. Selective hydrogenation of different N-heteroarenes using Co-pyromellitic acid@SiO_2-800. Reaction conditions: [a] 0.5 mmol substrate, 50 mg Co-pyromellitic acid @SiO_2-800, 50 bar H_2, 3 mL (i-PrOH:H_2O; 2:1), 120 °C, 24 h, yields of isolated products. [b] Same conditions as [a] but at 135 °C and 48 h. [c] Yields were determined by GC using *n*-hexadecane standard. [d] Same conditions as [a] but using t-BuOH as solvent.

SiO_2-800, 2-methyl-1,2,3,4-tetrahydroquinoline underwent dehydrogenation and provided 2-methylquinoline in 93% yield (Scheme 4). Such reactions are of general interest in the context of liquid organic hydrogen carriers (LOHC) technologies.[13]

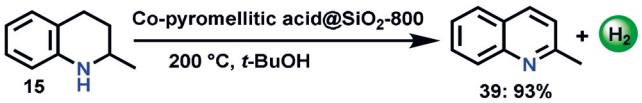

Scheme 4. Dehydrogenation reaction catalyzed by cobalt nanoparticles. Reaction conditions: 2 mmol substrate, 240 mg catalyst (11 mol% Co), 10 mL *t*-BuOH, 200 °C, 48 h, GC yield using *n*-hexadecane standard.

In conclusion, we report the preparation of novel supported Co/Co_3O_4 core–shell nanoparticles by template synthesis of Co-pyromellitic acid on silica and subsequent pyrolysis. These particles are shown to be active for general hydrogenation of variety of N-heteroarenes including pyridines, quinolines, acridine, phenanthroline, naphthyridine, quinoxaline, imidazo[1,2-*a*]pyridine, and indole. In addition, we believe this or similar catalysts also offer opportunities for other hydrogenation and dehydrogenation processes.

Acknowledgements

We gratefully acknowledge the support of the European Research Council (EU project 670986-NoNaCat) and the State of Mecklenburg-Vorpommern. Open access funding enabled and organized by Projekt DEAL.

Conflict of interest

The authors declare no conflict of interest.

Keywords: Co nanoparticles · hydrogenation · N-heteroarenes · pyridines · quinolines

[1] a) V. Sridharan, P. A. Suryavanshi, J. C. Menéndez, *Chem. Rev.* **2011**, *111*, 7157 – 7259; b) A. O'Byrne, P. Evans, *Tetrahedron* **2008**, *64*, 8067 – 8072; c) S. Källström, R. Leino, *Bioorg. Med. Chem.* **2008**, *16*, 601 – 635; d) R. P. Filho, C. M. de Souza Menezes, P. L. S. Pinto, G. A. Paula, C. A. Brandt, M. A. B. da Silveira, *Bioorg. Med. Chem.* **2007**, *15*, 1229 – 1236; e) R. Chen, X. Yang, H. Tian, X. Wang, A. Hagfeldt, L. Sun, *Chem. Mater.* **2007**, *19*, 4007 – 4015; f) K. W. Bentley, *Nat. Prod. Rep.* **2006**, *23*, 444 – 463; g) J. D. Scott, R. M. Williams, *Chem. Rev.* **2002**, *102*, 1669 – 1730; h) A. R. Katritzky, S. Rachwal, B. Rachwal, *Tetrahedron* **1996**, *52*, 15031 – 15070; i) R. J. Pagliero, S. Lusvarghi, A. B. Pierini, R. Brun, M. R. Mazzieri, *Bioorg. Med. Chem.* **2010**, *18*, 142 – 150; j) J.-P. Liou, Z.-Y. Wu, C.-C. Kuo, C.-Y. Chang, P.-Y. Lu, C.-M. Chen, H.-P. Hsieh, J.-Y. Chang, *J. Med. Chem.* **2008**, *51*, 4351 – 4355; k) J. Bálint, G. Egri, E. Fogassy, Z. Böcskei, K. Simon, A. Gajáry, A. Friesz, *Tetrahedron: Asymmetry* **1999**, *10*, 1079 – 1087.

[2] a) M. P. Wiesenfeldt, Z. Nairoukh, T. Dalton, F. Glorius, *Angew. Chem. Int. Ed.* **2019**, *58*, 10460 – 10476; *Angew. Chem.* **2019**, *131*, 10570 – 10586; b) Z. Nairoukh, M. Wollenburg, C. Schlepphorst, K. Bergander, F. Glorius, *Nat. Chem.* **2019**, *11*, 264 – 270; c) T. Mahdi, J. N. del Castillo, D. W. Stephan, *Organometallics* **2013**, *32*, 1971 – 1978; d) Y. Liu, H. Du, *J. Am. Chem. Soc.* **2013**, *135*, 12968 – 12971; e) W.-J. Tang, J. Tan, L.-J. Xu, K.-H. Lam, Q.-H. Fan, A. S. C. Chan, *Adv. Synth. Catal.* **2010**, *352*, 1055 – 1062; f) X.-B. Wang, W. Zeng, Y.-G. Zhou, *Tetrahedron Lett.* **2008**, *49*, 4922 – 4924; g) M. Studer, C. Wedemeyer-Exl, F. Spindler, H.-U. Blaser, *Monatsh. Chem.* **2000**, *131*, 1335 – 1343.

[3] a) M. Freifelder, *Advances in Catalysis*, *Vol. 14* (Eds.: D. D. Eley, H. Pines, P. B. Weisz), Academic Press, New York, **1963**, pp. 203 – 253; b) M. Freifelder, R. M. Robinson, G. R. Stone, *J. Org. Chem.* **1962**, *27*, 284 – 286; c) L. Hegedűs, V. Háda, A. Tungler, T. Máthé, L. Szepesy, *Appl. Catal. A* **2000**, *201*, 107 – 114; d) M. Maruoka, *Nippon Kagaku Zasshi* **1961**, *82*, 1257 – 1262; e) G. N. Walker, *J. Org. Chem.* **1962**, *27*, 2966 – 2967; f) H. Yasui, H. Ochi, *Aromatikkusu* **1969**, *21*, 264 – 267; g) M. Freifelder, G. R. Stone, *J. Org. Chem.* **1961**, *26*, 3805 – 3808; h) M. Freifelder, *J. Org. Chem.* **1964**, *29*, 2895 – 2898; i) H. U. Blaser, H. Hönig, M. Studer, C. Wedemeyer-Exl, *J. Mol. Catal. A* **1999**, *139*, 253 – 257; j) S. A. Raynor, J. M. Thomas, R. Raja, B. F. G. Johnson, R. G. Bell, M. D. Mantle, *Chem. Commun.* **2000**, 1925 – 1926; k) F. Glorius, N. Spielkamp, S. Holle, R. Goddard, C. W. Lehmann, *Angew. Chem. Int. Ed.* **2004**, *43*, 2850 – 2852; *Angew. Chem.* **2004**, *116*, 2910 – 2913; l) L. Piras, E. Genesio, C. Ghiron, M. Taddei, *Synlett* **2008**, 1125 – 1128; m) M. Irfan, E. Petricci, T. N. Glasnov, M. Taddei, C. O. Kappe, *Eur. J. Org. Chem.* **2009**, 1327 – 1334; n) A. Karakulina, A. Gopakumar, İ. Akçok, B. L. Roulier, T. LaGrange, S. A. Katsyuba, S. Das, P. J. Dyson, *Angew. Chem. Int. Ed.* **2016**, *55*, 292 – 296; *Angew. Chem.* **2016**, *128*, 300 – 304; o) F. Chen, W. Li, B. Sahoo, C. Kreyenschulte, G. Agostini, H. Lund, K. Junge, M. Beller, *Angew. Chem. Int. Ed.* **2018**, *57*, 14488 – 14492; *Angew. Chem.* **2018**, *130*, 14696 – 14700.

[4] a) G. E. Dobereiner, A. Nova, N. D. Schley, N. Hazari, S. J. Miller, O. Eisenstein, R. H. Crabtree, *J. Am. Chem. Soc.* **2011**, *133*, 7547 – 7562; b) J. John, C. Wilson-Konderka, C. Metallinos, *Adv. Synth. Catal.* **2015**, *357*, 2071 – 2081; c) M. Rosales, L. J. Bastidas, B. González, R. Vallejo, P. J. Baricelli, *Catal. Lett.* **2011**, *141*, 1305 – 1310; d) Á. Vivancos, M. Beller, M. Albrecht, *ACS Catal.* **2018**, *8*, 17 – 21; e) T. Wang, L.-G. Zhuo, Z. Li, F. Chen, Z. Ding, Y. He, Q.-H. Fan, J. Xiang, Z.-X. Yu, A. S. C. Chan, *J. Am. Chem. Soc.* **2011**, *133*, 9878 – 9891; f) W.-B. Wang, S.-M. Lu, P.-Y. Yang, X.-W. Han, Y.-G. Zhou, *J. Am. Chem. Soc.* **2003**, *125*, 10536 – 10537; g) J. Wu, J. H. Barnard, Y. Zhang, D. Talwar, C. M. Robertson, J. Xiao, *Chem. Commun.* **2013**, *49*, 7052 – 7054.

[5] a) R. Adam, J. R. Cabrero-Antonino, A. Spannenberg, K. Junge, R. Jackstell, M. Beller, *Angew. Chem. Int. Ed.* **2017**, *56*, 3216 – 3220; *Angew. Chem.* **2017**, *129*, 3264 – 3268; b) S. Chakraborty, W. W. Brennessel, W. D. Jones, *J. Am. Chem. Soc.* **2014**, *136*, 8564 – 8567; c) R. Xu, S. Chakraborty, H. Yuan, W. D. Jones, *ACS Catal.* **2015**, *5*, 6350 – 6354.

[6] a) L. Bai, X. Wang, Q. Chen, Y. Ye, H. Zheng, J. Guo, Y. Yin, C. Gao, *Angew. Chem. Int. Ed.* **2016**, *55*, 15656 – 15661; *Angew. Chem.* **2016**, *128*, 15885 – 15890; b) N. A. Beckers, S. Huynh, X. Zhang, E. J. Luber, J. M. Buriak, *ACS Catal.* **2012**, *2*, 1524 – 1534; c) M. Fang, R. A. Sánchez-Delgado, *J. Catal.* **2014**, *311*, 357 – 368; d) Y. Gong, P. Zhang, X. Xu, Y. Li, H. Li, Y. Wang, *J. Catal.* **2013**, *297*, 272 – 280; e) Y.-G. Ji, K. Wei, T. Liu, L. Wu, W.-H. Zhang, *Adv. Synth. Catal.* **2017**, *359*, 933 – 940; f) H. Konnerth, M. H. G. Prechtl, *Green Chem.* **2017**, *19*, 2762 – 2767; g) M. Niu, Y. Wang, P. Chen, D. Du, J. Jiang, Z. Jin, *Catal. Sci. Technol.* **2015**, *5*, 4746 – 4749; h) H. Norifumi, T. Yusuke, H. Takayoshi, S. Shogo, M. Takato, M. Tomoo, J. Koichiro, K. Kiyotomi, *Chem. Lett.* **2010**, *39*, 832 – 834; i) D. Ren, L. He, L. Yu, R.-S. Ding, Y.-M. Liu, Y. Cao, H.-Y. He, K.-N. Fan, *J. Am. Chem. Soc.* **2012**, *134*, 17592 – 17598; j) X. Wang, W. Chen, L. Zhang, T. Yao, W. Liu, Y. Lin, H. Ju, J. Dong, L. Zheng, W. Yan, X. Zheng, Z. Li, X. Wang, J. Yang, D. He, Y. Wang, Z. Deng, Y. Wu, Y. Li, *J. Am. Chem. Soc.* **2017**, *139*, 9419 – 9422; k) T.-N. Ye, J. Li, M. Kitano, H. Hosono, *Green Chem.* **2017**, *19*, 749 – 756; l) S. Zhang, Z. Xia, T. Ni, Z. Zhang, Y. Ma, Y. Qu, *J. Catal.* **2018**, *359*, 101 – 111; m) Y. Zhang, J. Zhu, Y.-T. Xia, X.-T. Sun, L. Wu, *Adv. Synth. Catal.* **2016**, *358*, 3039 – 3045.

[7] a) B. Sahoo, C. Kreyenschulte, G. Agostini, H. Lund, S. Bachmann, M. Scalone, K. Junge, M. Beller, *Chem. Sci.* **2018**, *9*, 8134 – 8141; b) I. Sorribes, L. Liu, A. Doménech-Carbó, A. Corma, *ACS Catal.* **2018**, *8*, 4545 – 4557; c) Z. Wei, Y. Chen, J. Wang, D. Su, M. Tang, S. Mao, Y. Wang, *ACS Catal.* **2016**, *6*, 5816 – 5822; d) F. Chen, A.-E. Surkus, L. He, M.-M. Pohl, J. Radnik, C. Topf, K. Junge, M. Beller, *J. Am. Chem. Soc.* **2015**, *137*, 11718 – 11724; e) J. Li, G. Liu, X. Long, G. Gao, J. Wu, F. Li, *J. Catal.* **2017**, *355*, 53 – 62; f) C. Liu, Z. Rong, Z. Sun, Y. Wang, W. Du, Y. Wang, L. Lu, *RSC Adv.* **2013**, *3*, 23984 – 23988; g) W. M. Czaplik, J.-M. Neudörfl, A. J. von Wangelin, *Green Chem.* **2007**, *9*, 1163 – 1165; h) P. Ji, K. Manna, Z. Lin, A. Urban, F. X. Greene, G. Lan, W. Lin, *J. Am. Chem. Soc.* **2016**, *138*, 12234 – 12242; i) V. Papa, Y. Cao, A. Spannenberg, K. Junge, M. Beller, *Nat. Catal.* **2020**, *3*, 135 – 142.

[8] a) D.-S. Wang, Q.-A. Chen, S.-M. Lu, Y.-G. Zhou, *Chem. Rev.* **2012**, *112*, 2557 – 2590; b) Y.-G. Zhou, *Acc. Chem. Res.* **2007**, *40*, 1357 – 1366.

[9] a) P. Munnik, P. E. de Jongh, K. P. de Jong, *Chem. Rev.* **2015**, *115*, 6687 – 6718; b) M. Sankar, N. Dimitratos, P. J. Miedziak, P. P. Wells, C. J. Kiely, G. J. Hutchings, *Chem. Soc. Rev.* **2012**, *41*, 8099 – 8139; c) Y. Zhang, X. Cui, F. Shi, Y. Deng, *Chem. Rev.* **2012**, *112*, 2467 – 2505.

[10] a) R. V. Jagadeesh, A.-E. Surkus, H. Junge, M.-M. Pohl, J. Radnik, J. Rabeah, H. Huan, V. Schünemann, A. Brückner, M. Beller, *Science* **2013**, *342*, 1073 – 1076; b) L. He, F. Weniger, H. Neumann, M. Beller, *Angew. Chem. Int. Ed.* **2016**, *55*, 12582 – 12594; *Angew. Chem.* **2016**, *128*, 12770 – 12783; c) G. Hahn, P. Kunnas, N. de Jonge, R. Kempe, *Nat. Catal.* **2019**, *2*, 71 – 77; d) R. V. Jagadeesh, K. Murugesan, A. S. Alshammari, H. Neumann, M.-M. Pohl, J. Radnik, M. Beller, *Science* **2017**, *358*, 326 – 332; e) S. Dang, Q.-L. Zhu, Q. Xu, *Nat. Rev. Mater.* **2017**, *3*, 17075; f) K. Shen, X. Chen, J. Chen, Y. Li, *ACS Catal.* **2016**, *6*, 5887 – 5903; g) K. J. Lee, J. H. Lee, S. Jeoung, H. R. Moon, *Acc. Chem. Res.* **2017**, *50*, 2684 – 2692; h) M. Hu, J. Reboul, S. Furukawa, N. L. Torad, Q. Ji, P. Srinivasu, K. Ariga, S. Kitagawa, Y. Yamauchi, *J. Am. Chem. Soc.* **2012**, *134*, 2864 – 2867; i) K. Murugesan, T. Senthamarai, A. S. Alshammari, R. M. Altamimi, C. Kreyenschulte, M.-M. Pohl, H. Lund, R. V. Jagadeesh, M. Beller, *ACS Catal.* **2019**, *9*, 8581 – 8591; j) B. Guan, A. Kushima, L. Yu, S. Li, J. Li, X. W. Lou, *Adv. Mater.* **2017**, *29*, 1605902.

[11] a) H. Furukawa, K. E. Cordova, M. O'Keeffe, O. M. Yaghi, *Science* **2013**, *341*, 1230444; b) A. Corma, H. Garcia, F. X. L. i Xamena, *Chem. Rev.* **2010**, *110*, 4606 – 4655; c) H. Wang, Q.-L. Zhu, R. Zou, Q. Xu, *Chem* **2017**, *2*, 52 – 80; d) M. L. Foo, R. Matsuda, S. Kitagawa, *Chem. Mater.* **2014**, *26*, 310 – 322.

[12] a) B. Ernst, A. Bensaddik, L. Hilaire, P. Chaumette, A. Kiennemann, *Catal. Today* **1998**, *39*, 329 – 341; b) Y. Okamoto, K. Nagata, T. Adachi, T. Imanaka, K. Inamura, T. Takyu, *J. Phys. Chem.* **1991**, *95*, 310 – 319; c) G. Wei, J. S. Wainright, R. F. Savinell, *J. New Mater. Electrochem. Syst.* **2000**, *3*, 121 – 129.

[13] a) N. Brückner, K. Obesser, A. Bösmann, D. Teichmann, W. Arlt, J. Dungs, P. Wasserscheid, *ChemSusChem* **2014**, *7*, 229 – 235; b) M. Markiewicz, Y. Q. Zhang, A. Bösmann, N. Brückner, J. Thöming, P. Wasserscheid, S. Stolte, *Energy Environ. Sci.* **2015**, *8*, 1035 – 1045; c) P. Preuster, C. Papp, P. Wasserscheid, *Acc. Chem. Res.* **2017**, *50*, 74 – 85; d) Y. Han, Z. Wang, R. Xu, W. Zhang, W. Chen, L. Zheng, J. Zhang, J. Luo, K. Wu, Y. Zhu, C. Chen, Q. Peng, Q. Liu, P. Hu, D. Wang, Y. Li, *Angew. Chem. Int. Ed.* **2018**, *57*, 11262 – 11266; *Angew. Chem.* **2018**, *130*, 11432 – 11436.

Manuscript received: March 31, 2020
Accepted manuscript online: June 16, 2020
Version of record online: August 18, 2020

6. Appendix

Remaining publications

In chapter 6.1 the manuscript is submitted to the international journal at the time of submitting the thesis. In chapter 6.2 to 6.6 given published articles and my contribution to each work in detail.

6.1 Expanding the catalytic hydrogenation toolbox for synthesis of amines

Vishwas G. Chandrashekhar, Wolfgang Baumann, Matthias Beller* and Rajenahally V. Jagadeesh*

Journal: Submitted to *Science on 17th December 2021 (under revision)*

Author contributions:

In this paper, I have developed the catalyst, optimized experimental conditions, performed all catalytic reactions, isolated reported compounds, prepared molecularly defined complex, performed mechanistic experiments, and co-wrote the paper. My contribution as the first author of this paper is approximately 90%.

Signature of the student

(Vishwas G. Chandrashekhar)

Signature of the supervisor

(Prof. Dr. Matthias Beller)

6.2 Ultra-small cobalt nanoparticles from molecularly-defined Co-salen complexes for catalytic synthesis of amines

Thirusangumurugan Senthamarai,[a] Vishwas G. Chandrashekhar,[a] Manoj B. Gawande,[b] Narayana V. Kalevaru,[a] Radek Zbořil,[b] Paul C. J. Kamer,[a] Rajenahally V. Jagadeesh*[a] and Matthias Beller*[a]

Chem. Sci., 2020, **11,** 2973-2981.

Author contributions:

In this paper, I have involved in catalyst development, analysis of analytical data, and reproduced the results. My contribution as a co-author in this paper is approximately 20%.

Signature of the student

(Vishwas G. Chandrashekhar)

Signature of the supervisor

(Prof. Dr. Matthias Beller)

6.3 General and selective synthesis of primary amines using Ni-based homogeneous catalysts

Kathiravan Murugesan, Zhihong Wei, Vishwas G. Chandrashekhar, Haijun Jiao,* Matthias Beller* and Rajenahally V. Jagadeesh*

Chem. Sci., 2020, **11,** 4332-4339. (With back cover picture)

Author contributions:

In this paper, I have involved in performing catalytic experiments, along with isolation of products, performed revision experiments. My contribution as a co-author in this paper is approximately 30%.

Signature of the student

(Vishwas G. Chandrashekhar)

Signature of the supervisor

(Prof. Dr. Matthias Beller)

6.4 Reductive amination using cobalt-based nanoparticles for synthesis of amines

Kathiravan Murugesan, Vishwas G. Chandrashekhar, Thirusangumurugan Senthamarai, Rajenahally V. Jagadeesh* and Matthias Beller*

Nat Protoc, 2020, **15,** 1313-1337.

Author contributions:

In this paper, I have involved writing the procedure and checking the correction of manuscript. My contribution as the second author in this paper is approximately 20%.

Vishwas-G C

Signature of the student

(Vishwas G. Chandrashekhar)

Signature of the supervisor

(Prof. Dr. Matthias Beller)

6.5 Catalytic reductive aminations using molecular hydrogen for synthesis of different kinds of amines

Kathiravan Murugesan,† Thirusangumurugan Senthamarai,† Vishwas G. Chandrashekhar,† Kishore Natte, Paul C. J. Kamer, Matthias Beller* and Rajenahally V. Jagadeesh*

(†1st, 2nd & 3rd authors equal contribution)

Chem. Soc. Rev., 2020, **49,** 6273-6328.

Author contributions:

In this paper, I have searched, reviewed related articles, and co-wrote the manuscript. procedure and checking the correction of manuscript. My contribution as the first author in this paper is approximately 30%.

Signature of the student

(Vishwas G. Chandrashekhar)

Signature of the supervisor

(Prof. Dr. Matthias Beller)

6.6 A "universal" catalyst for aerobic oxidations to synthesize (hetero)aromatic aldehydes, ketones, esters, acids, nitriles, and amides

Thirusangumurugan Senthamarai, Vishwas G. Chandrashekhar, Nils Rockstroh, Jabor Rabeah, Stephan Bartling, Matthias Beller,* Rajenahally V. Jagadeesh*

Chem, 2022, **8,** 508-531.

Author contributions:

In this paper, I have involved in performing catalytic reactions, characterization of products reported in the paper, also involved in revision work, and co-wrote the manuscript. My contribution as the second author in this paper is approximately 25%.

Signature of the student

(Vishwas G. Chandrashekhar)

Signature of the supervisor

(Prof. Dr. Matthias Beller)

Expanding the catalytic hydrogenation toolbox for synthesis of amines

Vishwas G. Chandrashekhar, Wolfgang Baumann, Matthias Beller* and Rajenahally V. Jagadeesh*

Leibniz-Institut für Katalyse e.V., Albert-Einstein-Str. 29a, Rostock, D-18059, Germany.

*Corresponding authors.

E-mails: matthias.beller@catalysis.de; jagadeesh.rajenahally@catalysis.de

Amines play an important role in our daily life as an essential part of advanced materials and many life science products. Thus, the development of efficient and general methodologies for their synthesis continues to be an actual, yet challenging, goal of chemical research. Among the many known processes, catalytic hydrogenations are cost-effective and industrially proven reactions, which are used to produce a wide array of amines today. Here, we report a homogeneous nickel catalyst that allows the reductive cross coupling of a range of aromatic, heteroaromatic, and aliphatic nitriles with primary and secondary amines or ammonia. This general hydrogenation protocol allows for a straightforward and highly selective synthesis of >230 functionalized and structurally diverse amines including drug molecules and chiral amines. Applying this methodology, the late-stage functionalization of life science molecules and ^{15}N-isotope labeling can be easily performed, too.

Amines play an essential role as part of proteins, vitamins, and nucleic acids in living beings *(1-5)*. Since the beginning of the first rational synthesis of amines in the 19th century, their applications continue to provide new innovations in chemistry, medicine, and biology, as well as material, energy, and environmental sciences *(1-5)*. Thus, over the last century the production of amines has continuously grown and today >6 million metric tons per year of valuable fine and bulk chemicals are produced *(6-7)*. Also, for the next decade a worldwide production growth rate of the amine market by about 8% annually is predicted due to the growing global demand for high-quality food, clothing, and changing lifestyles (Fig. 1) *(6-7)*.

Today, amines are widely used in the manufacture of daily life products, advanced chemicals, pharmaceuticals, agrochemicals, materials, personal care products, and others (Fig. 1) *(1-7)*. As an example, most agrochemicals and more than 75% of top 200 selling drugs contain amine/nitrogen moieties, which play crucial roles in their activities *(5,7)*. Furthermore, there is a growing demand for new agrochemicals, drugs, and improved personal care products, which require the practical synthesis of new amine building blocks.

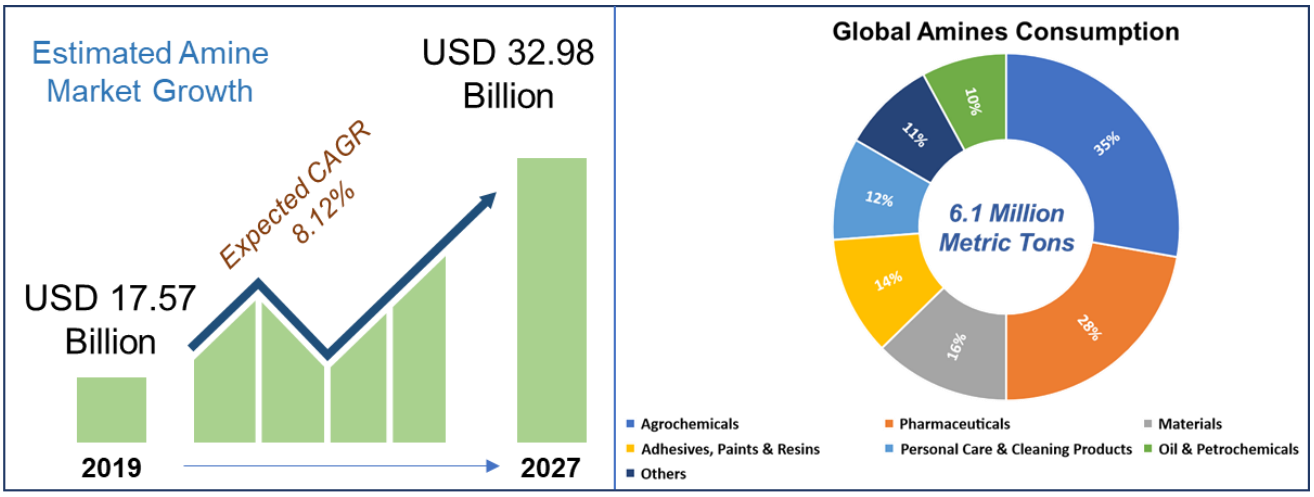

Fig. 1. Global amines production and consumption.

Based on the demand of amines, there is a constant need to improve their synthesis applying more economical and sustainable methodologies. According to the nature of the amine different methodologies prevail for their production. For example, catalytic hydrogenation of nitriles *(8-12)* and nitroarenes *(13-14)* are mainly used in industry for making primary aliphatic and aromatic amines, while reductive amination of carbonyl compounds *(15-18)*, amination of alcohols *(19-20),* substitution of halogenated compounds with amines *(21-22)* and hydroaminations *(23-24)* are mostly used for making secondary and tertiary amines. Among all the known methodologies, catalytic hydrogenation of nitriles represents a cost-effective and atom-economical industrial process to produce primary benzylic and aliphatic amines *(8-12)*. In fact, nitrile hydrogenation plays a key role in the bulk industrial production of nylon (utilizing 1,6-hexamethylenediamine), high performance plastics (1,4-diaminobutane), surfactants (alkyl dimethyl amines), emulsifiers (e.g. aminoethylpiperazine), and bioactive molecules. Noteworthy, many aromatic, heterocyclic, and aliphatic nitriles are easily accessible and produced on commercial scale. In addition, they occur in various animal and plant sources and more than hundred naturally occurring nitriles have been isolated from terrestrial and marine sources *(25-26)*. Hence, the direct catalytic hydrogenation of nitriles to produce primary amines

continues to attract significant attention for both academic synthesis and industry *(8-12)*. In contrast, the synthesis of diverse secondary and tertiary amines including *N*-methylamines from nitriles by cross-coupling is highly challenging and does not proceed with high selectivity *(27-32)*. As shown in Fig. 2, the hydrogenation of nitrile **1** generates primary imine **2**. This intermediate is reduced to form the primary amine **3**, which can further react with **2** to produce the secondary imine **4**. Subsequent hydrogenation leads to secondary amine **5** (homo-coupling pathway). Following a similar reaction pathway, the corresponding tertiary amine **6** can be formed. Alternatively, in the presence of different primary or secondary amines **7** and **8**, imine **2** can form imines **9** and **10**, which produce secondary or tertiary amines **11** and **12** (cross-coupling pathway). Further, secondary amine **11** can also reacts with **2** to produce **13**. Consequently, five different amines can result from the cross-coupling reaction of a given nitrile with a primary or secondary amine. In addition, the conversion of aromatic nitriles to give various heterocycles, especially 2,4,5-substituted imidazoles **14** under hydrogenation conditions has been described, too *(8)*.

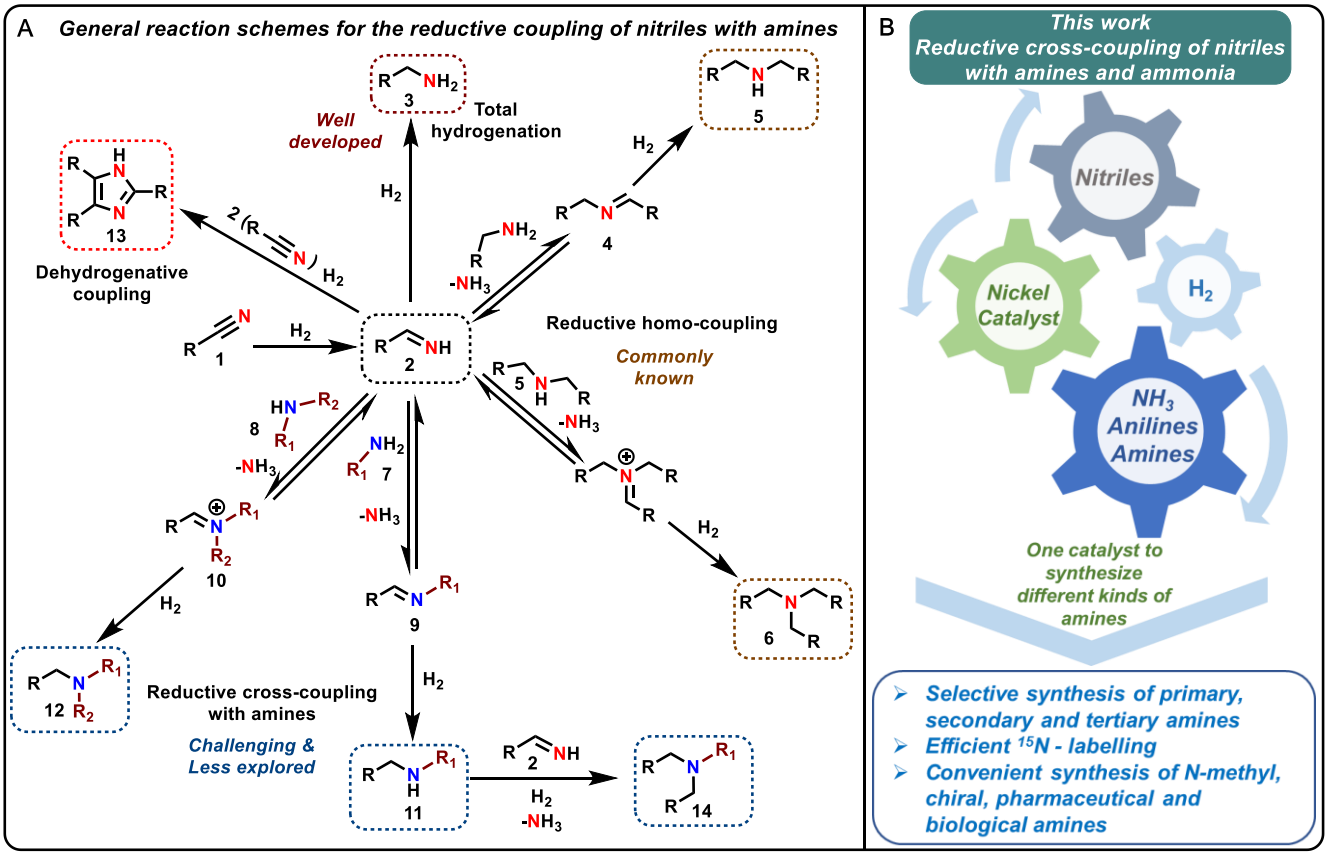

Fig. 2. Catalytic reductive cross-coupling of nitriles with primary or secondary amines or ammonia and formation of different products.

To perform reductive cross coupling of nitriles with amines in an efficient and selective manner, the design of suitable catalyst systems is crucial. Obviously, to obtain the desired products **11** or **12**, the rate for the hydrogenation step of the initially formed primary imine **2** should be slow compared to the corresponding secondary imines. In addition, reversible nucleophilic addition of the amine to the imine and elimination of ammonia should be fast, too. Ideally, the applied catalyst should be based on 3d-metals due to their availability and price. Here, we present a solution for these challenges and present a general homogeneous nickel catalyst system for the efficient reductive cross coupling of nitriles with ammonia or amines, which allows for the synthesis of functionalized and structurally diverse primary, secondary and tertiary benzylic, heterocyclic, and aliphatic amines including N-methyl amines and more complex drug targets.

Design of catalyst and reaction optimization

In recent years, multi-dentate phosphines became privileged ligand scaffolds for the preparation of defined metal complexes with specific catalytic activity for demanding hydrogenation reactions *(33-44)*. In this respect, the unique behavior of such catalysts for the hydrogenation of esters to ethers *(36-37)*, carbon dioxide to methanol *(38-40)* and carboxylic acids to alcohols *(41-42)* as well as amides to amines *(43-44)* has been demonstrated. Based and inspired by these works, we started to investigate the performance of 3d-metals in combination with selected di-, tri-, and tetradentate phosphines for cross coupling of 4-methylbenzonitrile **15** with 4-anisidine **16** to produce 4-methoxy-*N*-(4-methylbenzyl)aniline **17** in presence of molecular hydrogen as the model reaction (Fig. 3 and Table S1). At this point, it should be noted that the coupling of **16** is also demanding because of the lower nucleophilicity compared to the benzylic amine **18**, which obviously leads to self-coupling. Initially, we tested Fe-, Mn-, Co-, and Ni-salts in combination with bis-(2-diphenylphosphino-ethyl)phenylphosphine (linear-triphos **L1**), tris[2-(diphenylphosphino)ethyl]phosphine (tetraphos **L2**), and (4,5-bis(diphenylphosphino)-9,9-dimethylxanthene (xantphos **L3**). To increase the reactivity of the resulting complexes, metal salts with non-coordinating anions, e.g. tetrafluoroborates and triflates, were tested, too. In general, compared to Co and Ni, the *in situ* generated Fe and Mn complexes showed no or very low catalytic activity in the model reaction (Fig. 3 and Table S1; entries 1-9). Comparing Ni- and Co-complexes, excellent activity, and selectivity for the formation of **17** (91% yield) is observed in the presence of Ni-**L1**. Testing other nickel salts in the presence of this ligand revealed significantly less active catalysts (Table S1; entries 28-29). However, the high activity can be restored in presence of $Zn(OTf)_2$ (Table S1; entry 30). Due to the superior behavior of nickel, other ligands (**L4-L9**) were also tested with $Ni(OTf)_2$ in the model reaction. Notably, the *in situ* generated Ni-complexes with **L4**, **L5**,

and **L8** gave moderate to good yields (40-62% of **17**), while **L7** and **L9** exhibited only poor selectivity (16-24% of **17**), and **L6** provided no desired product (Fig. 3 and Table S1; entries 22-27).

Fig. 3. Reductive coupling of 4-methylbenzonitrile and 4-anisidine using *in situ* generated metal-phosphine complexes.

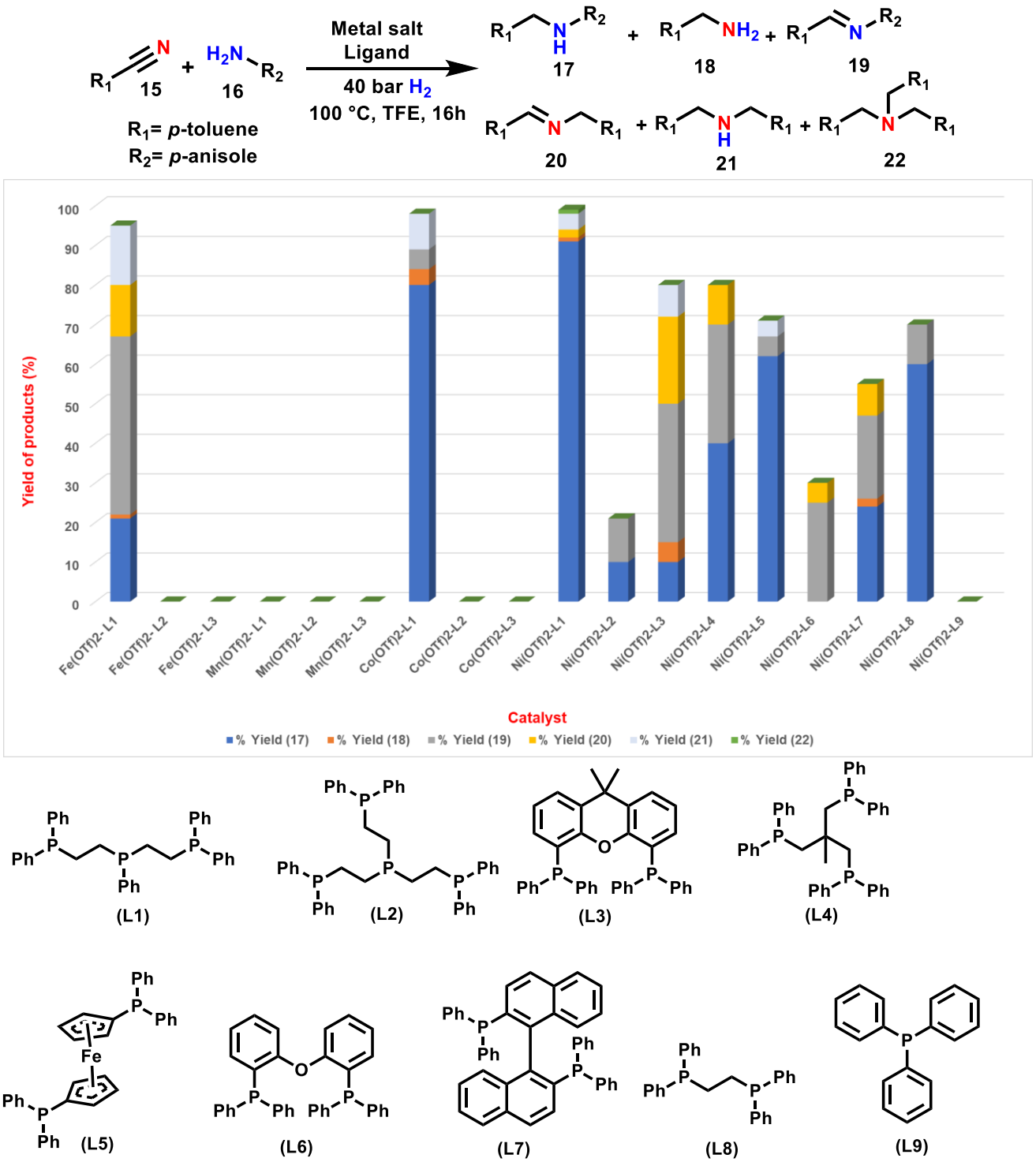

Reaction conditions: 0.5 mmol p-tolunitrile, 0.75 mmol p-anisidine, 4 mol% metal salt, 5 mol% ligand, 40 bar H_2, 3 mL TFE, 100 °C, 16 h, yields were determined by GC using 4-flourotoluene as standard.

After optimization of key parameters (e.g., catalyst amount, temperature, H_2 pressure, solvent) of the model reaction applying Ni-**L1** system, an excellent yield (91% of **17**) was obtained in trifluoroethanol (TFE) with 40 bar of hydrogen at 100 °C (Tables S2-S3). While most of the catalyst evaluation studies were performed with *in-situ* generated catalysts, we also prepared the defined $Ni(OTf)_2$-**L1** complex, which was characterized by NMR, HRMS and IR. According to the obtained analytical data formation of 1:1 Ni-L complex is assumed. This isolated complex (Complex **A**) exhibited similar activity and selectivity to that of the in-situ system (Table S2; entry 4).

Monitoring the progress of the model reaction at different time intervals in the presence of the optimal Ni-**L1** system revealed initial formation of the secondary imine **19** which is subsequently reduced in a highly selective manner to the desired amine **17**. As shown in Fig. S1 the reaction is finished after 12 h and the hydrogenation of **19** is rate determining. Looking at the different elementary reaction steps (Fig. S2) first the catalytic reduction of nitrile **15** takes place to generate primary imine **15A**. This intermediate is unstable and immediately couples with aniline **16** to form aminal **15B**, which yields the stable secondary imine **19** upon elimination of ammonia. Finally, **19** undergoes reduction to give the desired secondary amine **17**. The first hydrogenation step as well as the imine formation are fast compared to subsequent formation of **17**. The high chemoselectivity is explained by the slow hydrogenation of the primary imine **15A** compared to the cross-coupling step. Thus, also other unwanted side products like the symmetrical secondary amine **21** are minimized.

Reductive cross-coupling of nitriles with primary and secondary amines

After having identified the optimal catalyst system Ni-**L1** in the benchmark reaction, we explored its applications for the synthesis of different kinds of amines (Figs. 4-8). First, we performed reductive cross-coupling reactions of substituted and functionalized aromatic, heterocyclic, and aliphatic nitriles with *p*-anisidine or aniline to produce the corresponding amines in good to excellent selectivity and yields (Fig. 4A). For example, sterically hindered 2,6-dimethyl-benzonitrile and different halogenated benzonitriles reacted smoothly in up to 90% yield (Fig. 4A; products **24**, **26-34**). Similarly, di- and tri-substituted benzonitriles gave the respective secondary amines in up to 90% yield (Fig. 4A; products **30-34**, **37-38**). More challenging substrates such as benzonitriles containing reducible functional groups were smoothly reacted and yielded corresponding amines (Fig. 4A; products **39-42**). Specifically, functional groups such as (thio)ether, ester, amide, and boronic acid ester are well tolerated. Next, heterocyclic amines based on pyridine, furan, benzodioxole, 1,3-dihydroisobenzofuran were prepared in 80-92% (Fig. 4A; products **43-48**). Further, various araliphatic

and aliphatic nitriles including fatty nitriles efficiently underwent cross coupling with *p*-anisidine (Fig. 4A; products **49-55**).

Like the nitrile part, also a broad variety of structurally diverse primary amines can be selectively coupled (Fig. 4B). Exemplarily, we used in these studies 4-toluonitrile as the main substrate (Fig. 4B; products **56-95**). *Trans*-4-aminocyclohexanol, morpholine, and piperazine, which represent important motifs in drugs and natural products, were easily coupled and gave the corresponding amines in high yields (Fig. 4B; products **88, 91-92)**. Apart from primary amines, different secondary amines including less reactive indole were coupled with 4-tolunitrile and produced corresponding tertiary amines in up to 94% yields (Fig. 4B; products **89-95**). In addition, α-methyl amines also reacted smoothly with different nitriles to provide the desired products in up to 91% yield (Fig. 4C; products **96-100**). Simple methyl- and dimethylamine constitute inexpensive bulk chemicals, which are produced on 4 million tons/annum; however, their widespread use in organic synthesis is hampered by their physical properties (gas) and strong binding ability to many metal complexes. Gratifyingly, the Ni-**L1** system exhibited good to excellent activity and selectivity for the reaction of all kinds of aromatic nitriles with dimethyl- and monomethylamine and provided the corresponding *N*-methylated products in up to 92% yields (Fig. 5A and 5B; products **101-139**). This class of compounds is of special importance as the *N*-methyl group represents a ubiquitous motif and integral part of many drugs and biomolecules, which also plays a significant role in regulating biological activities. Remarkably, many aliphatic nitriles including dinitriles underwent selective cross coupling with methyl- and dimethylamine, too (Fig. 5A; products **120-124** and Fig. 5B; products **137-139**), albeit oligomerization and polymerization can be expected as side reactions.

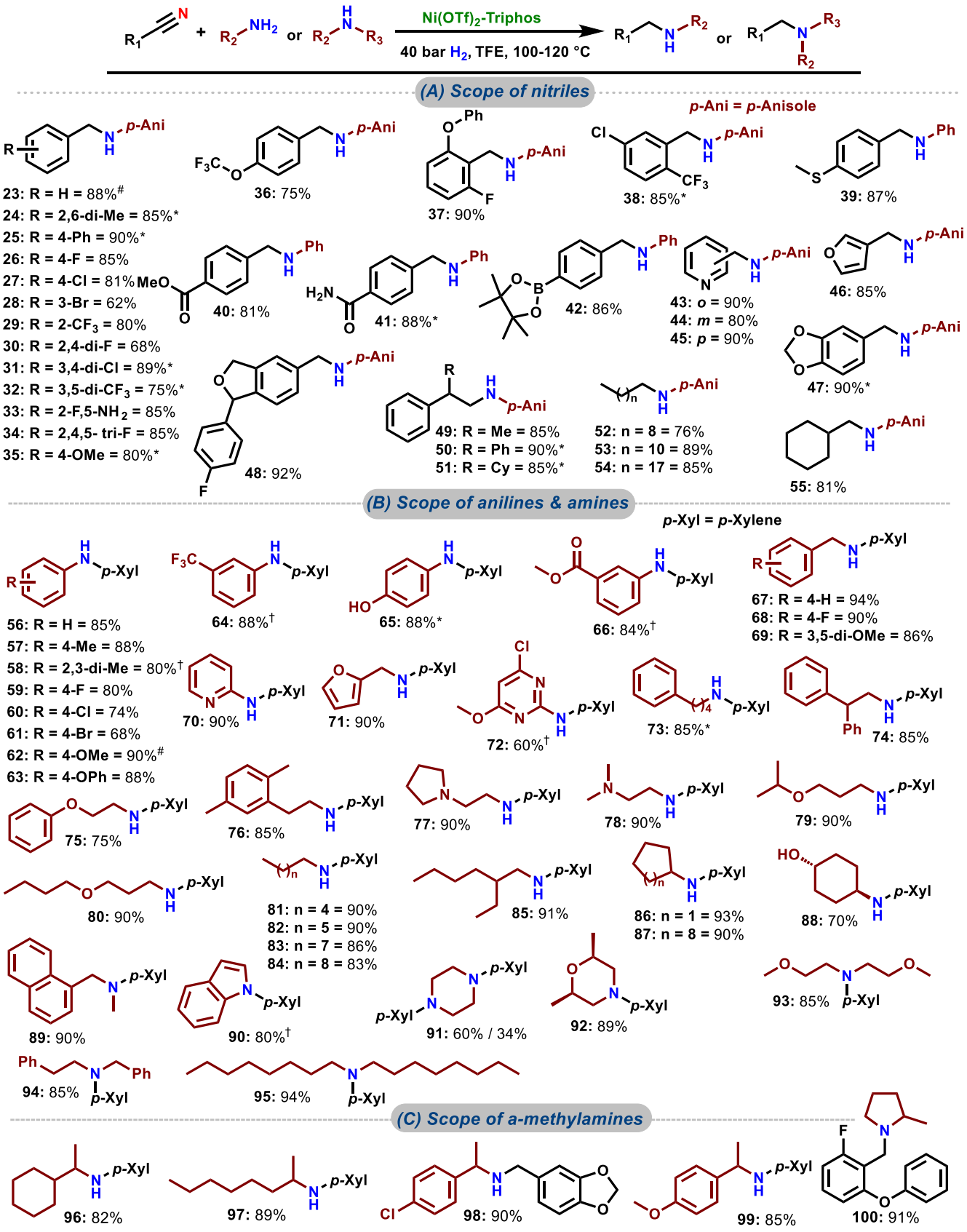

Fig. 4. Synthesis of secondary and tertiary amines by Ni-catalyzed reductive cross-coupling of nitriles and amines.

Reaction conditions: 0.5 mmol nitrile, 0.75 mmol amine, 4 mol% $Ni(OTf)_2$, 5 mol% linear triphos (**L1**), 40 bar H_2, 3 mL TFE, 100 °C, 16 h, isolated yields. *With 5 mol% $Ni(OTf)_2$ and 6 mol% linear triphos (**L1**) at 120 °C. †With 2 mmol amine. #GC yields using 4-flourotoluene as standard.

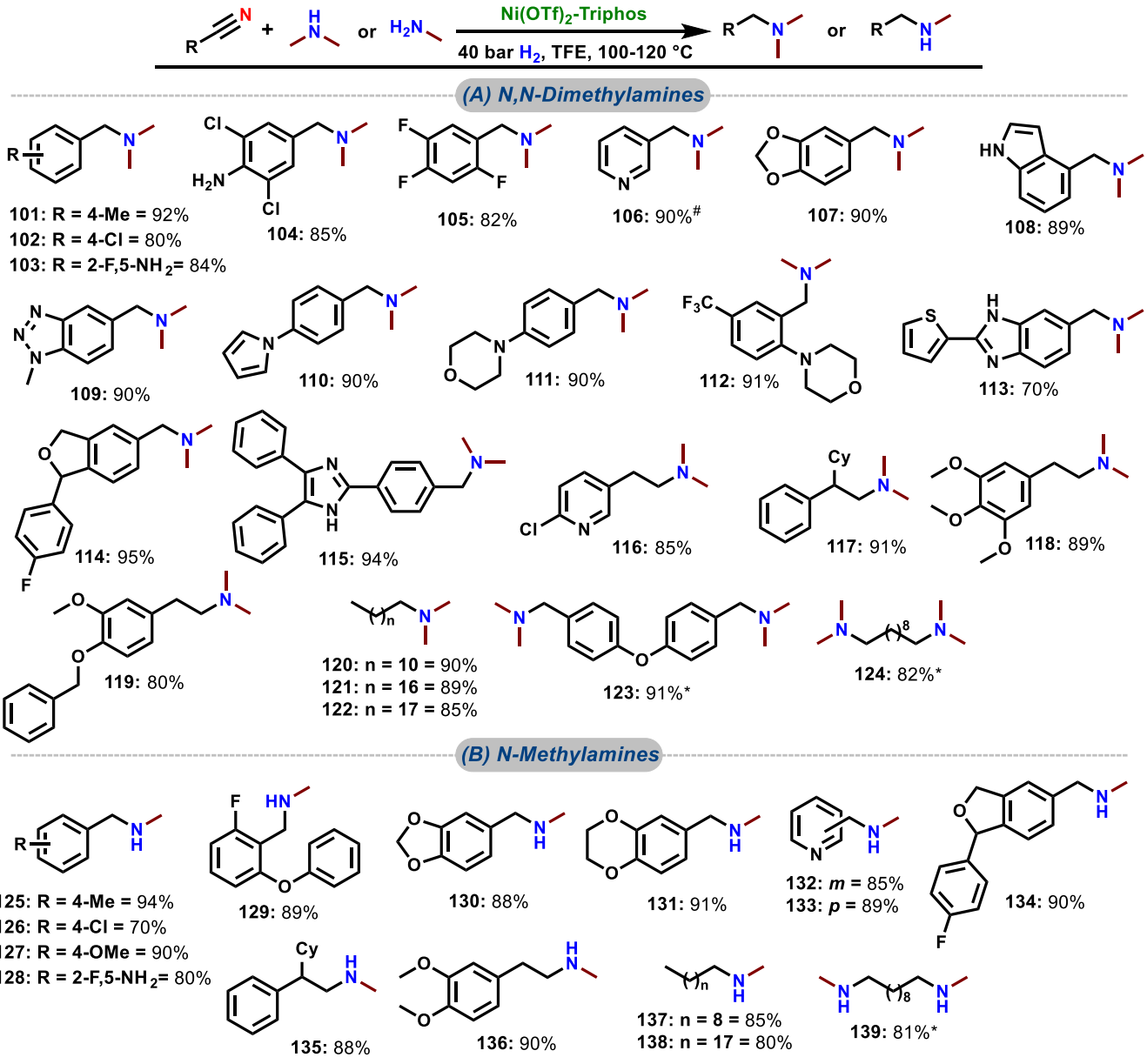

Fig. 5. Ni-catalyzed synthesis *N*-methylated amines.

Reaction conditions: 0.5 mmol nitrile, 150µL *N,N*-dimethylamine or *N*-methylamine (12 M in ethanol), 5 mol% $Ni(OTf)_2$, 6 mol% linear triphos (**L1**), 40 bar H_2, 2 mL TFE, 120 °C, 8 h, isolated yields. *With 7 mol% $Ni(OTf)_2$ and 8 mol% linear triphos (**L1**). #GC yields using 4-flourotoluene as standard.

Reductive cross-coupling of nitriles with ammonia

After the successful synthesis of a plethora of secondary, tertiary amines by reductive cross coupling, we turned our interest to ammonia as amine source. Obviously, products in this case are the corresponding primary amines, which are typically prepared by traditional hydrogenation of nitriles. To the best of our knowledge no homogeneous Ni-based catalyst was described for the hydrogenation of nitriles yet. Indeed, simple hydrogenation of p-toluonitrile **15** under standard conditions in the presence of Ni/**L1** did not provide the desired 4-methylbenzylamine **18**. Instead, the formation of the self-coupled secondary amine **21** as the main product in 85% yield and 10-12% of the tertiary amine **22** was observed. However, conducting the reaction in presence of ammonia gas at 120 °C, we obtained 87% of the desired 4-methylbenzylamine **18**. To understand this behavior and to know more about the role of ammonia, we conducted the hydrogenation of p-toluonitrile **15** in presence of ^{15}N-labeled ammonium acetate. Surprisingly, in this case LCMS and NMR analysis showed the predominant formation of the ^{15}N-labelled 4-methylbenzylamine (86% yield; 89% / 11% ^{15}N/^{14}N-selectivity) (Figs. S9-S11). This result clearly shows that this transformation does not proceed as a simple hydrogenation, but alternatively as a reductive coupling process. Indeed, increasing the amount of ^{15}N-labeled ammonium acetate in the hydrogenation of **15** the incorporation of ^{15}N is increased and we obtained 89% labelled product using 5 equiv. of $^{15}NH_4OAc$ (Figs. S9-S10). This indicates an equilibrium between the ^{15}N-labeled and non-labelled imine via the corresponding aminal. Notably, the selective formation of primary amine in presence of ammonia requires slightly higher temperature compared to the cross-coupling of the nitrile with aniline. Interestingly, in the presence of ammonia instead of 4-methoxyaniline the overall reaction is faster (Fig. S3), but less selective and significant amounts of the self-coupling product **21** are obtained at 100°C. However, increasing the temperature to 120 °C gave selectively the corresponding primary amine **18**.

Like the reactions with primary and secondary amines, the Ni-triphos catalyst is both active and selective for the reductive coupling of various nitriles with ammonia to produce corresponding primary amines (Fig. 6A; products **140-194**). For example, mono-, di-, and tri-halogen substituted benzylic amines were efficiently prepared in up to 93% yield (Fig. 6A; products **144-146**, **156-163**). Again, functional groups such as thioether, ketone, ester, amide, hydroxy are well tolerated. Furthermore, different heterocyclic nitriles based on pyridine, benzothiazole, thiazole, benzotriazole, furan, isobenzofuran-1(3H)-one, 1,3-dihydroisobenzofuran, 1-phenyl-1H-pyrrole, 4-phenyl-morpholine, and 2-(thiophen-2-yl)-1H-benzoimidazole smoothly underwent reductive coupling and provided the corresponding heterocyclic primary amines (Fig. 6A; products **164-174**). Finally, different araliphatic,

and (cyclo)aliphatic primary amines were successfully prepared using this catalyst system (Fig. 6A; products **175-183**). Among the latter reactions, the selective conversion of fatty nitriles to fatty amines represents an important industrial process *(45-46)*. Indeed, >800.000 tons of fatty amines are produced per annum for the manufacture of fabric softeners, flotation agents, emulsifiers, corrosion inhibitors, and lubricating additives. Gratifyingly, applying this Ni-triphos catalyst system, different fatty nitriles were coupled with ammonia to the corresponding fatty amines in 88-90% yield (Fig. 6A; products **184-186** and **191-192**).

Likewise, the synthesis of primary amines, a variety of ^{15}N-labeled primary amines can be prepared using the corresponding nitriles and $^{15}NH_4OAc$. Such transformations are interesting for isotope labeling applications, which help to understand the metabolism of bio-active compounds and to identify specific metabolites *(47-48)*. To showcase the utility under optimized conditions, eleven ^{15}N-labled primary amines were prepared including 3 bioactive molecules. In all these cases up to 91% of ^{15}N incorporation is observed (Fig. 6B; products **195-204**).

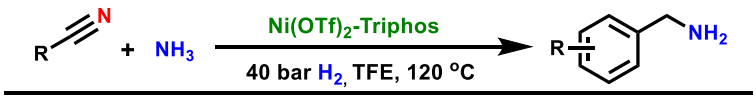

(A) Primary amines

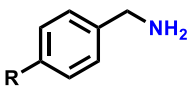

140: R = H = 90%#
141: R = Me = 87%#
142: R = *t*-Bu = 90%*
143: R = Ph = 93%*
144: R = F = 93%
145: R = Cl = 85%#
146: R = Br = 74%
147: R = OMe = 94%
148: R = OPh = 90%
149: R = OBn = 90%
150: R = CF_3 = 89%
151: R = OCF_3 = 89%
152: R = SMe = 91%
153: R = COOMe = 90%
154: R = $CONH_2$ = 92%*

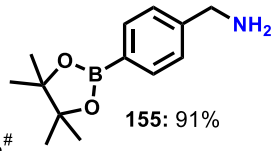

155: 91%

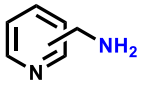

164: *m* = 90%
165: *p* = 90%

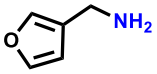

166: 85%

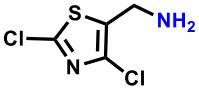

167: 60%

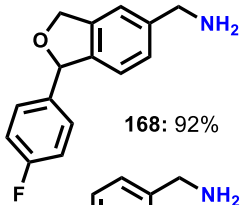

168: 92%

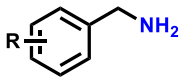

156: R = 3,4-Cl = 85%*
157: R = 3,4-CF_3 = 86%
158: R = 2-F, 5-NH_2 = 80%
159: R = 3-F, 4-CH_2OH = 70%
160: R = 2-F, 6-OPh = 90%
161: R = 2,4,5-tri-F = 85%
162: R = 3-Cl, 4-NH_2, 5-Me = 88%
163: R = 3,5-di-Cl, 4-NH_2 = 85%

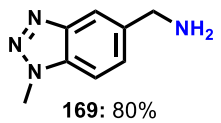

169: 80%

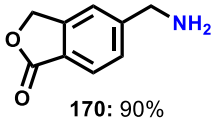

170: 90%

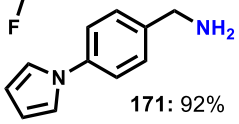

171: 92%

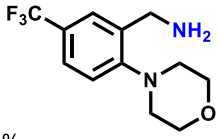

172: 84%*

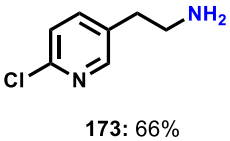

173: 66%

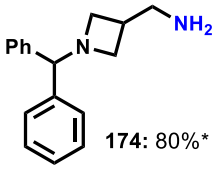

174: 80%*

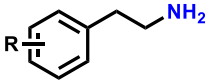

175: R = H = 90%
176: R = 2-Cl = 92%
177: R = 4-CF_3 = 90%
178: R = 3,4,5-OMe = 80%

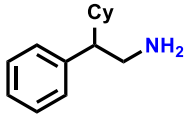

179: R = Cy = 89%*
180: R = Ph = 85%*

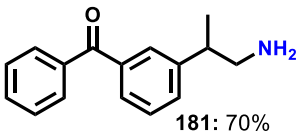

181: 70%

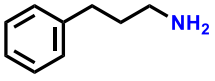

182: 91%

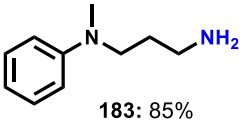

183: 85%

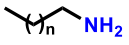

184: n = 6 = 91%
185: n = 10 = 90%
186: n = 12 = 89%

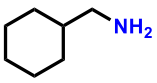

187: 85%

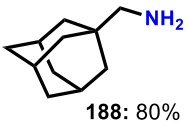

188: 80%

189: 1,3 = 88%†
190: 1,4 = 90%†

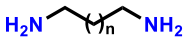

191: n = 6 = 87%†
192: n = 8 = 85%†

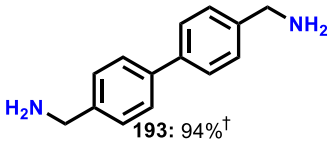

193: 94%†

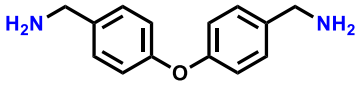

194: 91%†

(B) ^{15}N-Labeled primary amines

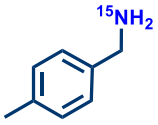

195: 86%
(89% ^{15}N)

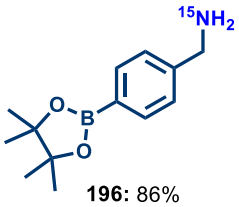

196: 86%
(86% ^{15}N)

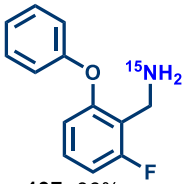

197: 86%
(>90% ^{15}N)

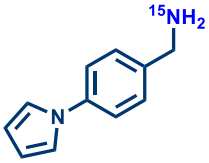

198: 86%
(91% ^{15}N)

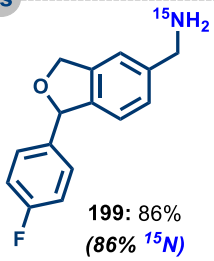

199: 86%
(86% ^{15}N)

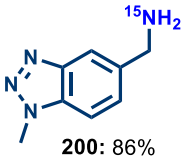

200: 86%
(86% ^{15}N)

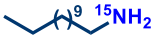

201: 86%
(91% ^{15}N)

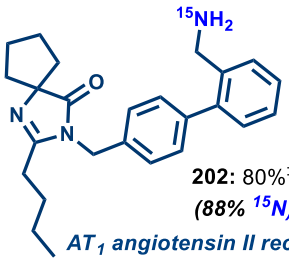

202: 80%‡
(88% ^{15}N)
AT_1 angiotensin II receptor antagonist analogue-$^{15}NH_2$

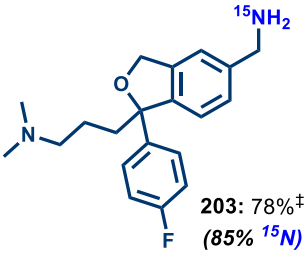

203: 78%‡
(85% ^{15}N)
Citalopram-$^{15}NH_2$

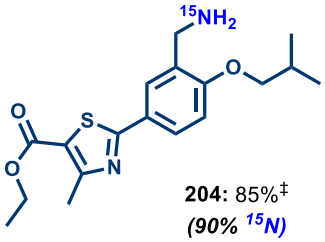

204: 85%‡
(90% ^{15}N)
Febuxostat ester-$^{15}NH_2$

Fig. 6. Ni-catalyzed reductive cross-coupling of nitriles with ammonia for the synthesis of primary amines.

Reaction conditions: A: 0.5 mmol nitrile, 5-7 bar NH_3, 5 mol% $Ni(OTf)_2$, 6 mol% linear triphos (**L1**), 40 bar H_2, 2 mL TFE, 120 °C, 5 h. Isolated as free primary amines and converted to hydrochloride salts for measuring NMR. *For 10 h. †With 7 mol% $Ni(OTf)_2$ and 8 mol% linear triphos (**L1**), 10 h. #GC yields using 4-flourotoluene as standard. **B:** 0.5 mmol nitrile, 2.5 mmol $^{15}NH_4OAc$, 5 mol% $Ni(OTf)_2$, 6 mol% linear triphos (**L1**), 40 bar H_2, 2 mL TFE, 120 °C, 5 h. Isolated as free primary amines and converted to hydrochloride salts for measuring NMR. ^{15}N incorporation was determined by ^{1}H-NMR. ‡With 0.25 mmol nitrile and 1.3 mmol $^{15}NH_4OAc$.

Applications: N-alkylation of chiral amines with nitriles

As demonstrated *vide supra*, the presented catalyst system exhibited good functional groups tolerance, which is important for synthetic applications. To highlight the catalyst's ability for medicinal and organic chemistry, further on the functionalization of chiral molecules was studied. As shown in Fig. 7A, N-alkylation of various chiral primary and secondary amines with different nitriles proceeded smoothly in presence of molecular hydrogen to achieve N-alkylated chiral secondary and tertiary amines with retention of chirality. Exemplarily, (R)-1-phenylethan-1-amine and (S)-1-phenylethan-1-amine as well as (S)-1-(naphthalen-1-yl)ethan-1-amine reacted selectively with 4-methylbenzonitrile to the corresponding chiral benzyl amines in up to 90% yields and 98% ee (Fig. 7A; products **205-207**). Similarly, bromo-substituted chiral 1-phenylethan-1-amines gave the desired N-alkylated amines with retention of chirality (Fig. 7A; products **208-209**). In addition to primary amines, secondary amines led to reductive coupling with nitriles and provided tertiary chiral amines in up to 85% yields and 99% ee (Fig. 7A; products **214-215**).

Applications: Synthesis of drugs and late-stage functionalization of bio-active compounds

Next, the importance of this methodology for life science applications and industrial process chemistry was showcased by the preparation of 13 existing drug molecules (Fig. 7B; products **216-230**). Without further optimizations, the corresponding nitriles and secondary or primary amines reacted selectively in presence of the Ni-triphos catalyst system and molecular hydrogen and gave the desired molecules in up to 91% yield. For example, Cinacalcet and Tecalcet, which are used to treat secondary hyperparathyroidism, parathyroid carcinoma, and primary hyperparathyroidism, were prepared in both chiral (98-99% ee) and racemic form (Fig. 7B; products **223-226**).

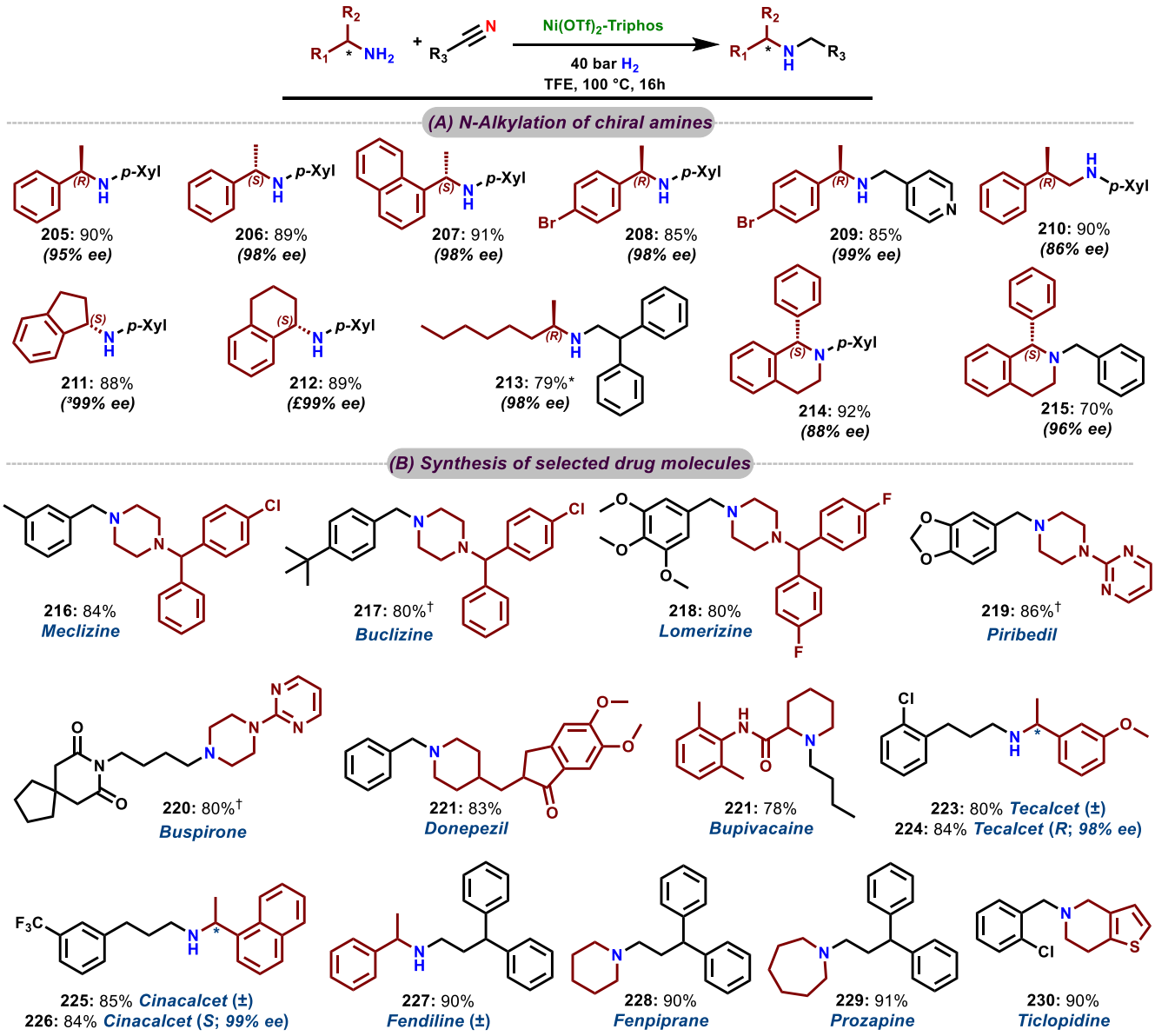

Fig. 7. Applicability of Ni-catalyzed cross coupling reactions for the N-alkylation of chiral amines with nitriles and synthesis of selected drug molecules.

Reaction conditions: 0.25 mmol nitrile, 0.37 mmol amine, 4 mol% $Ni(OTf)_2$, 5 mol% linear triphos (**L1**), 40 bar H_2, 3 mL TFE, 100 °C, 16 h, isolated yields. *At 120 °C. †With 5 mol% $Ni(OTf)_2$ and 6 mol% linear triphos (**L1**), 120 °C.

In addition, late-stage functionalization (LSF) represents an important strategy to introduce specific chemical groups/functionalities in the very last steps of the synthesis *(49-50)*. This process allows to speed up the preparation of novel intermediates and diverse chemical libraries for drug discovery *(49-50)*. In this respect, nitrile-containing pharmaceuticals, agrochemicals, and biomolecules *(26)* can be selectively functionalized to even more valuable amines.

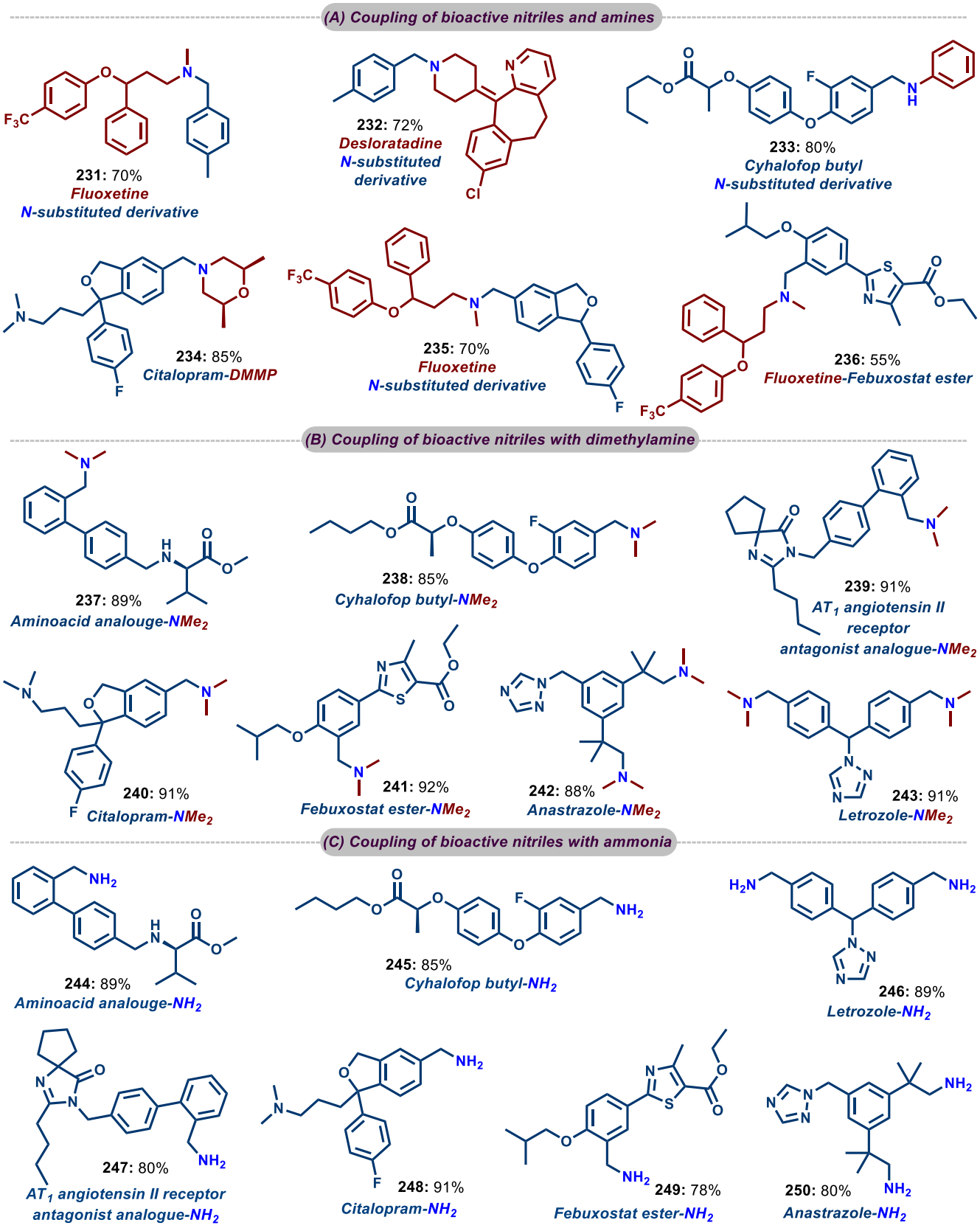

Fig. 8. Late-stage functionalization of biologically active nitriles and amines.

Reaction conditions: A: 0.25 mmol nitrile, 0.37 mmol amine, 5 mol% $Ni(OTf)_2$, 6 mol% linear triphos (**L1**), 40 bar H_2, 3 mL TFE, 100 °C, 16 h. **B:** 0.25 mmol nitrile, 75 µL *N,N*-dimethylamine (12 M in ethanol), 5 mol% $Ni(OTf)_2$, 6 mol% linear triphos (**L1**), 40 bar H_2, 2 mL TFE, 120 °C, 10 h. **C:** 0.25 mmol nitrile, 5-7 bar NH_3, 5 mol% $Ni(OTf)_2$, 6 mol% linear triphos (**L1**), 40 bar H_2, 2 mL TFE, 120 °C, 10 h. All are isolated yields.

Indeed, using our Ni-based protocol, the cross-coupling of Cyhalofop-butyl, Citalopram, amino acid analogues, as well as AT1 angiotensin II receptor antagonist analogue, Febuxostat ester, Letrozole, and Anastrazole with amines and ammonia (Fig. 8; products **231-250**) proceeded smoothly. In all these cases the -CN groups reacted with amines or ammonia in a highly selective manner without affecting the core structure of the nitriles. Similarly, derivatives of bio-active amines, e.g., Fluoxetine, Desloratadine, can be easily alkylated with various nitriles. Finally, to demonstrate the applicability of this homogeneous catalyst for the synthesis of interesting bio-relevant products, selected examples were upscaled to multi-gram level without problems (Fig. S12; products **216, 221**). In addition, also the synthesis of primary- (Fig. S12; product **179**) dimethyl- (Fig. S12; product **121**) and secondary amines (Fig. S12; product **31**) were exemplarily upscaled.

REFERENCES AND NOTES

1. F. Franzen, K. Eysell, *Biologically Active Amines Found in Man: Their Biochemistry, Pharmacology, and Pathophysiological Importance* (Elsevier, 1st Ed, 1969).
2. C. Proestos, *Biogenic Amines* (IntechOpen, 2019)
3. S. A. Lawrence, *Amines: Synthesis, Properties and Applications* (Cambridge University Press, 2004).
4. A. Ricci, *Amino Group Chemistry: From Synthesis to the Life Sciences* (Wiley-VCH, 2008).
5. https://njardarson.lab.arizona.edu/sites/njardarson.lab.arizona.edu/files/Top%20200%20Pharmaceuticals%20By%20Retail%20Sales%202020V3.pdf . *Top 200 Pharmaceuticals by Retail Sales in 2020*.
6. https://www.mordorintelligence.com/industry-reports/aminesmarket
7. https://www.grandviewresearch.com/industry-analysis/amines-industry
8. J. A. Garduño, J. J. García, *ACS Catal* **10**, 8012-8022 (2020).
9. C. Bornschein *et al.*, *Nat. Commun.* **5**, 4111 (2014).
10. K. Murugesan *et al.*, *Chem. Sci.* **9**, 8553-8560 (2018).
11. Y. Saito, H. Ishitani, M. Ueno, S. Kobayashi, *ChemistryOpen* **6**, 211-215 (2017).
12. A. Mukherjee, D. Srimani, S. Chakraborty, Y. Ben-David, D. Milstein, *J. Am. Chem. Soc.* **137**, 8888-8891 (2015).

13. D. Formenti, F. Ferretti, F. K. Scharnagl, M. Beller, *Chem. Rev.* **119**, 2611-2680 (2019).
14. R. V. Jagadeesh *et al.*, *Science* **342**, 1073-1076 (2013).
15. T. Irrgang, R. Kempe, *Chem. Rev.* **120**, 9583-9674 (2020).
16. O. I. Afanasyev, E. Kuchuk, D. L. Usanov, D. Chusov, *Chem. Rev.* **119**, 11857-11911 (2019).
17. K. Murugesan *et al.*, *Chem. Soc. Rev.* **49**, 6273-6328 (2020).
18. T. Yasukawa, R. Masuda, S. Kobayashi, *Nat. Catal.* **2**, 1088-1092 (2019).
19. T. Yan, B. L. Feringa, K. Barta, *Nat. Commun.* **5**, 5602 (2014).
20. T. Irrgang, R. Kempe, *Chem. Rev.* **119**, 2524-2549 (2019).
21. P. Ruiz-Castillo, S. L. Buchwald, *Chem. Rev.* **116**, 12564-12649 (2016).
22. J. F. Hartwig, *Acc. Chem. Res.* **41**, 1534-1544 (2008).
23. S. Streiff, F. Jérôme, *Chem. Soc. Rev.* **50**, 1512-1521 (2021).
24 J. Gui *et al.*, *Science* **348**, 886-891 (2015).
25. F. F. Fleming, *Nat. Prod. Rep.* **16**, 597-606 (1999).
26. F. F. Fleming, L. Yao, P. C. Ravikumar, L. Funk, B. C. Shook, *J. Med. Chem.* **53**, 7902-7917 (2010).
27. S. Chakraborty, G. Leitus, D. Milstein, *Angew. Chem. Int. Ed.* **56**, 2074-2078 (2017).
28. J. H. Cho, S. Byun, A. Cho, B. M. Kim, *Catal. Sci. Technol.* **10**, 4201-4209 (2020).
29. S. Lu, J. Wang, X. Cao, X. Li, H. Gu, *Chem. Commun.* **50**, 3512-3515 (2014).
30. Z. Shao, S. Fu, M. Wei, S. Zhou, Q. Liu, *Angew. Chem. Int. Ed.* **55**, 14653-14657 (2016).
31. S. K. Sharma *et al.*, *Catal. Sci. Technol.* **3**, 85-88 (2013).
32. T. Schönauer, S. L. J. Thomä, L. Kaiser, M. Zobel, R. Kempe, *Chem. Eur. J.* **27**, 1609-1614 (2021).
33. L. M. Pignolet, *Homogeneous Catalysis with Metal Phosphine Complexes*, (Springer, 2013)
34. P. C. J. Kamer, P. W. N. M. van Leeuwen, *Phosphorus(III) Ligands in Homogeneous Catalysis: Design and Synthesis* (John Wiley & Sons, Ltd, 2012).
35. Z. Fei, P. J. Dyson, *Coord. Chem. Rev.* **249**, 2056-2074 (2005).
36. T. vom Stein *et al.*, *J. Am. Chem. Soc.* **136**, 13217-13225 (2014).
37. Y. Li, C. Topf, X. Cui, K. Junge, M. Beller, *Angew. Chem. Int. Ed.* **54**, 5196-5200 (2015).
38. S. Wesselbaum, T. vom Stein, J. Klankermayer, W. Leitner, *Angew. Chem. Int. Ed.* **51**, 7499-7502 (2012).
39. J. Kothandaraman, A. Goeppert, M. Czaun, G. A. Olah, G. K. S. Prakash, *J. Am. Chem. Soc.* **138**, 778-781 (2016).

40. J. Schneidewind, R. Adam, W. Baumann, R. Jackstell, M. Beller, *Angew. Chem. Int. Ed.* **56**, 1890-1893 (2017).
41. T. J. Korstanje, J. I. v. d. Vlugt, C. J. Elsevier, B. d. Bruin, *Science* **350**, 298-302 (2015).
42. X. Cui, Y. Li, C. Topf, K. Junge, M. Beller, *Angew. Chem. Int. Ed.* **54**, 10596-10599 (2015).
43. A. A. N. Magro, G. R. Eastham, D. J. Cole-Hamilton, *Chem. Commun.* 3154-3156 (2007).
44. J. R. Cabrero-Antonino, R. Adam, V. Papa, M. Beller, *Nat. commun.* **11**, 3893 (2020).
45. A. Hinzmann, H. Gröger, *Eur. J. Lipid Sci. Technol.* **122**, 1900163 (2020).
46. https://www.grandviewresearch.com/industry-analysis/fatty-amines-market. *Fatty Amines Market Size, Share & Trends Analysis Report By Product.*
47. R. Schoenheimer, D. Rittenberg, *Science* **87**, 221-226 (1938).
48. J. Buček et al., *R. Soc. open sci.* **5**, 181322 (2018).
49. T. Cernak, K. D. Dykstra, S. Tyagarajan, P. Vachal, S. W. Krska, *Chem. Soc. Rev.* **45**, 546-576 (2016).
50. M. Moir, J. J. Danon, T. A. Reekie, M. Kassiou, *Expert Opin. Drug Discovery* **14**, 1137-1149 (2019).

ACKNOWLEDGMENTS

We gratefully acknowledge the European Research Council (EU project 670986-NoNaCat) and the State of Mecklenburg-Vorpommern for financial and general support. We thank the analytical team of the Leibniz-Institut für Katalyse e.V. for their excellent service.

SUPPLEMENTARY MATERIALS

Materials and Methods
Experimental procedures
Figs. S1 to S12
Tables S1 to S3
NMR data and spectra

Chemical Science

ROYAL SOCIETY OF CHEMISTRY

EDGE ARTICLE

View Article Online
View Journal

Cite this: DOI: 10.1039/c9sc04963k

All publication charges for this article have been paid for by the Royal Society of Chemistry

Ultra-small cobalt nanoparticles from molecularly-defined Co–salen complexes for catalytic synthesis of amines†

Thirusangumurugan Senthamarai,[a] Vishwas G. Chandrashekhar,[a] Manoj B. Gawande,[b] Narayana V. Kalevaru,[a] Radek Zbořil,[b] Paul C. J. Kamer,[a] Rajenahally V. Jagadeesh *[a] and Matthias Beller *[a]

Received 2nd October 2019
Accepted 3rd February 2020

DOI: 10.1039/c9sc04963k

rsc.li/chemical-science

We report the synthesis of *in situ* generated cobalt nanoparticles from molecularly defined complexes as efficient and selective catalysts for reductive amination reactions. In the presence of ammonia and hydrogen, cobalt–salen complexes such as cobalt(II)–*N*,*N*′-bis(salicylidene)-1,2-phenylenediamine produce ultra-small (2–4 nm) cobalt-nanoparticles embedded in a carbon–nitrogen framework. The resulting materials constitute stable, reusable and magnetically separable catalysts, which enable the synthesis of linear and branched benzylic, heterocyclic and aliphatic primary amines from carbonyl compounds and ammonia. The isolated nanoparticles also represent excellent catalysts for the synthesis of primary, secondary as well as tertiary amines including biologically relevant *N*-methyl amines.

Introduction

In recent years, 3d metal-based nanoparticles (NPs) emerged as promising catalysts for the synthesis of functionalized and complex organic molecules for advanced applications in life and material sciences.[1] Traditionally, such syntheses are performed using homogeneous organometallic complexes,[2] which are often sensitive and more difficult to recycle compared to heterogeneous materials.[1,2] For the preparation of stable but at the same time active and selective NPs, the use of suitable precursors and optimal methods is crucial.[1] Commonly, nanoparticles are prepared by chemical reduction processes, calcination or pyrolysis in the presence of suitable supports and metal precursors. The resulting materials are applied particularly in industrially-relevant bench mark reactions of less functionalized molecules.[3] However, in recent years there is an increasing interest to use such catalysts for advanced organic synthesis, specifically for the preparation of life science products.[1] In this respect, the preparation of specific NPs by immobilization and pyrolysis of organometallic complexes or metal organic frameworks (MOFs) on heterogeneous supports attracted also attention.[1,4] These supported NPs show high activity and selectivity for the preparation of functionalized amines,[1d–i] nitriles,[1k,4c] carboxylic acid derivatives,[1f,k] and cycloaliphatic compounds.[1j] Although this preparation represents a highly useful tool to produce novel nano-structured catalysts on lab-scale, the upscaling can be difficult and requires specialized equipment.[1,4] Thus, the use of alternative, more convenient methods is highly desired. One possibility is the practical *in situ* generation of active heterogeneous NPs.[5] Based on this idea, herein we report a straightforward approach for the generation of cobalt-based NPs *in situ* from molecularly-defined metal complexes and their application in reductive amination reactions using ammonia and molecular hydrogen (Fig. 1).

The resulting amines represent privileged molecules widely used in chemistry, medicine, biology, and material science.[6] For their synthesis, catalytic reductive amination of carbonyl compounds using molecular hydrogen is widely applied as cost-

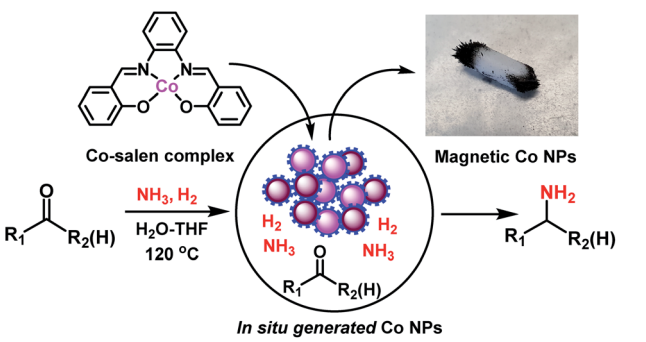

Fig. 1 *In situ* generation of Co-NPs for reductive aminations.

[a]Leibniz-Institut für Katalyse e. V. an der Universität Rostock, Albert-Einstein-Str. 29a, 18059 Rostock, Germany. E-mail: jagadeesh.rajenahally@catalysis.de; matthias.beller@catalysis.de

[b]Regional Centre of Advanced Technologies and Materials, Department of Physical Chemistry, Faculty of Science, Palacký University, Olomouc, Šlechtitelů 27, Olomouc, 78371, Czech Republic

† Electronic supplementary information (ESI) available. See DOI: 10.1039/c9sc04963k

effective methodology in both academic research and industry.[1e,h,7–10] Among reductive aminations, the synthesis of primary amines, which can be easily functionalized to high value products, continues to be especially important.[1e,h,j,8–10] Regarding catalysts for this reaction, precious metals-based ones are known to a large extent.[8,9] However, in recent years Co-[1e] and Ni[1h,i]-based nanocatalysts have successfully been developed in addition to RANEY® nickel.[10]

Results and discussion

In situ generation of Co-NPs and their activities

Following our concept, we initially investigated the reaction of cobalt salen complexes to obtain NPs. For example, using the cobalt–*N*,*N*′-bis(salicylidene)-1,2-phenylenediamine (complex **I**) in water–THF as solvent in the presence of ammonia and molecular hydrogen at 120 °C a black precipitate of Co NPs is formed, which can be magnetically separated (Fig. 1 and S3†). To explore their reactivity, preliminary catalytic experiments were carried out for the reductive amination of 4-bromobenzaldehyde **1** to 4-bromobenzylamine **2** in presence of ammonia and molecular hydrogen (Fig. 2). Indeed, using a mixture of cobalt(II) acetate and *N*,*N*′-bis(salicylidene)-1,2-phenylenediamine (**L1**) led to the formation of 15% of **2**. In contrast, testing simple cobalt(II) acetate under the same conditions produced no desired product. Remarkably, the defined complex Co-**L1** (complex **I**) exhibited excellent activity as well as selectivity in the bench mark reaction (98% of 4-bromobenzylamine). In addition, other molecularly-defined Co–salen complexes have also been tested (Fig. S1†) and complexes **II–IV** showed good activity (85–90% yield), while complex **V** resulted in lower product yield (50%). In all cases of active complexes, the reaction mixtures turned black after some hours. Hence, we assumed the *in situ* formed cobalt-NPs are the "real" active species for the reductive amination reaction. To confirm this, we performed a standard mercury test in the presence of complex **I** and after addition of 15 mg Hg the reductive amination reaction did not occur. Hot filtration of NPs and testing the filtrate for the reaction showed that Co-NPs did not go into solution as soluble particles. Studying the course of the benchmark reaction at different intervals of time showed a prolonged catalyst preformation time and only after 10 h 4-bromobenzylamine started to form (Fig. S3†). Apparently, complex **I** generated nanoparticles slowly, which then catalyze the desired amination process. For comparison, we also prepared cobalt nanoparticles separately by mixing complex **I**, ammonia and hydrogen (see S7a†). After isolation, they were tested under similar conditions and exhibited comparable activity and selectivity to that of *in situ* generated ones. Due to their physical properties, the Co NPs could be magnetically separated and were conveniently re-used up to three times (Fig. 2). However, after the third cycle we observed a significant decrease in activity and selectivity. In addition, the stability of the catalyst system was also confirmed by recycling the NPs after reduced reaction time (Fig. S4†). Next, we compared the reactivity of these active NPs with related supported NPs. However, addition of carbon or silica support to the reaction led to completely inactive materials (Fig. 2). On the other hand, materials prepared by immobilization of complex **I** on carbon or silica and subsequent pyrolysis produced catalysts with moderate activity (Fig. 2; 40–50% yield of **2**). In addition, specific cobalt nanoparticles have been prepared by using chemical reduction of cobalt salts[11] and tested for their activities. However, none of these cobalt nanoparticles formed the desired product, 4-bromobenzylamine (Table S1,† entries 5–6). All these results reveal the superiority of the simply *in situ* generated Co NPs (Fig. 3).

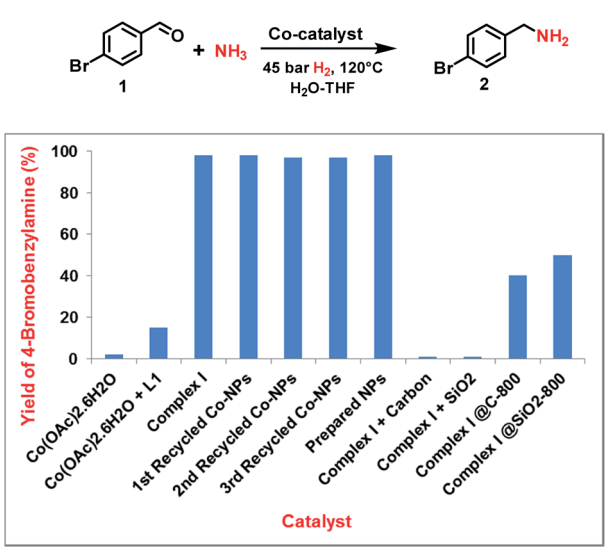

Fig. 2 Reductive amination of 4-bromobenzaldehyde: Activity of cobalt catalysts[a]. [a]Reaction conditions: 0.5 mmol 4-bromobenzaldehyde, 6 mol% Co-complex, (Co NPs), 5 bar NH_3, 45 bar H_2, 2.5 mL H_2O–THF (1.5 : 1), 120 °C, 24 h, GC yields using *n*-hexadecane as standard.

Characterization of *in situ* Co-NPs

To understand the reactivity and to know the structural features of the most active cobalt nanoparticles, we performed detailed

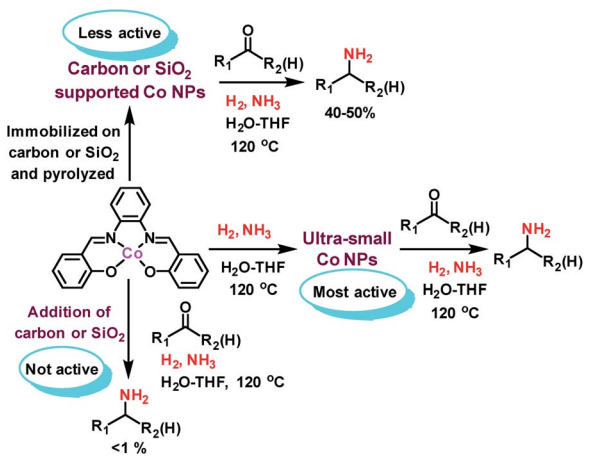

Fig. 3 Reductive amination of carbonyl compounds in presence of NH_3 and H_2 using different Co NPs produced from cobalt–salen complex.

characterizations using transmission electron microscopy (TEM), energy dispersive X-ray spectroscopy (EDX), X-ray diffraction (XRD), and X-ray photoelectron spectroscopy (XPS).

TEM analysis of cobalt-particles at different magnification showed sheets and at some places thread bundles like morphology where cobalt nanoparticles are embedded in carbon and nitrogen framework (Fig. 4). Further detailed morphological investigations were performed by HRTEM-STEM analysis. A close inspection of HRTEM images at 20 nm, revealed the presence of ultra-small (range 2–4 nm) cobalt nanoparticles (Fig. 4 and S6†) supported on graphitic carbon. The HAADF-elemental mapping displayed a homogeneous distribution of the cobalt nanoparticles (Fig. 4). In case of the recycled catalyst, we observed that these particles were still intact and there are no noticeable changes in the morphology (Fig. S8†).

XRD patterns of *in situ* generated and reused Co-nanoparticles do not show variations on the phase composition (Fig. S9†). Two allotropes of metallic cobalt have been identified, one with face centered cubic arrangement (Co-fcc, space group $Fm\bar{3}m$, PDF card 01-089-7093), and the other one with hexagonal closed packing (Co-hcp, space group $P6_3/mmc$, PDF card 01-089-7373). Elemental analysis of the bulk material showed 96.8 wt% of Co, 0.15 wt% of C and only 0.5 wt% of N. Complementary, XPS analysis displayed the presence of larger amounts of C, N, and O (C = 34.4, N = 1.2, O = 47.24 and Co = 16.8 at%) on the surface (Fig. S10†). The high resolution XP spectra of NPs in C1s region can be deconvoluted into five peak components with binding energies of 284.6, 285.6, 286.5, 288.5 and 289.4 eV corresponding to C–C sp^2, C–C sp^3, C–O/C–N, and C=O, and O=C–O type bonds with individual atomic% of 64.09, 19.30, 8.59, 3.20 and 4.82 respectively, showing the graphitic nature of the carbon material (Fig. 5a). The presence of a specific N1s peak at 399.7 confirms pyrrolic nitrogen (Fig. 5b). The three peak components at 529.5, 531.4, and 532.9 eV in O1s spectra originate from the presence of $Co(OH)_2$ (6.99%), C=O (73.09%), and O–C on the surface of cobalt (19.92%). This reveals partial oxidation at the surface of the optimal material (Fig. 5c). In agreement, the two main component peaks having binding energy at 780.7 eV (50.81%) and 782.5 eV (22.54%) confirm the presence of Co^{2+} ($Co(OH)_2$) (Fig. 5d).[12a] Three small peaks having binding energies at 778.09 (2.45%), 781.09 (0.59%) and 783.09 (0.35%) eV indicate the presence of metallic cobalt.[12b]

The HR-XPS of reused catalysts revealed that there is no shifting of binding energy in Co $2p_{3/2}$ peak but the ratio of metallic cobalt *vs.* cobalt hydroxide was slightly changed (Fig. S11d†). On the other hand, no perceptible change in the binding energies of C1s and N1s was discerned except for the slight shifting of the pyrrolic nitrogen peak from 399.7 eV to 400.2 eV, thus reiterating no apparent alteration in the chemical nature of the carbon shell of the catalyst (Fig. S11a and b†).

It is interesting to note that these cobalt-particles exhibit ferromagnetic behaviour with distinct values of coercivity field and remanent magnetization (Fig. S12†). Ferromagnetic behaviour at room temperature is due to the stronger effect of the magnetic dipole interaction compared with thermal fluctuations. We do not observe any blocking temperature suggesting the size of nanoparticles above 10–15 nm (*e.g.* the system is not superparamagnetic at room temperature).

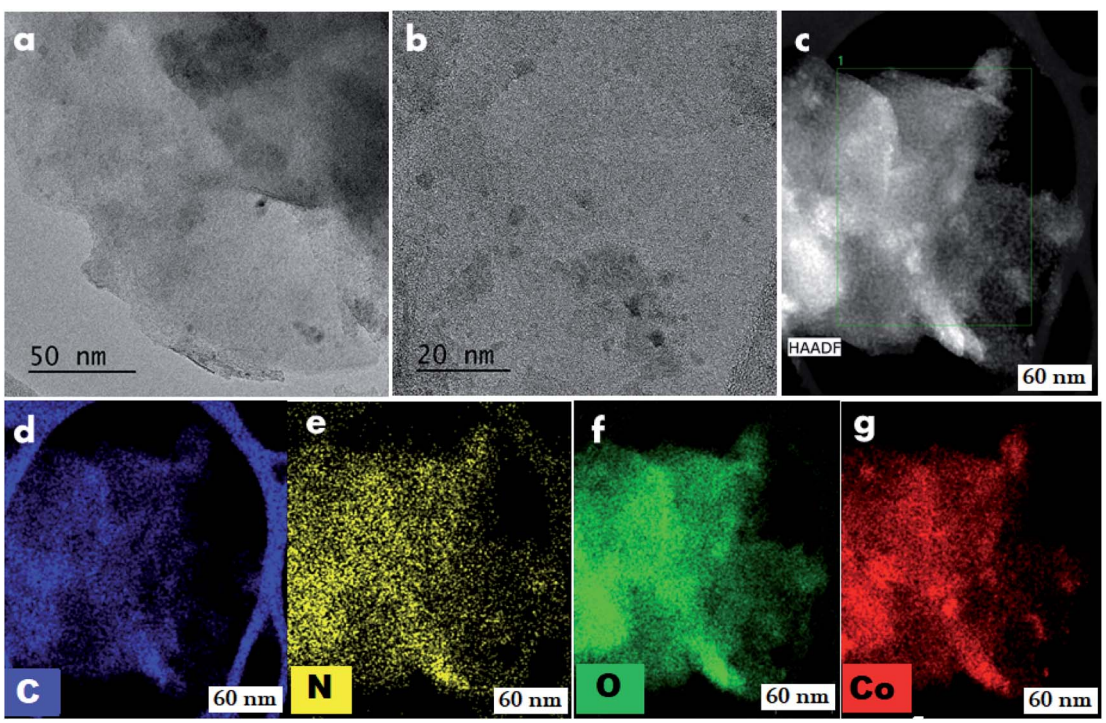

Fig. 4 TEM images of *in situ* generated Co-NPs from complex **I**. (a and b) HRTEM images of cobalt catalyst, (C) magnified STEM image, (d–g) elemental mapping images where C, N, O and Co are in blue, yellow, green and red colours.

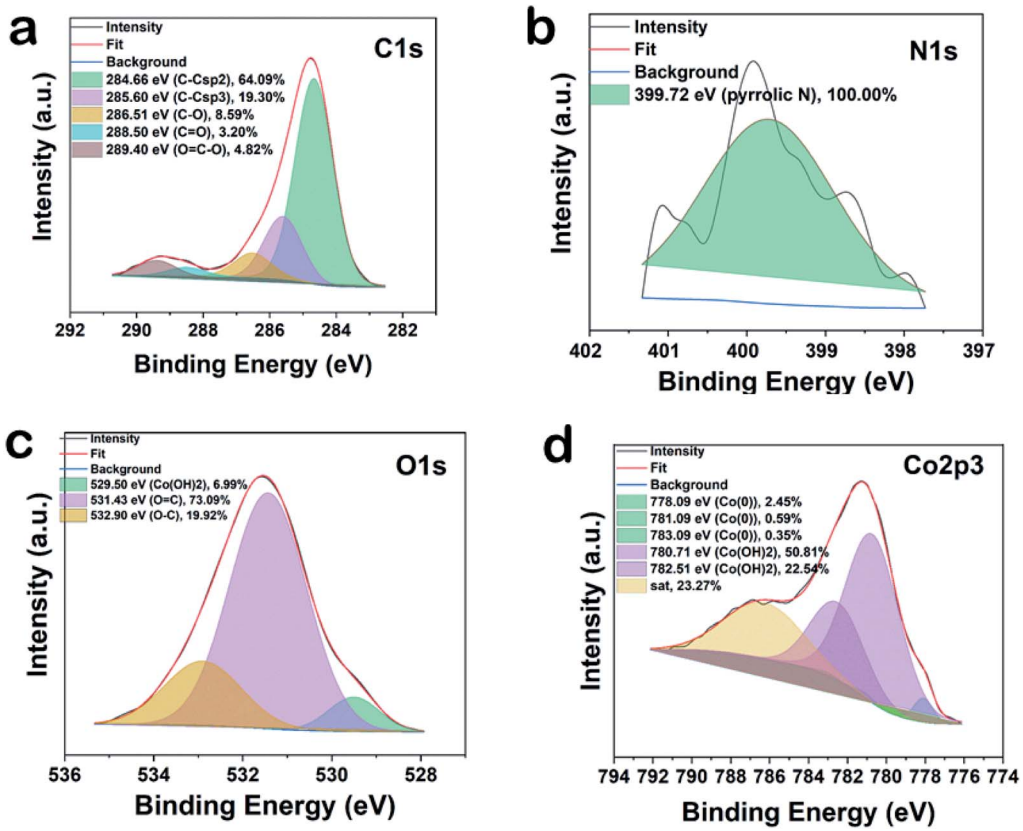

Fig. 5 HR-XPS spectra of *in situ* generated Co NPs.

Synthesis of linear primary amines

Then, we tested the general applicability of our *in situ* generated nanoparticles for the synthesis of primary amines. As shown in Schemes 1 and 2, a variety of structurally diverse and functionalized benzylic, heterocyclic and aliphatic linear and branched primary amines can be prepared in good to excellent yields. Simple and substituted aldehydes underwent smooth reaction to give primary benzylic amines in up to 92% yield (Scheme 1, products **3–7**). For example, fluoro-, chloro-, and bromo-substituted benzaldehydes produced corresponding amines without significant dehalogenations in 86–92% yields (Scheme 1, entries **8–12**). Different functionalized benzylic amines containing methoxy, trifluoromethoxy, dimethylamino, and ester groups as well as C–C double bonds were synthesized in up to 95% yield (Scheme 1, products **14–23**). In addition to benzylic amines, primary aliphatic ones were also prepared under similar conditions (Scheme 1, products **25–27**). Interestingly, the natural product perillaldehyde was successfully aminated to produce the corresponding amine in 87% yield (product **27**).

Synthesis of branched primary amines

Next, we tested the reductive amination of ketones (Scheme 2), which is more challenging compared to aldehydes.

Nevertheless, at higher temperature (130 °C) nine aromatic and six aliphatic branched primary amines were prepared in up to 92% yield. In addition, separately prepared Co NPs from complex **I**, gave similar yields of amines to those obtained by *in situ* generated nanoparticles.

Synthesis of secondary and tertiary amines

Apart from primary amines synthesis, we explored the applicability of Co-NPs for the synthesis of secondary and tertiary amines. Interestingly, testing complex **I** which generates the active NPs *vide supra* for the reaction of benzaldehyde and aniline at 120 °C in presence of molecular hydrogen (40 bar) led to the formation of imine (*N*-benzylideneaniline) as the sole product. Under these conditions no nanoparticles could be isolated after the reaction.

Apparently, the presence of both ammonia and hydrogen are required for the generation of the active NPs! Indeed, using isolated Co NPs, which were prepared from complex **I**, ammonia and hydrogen, led to excellent activity and selectivity for the synthesis of secondary and tertiary amines including *N*-methyl amines (Scheme 3). As representative examples different benzaldehydes were reacted with substituted anilines and the corresponding *N*-benzylanilines were obtained in 87–98% yields (Scheme 1; products **41–45**). Similarly, reactions of different benzaldehydes with benzylic and aliphatic amines produced selectively the corresponding secondary and tertiary amines (Scheme 3; products **46–55**). In addition, aliphatic aldehydes and 4-fluoroaniline underwent reductive amination and gave the corresponding secondary amines (Scheme 3, products **56–57**). Finally, *N*,*N*′-dimethylamines

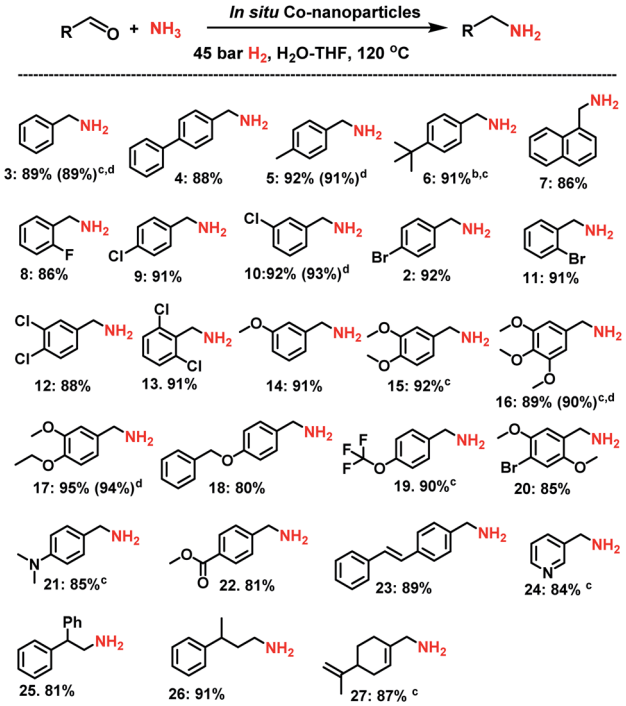

Scheme 1 *In situ* generated Co-nanoparticles catalyzed synthesis of linear primary amines from aldehydes[a]. [a]Reaction conditions: 0.5 mmol aldehyde, 6 mol% complex **I** (22 mg), 5–7 bar NH_3, 45 bar H_2, 2.5 mL H_2O–THF (1.5 : 1), 120 °C, 24h, isolated yields. [b] Same as 'a' at 130 °C. [c] Same as 'a' in 2.5 mL H_2O. [d] same as 'a' using prepared and isolated Co-NPs from complex **I** (2 mg; 6.5 mol% Co).

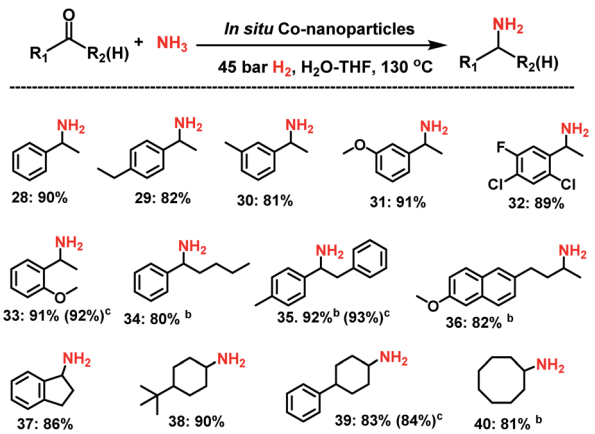

Scheme 2 Synthesis of branched primary amines from ketones using *in situ* generated Co-nanoparticles[a]. [a]Reaction conditions: 0.5 mmol ketone, 6 mol% complex **I** (22 mg) 5–7 bar NH_3, 45 bar H_2, 2.5 mL H_2O, 130 °C, 24 h, isolated yields. [b] Same as 'a' in H_2O–THF (1.5 : 1 ratio). [c]Using prepared and isolated Co-NPs from complex **I** (2 mg; 6.5 mol% Co).

were also prepared from three different aldehydes and aqueous *N*,*N*′-dimethyl amine (Scheme 3, products **58–60**).

Reaction upscaling

In order to demonstrate the synthetic utility of this novel reductive amination protocol, we performed the amination of 5

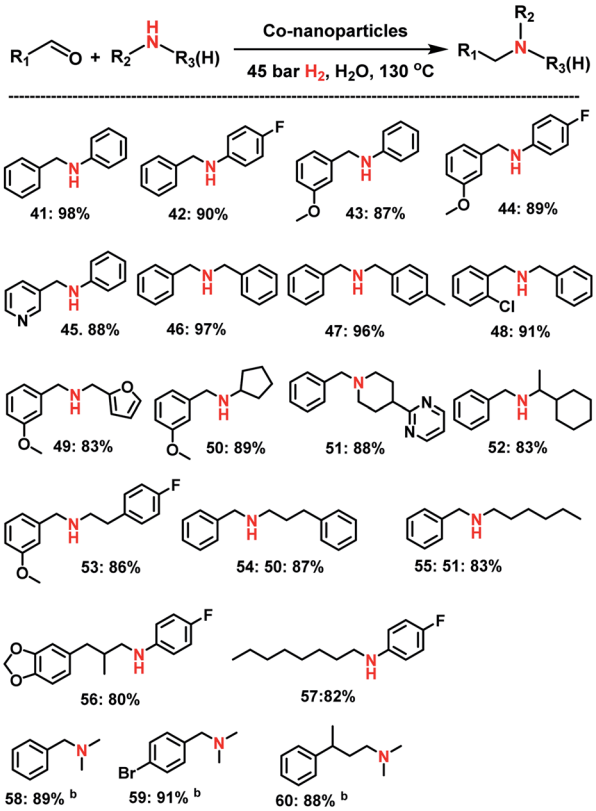

Scheme 3 Synthesis of secondary, tertiary and *N*-methyl amines using Co-nanoparticles prepared from complex **I**[a]. [a]Reaction conditions: 0.6 mmol aldehyde, 0.5 mmol amine, 2 mg Co-NPS (6.5 mol% Co), 45 bar H_2, 2.5 mL H_2O, 130 °C, 20 h, isolated yields. [b]Same as 'a' using 1 mL aq. *N*,*N*′-dimethylamine instead of amine.

carbonyl compounds in 5–10 g scale (Scheme 4). As expected, all the tested reactions could be successfully upscaled and the yields (92–96%) of the corresponding primary amines were comparable to that of small scale (0.5 mmol) reactions.

Experimental

General considerations

All substrates were obtained commercially from various chemical companies and their purity has been checked before use. Cobalt(II) acetate tetrahydrate (cat no. 208396–50G), salicylaldehyde, phenylenediamine and other ligand precursors were purchased from Sigma-Aldrich. Silica (silicon(IV) oxide,

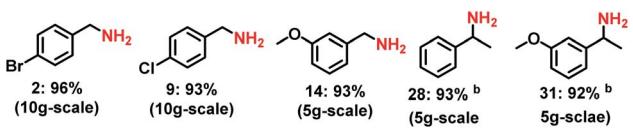

Scheme 4 Gram-scale synthesis of selected primary amines using *in situ* generated Co-NPs [a]. [a]Reaction conditions: 5–10 g of carbonyl compound, weight of complex **I** corresponds to 6 mol%, 5–7 bar NH_3, 45 bar H_2, 75–150 mL H_2O–THF (1 : 1), 120 °C, 24h, isolated yields. [b] Same as 'a' at 130 °C in 75 mL H_2O.

amorphous fumed, S.A. 300–350 $m^2 g^{-1}$) was obtained from Alfa Aesar. Carbon powder, VULCAN® XC72R with Code XVC72R and CAS No. 1333-86-4 was obtained from Cabot Corporation Prod. The pyrolysis experiments were carried out in a Nytech-Qex oven.

X-ray diffraction patterns were recorded with an Empyrean (PANalytical, The Netherlands) diffractometer in the Bragg–Brentano geometry, Co-Kα radiation (40 kV, 30 mA, $\lambda = 0.1789$ nm) equipped with a PIXcel3D detector (1D mode) and programmable divergence and diffracted beam anti-scatter slits. The measurement range was 2θ: 5–105°, with a step size of 0.026°. The identification of crystalline phases was performed using the High Score Plus software (PANalytical) that includes the PDF-4$^+$ database.

TEM images were obtained using a HRTEM TITAN 60-300 with X-FEG type emission gun, operating at 80 kV. This microscope is equipped with a Cs image corrector and a STEM high-angle annular dark-field detector (HAADF). The point resolution is 0.06 nm in TEM mode. The elemental mappings were obtained by STEM-Energy Dispersive X-ray Spectroscopy (EDS) with an acquisition time of 20 min. For HRTEM analysis, the powder samples were dispersed in ethanol and ultrasonicated for 5 min. One drop of this solution was placed on a copper grid with holey carbon film.

XPS surface investigation has been performed on the PHI 5000 VersaProbe II XPS system (Physical Electronics) with monochromatic Al-Kα source (15 kV, 50 W) and photon energy of 1486.7 eV. Dual beam charge compensation was used for all measurements. All the spectra were measured in the vacuum of 1.3×10^{-7} Pa and at room temperature of 21 °C. The analyzed area on each sample was a spot of 200 μm in diameter. The survey spectra were measured with pass energy of 187.850 eV and electronvolt step of 0.8 eV while for the high resolution spectra was used pass energy of 23.500 eV and electronvolt step of 0.2 eV. The spectra were evaluated with the MultiPak (Ulvac – PHI, Inc.) software. All binding energy (BE) values were referenced to the carbon peak C 1s at 284.80 eV.

Magnetic properties of cobalt-nanoparticles were analyzed using a Quantum Design Physical Properties Measurement System (PPMS Dynacool system) with the vibrating sample magnetometer (VSM) option. The experimental data were corrected for the diamagnetism and signal of the sample holder. The temperature dependence of the magnetization was recorded in a sweep mode of 1 K min^{-1} in the zero-field-cooled (ZFC) and field-cooled (FC) measuring regimes. To get the ZFC magnetization curve, the sample was firstly cooled down from 300 to 5 K in a presence of zero magnetic field and the measurement was carried out on warming from 5 to 300 K under the external magnetic field (1000 Oe). In the case of the FC magnetization measurements, the sample was cooled from 300 to 5 K in an external magnetic field (1000 Oe) and the measurement was carried out on warming from 5 to 300 K at the same value of the external magnetic field (1000 Oe). Hysteresis loops were measured at room temperature (300 K) and at low temperature (5 K).

GC conversion and yields were determined by GC-FID, HP6890 with FID detector, column HP530 m × 250 mm × 0.25 μm. ^{1}H, ^{13}C, NMR data were recorded on a Bruker ARX 300 and Bruker ARX 400 spectrometers using DMSO-d_6 and $CDCl_3$ solvents.

All catalytic reactions were carried out in 300 mL and 100 mL autoclaves (PARR Instrument Company). In order to avoid unspecific reactions, catalytic reactions were carried out either in glass vials, which were placed inside the autoclave, or glass/Teflon vessel fitted autoclaves.

Preparation of Co–salen complexes (see scheme S1†)

(a) Preparation of salen ligand (L1). Salicylaldehyde (4 mmol; in 15 mL ethanol), 1,2-phenylenediamine (2 mmol; in 10 mL ethanol) were separately dissolved in ethanol. Then, the ethanolic solution of 1,2-phenylenediamine was slowly added to salicylaldehyde solution. The resulting reaction mixture was refluxed at 80 °C for 8 h to obtain a solid compound. The reaction mixture was cooled to room temperature and the product was isolated by filtration. Then, the solid product was washed with 30 mL of cold ethanol twice and dried *in vacuo* to get corresponding salen ligand (**L1**) in 98% yield. Other salen ligands were prepared by using similar method.

(b) Preparation of Co–salen complex (complex I).[13] 1 g of $Co(OAc)_2 \cdot 4H_2O$, (4 mmol; in 15 mL ethanol) and 1.28 g of *N*,*N*′-bis(salicylidene)-1,2-phenylenediamine (ligand **L1**) (4 mmol; in 20 mL ethanol) were separately dissolved in ethanol. The cobalt acetate solution was slowly added to the solution of ligand. The resulting red suspension was refluxed for 18 h at 80 °C to give a reddish-brown solid compound. The obtained solid compound was filtered. Then the obtained solid compound was washed with 10 mL of cold ethanol and dried *in vacuo* to get corresponding cobalt salen complex **I** in 94% yield. The same procedure was applied to prepare other cobalt salen complexes using different salen ligands.

Procedure for reductive amination

(a) Procedure for the synthesis of primary amines. The magnetic stirring bar, 0.5 mmol of the carbonyl compound (aldehyde or ketone) and 22 mg complex **I** (in case of *in situ* generated Co NPs) or 2 mg of prepared and isolated Co NPs were transferred to an 8 mL glass vial. Then, 2 mL of solvent (water or THF/H_2O (1.5 : 1)) was added and the vial was fitted with septum, cap and needle. The reaction vials (8 vials with different substrates at a time) were placed into a 300 mL autoclave. The autoclave was flushed with hydrogen twice at 40 bar pressure and then it was pressurized with 5–7 bar ammonia and 45 bar hydrogen. The autoclave was placed into an aluminium block preheated at 135 °C in case of aldehydes and 145 °C in case of ketones and the reactions were stirred for the required time. During the reaction, the inside temperature of the autoclave was measured to be 120 °C in case of aldehydes and 130 °C in case of ketones and this temperature was used as the reaction temperature. After completion of the reactions, the autoclave was cooled to room temperature. The remaining ammonia and hydrogen were discharged and the vials containing reaction products were removed from the autoclave. The reaction mixtures containing the products were filtered off and washed

thoroughly with ethanol. The reaction products were analyzed by GC-MS. The crude product was purified by column chromatography using ethyl acetate and *n*-heptane as the eluent. The corresponding primary amines were converted to their respective hydrochloride salt and characterized by NMR and GC-MS analysis. For converting into hydrochloride salt of amine, 0.3–0.5 mL 7 M HCl in dioxane or 1.5 M HCl in methanol was added to the dioxane solution of respective amine and stirred at room temperature for 4–5 h. Then, the solvent was removed and the resulted hydrochloride salt of amine was dried under high vacuum. The yields were determined by GC for the selected amines: after completing the reaction, *n*-hexadecane (100 μL) as standard was added to the reaction vials and the reaction products were diluted with ethyl acetate followed by filtration using plug of silica and then analyzed by GC.

(b) Procedure for the synthesis of secondary and tertiary amines. The magnetic stir bar, 0.5 mmol of amine and 0.6 mmol aldehyde were transferred to an 8 mL glass vial. Then 2 mg of Co NPs and 2 mL of water as solvent were added. The vial was fitted with septum, cap and needle. The reaction vials (8 vials with different substrates at a time) were placed into a 300 mL autoclave. The autoclave was flushed with hydrogen twice at 40 bar pressure and then it was pressurized 45 bar hydrogen. The autoclave was placed into an aluminium block preheated at 145 °C and the reactions were stirred for the required time. During the reaction, the inside temperature of the autoclave was measured to be 130 °C and this temperature was used as the reaction temperature. After completion of the reactions, the autoclave was cooled to room temperature. The remaining hydrogen was discharged and the vials containing the reaction products were removed from the autoclave. The reaction mixtures containing the products were filtered off and washed thoroughly with ethanol. The reaction products were analyzed by GC-MS. The crude product was purified by column chromatography using ethyl acetate and *n*-heptane as the eluent. The corresponding amines were characterized by NMR and GC-MS analysis.

Isolation of *in situ* generated cobalt nanoparticles

After the completion of the reductive amination reaction of carbonyl compound in presence of ammonia and hydrogen as described in Section S3a,† the *in situ* generated cobalt nanoparticles from the solution containing products were separated using the magnetic stir bar. Then, they were separated from the magnetic stir bar and washed with water and ethanol. Finally the recycled Co NPs were dried under vacuum and stored in a glass vial.

Elemental analysis (wt%): Co = 96.8% C = 0.15% and N = 0.5%.

Recycling of *in situ* generated cobalt-nanoparticles

A magnetic stirring bar and 5 mmol 4-bromobenzaldehyde were transferred to a glass fitted 100 mL autoclave and then 20 mL THF–water (1.5 : 1) was added. Subsequently, 20 mg isolated *in situ* generated Co NPs were added. The autoclave was flushed with 40 bar hydrogen and then it was pressurized with 5–7 bar ammonia gas and 45 bar hydrogen. The autoclave was placed into the heating system and the reaction was allowed to progress at 120 °C (temperature inside the autoclave) by stirring for 24 h. After completion of the reaction, the autoclave was cooled and the remaining ammonia and hydrogen pressure was discharged. To the reaction products, 200 μL *n*-hexadecane as standard was added. The catalyst was then separated by centrifugation and the supernatant containing the reaction products was subjected to GC analysis for determining conversion and yield. The separated catalyst was then washed with ethanol, dried under vacuum and used without further purification or reactivation for the next run.

Gram-scale reactions

The Teflon or glass fitted 300 mL autoclave was charged with a magnetic stirring bar and 5–10 g of carbonyl compound (aldehyde or ketone) and complex **I** (weight of complex **I** corresponds 6 mol%). Then, 75–150 mL of solvent (THF/H_2O (1.5 : 1) in case of aldehyde and H_2O in case of ketones) was added and the autoclave was flushed with hydrogen twice at 40 bar pressure. Afterwards, it was pressurized with 5–7 bar ammonia and 45 bar hydrogen. The autoclave was placed into an aluminium block preheated at 135 °C in case of aldehydes and 145 °C in case of ketones and the reactions were stirred for the required time. During the reaction, the inside temperature of the autoclave was measured to be 120 °C in case of aldehydes and 130 °C in case of ketones and this temperature was used as the reaction temperature. After completion of the reaction, the autoclave was cooled to room temperature and the remaining ammonia and hydrogen were discharged. The reaction mixtures containing the products were filtered off and washed thoroughly with ethanol. The reaction products were analysed by GC-MS and the crude primary amine product was purified by column chromatography using ethyl acetate and *n*-heptane as the eluent.

Preparation of cobalt-nanoparticles

(a) Preparation of Co NPs from complex I. A magnetic stir bar and 1.0 g of cobalt–salen complex (complex **I**) were transferred to a glass fitted 100 mL autoclave. Then, 20 mL THF–water (1 : 1) was added. The autoclave was flushed with 40 bar hydrogen and then it was pressurized with 5–7 bar ammonia and 45 bar hydrogen. The autoclave was placed into the heating system and the reaction was allowed to progress at 120 °C (temperature inside the autoclave) by stirring for 24 h. After 24 h of reaction time, the autoclave was removed from the heating system and cooled to room temperature. The remaining ammonia and hydrogen pressure was discharged. The cobalt nanoparticles formed were separated from solution by using the magnetic stir bar. Then, the nanoparticles were separated from the magnetic stir bar and washed with water and ethanol. Finally obtained nanoparticles were dried under vacuum and stored in a glass vial.

(b) Preparation of carbon and silica supported Co-nanoparticles. In a 50 mL round bottomed flask, cobalt salen complex (316.8 mg) and 25 mL of ethanol were refluxed at 80 °C

for 15 minutes. To this, 700 mg of Vulcan XC 72R carbon powder or SiO_2 was added and then the whole reaction mixture was refluxed at 80 °C for 4–5 h. The reaction mixture was cooled to room temperature and the ethanol was removed in vacuum. The solid sample obtained was dried in high vacuum, after which it was grinded to a fine powder. Then, the grinded powder was pyrolyzed at 800 °C for 2 hours under an argon atmosphere and cooled to room temperature.

(c) Preparation of other cobalt nanoparticles reported in literature.[11] *Method-I*: 1.0 g of cobalt acetate and 1.5 mL of oleic acid were mixed in 40 mL of diphenyl ether (DPE) and the reaction mixture was heated to 200 °C under N_2 atmosphere. Then, 1.0 mL of TOP (trioctylphosphine) was added and the mixture was again heated to 250 °C. Subsequently, the reducing solvent such as 4.0 g of 1,2-dodecanediol dissolved in 10 mL DPE at 80 °C, was injected into the reaction mixture. Then whole reaction mixture was held at 250 °C for 30 min until the completion of the reduction. The reaction products were cooled to room temperature and ethanol was added to precipitate nanoparticles. The formed cobalt nanoparticles were separated by centrifugation and were finally dried and stored in glass vial.

Method-II: 2 mmol of cobalt acetate and 0.4 mmol of oleic acid were mixed in 1 mL ethanol. Then, 3 mmol of $NaBH_4$ dissolved in 1 mL of ethanol, was slowly added to the above mixture at room temperature under stirred condition. The whole mixture was stirred at room temperature for 4 h. The formed cobalt nanoparticles were separated by centrifugation and finally dried and stored in glass vial.

Conclusions

In conclusion, we demonstrated that the *in situ* formation of cobalt nanoparticles from molecularly defined precursors is straightforward and convenient. Such approach can be used as a versatile tool to prepare selective and active heterogeneous catalysts. In our specific case, Co NPs are formed from cobalt–salen complexes (*e.g.* cobalt(II)–*N*,*N*′-bis(salicylidene)-1,2-phenylenediamine) in the presence of ammonia and hydrogen. Thereby, well-defined ultra-small metallic cobalt and cobalt hydroxide nanoparticles embedded in a cobalt–nitrogen framework are formed. The resulting NPs are stable in the presence of air and water and allow for the preparation of various functionalized and structurally diverse linear and branched benzylic, heterocyclic and aliphatic primary amines as well as secondary and tertiary amines. Moreover, they can be easily magnetically separated enabling easy catalyst recycling and product purification.

Conflicts of interest

There are no conflicts to declare.

Acknowledgements

We gratefully acknowledge the European Research Council (EU project 670986-NoNaCat), and the State of Mecklenburg-Vorpommern for financial and general support. We thank the analytical team of the Leibniz-Institute for Catalysis, Rostock for their excellent service. We gratefully thank Ondrej Tomanec, and Martin Petr (both from Palacky University) for HRTEM elemental mapping and XPS data respectively. The authors gratefully acknowledge the support by the Operational Programme Research, Development and Education – European Regional Development Fund, projects no. CZ.02.1.01/0.0/0.0/16_019/0000754 and CZ.02.1.01/0.0/0.0/15_003/0000416 of the Ministry of Education, Youth and Sports of the Czech Republic.

Notes and references

1 (*a*) D. Wang and D. Astruc, *Chem. Soc. Rev.*, 2017, **46**, 816–854; (*b*) L. Liu and A. Corma, *Chem. Rev.*, 2018, **8**, 4981–5079; (*c*) X. Cui, X. Dai, Y. Deng and F. Shi, *Chem.–Eur. J.*, 2013, **19**, 3665–3675; (*d*) R. V. Jagadeesh, A.-E. Surkus, H. Junge, M.-M. Pohl, J. Radnik, J. Rabeah, H. Huan, V. Schünemann, A. Brückner and M. Beller, *Science*, 2013, **342**, 1073–1076; (*e*) R. V. Jagadeesh, K. Murugesan, A. S. Alshammari, H. Neumann, M.-M. Pohl, J. Radnik and M. Beller, *Science*, 2017, **358**, 326–332; (*f*) L. He, F. Weniger, H. Neumann and M. Beller, *Angew. Chem., Int. Ed.*, 2016, **55**, 12582–12594; (*g*) T. Schwob and R. Kempe, *Angew. Chem., Int. Ed.*, 2016, **55**, 15175–15179; (*h*) G. Hahn, P. Kunnas, N. de Jonge and R. Kempe, *Nat. Catal.*, 2018, **2**, 71–77; (*i*) K. Murugesan, M. Beller and R. V. Jagadeesh, *Angew. Chem., Int. Ed.*, 2019, **58**, 5064–5068; (*j*) K. Murugesan, T. Senthamarai, A. S. Alshammari, R. M. Altamimi, C. Kreyenschulte, M.-M. Pohl, H. Lund, R. V. Jagadeesh and M. Beller, *ACS Catal.*, 2019, **9**, 8581–8591; (*k*) R. V. Jagadeesh, T. Stemmler, A.-E. Surkus, M. Bauer, M.-M. Pohl, J. Radnik, K. Junge, H. Junge, A. Brückner and M. Beller, *Nat. Protoc.*, 2015, **10**, 916–926; (*l*) T. Schwob, P. Kunnas, N. de Jonge, C. Papp, H. P. Steinrück and R. Kempe, *Sci. Adv.*, 2019, **5**, eaav3680; (*m*) T. Schwob, M. Ade and R. Kempe, *ChemSusChem*, 2019, **12**, 3013–3017.

2 (*a*) G. W. Parshall and S. D. Ittel, *Homogeneous Catalysis: The Applications and Chemistry of Catalysis by Soluble Transition Metal Complexes*, Weily, 1992; (*b*) P. W. N. M. van Leeuwen and J. C. Chadwick, *Homogeneous Catalysts: Activity – Stability – Deactivation*, Wiley-VCH, 2011; (*c*) B. Cornils, W. A. Herrmann, M. Beller and R. Paciello, *Applied Homogeneous Catalysis with Organometallic Compounds*, Wiley-VCH, 2017; (*d*) B. A. Averill, J. A. Moulijn, R. A. van Santen and P. W. N. M. van Leeuwen, *Catalysis: An integrated approach*, Elsevier, 1997.

3 (*a*) L. Filipponi and D. Sutherland, *Nanotechnologies: Principles, Applications, Implications and Hands-on Activities*, European Commission, European Union, 2012; (*b*) M. B. Gawande, S. P. Branco and R. S. Varma, *Chem. Soc. Rev.*, 2013, **42**, 3371–3393; (*c*) M. B. Gawande, A. Goswami, T. Asefa, H. Guo, A. V. Biradar, D. L. Peng, R. Zboril and R. S. Varma, *Chem. Soc. Rev.*, 2015, **44**, 7540–7590; (*d*) P. Munnik, P. E. De Jongh and K. P. De Jong, *Chem. Rev.*, 2015, **115**, 6687–6718; (*e*) M. Sankar, N. Dimitratos, P. J. Miedziak, P. P. Wells, C. J. Kielye and G. J. Hutchings,

Chem. Soc. Rev., 2012, **41**, 8099–8139; (*f*) F. Tao, *Metal Nanoparticles for Catalysis: Advances and Applications*, Royal Society of Chemistry, 2014; (*g*) E. M. van Schrojenstein Lantman, T. Deckert-Gaudig, A. J. G. Mank, V. Deckert and B. M. Weckhuysen, *Nat. Nanotechnol.*, 2012, **7**, 583–586; (*h*) J. J. H. B. Sattler, J. Ruiz-Martinez, E. Santillan-Jimenez and B. M. Weckhuysen, *Chem. Rev.*, 2014, **114**, 10613–10653; (*i*) A. Balanta, C. Godard and C. Claver, *Chem. Soc. Rev.*, 2011, **40**, 4973–4985.

4 (*a*) S. Dang, Q.-L. Zhu and Q. Xu, *Nat. Rev. Mater.*, 2017, **3**, 17075; (*b*) J. Tang and Y. Yamauchi, *Nat. Chem.*, 2016, **8**, 638–639; (*c*) K. Shen, X. Chen, J. Chen and Y. Li, *ACS Catal.*, 2016, **6**, 5887–5903.

5 (*a*) N. Yan, Y. Yuan and P. J. Dyson, *Dalton Trans.*, 2013, **42**, 13294–13304; (*b*) Da. Cantillo, M. Baghbanzadeh and C. O. Kappe, *Angew. Chem., Int. Ed.*, 2012, **51**, 10190–10193; (*c*) J. Holz, C. Pfeffer, H. Zuo, D. Beierlein, G. Richter, E. Klemm and R. Peters, *Angew. Chem., Int. Ed.*, 2019, **58**, 10330–10334; (*d*) L. Zadoina, K. Soulantica, S. Ferrere, B. Lonetti, M. Respaud, A. F. Mingotaud, A. Falqui, A. Genovese, B. Chaudret and M. Mauzac, *J. Mater. Chem.*, 2011, **21**, 6988–6994.

6 (*a*) A. Ricci, *Amino group chemistry: From synthesis to the life sciences*, Wiley-VCH, 2008; (*b*) Top 200 drugs production, National Science Foundation, *J Chem. Educ.*, 2010, **87**, 1348; (*c*) S. A. Lawrence, *Amines: synthesis, properties and applications*, Cambridge University Press, 2004; (*d*) F. Shi and X. Cui, *Catalytic amination for N-alkyl amine synthesis*, Academic Press, 2018; (*e*) W. R. Meindl, E. V. Angerer, H. Schoenenberger and G. Ruckdeschel, *Med. Chem.*, 1984, **27**, 1111–1118; (*f*) V. Froidevaux, C. Negrell, S. Caillol, J.-P. Pascault and B. Boutevin, *Chem. Rev.*, 2016, **116**, 14181–14224; (*g*) T. Yan, B. L. Feringa and K. Barta, *Nat. Commun.*, 2014, **5**, 5602.

7 (*a*) S. Gomez, J. A. Peters and T. Maschmeyer, *Adv. Synth. Catal.*, 2002, **344**, 1037–1057; (*b*) H. Alinezhad, H. Yavari and F. Salehian, *Curr. Org. Chem.*, 2015, **19**, 1021–1049; (*c*) T. C. Nugenta and M. El-Shazlya, *Adv. Synth. Catal.*, 2010, **352**, 753–819; (*d*) K. Natte, H. Neumann, R. V. Jagadeesh and M. Beller, *Nat. Commun.*, 2017, **8**, 1344; (*e*) https://reagentguides.com/reagent-guides/reductive-amination/list-of-reagents/hydrogen-metal-catalysts-precious-and-base-metal; (*f*) K. N. Gusak, Z. V. Ignatovich and E. V. Koroleva, *Russ. Chem. Rev.*, 2015, **84**, 288–309.

8 (*a*) Y. Nakamura, K. Kon, A. S. Touchy, K.-I. Shimizu and W. Ueda, *ChemCatChem*, 2015, **7**, 921–924; (*b*) G. Liang, A. Wang, L. Li, G. Xu, N. Yan and T. Zhang, *Angew. Chem., Int. Ed.*, 2017, **56**, 3050–3054; (*c*) T. Komanoya, T. Kinemura, Y. Kita, Y. K. Kamata and M. Hara, *J. Am. Chem. Soc.*, 2017, **139**, 11493–11499; (*d*) M. Chatterjee, T. Ishizakaa and H. Kawanami, *Green Chem.*, 2016, **18**, 487–496.

9 (*a*) T. Gross, A. M. Seayad, M. Ahmad and M. Beller, *Org. Lett.*, 2002, **4**, 2055–2058; (*b*) T. Riermeier, K.-J. Haack, U. Dingerdissen, A. Börner, V. Tararov and R. Kadyrov, *US Pat.*, 6884887B1, 2005; (*c*) J. Gallardo-Donaire, M. Ernst, O. Trapp and T. Schaub, *Adv. Synth. Catal.*, 2016, **358**, 358–363; (*d*) J. Gallardo-Donaire, M. H. Wysocki, M. Ernst, F. Rominger, O. Trapp, A. Stephen, L. Hashmi, A. Schaefer, P. Comba and T. Schaub, *J. Am. Chem. Soc.*, 2018, **140**, 355–361; (*e*) S. Ogo, K. Uehara, T. Abura and S. Fukuzumi, *J. Am. Chem. Soc.*, 2014, **126**, 3020–3021; (*f*) R. Kadyrov and T. H. Riermeier, *Angew. Chem., Int. Ed.*, 2003, **42**, 5472–5474; (*g*) T. Senthamarai, K. Murugesan, J. Schneidewind, N. V. Kalevaru, W. Baumann, H. Neumann, P. C. J. Kamer, M. Beller and R. V. Jagadeesh, *Nat. Commun.*, 2018, **9**, 4123; (*h*) X. Tan, S. Gao, W. Zeng, S. Xin, Q. Yin and X. Zhang, *J. Am. Chem. Soc.*, 2018, **140**, 2024–2027.

10 (*a*) Z. Wang, *"Mignonac reaction" in comprehensive organic name reactions and reagents*, Wiley, 2010; (*b*) https://erowid.org/archive/rhodium/chemistry/reductive.amination.html, 2004.

11 A. S. Zola, R. U. Ribeiro, J. M. C. Bueno, D. Zanchet and P. A. Arroyo, *J. Exp. Nanosci.*, 2014, **9**, 398–405.

12 (*a*) J. Yang, H. Liu, W. N. Martens and R. L. Frost, *J. Phys. Chem.*, 2010, **114**, 111–119; (*b*) C. D. Wagner, L. E. Davis, J. F. Moulder and G. E. Mullenberg, *Handbook of X-ray Photoelectron Spectroscopy*, Minnesota: Perkin-Elmer Corporation, 1978.

13 (*a*) A. A. Khandar, B. Shaabani, F. Belaj and A. Bakhtiari, *Inorg. Chim. Acta*, 2007, **360**, 3255–3264; (*b*) A. van Den Bergen, K. S. Murray and B. O. West, *J. Organomet. Chem.*, 1971, **33**, 89–96.

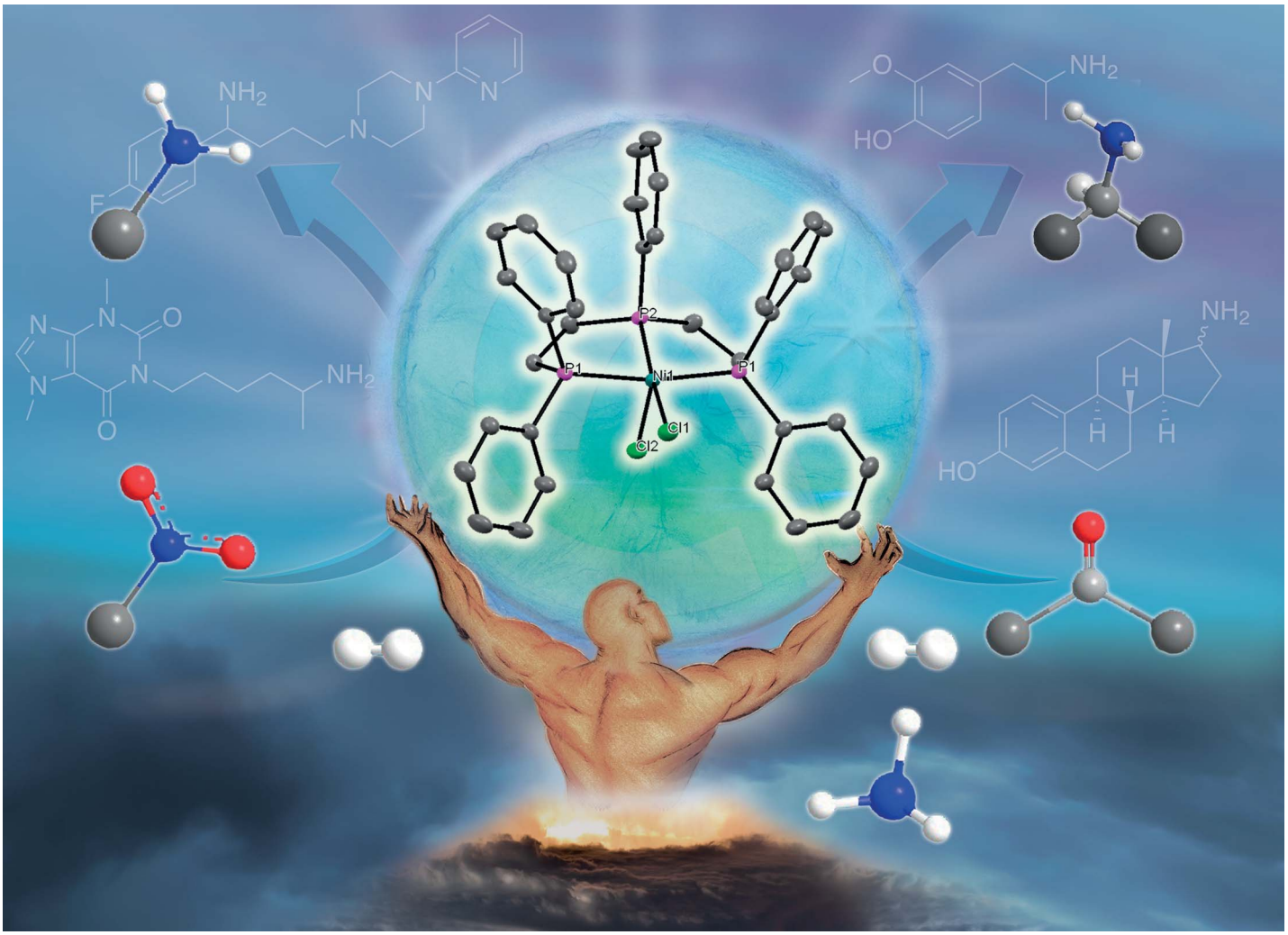

Showcasing research from Dr. Jagadeesh Rajenahally's laboratory, Department of Prof. Matthias Beller, Leibniz Institute for Catalysis, Germany.

General and selective synthesis of primary amines using Ni-based homogeneous catalysts

The development of base metal catalysts for industrially relevant amination and hydrogenation processes by applying abundant and green reagents is of central importance to produce amines, which represent highly privileged compounds widely used in chemistry, medicine, biology, energy, materials and the environment. Here, a Ni-triphos complex has been introduced as the first Ni-based homogeneous catalyst for both reductive amination of carbonyl compounds with ammonia and hydrogenation of nitroarenes to access all kinds of primary amines including the synthesis and amination of complex drug molecules and steroid derivatives.

As featured in:

See Haijun Jiao, Matthias Beller, Rajenahally V. Jagadeesh *et al.*, *Chem. Sci.*, 2020, **11**, 4332.

ROYAL SOCIETY OF CHEMISTRY

rsc.li/chemical-science

Registered charity number: 207890

Chemical Science

ROYAL SOCIETY OF CHEMISTRY

EDGE ARTICLE

View Article Online
View Journal | View Issue

Cite this: *Chem. Sci.*, 2020, **11**, 4332

All publication charges for this article have been paid for by the Royal Society of Chemistry

General and selective synthesis of primary amines using Ni-based homogeneous catalysts†

Kathiravan Murugesan, Zhihong Wei, Vishwas G. Chandrashekhar, Haijun Jiao,* Matthias Beller* and Rajenahally V. Jagadeesh*

The development of base metal catalysts for industrially relevant amination and hydrogenation reactions by applying abundant and atom economical reagents continues to be important for the cost-effective and sustainable synthesis of amines which represent highly essential chemicals. In particular, the synthesis of primary amines is of central importance because these compounds serve as key precursors and central intermediates to produce value-added fine and bulk chemicals as well as pharmaceuticals, agrochemicals and materials. Here we report a Ni-triphos complex as the first Ni-based homogeneous catalyst for both reductive amination of carbonyl compounds with ammonia and hydrogenation of nitroarenes to prepare all kinds of primary amines. Remarkably, this Ni-complex enabled the synthesis of functionalized and structurally diverse benzylic, heterocyclic and aliphatic linear and branched primary amines as well as aromatic primary amines starting from inexpensive and easily accessible carbonyl compounds (aldehydes and ketones) and nitroarenes using ammonia and molecular hydrogen. This Ni-catalyzed reductive amination methodology has been applied for the amination of more complex pharmaceuticals and steroid derivatives. Detailed DFT computations have been performed for the Ni-triphos based reductive amination reaction, and they revealed that the overall reaction has an inner-sphere mechanism with H_2 metathesis as the rate-determining step.

Received 23rd February 2020
Accepted 25th March 2020

DOI: 10.1039/d0sc01084g

rsc.li/chemical-science

Introduction

Catalytic reductive aminations and hydrogenations constitute essential processes widely applied in research laboratories and industries for the synthesis of fine and bulk chemicals as well as molecules used in life sciences.[1] In particular, the selective and efficient synthesis of amines by applying these processes starting from inexpensive and easily available starting materials, and green and abundant reagents using non-noble metal-based catalysts continues to be an important goal of chemical research. In general, amines are highly essential fine and bulk chemicals used in chemistry, medicine, biology and materials.[2] Noteworthily, amine functionalities constitute integral parts of a large number of life science molecules and play significant roles in their activities.[2] As an example, more than 75% of 200 top selling drugs of the year 2018 contain amine/nitrogen moieties.[2e] Among different kinds of amines, primary amines are highly valued because these compounds serve as key precursor and central intermediates for the synthesis of advanced chemicals, pharmaceuticals, agrochemicals and materials. The reductive amination of carbonyl compounds with ammonia[3] and the hydrogenation of nitroarenes[4] are found to be more expedient processes to synthesize benzylic, aliphatic and aromatic primary amines.[3,4] Notably for the advancement of more sustainable and cost-effective synthesis of this class of amines, the development of base metal catalysts is highly desired and continues to attract scientific interest. Catalytic reductive aminations, especially for the synthesis of primary amines are challenging processes and are often non-selective and suffer from side reactions such as over alkylation and reduction to the corresponding alcohols.[3] Hence in order to perform these reactions in an efficient and highly selective manner the development of suitable catalysts is of central importance. Regarding potential catalysts for reductive amination to prepare primary amines from carbonyl compounds using ammonia and molecular hydrogen, mainly heterogeneous catalysts based on Rh,[3k,s] Ru,[3k–m,q,r] Ni[3d,h,n] and Co[3a] are applied. Compared to that of heterogeneous materials, the design of homogeneous catalysts for this reaction is highly challenging due to the inactivation of metal complexes in the presence of ammonia by forming Werner-amine type complexes and common problems such as formation of secondary and/or tertiary amines and over hydrogenation of carbonyl compounds to corresponding alcohols associated with reductive aminations.[3] Nevertheless, in recent years, a few Rh,[3i] Ru,[3c,f,g,j] Ir[3p] and Co[3e]-based complexes have been established to catalyze the synthesis of primary amines from carbonyl compounds and

Leibniz-Institut für Katalyse e. V., Albert Einstein-Str. 29a, 18059 Rostock, Germany. E-mail: haijun.jiao@catalysis.de; matthias.beller@catalysis.de; jagadeesh.rajenahally@catalysis.de

† Electronic supplementary information (ESI) available. See DOI: 10.1039/d0sc01084g

ammonia. Despite these achievements, still the development of base metal homogeneous catalysts for the synthesis of benzylic and aliphatic primary amines is highly desired and attracts scientific interest.

The catalytic hydrogenation of nitroarenes represents an indispensable and widely applied process for the synthesis of aromatic amines (anilines).[1c,d,4] In general this reaction mainly relies on heterogeneous catalysts. Unfortunately, homogeneous catalysts for the hydrogenation of nitro compounds are scarcely explored and using them remains a challenge.[4c–f] Hence the development of suitable homogeneous catalysts, especially based on non-noble metals, for the synthesis of functionalized anilines continues to be important is also of significant interest. Here, we report a Ni-based complex for both reductive amination of carbonyl compounds with ammonia and hydrogenation of nitroarenes for the general synthesis of all kinds of primary amines.

Ni-based complexes are well known to catalyze a number of synthetic processes[5–11] including hydrogenations,[6] CH-activations,[7] coupling reactions[8] and amination of alcohols,[8,9] as well as polymerizations[10] and photo-redox reactions.[11] The key to success for this Ni-catalysis in organic synthesis is the use of a broad variety of complexes based on specific ligands.[5–11] Although Ni-based homogeneous catalysts are well recognized for a variety of reactions, they are still underdeveloped for reductive aminations as well as for the hydrogenation of nitro compounds.[5–11] To the best of our knowledge until now there has been no homogeneous Ni-based catalyst known for both of these reactions to synthesize primary amines. Certainly, there is potential interest in the development of homogeneous Ni-based reductive amination and hydrogenation catalysts for the general and selective synthesis of primary amines. In addition to synthetic applications, it is also important to know the mode of action of Ni-complexes, formation of catalytically active species, and reactivity and selectivity towards reductive amination as well as their compatibility with ammonia. In this respect, here we report a Ni-linear triphos (bis(diphenylphosphinoethyl) phenylphosphine) complex as the first homogeneous Ni-based catalyst for both reductive amination and hydrogenation of nitroarenes. Remarkably, this Ni-triphos complex enabled the synthesis of functionalized and structurally diverse benzylic, heterocyclic, and aliphatic linear and branched primary amines as well as aromatic primary amines starting from inexpensive and easily accessible carbonyl compounds (aldehydes and ketones) and nitroarenes using ammonia and molecular hydrogen. In addition, we also performed DFT studies to know the active catalytic species and mode of reactivity as well as to propose the plausible Ni-based reductive amination mechanism.

Results and discussion

Design of the Ni-catalyst for the reductive amination reaction

In recent years triphos-based non-noble metal complexes have emerged as promising catalysts for hydrogenation[6a,12a–c,12f–k] and amination reactions.[3e,12d,e] Due to the strong coordination nature to the central metal atom, triphos-based complexes are suitable to activate hydrogen and ammonia. Inspired by previous amination[3e,12d,e] and hydrogenation[6a,12a–c,12f–k] processes, we started to design tridentate-Ni complexes for the synthesis of different kinds of primary amines by reductive amination of carbonyl compounds and hydrogenation of nitroarenes.

First we tested the combination of $Ni(BF_4)_2 \cdot 6H_2O$ and linear triphos (**L1**; bis(diphenylphosphinoethyl) phenylphosphine) as the *in situ* catalyst for the reductive amination of veratraldehyde **1** (3,4-dimethoxy benzaldehyde) to veratrylamine **2** (3,4-dimethoxy benzylamine) in the presence of ammonia and molecular hydrogen as a benchmark reaction (Table 1). Gratifyingly, this *in situ* complex exhibited high activity and selectivity for the reductive amination of veratraldehyde **1** and obtained 96% of the desired product, veratrylamine **2** (Table 1, entry 1). In order to know the reactivity of other tridentate ligands, we tested

Table 1 Ni-catalyzed reductive amination of veratraldehyde: activity and selectivity of Ni-complexes[a]

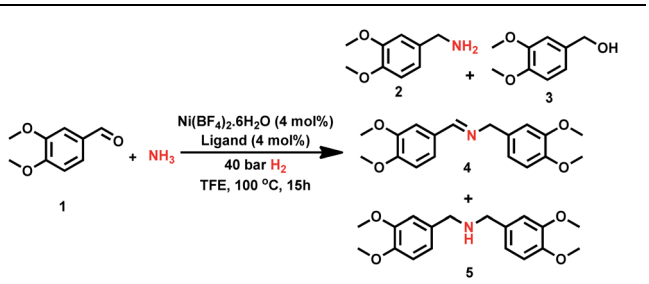

			Yield (%)			
Entry	Ligand	Conv. (%)	2	3	4	5
1[a]	**L1**	>99	96	—	3	—
2[a]	**L2**	15	—	—	13	—
3[a]	**L3**	23	—	—	21	—
4[a]	**L4**	20	—	—	18	—
5[a]	**L5**	12	—	—	10	—
6[a]	**L6**	5	—	—	3	—
7[a]	**L7**	5	—	—	3	—
8[b]	**L1**	>99	92	—	6	—
9[c]	**L1**	>99	91	—	7	—
10[d]	**L1**	>99	93	—	5	—
11[a]	—	10	—	—	8	—

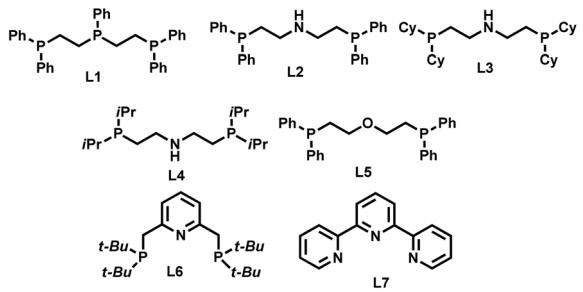

[a] Reaction conditions: 0.5 mmol veratraldehyde, 4 mol% $Ni(BF_4)_2 \cdot 6H_2O$, 4 mol% ligand, 5 bar NH_3, 40 bar H_2 2 mL trifluoroethanol (TFE), 100 °C, 15 h, and GC yields using *n*-hexadecane as the standard. [b] Same as 'a' with 20 bar H_2. [c] Same as 'a' at 80 °C. [d] Same as 'a' with 3 mol% catalyst.

different PNP, POP and NNN ligands (Table 1, entries 2 to 7). All these tested tridentate ligands (**L2–L7**) showed poor activity with a conversion of up to 25% and in none of these cases the formation of primary amine **1** was observed (Table 1, entries 2 to 7). Notably, the Ni-triphos system was well tolerated with ammonia and due to strong coordination, and this PPP-ligand was found to be appropriate to avoid the formation of a Werner-type ammonia complex. Applying this active system ($Ni(BF_4)_2$–**L1**), next we performed the optimization of the benchmark reaction by evaluating the effect of hydrogen pressure, reaction temperature and catalyst loading (Table 1; entries 8–10). These results revealed that in order to achieve the best yield of **2**, a 40 bar hydrogen pressure, 5 bar ammonia pressure, 100 °C reaction temperature and 4 mol% catalyst (1 : 1 $Ni(BF_4)_2 \cdot 6H_2O$–**L1**) are required. Further to know the effect of solvents, different polar (MeOH, EtOH, *t*-BuOH, *t*-amyl alcohol, TFE) and non-polar solvents (toluene, THF) were tested (Table S1†). Among these solvents, trifluoroethanol (TFE) was found to be the best solvent. However, in other tested solvents, we did not observe the formation of the desired product, primary amine **2**.

After having obtained the best results with the *in situ* generated, $Ni(BF_4)_2 \cdot 6H_2O$–**L1** system, we were interested in preparing a molecularly defined complex and testing its activity in the model reaction. Unfortunately, we could not isolate $Ni(BF_4)_2$–**L1** complex due its stability problem. However, the $NiCl_2$–**L1** complex was prepared, isolated and tested in the benchmark reaction (see the ESI†)[6a]. Noteworthily, this defined complex also exhibited similar activity to the *in situ* $Ni(BF_4)_2 \cdot 6H_2O$–**L1** complex and obtained 97% of veratrylamine **2**. In addition, the *in situ* $NiCl_2$–**L1** complex also showed good activity and obtained 90% of the desired primary amine **2**. We attempted to isolate a nickel hydride complex; however, we could not due to its highly unstable nature. In order to know the nature of the reaction, catalytic poisoning tests were performed with Hg and PPh_3 (Table S3†). Addition of either Hg or PPh_3 to the reaction under standard conditions did not affect either the activity or selectivity of the active Ni-complex. These results showed that the reaction proceeds *via* homogeneous catalysis.

DFT computational study

Parallel to our experimental studies we carried out detailed density functional theory computations on the reductive amination reaction mechanisms. Since both *in situ* $Ni(BF_4)_2 \cdot 6H_2O$-triphos (**L1**) and the well-defined $NiCl_2$–**L1** complexes showed the same activity and selectivity, we used this well-defined complex as the pre-catalyst, which can be converted with NH_3 to the active catalyst bearing the Ni–H bond $[\mathbf{L1}NiH]^+$(**I**). In our computations we used the real-size catalyst as well as phenylmethanimine (Ph–CH=NH) for benzaldehyde as the substrate for the reaction. To evaluate the effect of the van der Waals dispersion correction (GD3BJ) and solvation (SMD) of 2,2,2-trifluoroethanol (TFE) we tested different combinations and several functionals. Based on these testing results, we discussed our results including dispersion and solvation (B3PW91–GD3BJ–SMD). The computational details for the models and methods are listed in the ESI(S7).†

Since complex **I** can have *fac* (facial) and *mer* (meridional) conformations, we first computed their relative energy (Fig. 1). It is found that the **I**-*mer* is more stable than **I**-*fac* by 4.6 kcal mol; and **I**-*mer* should be the dominant isomer under equilibrium (>99.9%). Since complex **I** has 16 valence electrons, we tested the stability of the triplet state, and the singlet state is more stable than the corresponding triplet state by 51.8 and 50.2 kcal mol^{-1} for the *fac*- and *mer*-coordination, respectively. Under the coordination of imines, however, the complex (**M1**-*fac-syn*) from **I**-*fac* is more stable than that (**M1**-*mer*) from **I**-*mer* by 3.2 kcal mol^{-1} (>99%), indicating that **M1**-*fac-syn* should be the major component in the reaction medium and this indicates the stability change upon substrate coordination. Indeed, imine coordination to **I**-*mer* is slightly endergonic by 0.2 kcal mol^{-1}, while imine coordination to **I**-*fac* is exergonic by 7.6 kcal mol^{-1}. It is also noted that **M1**-*fac-syn* is more stable than **M1**-*fac-anti* by 2.4 kcal mol^{-1}.

Therefore, we used **M1**-*fac-syn* for our computations. It is also noted that only the potential energy surface of the *fac*-coordination has been obtained; and it is not possible to have the potential energy surface for the *mer*-coordination. For the *mer*-coordination, only the complexes of imine and amine coordination have been found and they have higher energy and are less stable than the *fac*-coordination. The computed potential free energy surface is shown in Fig. 2.

In **M1**-*fac-syn*, imine coordination is the nitrogen lone pair instead of the expected C=N double bond. Starting from **M1**-*fac-syn*, the first step is the transfer of the hydride to the carbon center of the C=N double bond *via* the transition state (**TS1**) due to the different electronegativities of C and N atoms. This hydride transfer results in the formation of an amido complex with C–H agostic interaction with the Ni center, **M2**. This hydride transfer needs a free energy barrier of 11.0 kcal mol^{-1} and is endergonic by 10.6 kcal mol^{-1}. The next step is the

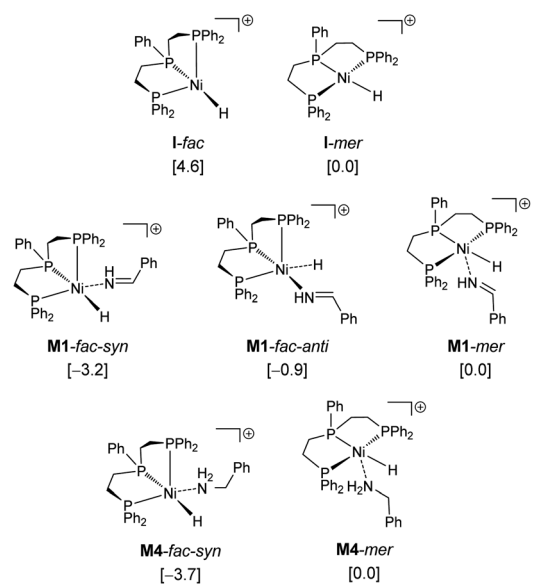

Fig. 1 Relative energies (kcal mol^{-1}) of the Ni-catalyst and Ni-complexes.

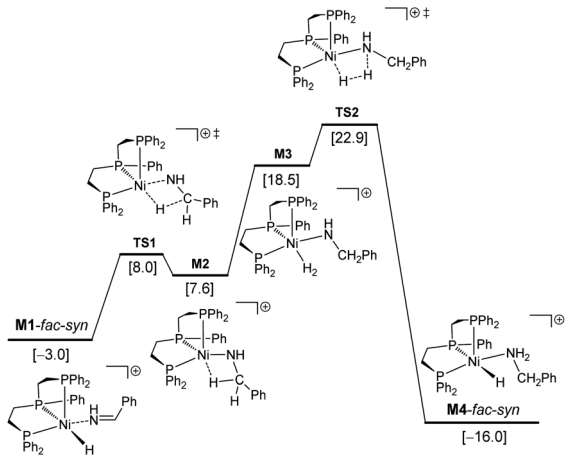

Fig. 2 Potential free energy surface (kcal mol^{-1}) with the reference of I-*mer*, Ph–CH=NH and H_2.

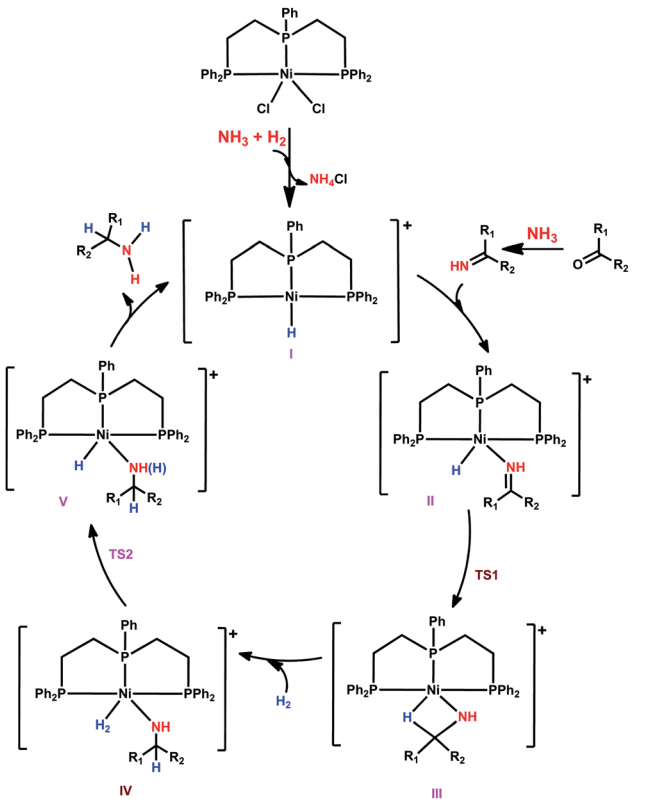

Scheme 1 Plausible reaction mechanism for the $NiCl_2$-triphos catalyzed reductive amination for the synthesis of primary amines.

breaking of the C–H agostic interaction *via* H_2 coordination with the formation of intermediate **M3**, and this step is endergonic by 10.9 kcal mol^{-1}. In **M3**, molecular H_2 coordination has been found instead of oxidative addition. Having formed **M3** with molecular H_2 coordination, the next step is metathesis (hydrogenolysis) instead of reductive elimination and the formed amine (Ph–CH_2–NH_2) still coordinates to the Ni center, **M4**. This step needs a free energy barrier of 4.4 kcal mol^{-1} and is strongly exergonic by 34.5 kcal mol^{-1}.

On the basis of **I**-*mer* and Ph–CH=NH, the apparent free energy barrier is 22.9 kcal mol^{-1}, and this barrier is in reasonable agreement with an applied high reaction temperature of 100–120 °C and a long reaction time of 24 hours. In addition, the endergonic molecular H_2 coordination and the high apparent barrier reasonably explain the need for a high H_2 pressure of 40–50 bar. It is noted that the computed apparent barrier is 41.6 kcal mol^{-1} in the gas phase, and 41.9 kcal mol^{-1} under the consideration of the solvation effect. In the case of van der Waals dispersion correction, the apparent barrier becomes 19.2 in the gas phase. In the case of solvation and dispersion corrections, the apparent barrier is 22.9 kcal mol^{-1}. This demonstrates the effect of dispersion correction. In addition, we tested other functional methods including solvation and dispersion corrections and found that the apparent barrier is 28.1, 21.1, 25.4 and 27.8 kcal mol^{-1} for B3LYP, BP86, M06L and MN15, respectively.

Having studied the catalytically active species by DFT calculations, we proposed the plausible mechanism for the Ni-triphos catalyzed reductive amination of carbonyl compounds with ammonia and molecular hydrogen (Scheme 1). After the generation of the active catalyst with the Ni–H functionality (**I**), the mechanism has three main steps, (i) substrate coordination (**II**) followed by the Ni–H selective insertion into the C=N double bond (**TS1**) and the formation of agostically interacting intermediate (**III**); and (ii) H_2 coordination (**IV**) followed by H_2 metathesis (**TS2**) and the formation of amine coordinated intermediate (**V**). The final step is the release of the amine and regeneration of the active catalyst. Overall, the reaction has an inner-sphere mechanism and the rate-determining step is H_2 metathesis, and the apparent barrier is about 23 kcal mol^{-1}. All this reasonably explains the need for a high H_2 pressure of 40–50 bar and the long reaction time (Table 1).

Synthesis of benzylic and aliphatic linear primary amines

After having investigated the nickel-triphos (**L1**) as the most active catalyst system, we explored its (*in situ* system) general applicability for the preparation of various primary amines starting from carbonyl compounds. As shown in Schemes 2 and 3 this Ni-triphos catalyst allowed for the amination of both aldehydes and ketones with ammonia in the presence of molecular hydrogen and obtained structurally diverse and functionalized linear and branched primary amines. Simple aldehydes and substrate bearing electron -donating and -withdrawing groups including halide substituted ones were reacted smoothly and the corresponding primary amines were obtained in good to excellent yields (Scheme 2, products **6–11**). For any given amination/hydrogenation catalyst, achieving a high degree of chemoselectivity is challenging and important in organic synthesis and drug discovery.

To demonstrate this aspect, reductive amination of various functionalized aldehydes was performed. Interestingly, the functionalized aldehydes containing ether, phenolic, C–C double bond, ester, boronic acid ester and thioether groups were all highly selectively aminated and the corresponding linear primary amines were obtained in up to 96% yield,

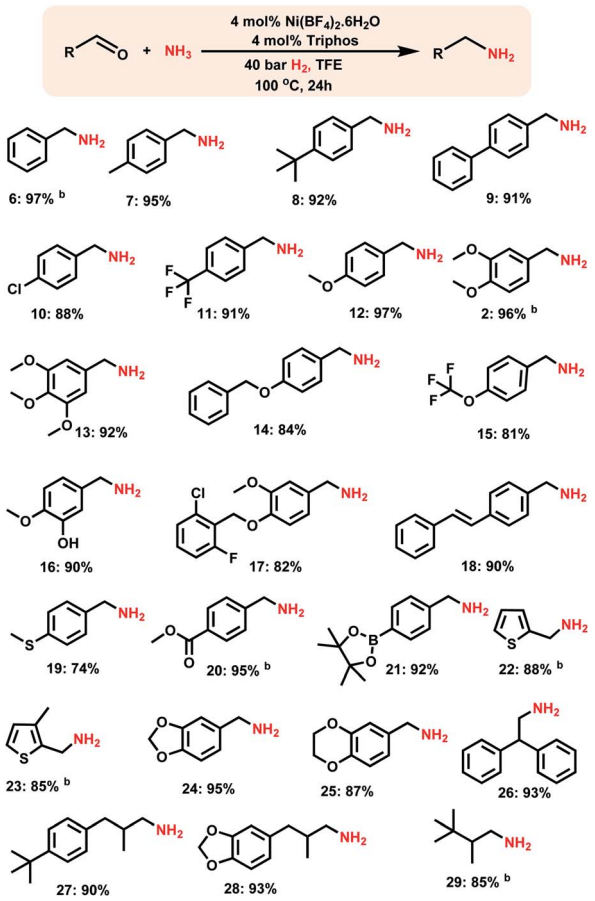

Scheme 2 Synthesis of linear primary amines using the Ni-triphos complex.[a] [a]Reaction conditions: 0.5 mmol aldehyde, 4 mol% $Ni(BF_4)_2{\cdot}6H_2O$, 4 mol% triphos (**L1**), 5–7 bar NH_3, 40 bar H_2, 2 mL degassed trifluoroethanol (TFE), 100 °C, 24 h, and isolated yields. [b]GC yields using *n*-hexadecane as the standard. Isolated as free amines and converted to hydrochloride salts. The corresponding hydrochloride salts were subjected to NMR analysis.

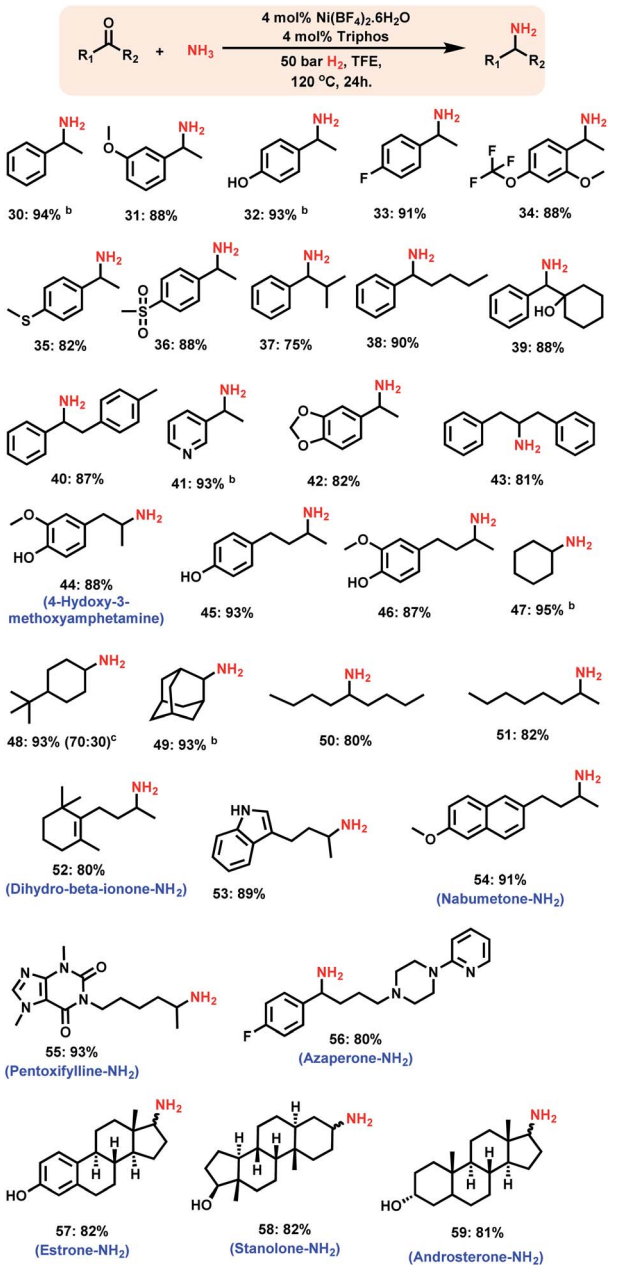

Scheme 3 Nickel-triphos catalysed synthesis of branched primary amines.[a] [a]Reaction conditions: 0.5 mmol ketone, 4 mol% $Ni(BF_4)_2{\cdot}6H_2O$, 4 mol% triphos (**L1**), 5–7 bar NH_3, 50 bar H_2, 2 mL degassed trifluoroethanol (TFE), 120 °C, 24 h, and isolated yields. [b]GC yields using *n*-hexadecane as the standard. Isolated as free amines and converted to hydrochloride salts. The corresponding hydrochloride salts were subjected to NMR analysis.

without the reduction of other functional groups (Scheme 2, products **12–21**). In addition, heterocyclic primary amines were prepared in up to 95% yield (Scheme 2, products **22–25** and **28**). Primary amines of 3,4-methylenedioxy and benzo-1,4-dioxane, which represent versatile motifs in many drugs and natural products, were prepared in up to 96% yield (Scheme 2, products **24** to **25** and **28**). Further, aliphatic aldehydes, which are difficult to react were also aminated and the corresponding primary amines were obtained in good to excellent yields (Scheme 2; products **26–29**).

Synthesis of branched primary amines from ketones

Compared to that of linear primary amines, the synthesis of branched primary amines starting from ketones is more challenging, because the reduction of corresponding imines from ketones is more difficult than that of the imines of corresponding aldehydes.

Remarkably, the Ni-triphos complex is highly active and selective for the reductive amination of ketones with ammonia and hydrogen. As a result, all kinds of ketones were efficiently aminated to produce corresponding branched primary amines in high yields (Scheme 3). In addition to the simple and functionalized ketones, the ones bearing easily coordinating groups such as –NH, and –OH phenolic groups as well as pyridines to metals were also smoothly reacted with ammonia and gave corresponding primary amines in up to 94% yield (Scheme 3, products **41**, **44–46**, **53** and **56**). In addition, the synthesis of

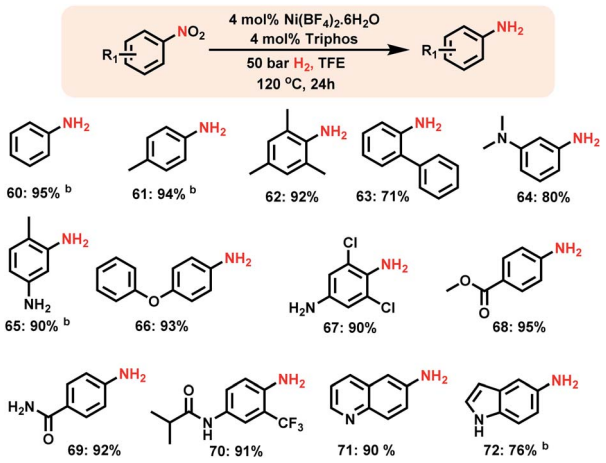

Scheme 4 Homogeneous Ni-catalyzed synthesis of aromatic primary amines.[a] [a]Reaction conditions: 0.5 mmol substrate, 4 mol% $Ni(BF_4)_2 \cdot 6H_2O$, 4 mol% triphos (**L1**), 50 bar H_2, 2 mL degassed trifluoroethanol (TFE), 120 °C, 24 h, and [b]GC yields using *n*-hexadecane as the standard.

various aliphatic branched primary amines, which are difficult to prepare,[3i,n] was performed with different ketones using this Ni-triphos system (Scheme 3, products **44–51**). A more valuable application of this Ni-based protocol has been demonstrated by performing the amination of structurally complex life science molecules and steroid derivatives (Scheme 3). Gratifyingly, by applying the Ni-triphos catalyst the $-NH_2$ moiety has been introduced in nabumetone, pentoxifylline, azaperone, estrone, androsterone and stanolone (Scheme 3, products **54–60**).

Synthesis of aromatic primary amines by Ni-catalyzed hydrogenation of nitroarenes

The design of homogeneous catalysts for the hydrogenation of nitroarenes to anilines continues to be challenging.[4c–f] Here we explored the applicability of Ni-triphos as a homogeneous catalyst for the hydrogenation of nitroarenes. Advantageously this *in situ* generated Ni–**L1** complex also exhibited excellent activity for the hydrogenation of nitroarenes (Scheme 4).

Nitrobenzenes containing both electron-donating and -withdrawing groups were selectively hydrogenated to obtain corresponding anilines in up to 95% yield (Scheme 4, products **62** to **72**). Functionalized nitroarenes containing esters, amides and ethers as well as halide groups were hydrogenated to anilines by tolerating these functional groups without being reduced (Scheme 4, products **66–70**).

Conclusions

In conclusion, for the first time we introduced a homogeneous Ni-based catalyst for both reductive amination of carbonyl compounds and hydrogenation of nitroarenes to prepare all kinds of primary amines. The key to success for this synthesis is the use of a linear triphos-ligated Ni-complex. By applying this Ni-based homogeneous catalyst, starting from inexpensive and easily available carbonyl compounds and nitroarenes using abundant and atom economical reagents such as ammonia and molecular hydrogen, commercially and industrially important as well as pharmaceutically relevant aromatic, heterocyclic, and aliphatic primary amines were synthesized in good to excellent yields. DFT computations revealed that the overall reaction has an inner-sphere mechanism with H_2 metathesis as the rate-determining step and this reasonably explains the need for the high H_2 pressure and long reaction time on the basis of the computed apparent barriers.

Conflicts of interest

The authors declare no competing financial interest.

Acknowledgements

We gratefully acknowledge the European Research Council, (EU project 670986-NoNaCat), the State of Mecklenburg-Vorpommern and the Leibniz Foundation (ZW, Leibniz Competition, SAW-2016-LIKAT-1). We thank the analytical staff of the Leibniz-Institute for Catalysis, Rostock for their excellent service.

Notes and references

1 (*a*) S. Gomez, J. A. Peters and T. Maschmeyer, *Adv. Synth. Catal.*, 2002, **344**, 1037–1057; (*b*) A. Heshmatollah, Y. Hossein and S. Fatemeh, *Curr. Org. Chem.*, 2015, **19**, 1021–1049; (*c*) M. Orlandi, D. Brenna, R. Harms, S. Jost and M. Benaglia, *Org. Process Res. Dev.*, 2018, **22**, 430–445; (*d*) D. Formenti, F. Ferretti, F. K. Scharnagl and M. Beller, *Chem. Rev.*, 2019, **119**, 2611–2680; (*e*) F. Pohlki and S. Doye, *Chem. Soc. Rev.*, 2003, **32**, 104–114; (*f*) D. B. Bagal and B. M. Bhanage, *Adv. Synth. Catal.*, 2015, **357**, 883–900; (*g*) D. B. Bagal and B. M. Bhanage, Recent Advances in Transition Metal-Catalyzed Hydrogenation of Nitriles, *Adv. Synth. Catal.*, 2015, **357**, 883–900; (*h*) J. G. de Vries and C. J. Elsevier, in *Handbook of Homogeneous Hydrogenation*, Wiley-VCH, NewYork, 2007; (*i*) S. Nishimura, *Handbook of Heterogeneous Catalytic Hydrogenation for Organic Synthesis*, Wiley, New York, 2001; (*j*) F. Shi and X. Cui, in *Catalytic Amination for N-Alkyl Amine Synthesis*, Academic Press, 2018; (*k*) *Reductive amination review*, https://erowid.org/archive/rhodium/chemistry/reductive.amination.html, 2004; (*l*) T. Yan, B. L. Feringa and K. Barta, *Nat. Commun.*, 2014, **5**, 5602; (*m*) T. Yan, B. L. Feringa and K. Barta, *Sci. Adv.*, 2017, **3**, eaao6494; (*n*) T. Yasukawa, R. Masuda and S. Kobayashi, *Nat. Catal.*, 2019, **2**, 1088–1092; (*o*) C. Gunanathan and D. Milstein, *Angew. Chem. Int. Ed.*, 2008, **47**, 8661–8664.

2 (*a*) S. D. Roughley and A. M. Jordan, *J. Med. Chem.*, 2011, **54**, 3451–3479; (*b*) V. Froidevaux, C. Negrell, S. Caillol, J.-P. Pascault and B. Boutevin, *Chem. Rev.*, 2016, **116**, 14181–14224; (*c*) S. A. Lawrence, *Amines: Synthesis, Properties and Applications*, Cambridge University Press, Cambridge, UK, 2004; (*d*) A. Ricci, *Amino Group Chemistry: From Synthesis to the Life Sciences*, Wiley VCH, Weinheim, 2008; (*e*) https://njardarson.lab.arizona.edu/sites/

njardarson.lab.arizona.edu/files/2018Top200PharmaceuticalRetailSalesPosterLowResFinalV2.pdf.

3 (*a*) R. V. Jagadeesh, K. Murugesan, A. S. Alshammari, H. Neumann, M.-M. Pohl, J. Radnik and M. Beller, *Science*, 2017, **358**, 326–332; (*b*) K. Murugesan, T. Senthamarai, M. Sohail, A. S. Alshammari, M.-M. Pohl, M. Beller and R. V. Jagadeesh, *Chem. Sci.*, 2018, **9**, 8553–8560; (*c*) T. Senthamarai, K. Murugesan, J. Schneidewind, N. V. Kalevaru, W. Baumann, H. Neumann, P. C. J. Kamer, M. Beller and R. V. Jagadeesh, *Nat. Commun.*, 2018, **9**, 4123; (*d*) K. Murugesan, M. Beller and R. V. Jagadeesh, *Angew. Chem., Int. Ed.*, 2019, **58**, 5064–5068; (*e*) K. Murugesan, Z. Wei, V. G. Chandrashekhar, H. Neumann, A. Spannenberg, H. Jiao, M. Beller and R. V. Jagadeesh, *Nat. Commun.*, 2019, **10**, 5443; (*f*) J. Gallardo-Donaire, M. Ernst, O. Trapp and T. Schaub, *Adv. Synth. Catal.*, 2016, **358**, 358–363; (*g*) J. Gallardo-Donaire, M. Hermsen, J. Wysocki, M. Ernst, F. Rominger, O. Trapp, A. S. K. Hashmi, A. Schäfer, P. Comba and T. Schaub, *J. Am. Chem. Soc.*, 2018, **140**, 355–361; (*h*) G. Hahn, P. Kunnas, N. de Jonge and R. Kempe, *Nat. Catal.*, 2018, **2**, 71–77; (*i*) T. Gross, A. M. Seayad, M. Ahmad and M. Beller, *Org. Lett.*, 2002, **4**, 2055–2058; (*j*) X. Tan, S. Gao, W. Zeng, S. Xin, Q. Yin and X. Zhang, *J. Am. Chem. Soc.*, 2018, **140**, 2024–2027; (*k*) M. Chatterjee, T. Ishizaka and H. Kawanami, *Green Chem.*, 2016, **18**, 487–496; (*l*) B. Dong, X. Guo, B. Zhang, X. Chen, J. Guan, Y. Qi, S. Han and X. Mu, *Catalysts*, 2015, **5**, 2258–2270; (*m*) S. Nishimura, K. Mizuhori and K. Ebitani, *Res. Chem. Intermed.*, 2016, **42**, 19–30; (*n*) J. Krupka, L. Dluhoš and L. Mrózek, *Chem. Eng. Technol.*, 2017, **40**, 870–877; (*o*) Z. Wang, *Mignonac reaction, in Comprehensive organic name reactions and reagents*, John Wiley & Sons, New Jersey, 2010; (*p*) T. Riermeier, K.-J. Haack, U. Dingerdissen, A. Boerner, A. V. Tararov and R. Kadyrov, *Method for producing amines by homogeneously catalyzed reductive amination of carbonyl compounds*, Weniger, US, 2005, vol. 6, pp. 884–887B1; (*q*) T. Komanoya, T. Kinemura, Y. Kita, K. Kamata and M. Hara, *J. Am. Chem. Soc.*, 2017, **139**, 11493–11499; (*r*) G. Liang, A. Wang, L. Li, G. Xu, N. Yan and T. Zhang, *Angew. Chem., Int. Ed.*, 2017, **56**, 3050–3054; (*s*) J. Bódis, L. Lefferts, T. E. Müller, R. Pestman and J. A. Lercher, *Catal. Lett.*, 2005, **104**, 23–28.

4 (*a*) T. Schwob and R. Kempe, *Angew. Chem., Int. Ed.*, 2016, **55**, 15175–15179; (*b*) R. V. Jagadeesh, A.-E. Surkus, H. Junge, M.-M. Pohl, J. Radnik, J. Rabeah, H. Huan, V. Schünemann, A. Brückner and M. Beller, *Science*, 2013, **342**, 1073–1076; (*c*) J. F. Knifton, *J. Org. Chem.*, 1976, **41**, 1200–1206; (*d*) R. M. Deshpande, A. N. Mahajan, M. M. Diwakar, P. S. Ozarde and R. V. Chaudhari, *J. Org. Chem.*, 2004, **69**, 4835–4838; (*e*) G. Wienhöfer, M. Baseda-Krüger, C. Ziebart, F. A. Westerhaus, W. Baumann, R. Jackstell, K. Junge and M. Beller, *Chem. Commun.*, 2013, **49**, 9089–9091; (*f*) Z.-J. Yao, J.-W. Zhu, N. Lin, X.-C. Qiao and W. Deng, *Dalton Trans.*, 2019, **48**, 7158–7166; (*g*) G. Hahn, J.-K. Ewert, C. Denner, D. Tilgner and R. Kempe, *ChemCatChem*, 2016, **8**, 2461–2465; (*h*) P. Ryabchuk, G. Agostini, M.-M. Pohl, H. Lund, A. Agapova, H. Junge, K. Junge and M. Beller, *Sci. Adv.*, 2018, **4**, eaat0761; (*i*) Y. Hu, Y. Yu, X. Zhao, H. Yang, B. Feng, H. Li, Y. Qiao, L. Hua, Z. Pan and Z. Hou, *Sci. China Chem.*, 2010, **53**, 1541–1548; (*j*) S. Pisiewicz, D. Formenti, A.-E. Surkus, M.-M. Pohl, J. Radnik, K. Junge, C. Topf, S. Bach-mann, M. Scalone and M. Beller, *ChemCatChem*, 2016, **8**, 129–134; (*k*) F. Yang, M. Wang, W. Liu, B. Yang, Y. Wang, J. Luo, Y. Tang, L. Hou, Y. Li, Z. i. Li, B. Zhang, W. Yang and Y. Li, *Green Chem.*, 2019, **21**, 704–711; (*l*) N. Mahata, A. F. Cunha, J. J. M. Órfão and J. L. Figueiredo, *Appl. Catal. Gen.*, 2018, **351**, 204–209; (*m*) W. She, T. Qi, M. Cui, P. Yan, S. W. Ng, W. Li and G. Li, *ACS Appl. Mater. Interfaces*, 2018, **10**, 14698–14707.

5 (*a*) S. Z. Tasker, E. A. Standley and T. F. Jamison, *Nature*, 2014, **509**, 299–309; (*b*) J. A. Garduno, A. Arevalo and J. J. Garcia, *Dalton Trans.*, 2015, **44**, 13419–13438.

6 (*a*) M. Beller, K. Murugesan, C. B. Bheeter, P. R. Linnebank, A. Spannenberg, J. N. H. Reek, R. V. Jagadeesh and M. Beller, *ChemSusChem*, 2019, **12**, 3363–3369; (*b*) N. G. Léonard and P. J. Chirik, *ACS Catal.*, 2018, **8**, 342–348; (*c*) T. J. Mooibroek, E. C. M. Wenker, W. Smit, I. Mutikainen, M. Lutz and E. Bouwman, *Inorg. Chem.*, 2013, **52**, 8190–8201; (*d*) K. V. Vasudevan, B. L. Scott and S. K. Hanson, *Eur. J. Inorg. Chem.*, 2012, **2012**, 4898–4906; (*e*) I. M. Angulo, A. M. Kluwer and E. Bouwman, *Chem. Commun.*, 1998, 2689–2690; (*f*) S. Chakraborty, P. Bhattacharya, H. Dai and H. Guan, *Acc. Chem. Res.*, 2015, **48**, 1995–2003.

7 (*a*) S. A. Johnson, *Dalton Trans.*, 2015, **44**, 10905–10913; (*b*) Y. Nakao, *Shokubai*, 2008, **50**, 705–709; (*c*) A. C. Williams, in *Nickel-catalyzed C–H activation*, CRC Press, 2015, pp. 113–144; (*d*) F. Juliá-Hernández, T. Moragas, J. Cornella and R. Martin, *Nature*, 2017, **545**, 84; (*e*) N. A. Harry, S. Saranya, S. M. Ujwaldev and G. Anilkumar, *Catal. Sci. Technol.*, 2019, **9**, 1726–1743; V. G. Landge, C. H. Shewale, G. Jaiswal, M. K. Sahoo, S. P. Midya and E. Balaraman, *Catal. Sci. Technol.*, 2016, **6**, 1946–1951.

8 (*a*) M. Henrion, V. Ritleng and M. J. Chetcuti, *ACS Catal.*, 2015, **5**, 1283–1302; (*b*) R. Shi, Z. Zhang and X. Hu, *Acc. Chem. Res.*, 2019, **52**, 1471–1483; (*c*) C. M. Lavoie and M. Stradiotto, *ACS Catal.*, 2018, **8**, 7228–7250; (*d*) L. Guo and M. Rueping, *Acc. Chem. Res.*, 2018, **51**, 1185–1195; (*e*) M. O. Konev and E. R. Jarvo, *Angew. Chem., Int. Ed.*, 2016, **55**, 11340–11342; (*f*) C. Liu, S. Tang, D. Liu, J. Yuan, L. Zheng, L. Meng and A. Lei, *Angew. Chem., Int. Ed.*, 2012, **51**, 3638–3641.

9 (*a*) J. B. Sweeney, A. K. Ball, P. A. Lawrence, M. C. Sinclair and L. J. Smith, *Angew. Chem., Int. Ed.*, 2018, **57**, 10202–10206; (*b*) M. Vellakkaran, K. Singh and D. Banerjee, *ACS Catal.*, 2017, **7**, 8152–8158.

10 (*a*) F. AlObaidi, Z. Ye and S. Zhu, *Polymer*, 2004, **45**, 6823–6829; (*b*) R. P. Quirk and W. Yu, *High Perform. Polym.*, 2005, **17**, 349–360; (*c*) D. G. Yakhvarov, K. R. Basvani, M. K. Kindermann, A. B. Dobrynin, I. A. Litvinov, O. G. Sinyashin, P. G. Jones and J. Heinicke, *Eur. J. Inorg. Chem.*, 2009, 1234–1242.

11 (*a*) J. A. Milligan, J. P. Phelan, S. O. Badir and G. A. Molander, *Angew. Chem., Int. Ed.*, 2019, **58**, 6152–6163; (*b*) J. Twilton, C. Le, P. Zhang, M. H. Shaw, R. W. Evans and D. W. C. MacMillan, *Nat. Rev. Chem.*, 2017, **1**, 0052; (*c*) K. L. Skubi, T. R. Blum and T. P. Yoon, *Chem. Rev.*, 2016, **116**, 10035–10074.

12 (*a*) Z. Liu, Z. Yang, P. Wang, X. Yu, Y. Wu, H. Wang and Z. Liu, *ACS Sustainable Chem. Eng.*, 2019, **7**, 18236–18241; (*b*) L. Iffland, A. Khedkar, A. Petuker, M. Lieb, F. Wittkamp, M. van Gastel, M. Roemelt and U.-P. Apfel, *Organometallics*, 2019, **38**, 289–299; (*c*) F. Ferretti, F. K. Scharnagl, A. Dall'Anese, R. Jackstell, S. Dastgir and M. Beller, *Catal. Sci. Technol.*, 2019, **9**, 3548–3553; (*d*) B. Emayavaramban, P. Chakraborty and B. Sundararaju, *ChemSusChem*, 2019, **12**, 3089–3093; (*e*) W. Liu, B. Sahoo, A. Spannenberg, K. Junge and M. Beller, *Angew. Chem., Int. Ed.*, 2018, **57**, 11673–11677; (*f*) A. Cavaille, B. Joyeux, N. Saffon-Merceron, N. Nebra, M. Fustier-Boutignon and N. Mezailles, *Chem. Commun.*, 2018, **54**, 11953–11956; (*g*) J. Schneidewind, R. Adam, W. Baumann, R. Jackstell and M. Beller, *Angew. Chem., Int. Ed.*, 2017, **56**, 1890–1893; (*h*) J. R. Cabrero-Antonino, R. Adam, V. Papa, M. Holsten, K. Junge and M. Beller, *Chem. Sci.*, 2017, **8**, 5536–5546; (*i*) T. M. Buscagan, P. H. Oyala and J. C. Peters, *Angew. Chem., Int. Ed.*, 2017, **56**, 6921–6926; (*j*) T. J. Korstanje, J. Ivar van der Vlugt, C. J. Elsevier and B. de Bruin, *Science*, 2015, **350**, 298–302; (*k*) F. K. Scharnagl, M. F. Hertrich, G. Neitzel, R. Jackstell and M. Beller, *Adv. Synth. Catal.*, 2019, **361**, 374–379.

nature protocols

PROTOCOL

https://doi.org/10.1038/s41596-019-0258-z

Check for updates

Reductive amination using cobalt-based nanoparticles for synthesis of amines

Kathiravan Murugesan, Vishwas G. Chandrashekhar, Thirusangumurugan Senthamarai, Rajenahally V. Jagadeesh✉ and Matthias Beller✉

Reductive aminations are an essential class of reactions widely applied for the preparation of different kinds of amines, as well as a number of pharmaceuticals and industrially relevant compounds. In such reactions, carbonyl compounds (aldehydes, ketones) react with ammonia or amines in the presence of a reducing agent and form corresponding amines. Common catalysts used for reductive aminations, especially for the synthesis of primary amines, are based on precious metals or Raney nickel. However, their drawbacks and limited applicability inspired us to look for alternative catalysts. The development of base-metal nanostructured catalysts is highly preferable and is crucial to the advancement of sustainable and cost-effective reductive amination processes. In this protocol, we describe the preparation of carbon-supported cobalt-based nanoparticles as efficient and practical catalysts for synthesis of different kinds of amines by reductive aminations. Template synthesis of a cobalt–triethylenediamine–terephthalic acid metal–organic framework on carbon and subsequent pyrolysis to remove the organic template resulted in the formation of supported single cobalt atoms and nanoparticles. Applying these catalysts, we have synthesized structurally diverse benzylic, aliphatic and heterocyclic primary, secondary and tertiary amines, including pharmaceutically relevant products, starting from inexpensive and easily accessible carbonyl compounds with ammonia, nitro compounds or amines and molecular hydrogen. To prepare this cobalt-based catalyst takes 26 h, and the reported catalytic reductive amination reactions can be carried out within 18–28 h.

Introduction

Among different kinds of chemicals, amines represent highly valuable compounds widely applied in many science areas, including chemistry, biology, medicine, materials and energy[1–7]. As an example, the majority of top-selling drugs contain nitrogen and/or amino groups, which constitute integral parts and play vital roles in their activities[3]. For the synthesis and functionalization of amines, catalytic reductive aminations using molecular hydrogen represent a resourceful method used in both academic laboratories and industry[8–26]. Common catalysts known for these reactions are based on precious metals[8–19] and Raney nickel[8,9,20]. However, for the advancement of cost-effective and selective reductive amination processes, the development of non-noble metal-based catalysts is preferable and continues to attract substantial interest. Compared to traditional homogeneous catalysts, heterogeneous catalysts offer advantages such as stability and recyclability. Among heterogeneous catalysts, supported nanoparticles[23–35], or single metal atoms[35–37] are of prime importance because of their low energy consumption and high activities and selectivities. In this regard, in recent years these materials have become the subject of increasing interest as catalysts for organic synthesis[6,23–39]. With respect to reductive aminations using molecular hydrogen, to our knowledge, only a few nanocatalysts have been developed[21–26]. Among these, carbon-supported Co_3O_4 nanoparticles surrounded by nitrogen-doped graphene layers, developed by our group, represent excellent catalysts for oxidation and hydrogenation reactions, as well as reductive amination[24]. These cobalt oxide nanoparticles are prepared by the immobilization of a cobalt–phenanthroline complex on carbon and subsequent pyrolysis at 800 °C under argon for 2 h. This cobalt oxide–based nanocatalyst worked well for the reductive amination of aldehydes and nitro compounds or amines to produce secondary/tertiary amines[24]. Unfortunately, this catalyst is not active for the synthesis of primary amines from carbonyl compounds and ammonia in presence of molecular hydrogen.

Leibniz-Institut für Katalyse e.V. an der Universität Rostock, Rostock, Germany. ✉e-mail: jagadeesh.rajenahally@catalysis.de; matthias.beller@catalysis.de

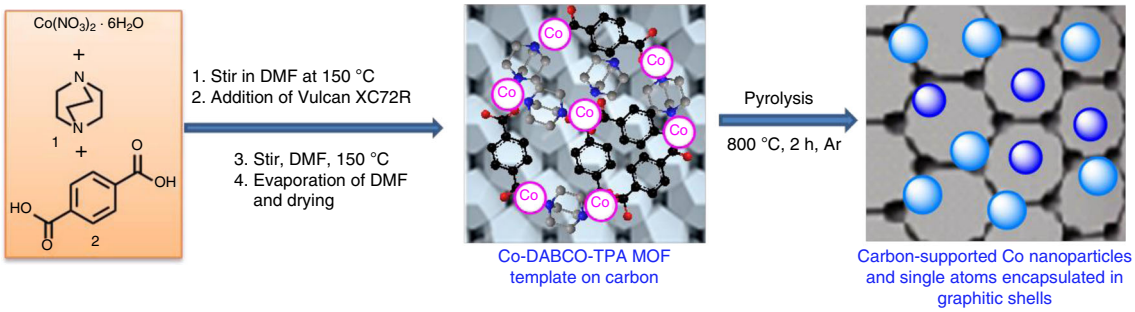

Fig. 1 | Preparation of carbon-supported single cobalt atoms and nanoparticles encapsulated within graphitic shells using a MOF template.

We recently developed a new type of carbon-supported cobalt nanoparticle and single atom–based catalysts[25]. The ordered arrangement of cobalt nanoparticles and single atoms is achieved by using a cobalt metal–organic framework (MOF) as a template on carbon and subsequent pyrolysis under an inert atmosphere[25]. The resulting cobalt nanoparticles were found to be general and selective catalysts for reductive aminations to prepare different kinds of amines[25].

Here, we describe the detailed procedure for the synthesis of these cobalt-based nanocatalysts and their application to obtain various amines of commercial and industrial importance. Notably, MOFs represent suitable precursors and self-scarifying templates for the preparation of nanomaterials under pyrolytic methods[6,25,39].

In a representative procedure, the most active material is prepared by immobilization of an in situ–generated cobalt–triethylenediamine (DABCO; **1**)–terephthalic acid (TPA; **2**) (Co-DABCO-TPA) MOF on carbon and subsequent pyrolysis of the templated material under argon atmosphere (Fig. 1)[25]. To identify a suitable MOF precursor, different MOFs, such as Co-DABCO-TPA, Co-DABCO and Co-TPA, were generated in situ and used for the preparation of catalytic materials. In particular, cobalt nitrate, DABCO and TPA in a molar ratio of 1:3:3 are mixed in *N*,*N*-dimethylformamide (DMF) and stirred at 150 °C to generate the MOF used in this procedure. After MOF formation, carbon is added (Vulcan XC72R) and the mixture is stirred again at 150 °C. Slow evaporation of the solvent (DMF) generates the desired template material (Co-DABCO-TPA@C). Pyrolysis at 800 °C leads to the formation of carbon-supported single cobalt atoms and nanoparticles (Co-DABCO-TPA@C-800). Under a similar procedure, other cobalt materials using Co-MOFs containing single linkers such as Co-DABCO and Co-TPA are also prepared.

The resulting materials are characterized using Cs-corrected scanning transmission electron microscopy (STEM), energy-dispersive X-ray spectroscopy (EDXS), electron energy loss spectroscopy (EELS), X-ray photoelectron spectroscopy (XPS), and X-ray powder diffraction (XRD) spectral analysis[25] (see Supplementary Figures for detailed characterizations). The most active material (Co-DABCO-TPA@C-800) is characterized by the formation of graphitic shells encapsulating metallic cobalt particles with sizes ranging from <5 to 30 nm (Fig. 2, Supplementary Figs. 1a and 2a). The EDXS (Supplementary Fig. 4a, left) shows mainly the presence of metallic Co particles within the carbon matrix. In addition to these small metallic particles, single Co atoms, visible as bright dots by high-resolution, high-angle annular dark-field (HR-HAADF) STEM, were also detected within so-called cloudy regions of short-range ordered carbon (Fig. 2, Supplementary Figs. 1a and 2a, right). Apart from these, a small quantity of oxidic cobalt (Co(II)) in the surface of core shell particles is also present. To obtain information on Co, C and N relations, the parallel mapping of EDXS for all elements and EELS (Supplementary Fig. 1b) are performed. Compared to EDXS, the EELS technique allows the detection of nitrogen species because, in the case of EDXS, the overlap of the C and N edges minimizes, allowing visualization of small amounts of N. These analyses identified the presence of nitrogen located in the vicinity of metallic Co particles and single Co atoms within short-range ordered carbon (Supplementary Fig. 1). The XRD analysis of the Co-DABCO-TPA@C-800 catalyst also showed predominately the presence of metallic Co particles, along with small quantity of cobalt oxide particles (Supplementary Fig. 7). XPS analysis showed two states of nitrogen. One is correlated to imine-like N known from pyridine (~98 eV) and the other, displaying at higher binding energy, corresponds to N bonded to Co (Supplementary Fig. 10a, right). These characterization data are summarized in Table 1.

Hereafter, we denote the most active catalyst, Co-DABCO-TPA@C-800 as Co/GS@C, where 'GS' stands for graphitic shells.

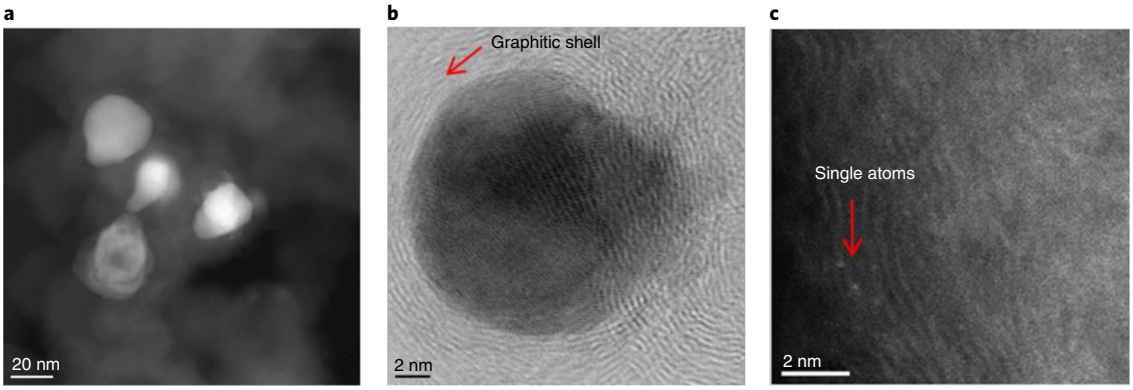

Fig. 2 | TEM images of Co/GS@C (Co-DABCO-TPA@C-800) catalyst. a, Distribution of cobalt nanoparticles. **b**, Graphitic shell encapsulated Co nanoparticles. **c**, Single cobalt atoms. Scale bars, 20 nm (**a**); 2 nm (**b**,**c**).

Table 1 | Characterization data for Co-DABCO-TPA@C-800 catalyst

Entry	Technique	Required analysis	Data found
2	STEM	Distribution, morphology, size and nature of nanoparticles	Graphitic shells encapsulated metallic cobalt particles with sizes from <5 nm to a maximum of 30 nm. Cobalt single atoms. Small quantity of cobalt oxide nanoparticles.
3	EDXS	Elemental detection and mapping	Metallic cobalt with small quantity of oxidic cobalt particles
4	EELS	Detection and distribution of nitrogen	Presence of nitrogen is detected and located in the vicinity of metallic Co particles and single Co atoms within short-range order carbon
5	XPS	Nature and states of nitrogen	XPS analysis showed two states of nitrogen. One is correlated with imine-like N known from pyridine (~398 eV) and the other, displaying at higher binding energy, corresponds to N bonded to Co
6	XRD	Different phases of cobalt	Predominate presence of metallic Co particles, along with small quantity of cobalt oxide particles

We tested commercial and prepared cobalt materials for the reductive amination of veratraldehyde (3,4-dimethoxybenzaldehyde; **3**) to veratrylamine (3,4-dimethoxybenzylamine; **4**) using ammonia and molecular hydrogen. In this benchmark reaction, the synthesis of the desired primary amine competes with the formation of unwanted secondary and tertiary amines/imines or alcohols. First, we tested commercial Raney nickel and Raney cobalt in the benchmark reaction and found that these two materials exhibited lower selectivity toward the formation of primary amine and as a results produced only 30–50% of veratrylamine (Table 2, entries 1-2). In these two cases, formation of the corresponding alcohol (45–64%) and secondary amine (2-3%) as side products was observed, which obviously lowered the selectivity toward the primary amine, a desired product in the present study. However, the cobalt materials prepared by the immobilization and pyrolysis of a Co-DABCO-TPA@C MOF on carbon (400–1,000 °C) exhibit significant activities (16–88% of **4**; Table 2, entries 3–6).

Among these materials, the ones pyrolyzed at 800 °C showed maximum activity and produced veratrylamine in an 88% yield (Table 2, entry 3). Pyrolysis of cobalt–MOF's on carbon using cobalt nitrate with either DABCO (Co-DABCO@C-800) or TPA (Co-TPA@C-800) alone yielded less active catalysts (15–20% yields; Table 2, entries 7-8). We also tested our previously reported[24] cobalt oxide–based nanocatalyst (Co-phenanthroline@C-800), prepared by the pyrolysis of Co-phenanthroline complex on carbon, and found that this catalyst is not active enough for the reductive amination to produce the desired primary amines (Table 2, entry 9). As expected, homogeneous cobalt salts, different cobalt-based MOFs, and non-pyrolyzed materials were completely inactive (Table 2, entries 10–13).

The general applicability of the Co/GS@C catalyst for the reductive amination of carbonyl compounds to access all kinds of amines is shown in Figs. 3–8 [25]. A series of functionalized and

Table 2 | Activity of supported cobalt nanoparticles and commercial heterogeneous catalysts for the reductive amination of veratrylamine using ammonia and hydrogen

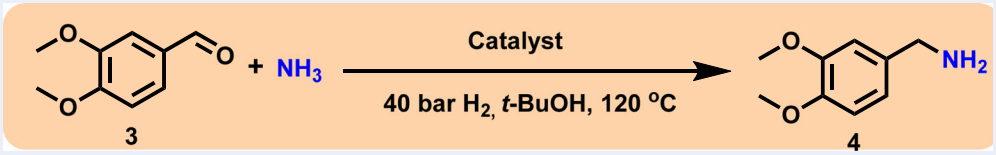

Entry	Catalyst	Yield of veratrylamine (%)
1	Raney nickel	50
2	Raney cobalt	30
3	Co-DABCO-TPA@C-800	88
4	Co-DABCO-TPA@C-400	16
5	Co-DABCO-TPA@C-600	75
6	Co-DABCO-TPA@C-1000	83
7	Co-DABCO@C-800	15
8	Co-TPA@C-800	20
9	Co-phenanthroline@C-800	1
10	$Co(NO_3)_2 \cdot 6H_2O$	1
11	Co-DABCO-TPA	1
12	Co-DABCO-TPA MOF	1
13	Co-DABCO-TPA@C	1

Reaction conditions: 0.5 mmol of 3,4-dimethoxybenzaldehyde, weight of catalyst corresponds to 3.5 mol% C, 5–7 bar NH_3, 40 bar H_2, 120 °C, 3 mL of *t*-BuOH, 15 h. Yields were determined by GC using n-hexadecane (100 μL) as standard. In the case of Raney nickel, 45% of corresponding alcohol and 2% of secondary amine were observed as side products. In the case of Raney cobalt, 64% of corresponding alcohol and 3% of secondary amine were observed as side products. The synthesis of Co-DABCO@C-800 and Co-DABCO-TPA MOF is described in Supplementary Method 2.

structurally diverse primary, secondary, and tertiary amines, including existing drug molecules, were prepared in good to excellent yields (**5**–**66**). Industrially relevant primary aliphatic amines were obtained from various aldehydes and ketones Fig. 3). Interestingly, this primary amine synthetic methodology can been applied for the introduction of an -NH_2 moiety in structurally complex and pharmaceutically applicable molecules, such as steroid derivatives, with high functional group tolerance (Fig. 4).

Next, various aldehydes were reacted directly with nitroarenes (products **37**–**44**) or amines (products **45**–**50**) in the presence of molecular hydrogen to obtain the corresponding secondary and tertiary amines (Fig. 5). For example, the alkylation of amino acid esters such as tyrosine methyl ester with different aldehydes proceeded smoothly in up to an 89% yield (products **47**–**49**), albeit racemization was observed. Under the present experimental reaction conditions, it is quite difficult to obtain retention of chirality without racemization in the case of reductive *N*-alkylation of amino acids. However, Fering et al. have shown the possibility of retention of chirality with single isomers in the case of *N*-alkylation of unprotected amino acids with alcohols by homogeneous Ru-catalyst[40]. By contrast, the reductive *N*-alkylation of (*S*)-(−)-α-methylbenzylamine and (*R*)-(+)-α-methylbenzylamine took place without racemization of the stereocenter (products **51**–**52**). Furthermore, we applied this cobalt catalyst for the preparation of *N*-methylamines (Fig. 6), which represent an important motif in numerous drugs (e.g.. Oxycontin, Venlafaxine, Lexapro). Hence, different carbonyl compounds were reacted with aqueous *N*,*N*-dimethylamine (DMA) to yield products **53**–**57**. In addition, *N*-methyl amines were also prepared directly from nitro compounds or amines using aqueous formaldehyde as a methylation source (products **58**–**61**).

The synthetic applicability of this novel amination protocol is showcased by applying the catalyst system to the preparation of different existing drug molecules such as piribedil (**62**), buclizine (**63**), fenpropimorph (**64**), befuraline (**65**), and fipexide (**66**) in good to excellent yields (Fig. 7).

Reaction scale-up was demonstrated by performing the reductive amination of three substrates at the 5- to 20-g scale (Fig. 8). In all these cases, excellent yields were obtained (similar to those of the small-scale reactions (100–150 mg). In addition to excellent activity and selectivity, our Co/GS@C catalyst exhibits high stability and can be easily recycled six times without any reactivation (Table 3; Box 1).

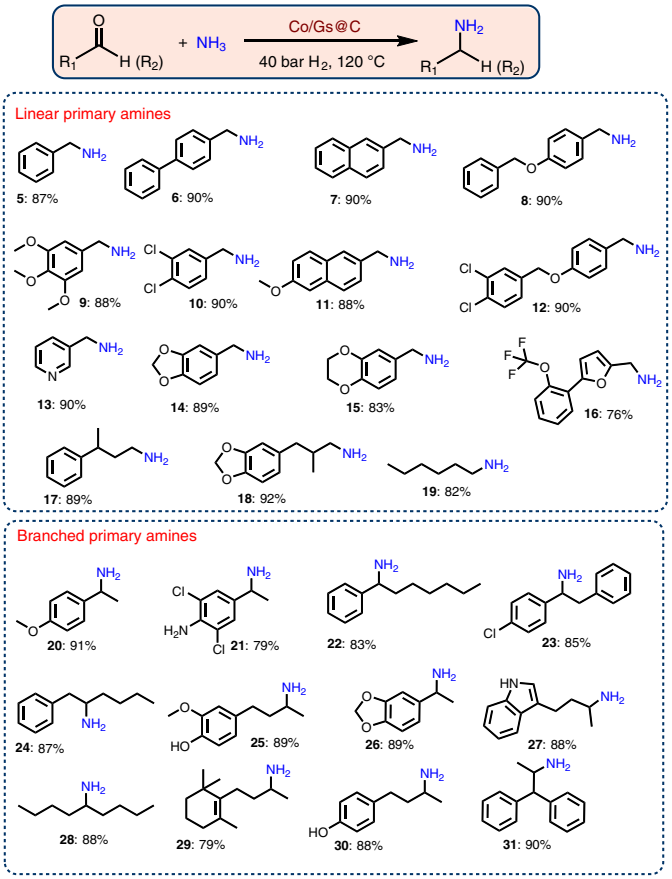

Fig. 3 | Co/GS@C-catalyzed reductive amination of aldehydes and ketones for the synthesis of linear and branched primary amines. Reaction conditions: 0.5 mmol of substrate, 25 mg of catalyst (3.5 mol% Co), 5–7 bar NH_3, 40 bar H_2, 3 mL *t*-BuOH, 120 °C, 15 h, with exceptions as follows. **20**–**30**: in THF (dry) solvent; **21**, **22**,**31**: for 20 h; **23**: for 30 h with 35 mg of catalyst. **24**: for 24 h. Isolated yields reported unless otherwise indicated. Isolated as free amines and converted to hydrochloride salts for measurement of NMR and HRMS spectra.

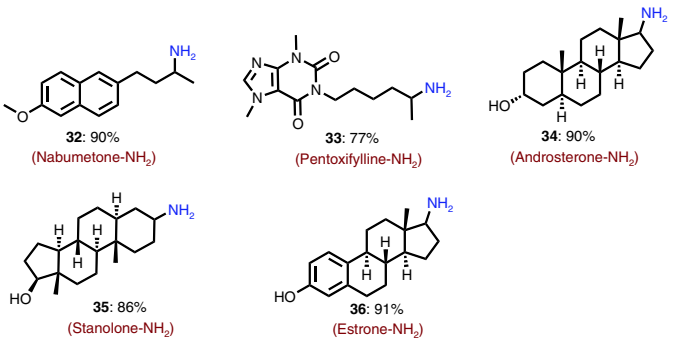

Fig. 4 | Co/GS@C-catalyzed amination of pharmaceuticals and steroid derivatives. Reaction conditions: 0.5 mmol of ketone, 25 mg of catalyst (3.5 mol% Co), 5–7 bar NH_3, 40 bar H_2, 3 mL of THF (dry), 120 °C, 15 h, with exceptions as follows. **33**, **34**: for 24 h. Isolated yields reported unless otherwise indicated. Isolated as free amines and converted to hydrochloride salts for measuring NMR and HRMS.

Although this cobalt-based reductive amination protocol can be applied to the synthesis of different kinds of amines, it still displays limitations such as (i) poor reactivity of ketones with amines to produce branched secondary or tertiary amines and, (ii) racemization of *N*-alkylated products of amino acids without retention of chirality.

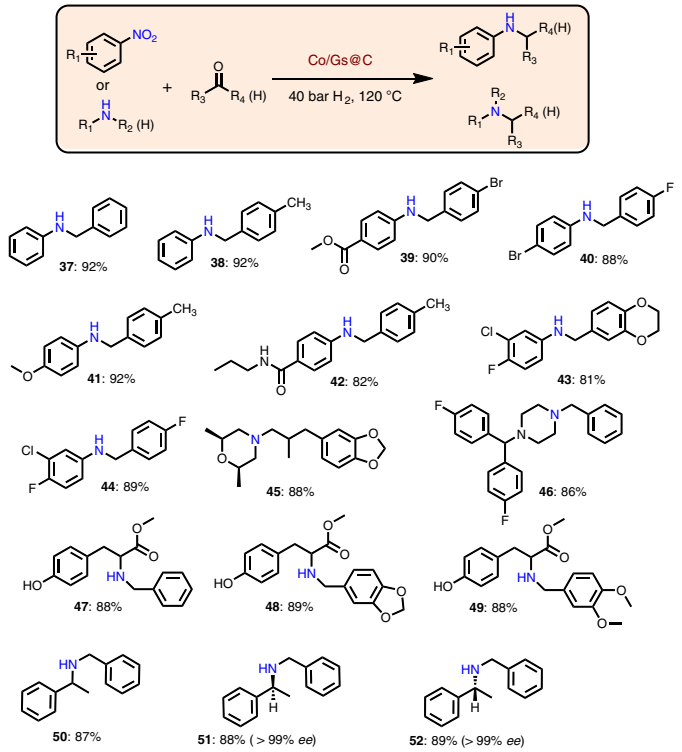

Fig. 5 | Co/GS@C-catalyzed synthesis of secondary and tertiary amines. Reaction conditions: 0.5 mmol of nitroarene, 0.75–1 mmol of aldehyde, 25 mg of catalyst (3.5 mol% Co), 20 mg of Amberlite IR-120, 3 mL of *t*-BuOH, 120 °C, 24 h, with exceptions as follows. **45**–**52**: 0.5 mmol of amine, 0.75 mmol of aldehyde. **46**: 30 mg of catalyst, 30 h. **50**–**52**: 10 mmol of amine, 15 mmol of benzaldehyde, 500 mg of catalyst (3.5 mol% Co), 400 mg of Amberlite IR-120, 15 mL of *t*-BuOH, 120 °C, 24 h. Isolated yields. ee, enantiomeric excess.

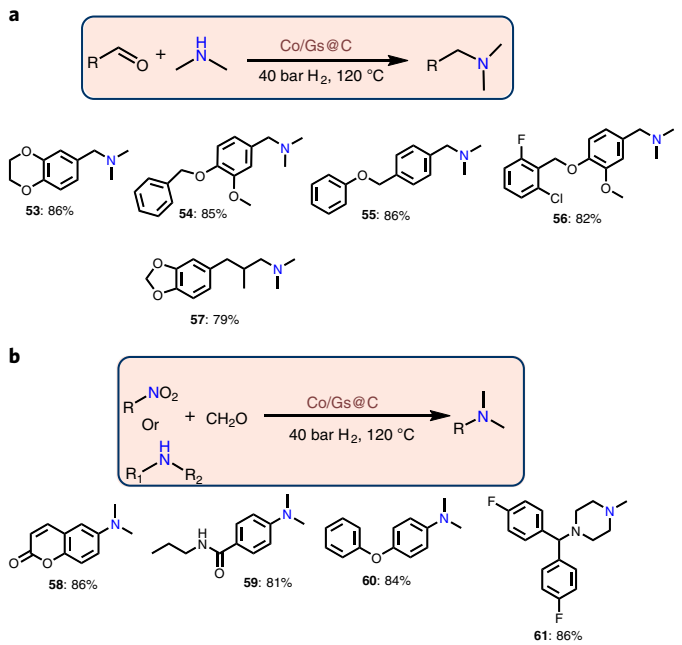

Fig. 6 | Co/Gs@C-catalyzed preparation of *N*-methylamines. a, Reactions of aldehydes with dimethylamine. Conditions: 0.5 mmol of aldehyde, 100 μL of aqueous dimethylamine (40 %), 25 mg of catalyst (3.5 mol% Co), 3 mL of *t*-BuOH, 120 °C, 24 h; isolated yields. **b**, Reactions of nitroarenes or amines with formaldehyde. Conditions: 0.5 mmol of nitroarene, 100–200 μL of aqueous formaldehyde (37%), 1:1 THF/H_2O (3 mL), with the following exception. **61**: 0.5 mmol of amine, 100–200 μL of aqueous formaldehyde (37%), 1:1 THF/H_2O (3 mL). Isolated yields.

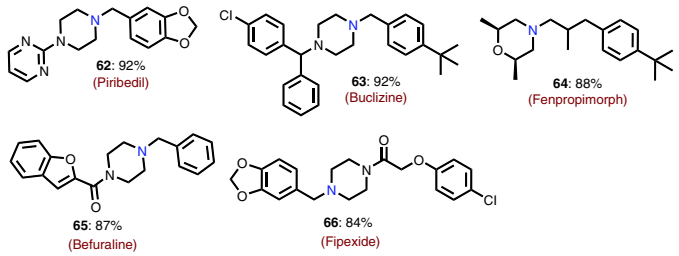

Fig. 7 | Preparation of drug molecules. Reaction conditions: 1 mmol of amine, 1.5 mmol of aldehyde, 50 mg of catalyst (3.5 mol% Co), 3 mL of *t*-BuOH, 120 °C, 24 h, with exceptions as follows. **65**, **66**: 2 mmol of amine, 1 mmol of aldehyde; synthesis of amine followed by acylation with acid chlorides (see Supplementary Method 2 for detailed procedure). Isolated yields.

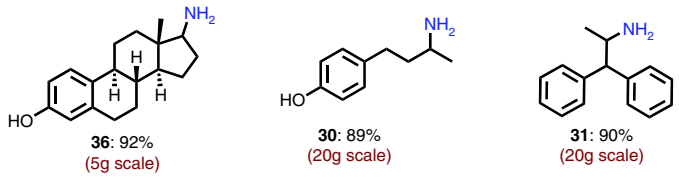

Fig. 8 | Reaction upscaling. Reaction conditions: 5–20 g of substrate, 25 mg of Co/Gs@C (3.5 mol% Co) for each 0.5 mmol of substrate, 5–7 bar NH_3, 40 bar H_2, 50–150 mL dry THF, 120 °C, 24 h. Isolated yields.

Table 3 | Recycling of Co/GS@C for the reductive amination of 4-(4-hydroxyphenyl)butan-2-one (67)

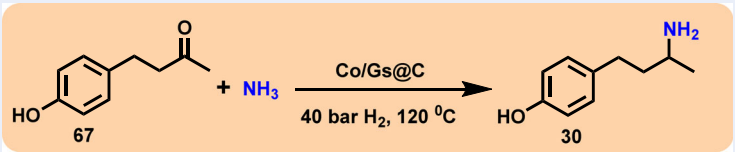

No. of runs	Yield of 4-(3-aminobutyl)phenol (%)
1	90
2	90
3	89
4	89
5	88
6	87
7	87

Reaction conditions: 5 mmol, 250 mg of catalyst (3.5 mol%), 5–7 bar NH_3, 40 bar H_2, 20 mL of dry THF, 120 °C, 15 h, isolated yields.

Experimental design

Catalyst preparation

The experimental procedure and setup reported below are applicable to the preparation of the catalyst on a 1- to 5-g scale. Following this experimental procedure, all the catalytic materials prepared exhibited similar activity and selectivity toward reductive amination reactions.

Characterization of catalysts

The catalytic materials have been systematically characterized using STEM, EDXS, EELS, XPS, and XRD spectral analysis.

Catalytic reactions

The described protocol was applied to reactions ranging from a 0.5-mmol to a 120-mmol scale. Similar yields were obtained in this range. The detailed experimental procedures to synthesize

Box 1 | Catalyst-recycling experiments with 4-(4-hydroxyphenyl)butan-2-one (Raspberry ketone)
● Timing 15 h

This reaction is performed to test and to demonstrate recycling and reusability of the catalyst. The catalyst can be recycled and reused up to six times without any substantial loss of catalytic activity or selectivity. In each step, after the reaction, the catalyst is separated (recycled) and reused without any reactivation (six times).

Procedure

1 Charge the Teflon or glass fitted 100-mL autoclave with a magnetic stir bar and 20 mL of THF solvent. Then add 821 mg of 4-(4-hydroxyphenyl)butan-2-one (5.0 mmol).
2 Weigh 250 mg (3.5 mol%) of the cobalt-based catalyst prepared in Step 8 of the main Procedure and add it to the autoclave.
3 Perform the reaction in an autoclave as described in Step 11A(iv–vi).
4 After completion of the reaction, let the autoclave cool to room temperature. Discharge the remaining ammonia and hydrogen and remove the reaction solution from the autoclave.
5 Transfer all of the reaction mixture to a centrifuge tube. Centrifuge the solution and separate the catalyst by decanting the supernatant.
▲ CRITICAL STEP Apply a centrifugation rate of 4,032*g* (6,000 r.p.m.) at room temperature (25 °C) for 5–10 min.
6 Wash the catalyst with an excess of ethyl acetate three times and dry the material in vacuo.
■ PAUSE POINT The dried catalyst can be stored for hours without further ado. Reuse it directly without further reactivation or purification for the next run.

the different amines given in Step 11A–E have been optimized (e.g., solvent, temperature, stirring time).

Different MOFs, such as Co-DABCO-TPA, Co-DABCO, and Co-TPA, were generated in situ under similar experimental procedures and have been used as precursors for the preparation of supported cobalt nanoparticles. The same procedure was applied to generate different MOFs and immobilize them on carbon, followed by pyrolysis to obtain cobalt nanoparticles.

Materials

Reagents

! CAUTION For the handling of reaction gases (hydrogen and ammonia), appropriate safety measures should be taken. Hydrogen is a flammable gas and hence it should be handled carefully. When filling the autoclave with hydrogen, care should be taken to avoid allowing the gas to leak out. Gaseous ammonia is corrosive and an irritant and can be fatal when inhaled. Check the material safety data sheets for hydrogen and ammonia before handling. The autoclaves should be handled carefully; hence, proper training is required. Convenient and pre-checked autoclaves should be used in order to avoid hydrogen leakage ▲ CRITICAL All solvents are used as received commercially without any purification.

- Cobalt(II) nitrate hexahydrate ($Co(NO_3)_2 \cdot 6H_2O$; Alfa Aesar, cat. no. 36418-100G)
- 1,4-Diazabicyclo[2.2.2]octane (DABCO; ReagentPlus, ≥99%; Sigma-Aldrich, cat. no. D27802-25G)
- Terephthalic acid (TPA, 98%; Sigma-Aldrich, cat. no.185361)
- Aqueous formaldehyde (37%, stabilizer with ~10% methanol; Sigma-Aldrich, cat. no. 252549)
- Aqueous dimethylamine solution (40 wt% in H_2O; Sigma-Aldrich, cat. no. 426458)
- Tetrahydrofuran (THF; 99.8%; stabilizer free; extra dry; Acros Organics, cat. no. 45070010)
- Methanol (MeOH; J.T. Baker, cat. no. 9070-01)
- Tertiary butanol (*t*-buOH, 99.8%; Acros Organics, cat. no. 390690025)
- *N*,*N*-Dimethylformamide (DMF, 99%; Sigma-Aldrich, cat. no. 348435000)
- Methanolic HCl (0.5 M HCl in methanol, Alfa Aesar, cat. no. H31570)
- Dioxane HCl (4 N HCl in dioxane; TCI Europe, cat. no. H1062)
- Vulcan XC72R carbon black (Cabot, cat. no. LOT-1584452)
- 3-Chloro-4-fluoronitrobenzene or 2-chloro-1-fluoro-4-nitrobenzene (98.0%; Sigma-Aldrich, cat. no. 233234)
- Ethyl acetate (Walther CMP, cat. no. WAL10521 5000)
- n-Hexane (Walther CMP, cat. no. BAK8669 9025)
- Hexadecane (ReagentPlus, 99%; Sigma-Aldrich, cat. no. H6703)
- Silica gel (high-purity grade, pore size 60 Å, 130–270 mesh, for column chromatography; Sigma-Aldrich, cat. no. 288608)
- Sodium sulfate (Na_2SO_4, ReagentPlus, ≥99.0%; Sigma-Aldrich, cat. no. S9627)

- Deionized water
- Hydrogen (99.999%; Air Liquide)
- Argon
- Helium (He)
- Ammonia gas (99.999%; Linde)
- Dimethylsulfoxide (DMSO-d_6) (Sigma-Aldrich, cat. no. 151874)
- Deuterated methanol (CD_3OD) (Sigma-Aldrich, cat. no. 151947)
- Deuterated chloroform ($CDCl_3$) (Sigma-Aldrich, cat. no. 151823)
- Holey carbon-supported Cu grid (mesh 300)
- 3,4,5-Trimethoxybenzaldehyde (98.0%; Sigma-Aldrich, cat. no. T68403)
- 4-(4-Hydroxyphenyl)butan-2-one (>99.0%; TCI Europe, cat. no. H0604)
- 2-Chloro-1-fluoro-4-nitrobenzene (98.0%; Sigma-Aldrich, cat. no. 233234)
- 2,3-Dihydrobenzo[b][1,4]dioxine-6-carbaldehyde (98.0%; Sigma-Aldrich, cat. no. 264598)
- Amberlite IR-120 (Sigma-Aldrich, cat. no. 1.15966)
- 4-(Phenoxymethyl)benzaldehyde (Maybridge, cat. no. CC63704CB)
- 4-Nitro-*N*-propylbenzamide (98.0%; Sigma-Aldrich, cat. no. 394130)

Equipment

- Round-bottom (RB) flasks (50, 100 and 250, pear-shaped, NS 29/32; Fisher Scientific, cat. no. 10303511)
- Teflon-coated magnetic stir bars (19 × 41.3 mm; VWR, cat. no. 58949-210,)
- Pasteur pipettes (glass, 230 mm, with cotton stoppers;, Carl Roth, cat. no. E327.1)
- Filter funnel (Buchner, 30 mL, glass-fritted disk, porosity = fine; VWR, cat. no. 89426-722)
- Magnetic stir plate with heating functionality (temperature range 50–300 °C, stirring speed 100–1,250 r.p.m.; Heidolph, model no. MR 3001 K)
- Aluminum block
- Weighing balance
- Vacuum pump
- Mortar and pestle (polytetrafluoroethylene (PTFE) stir bar, cylindrical, 10 × 6 mm; Cowie, cat. no. 001.110.6)
- Rotary evaporator
- Crucible and lid (china, 65 mL, 60 mm; Carl Roth, cat. nos. L222.1 and L239.1)
- Crucible and lid (china, 11 mL, 35 mm; Carl Roth, cat. nos. L218.1 and L235.1)
- Oven (Neytech Qex)
- Autoclaves (100, 300 mL; Parr Instrument)
- Glass centrifuge tube
- TEM instrument (JEOL, model no. JEM-ARM200F) equipped with corrector (CEOS), energy-dispersive X-ray-spectrometer (JEOL, model no. JED-2300), and a dual-EELS system (Gatan, Enfinium ER model)
- Diffractometer equipped with a linear position-sensitive detector (PSD; Stoe, STADI P model)
- X-ray photoelectron spectrometer (Thermo Fisher Scientific, model no. VG ESCALAB 220i XL)
- Gas chromatograph (Agilent, model no. 6890N network) equipped with a mass selective detector (Agilent, model no. 5973 network) and a 30 m × 0.250 mm × 0.25-μm column (Agilent, model no. HP-5MS; cat. no. 19091S-433)
- Gas chromatograph (Agilent 6890 series) with a flame ionization detector (FID) and a 30 m × 0.320 mm × 0.25-μm column (Agilent, model no. HP-5; cat. no. 19091J-413)
- Spectrometers (Bruker, model nos. AV 300 and AV 400)
- High-resolution electrospray ionization mass spectrometry (ESI-HRMS) instrument (HPLC system; Agilent, model no. 1200) and an electrospray ionization–time of flight–MS (ESI-TOF-MS) system (Agilent, model no. 6210)
- Electron ionization mass spectrometry (EI-HRMS) instrument (mass spectrometer; Thermo Fisher Scientific, model no. MAT 95XP)
- Reflux condenser
- Needles
- Aluminum plate
- Silica gel (pore size 3 or 4)
- Silica gel column (length, 200 mm; inner diameter, 15 mm; volume, 35 mL)
- Silica gel column (length, 1,000 mm; inner diameter, 75 mm; volume, 200 mL)
- Beaker

Fig. 9 | Heat treatment of the prepared Co-MOF@C material with a Neytech Qex oven.

Software

- WinX^{POW} (https://www.stoe.com/product/software-powder-xrd/)
- NMR-MestReNova (https://mestrelab.com/software/mnova/nmr/)

Equipment setup

Pyrolysis furnace (oven)

In our lab, a Neytech Qex oven is used to pyrolyze the material. The following temperature program is applied: conditions 25 °C/min, ~10 mL/min argon. The solid material to be pyrolyzed is transferred to a crucible and placed in the oven (Fig. 9). After placement of the crucible with lid, the chamber is closed and then the temperature of the oven is set to 100 °C. The air in the oven is evacuated by generating pre-vacuum for 5 min and then the chamber is flooded with argon for 60 s. The oven is heated again and evacuates another two times (three in total). The temperature of the oven is increased to 800 °C with constant argon flow and held at the same temperature (800 °C) for 2 h. After the completion of pyrolysis time, the oven is cooled to 100 °C and then the chamber is opened.

TEM

The TEM measurements are performed at 200 kV with an aberration-corrected instrument with a corrector. The microscope is equipped with an EDXS instrument and a dual-EELS system for chemical analysis. The aberration-corrected STEM imaging (HAADF and annular bright field (ABF)) is performed under the following conditions: HAADF and ABF imaging both are done with a spot size of approximately 0.1 nm, a convergence angle of 30–36° and collection semi-angles for HAADF and ABF of 90–170 mrad and 11–22 mrad, respectively. Dual EELS is done at a cathodoluminescence (CL) of 4 cm, an illumination semi-angle of 21.3 mrad and an entrance aperture semi-angle of 19.8 mrad.

XRD

XRD powder patterns are recorded on a Stoe STADI P diffractometer equipped with a linear PSD using Cu Kα radiation (λ = 1.5406 Å). Processing and assignment of the powder patterns is done using WinX^{POW} software (Stoe) and the Powder Diffraction File (PDF) database of the International Centre for Diffraction Data (ICDD).

XPS

XPS data are obtained with an X-ray photoelectron spectrometer with monochromatic Al Kα (1486.6 eV) radiation. The electron-binding energies (E_B) are obtained without charge compensation. For quantitative analysis, the peaks are deconvoluted with Gaussian–Lorentzian curves and the peak area is divided by a sensitivity factor obtained from the element-specific Scofield factor and the transmission function of the spectrometer.

Autoclaves for carrying out reductive amination reactions

All catalytic experiments are performed in either a 100- or 300-mL autoclave by placing it into a pre-heated aluminum block (Fig. 10). ▲ **CRITICAL** To avoid unspecific reactions, all catalytic reactions are performed in either glass vials, which were placed inside the autoclave, or Teflon/glass vessel-fitted autoclaves.

Gas chromatography–mass spectrometry

Perform gas chromatography–mass spectrometry (GC-MS; instrument coupled to both GC and MS instruments used for the analysis of organic compounds) analyses with column temperature limits of −60 °C to 325 °C and helium as carrier gas. A representative method for monitoring the reaction is shown in the table below.

Time (min)	Temperature (°C)	Temperature ramp
0–2	40	
2–11	250	21 °C/min
11–19	250	

Gas chromatography

Perform gas chromatography (GC) analysis on a GC system with an FID and a 30 m × 0.320 mm × 0.25-μm column, with column temperature limits of −60 °C to 325 °C and hydrogen as carrier gas. A representative method for monitoring the reaction is as shown in the table below.

Time (min)	Temperature (°C)	Temperature ramp
0–2	80	
2–10	160	10 °C/min
10–19	300	14 °C/min
19–24	300	

NMR spectral analysis

^{1}H, ^{13}C NMR data are recorded on spectrometers using DMSO-d_6, CD_3OD and $CDCl_3$ solvents. Temperature should be ~25 °C (unless stated otherwise). Chemical shift reference (shifts are given relative to tetramethylsilane) normal is 7.27 (^{1}H) and 77.0 (^{13}C) for $CDCl_3$; 3.32 (^{1}H) and 49.0 (^{13}C)

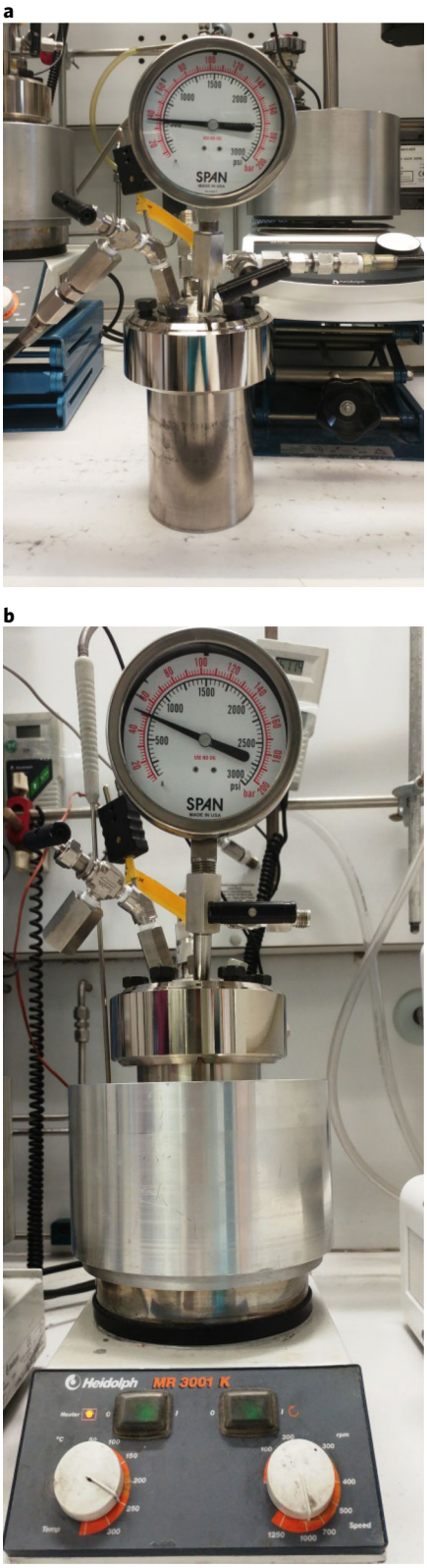

Fig. 10 | Equipment setup for reductive amination reactions. a, Pressurizing the autoclave. **b**, Autoclave placed into an aluminum block.

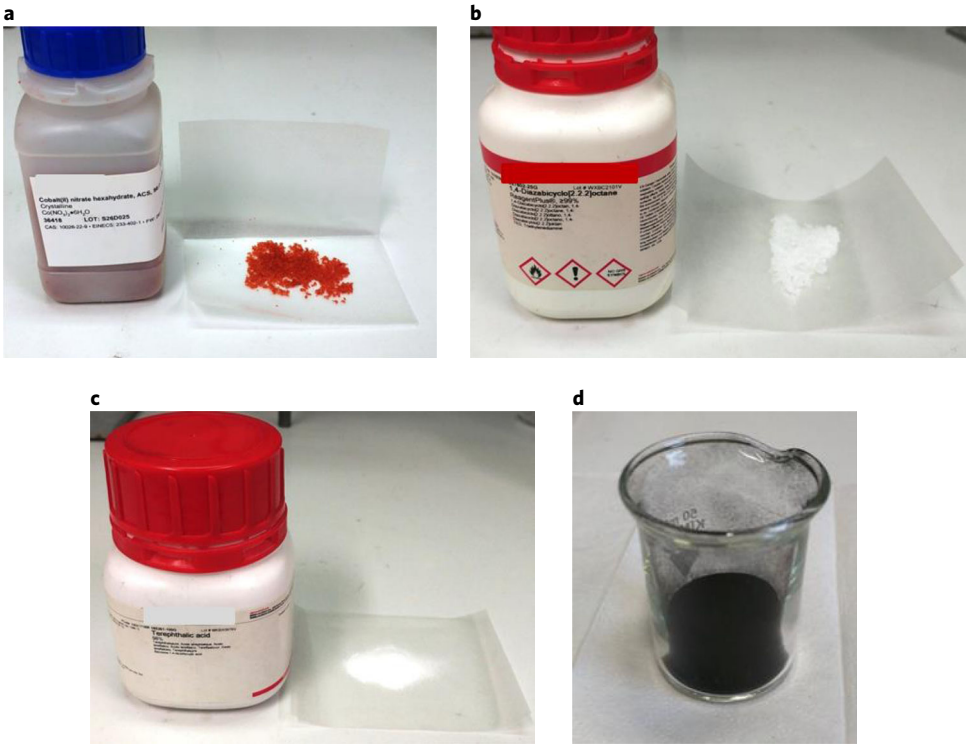

Fig. 11 | Starting materials for the preparation of Co/GS@C catalyst. a–d, Cobalt(II) nitrate hexahydrate ($Co(NO_3)_2$ $6H_2O$; **a**); 1,4-diazabicyclo[2.2.2]octane (DABCO; **b**); TPA (**c**); Vulcan XC72R carbon powder (**d**).

for CD_3OD; 2.49 (^1H) and 39.5 (^{13}C) for DMSO-d_6. NMR-MestReNova software is used to integrate the spectra.

HRMS spectral analysis

HRMS data were recorded on (i) an ESI-HRMS instrument and (ii) an EI-HRMS instrument, 70 eV.

Procedure

Catalyst preparation

▲ **CRITICAL** The catalyst preparation has been adapted for the different scales. All catalyst preparation steps (Steps 1–6) can be performed in air, except for the pyrolysis of the immobilized MOF on carbon (Step 8).

Wet impregnation of Vulcan XC72R carbon powder ● Timing 26 h

1 Calculate the appropriate weights of cobalt nitrate ($(Co(NO_3)_2 \cdot 6H_2O$), DABCO, TPA and Vulcan XC72R carbon powder required for the preparation of 1 g, 3 g or 5 g of catalyst (see entries 1–3 in the table below; Figs. 11–15). See Fig. 11 for starting materials.

Entry	Co/Gs@C (g)	$Co(NO_3)_2 \cdot 6H_2O$ (g)	DABCO (g)	TPA (g)	Vulcan XC72R (g)	DMF (mL)
1	1	0.148	0.171	0.253	0.5	20
2	3	0.444	0.513	0.761	1.5	40
3	5	0.740	0.855	1.265	2.5	60

2 Use a 100-mL RB flask for a 5-g-scale catalyst preparation and charge with $Co(NO_3)_2 \cdot 6H_2O$ and DABCO. For small-scale reactions, use smaller flasks as appropriate (50 mL).
? TROUBLESHOOTING

3 Add the appropriate amount of DMF (20 mL). Stir the mixture for 2–3 min at room temperature (25 °C), which leads to a dark blue solution. Set the speed of stirring to ~750 r.p.m.
? TROUBLESHOOTING

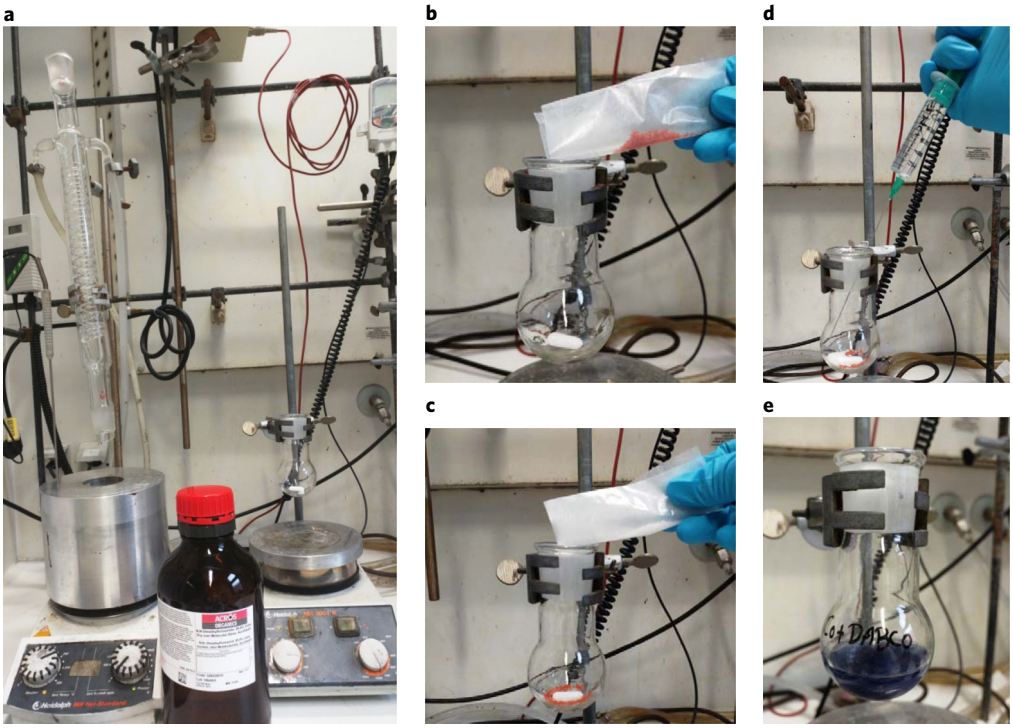

Fig. 12 | Addition of cobalt nitrate and DABCO in DMF. a–e, Reaction setup (**a**); addition of Cobalt(II) nitrate hexahydrate ($Co(NO_3)_2 \cdot 6H_2O$; **b**); addition of 1,4-diazabicyclo[2.2.2]octane (DABCO) to cobalt(II) nitrate hexahydrate (**c**); addition of DMF to the mixture of cobalt(II) nitrate and DABCO (**d**); after 2–3 min of stirring the mixture of cobalt(II) nitrate and DABCO in DMF (**e**).

4 Add the solution of TPA in hot DMF (15 mL) to the dark blue solution obtained in Step 3. The dark blue solution should turn into a solution with a light-blue precipitate. Then place the RB flask containing the reaction mixture into an aluminum block preheated to 150 °C and stir the mixture for 20–30 min with a fixed reflux condenser. The color of the solution should change to the pale green of the Co-DABO-TPA MOF after 20 min. Keep the stirring speed at ~750 r.p.m.
? TROUBLESHOOTING

5 Slowly add the appropriate amount of Vulcan XC72R carbon black powder to the solution, followed by addition of DMF (10 mL), and stir the suspension at 150 °C for 4 h. Keep the stirring speed at ~750 r.p.m.
▲CRITICAL STEP Vulcan XC72R carbon black is a fine powder and should be handled carefully while wearing protective clothes and with local exhaust ventilation. Note, the ratio of cobalt to linkers should be 1:3:3 ($Co(NO_3)_2 \cdot 6H_2O$/DABCO/TPA). TPA dissolves only in hot DMF.

6 Remove the reflux condenser and allow the RB flask containing the reaction products to stand without stirring or closing for 20 h at 150 °C in order to slowly evaporate the DMF and to grow the Co-MOF template on the carbon.
▲CRITICAL STEP After the evaporation of the solvent and ensuring that the material is completely dry, the material should be cooled to room temperature and ground to obtain a fine powder.

Heat treatment of the Co-MOF template on carbon ● Timing 8 h

7 Grind the dried material isolated in Step 6 into a fine powder and transfer it to a suitable crucible with a lid (Fig. 16).

8 Place the crucible in the chamber of the oven (Fig. 9) and pyrolyze the material at 800 °C for 2 h under an argon atmosphere (Equipment setup). The average percentage mass loss of the catalyst after pyrolysis was found to be ~50 %.
▲CRITICAL STEP After the pyrolysis, the catalytic material should be cooled to room temperature in the closed chamber.
■PAUSE POINT The obtained material can be stored for at least 4 months in closed glass vials at room temperature without taking any special precautions.

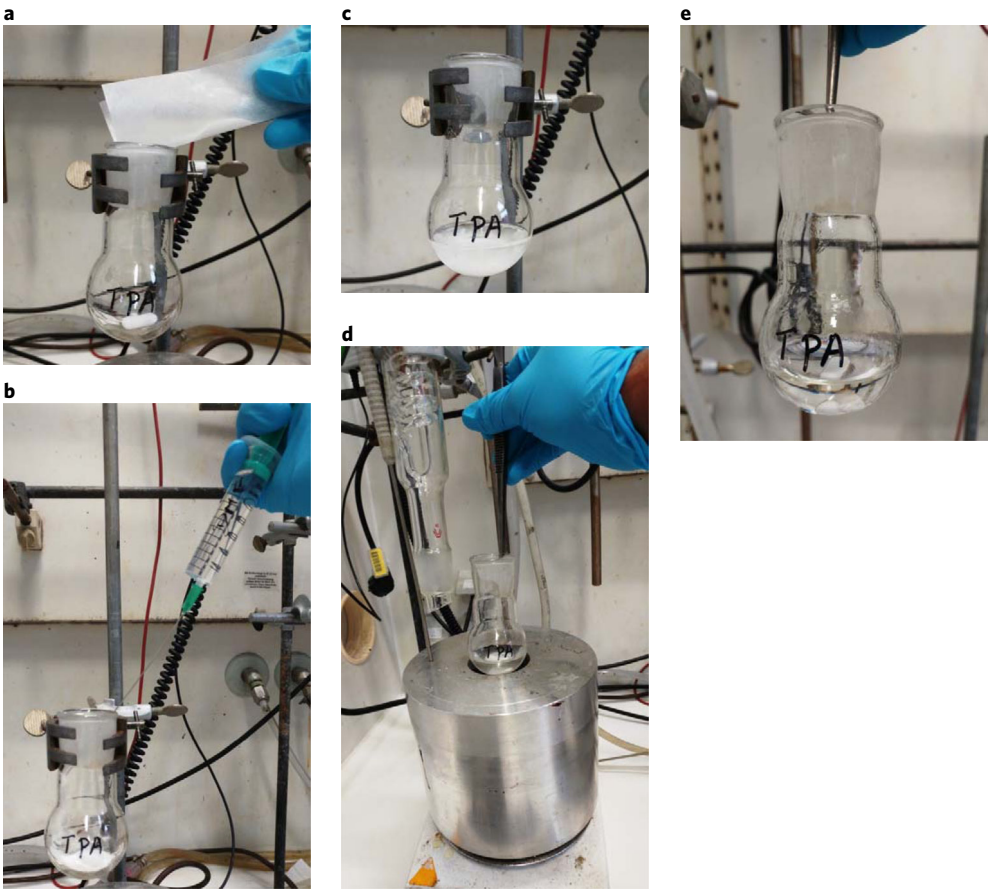

Fig. 13 | Preparation of TPA solution in DMF. a–e, Addition of TPA to the other RB flask (**a**); addition of DMF to TPA in RB flask (**b**); after addition of DMF to TPA at room temperature (**c**); placing the undissolved TPA in the aluminum block for heating at 150 °C for 5 min with stirring (**d**); TPA solution after 5 min of heating at 150 °C (**e**).

Catalyst characterization ● Timing variable

9 Characterize the material by STEM, EDXS, EELS, XPS, and XRD spectral analysis. Refer to the Materials section for setup of the TEM, XPS and XRD equipment. For TEM, deposit the samples on a holey carbon-supported Cu grid (mesh 300) without any pretreatment, and transfer it to the microscope.

10 Before using the material, check that the spectra are similar to those shown in the Supplementary Information (see also Table 1).

Amination reactions

11 The prepared catalyst can be used for reductive amination reactions (Fig. 17). Procedures for each reaction type are described in options A–E. Options A and B are used to prepare (3,4,5-trimethoxyphenyl)methanamine and 4-(3-aminobutyl)phenol, respectively. Option C is for reductive amination of nitro compounds and aldehydes, such as the synthesis of 3-chloro-*N*-((2,3-dihydrobenzo[b][1,4]dioxin-6-yl)methyl)-4-fluoroaniline. Options D and E are for the synthesis of tertiary amines. Option D is for reductive amination of carbonyl compounds and dimethyl amine to prepare, for example, *N*,*N*-dimethyl-1-(4-(phenoxymethyl)phenyl)methanamine. Option E is for reductive amination of nitro compounds with formaldehyde solution, for example, for the preparation of 4-(dimethylamino)-*N*-propylbenzamide.

(A) **Synthesis of (3,4,5-trimethoxyphenyl)methanamine hydrochloride ● Timing 15 h**

(i) Prepare the glass vial with a magnetic stir bar (Fig. 17a) and add 3 mL of *t*-buOH as solvent.

(ii) Add 98.1 mg of 3,4,5-trimethoxybenzaldehyde (0.5 mmol) to the prepared glass vial.

(iii) Weigh carefully 25 mg of the cobalt-based catalyst (3.5 mol%) prepared in Step 8 and add it to the reaction mixture. Fit the prepared vial with septum, cap and needle and place it in an aluminum plate inside a 300-mL autoclave (Fig. 17b).

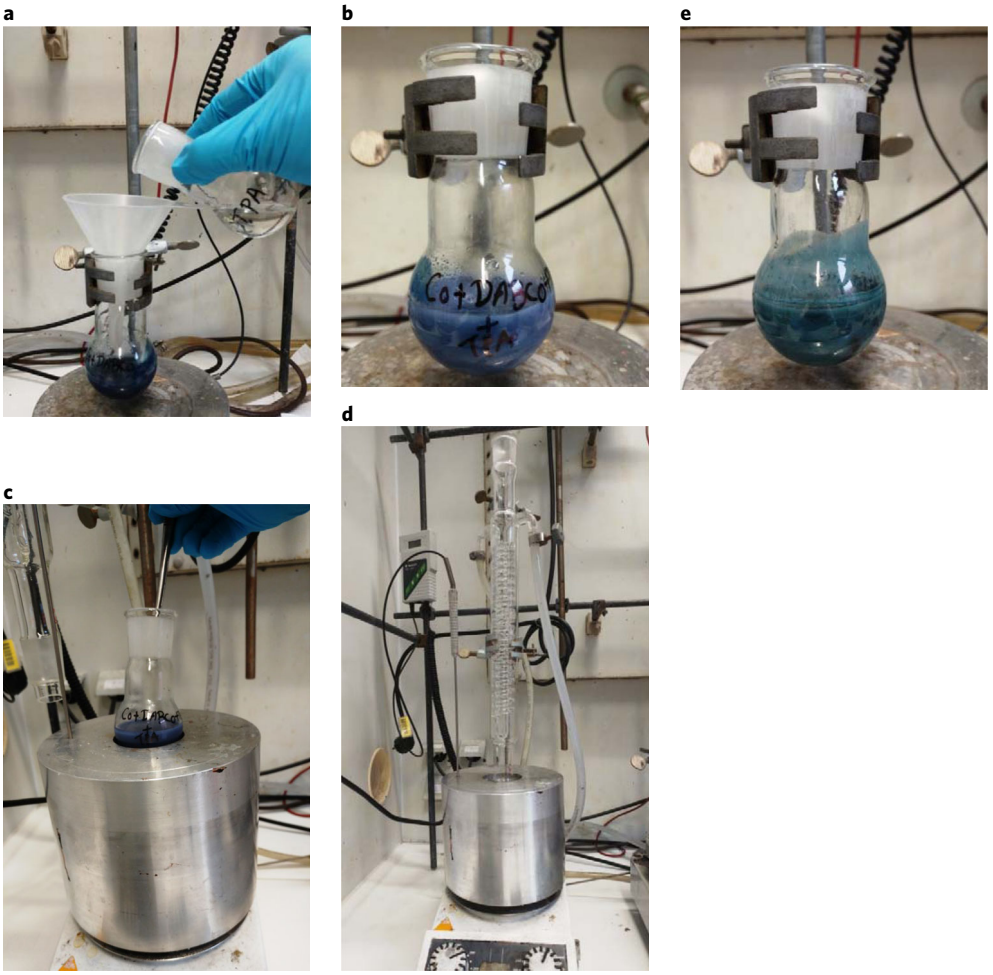

Fig. 14 | Preparation of Co-DABCO-TPA MOF. a–e, Addition of TPA solution to cobalt nitrate+DABCO mixture in DMF (**a**); color of the reaction mixture after addition of TPA solution to cobalt nitrate+DABCO mixture in DMF (**b**); placement of the reaction mixture in the aluminum block (**c**); fixation with reflux condenser and stirring at 150 °C (**d**); color of the reaction mixture after 30 min of stirring at 150 °C (**e**).

(iv) To evacuate the air, flush the autoclave with 40 bar hydrogen gas twice. Then, pressurize the autoclave with 5–7 bar ammonia gas and 40 bar hydrogen (Fig. 17b).

(v) Pre heat the aluminum block to 130 °C. Place the autoclave into the preheated aluminum block. Stir the reaction for 15 h, setting the speed of stirrer to 750 r.p.m. (Fig. 17b).
▲ **CRITICAL STEP** The temperature inside the autoclave and at the aluminum block might vary depending on the autoclave. To avoid this difference, the temperature of the aluminum block (heating system) should be verified and set to obtain the exact reaction temperature inside the autoclave. The temperature measured inside the autoclave is considered to be the reaction temperature. In our case, we observed 10 °C temperature differences between the aluminum block and inside the autoclave. For this reason, the temperature of the aluminum block is set to 130 °C (10 °C higher than the reaction temperature). When charging the autoclave with ammonia and hydrogen, ammonia should be pressurized first and then hydrogen.

(vi) After completion of the reaction, cool the autoclave to room temperature. Discharge the remaining hydrogen and ammonia and then remove the samples from the autoclave.
▲ **CRITICAL STEP** The reaction times differ between substrates (Fig. 3). Work up the sample using a Pasteur pipette with cotton stopper, filter off the catalyst from the reaction solution through a short plug of silica gel (~3 cm), and rinse it with 4 mL of ethyl acetate

(vii) For each reaction with a different kind of substrate (Fig. 3), monitor the progress of the reaction by GC-MS. To identify the desired product, take an aliquot (100 µl) of the filtrate and perform GC-MS as described in the 'Equipment setup' section.

Fig. 15 | Impregnation of Co-DABCO-TPA MOF on carbon. a–c, Addition of Vulcan XC72R carbon black support (**a**); after addition of Vulcan XC72R carbon powder support (**b**); after 20 h of drying by slow solvothermal process (**c**).

(viii) For quantitative analysis of products by GC, add hexadecane (100 μl) as a standard to the filtrate containing the reaction products. Take an aliquot (200 μl) of this filtrate for GC analysis with the calibrated method of the substrate and the product according to the instructions in the 'Equipment setup' section.

(ix) After completion of the reaction, cool the autoclave to room temperature. Discharge the remaining hydrogen and ammonia and then remove samples from the autoclave.
▲ **CRITICAL STEP** It should be noted that the reaction times differ between substrates (Fig. 3). Work up the sample using a Pasteur pipette with a cotton stopper, filter off the catalyst from the reaction solution through a short plug of silica gel (~3 cm) and rinse it with 4 mL of ethyl acetate.

(x) *Purification*. After completion of the autoclave reaction, remove the sample from the autoclave. Separate the catalyst from the solution using a 30-mL Buchner filter funnel with an embedded silica filter (pore size 3 or 4). Wash the catalyst along with the filter funnel, using ethyl acetate (3 × 5 mL).

(xi) Collect all the filtrate fractions and concentrate the solution under reduced pressure (at 240 mbar for 15 min, then further reduced to 10 mbar for 10 min), using a rotary evaporator at a temperature of 40 °C.

(xii) Purify the crude product by flash column chromatography. Use a silica gel column with the following size: length, 200 mm; inner diameter, 15 mm; and volume, 35 mL. As eluent, use a mixture of ethyl acetate and hexane (1:10 ethyl acetate/hexane progressively brought to 1:5 ethyl acetate/hexane).

(xiii) Collect the fractions of the pure product into a beaker, stir with anhydrous Na_2SO_4 for 5 min, and filter it off using a Buchner funnel.

(xiv) Remove the solvent from the filtrate under reduced pressure, using a rotary evaporator at a temperature of 40 °C, and dry the obtained product in vacuo.

(xv) Convert amines into their respective hydrochloride salts. To obtain the corresponding salts, add 1–2 mL of methanolic HCl or dioxane HCl (0.5 M HCl in methanol or 4 N HCl in dioxane) to the ether solution of the respective amine and stir the mixture at room temperature for 4–5 h. Then remove the solvent and dry the resulting hydrochloride salt of amine under vacuum.

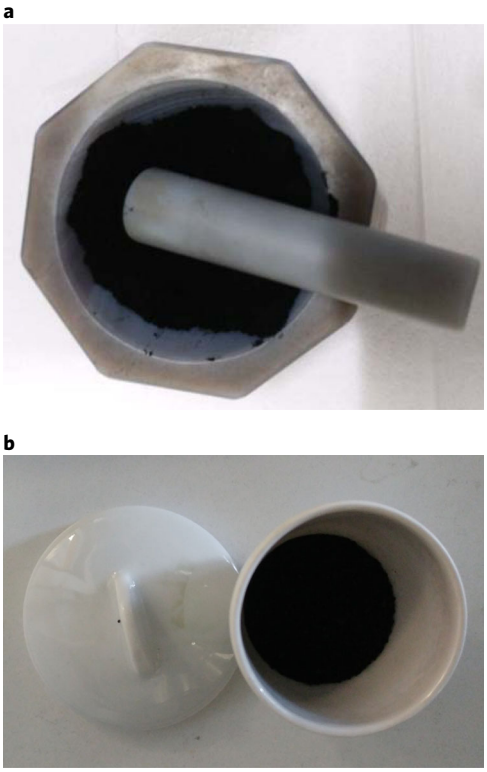

Fig. 16 | Grinding of the dried catalyst and pyrolysis. a,**b**, Grinding of the dried catalyst Co-DABCO-TPA solid material (**a**); used crucible with lid after pyrolysis (**b**).

(xvi) Analyze the structure and purity of the product by GC-MS, HRMS and NMR spectral analysis.
? TROUBLESHOOTING

(B) **Synthesis of 4-(3-aminobutyl)phenol hydrochloride** ● Timing **15 h**
▲ CRITICAL The reaction described here is at a 05-mmol scale. This reaction can be scaled up to a 20-g scale. Refer to Box 2 for a detailed procedure for doing this.
(i) Prepare the glass vial with a magnetic stir bar (Fig. 17a) and add 3 mL of dry THF.
? TROUBLESHOOTING
(ii) Add 82.1 mg of 4-(4-hydroxyphenyl)butan-2-one (0.5 mmol) to the prepared glass vial.
(iii) Weigh carefully 25 mg of the cobalt-based catalyst (3.5 mol%) prepared in Step 8 and add it to the glass vial containing the reaction mixture. Fit the prepared vial with septum, cap and needle and place it into an aluminum plate inside a 300-mL autoclave (Fig. 17b).
(iv) Perform the reaction in an autoclave as described in Step 11A (iv–xiii) to obtain 4-(3-aminobutyl)phenol hydrochloride.
(v) Analyze the structure and purity of the product by GC, GC-MS, HRMS and NMR spectral analysis.
? TROUBLESHOOTING

(C) **Reductive amination of 2,3-dihydrobenzo[b][1,4]dioxine-6-carbaldehyde with 2-chloro-1-fluoro-4-nitrobenzene** ● Timing **24 h**
(i) Place a magnetic stir bar in an 8-mL reaction vial and add 3 mL of *t*-buOH solvent (Fig. 17).
(ii) Add 87.7 mg of 2-chloro-1-fluoro-4-nitrobenzene (1.0 equiv.) and 82.1 mg of 2,3-dihydrobenzo [b][1,4]dioxine-6-carbaldehyde (1.5 equiv.) to the glass vial.
(iii) Add 25 mg of the cobalt-based catalyst (3.5 mol%) prepared in Step 8 and 20 mg of Amberlite IR-120 to the glass vial containing the reaction mixture.
? TROUBLESHOOTING
(iv) Flush the autoclave with hydrogen at 40 bar pressure twice and pressurize it with hydrogen to 40 bar.

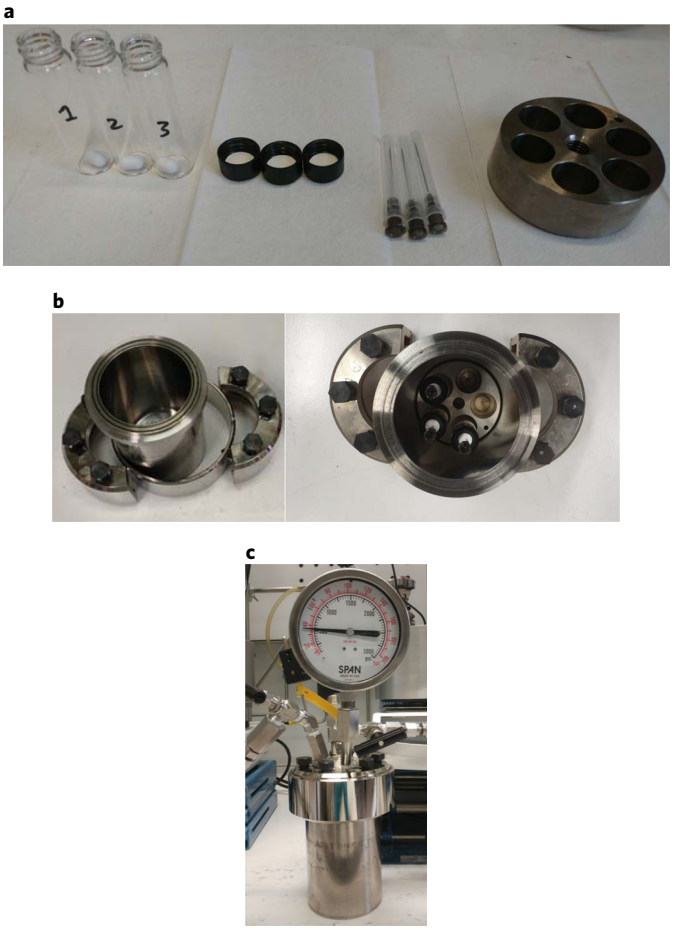

Fig. 17 | Glass reaction vials and autoclave setup. a–c, Glass vials with magnetic stir bars, caps with septa, needles and aluminum plate for placing vials (**a**); 300-mL autoclave (left) and autoclave with prepared reaction vials (right; **b**); pressurized autoclave (**c**).

(v) Place the autoclave into an aluminum block preheated to 130 °C and stir the reaction mixture for 24 h at 130 °C (Fig. 17a). Set the stirring rate to 650–700 r.p.m.
▲ **CRITICAL STEP** The temperature of the aluminum block (heating system) should be verified by a temperature sensor to obtain the required reaction temperature. While heating up the reaction system, a temperature gradient between the aluminum block and the reaction vial inside the autoclave occurs. Preheat the autoclave for 30 min in order to achieve the desired reaction temperature before starting to count the reaction time.

(vi) Implement Step 11A(vi–xii) to obtain the pure product of 3-chloro-*N*-((2,3-dihydrobenzo[b][1,4]dioxin-6-yl)methyl)-4-fluoroaniline as an oil. For the chromatographic purification of the desired product, use a silica gel column with the following size: length, 200 mm; inner diameter, 15 mm; and volume, 35 mL. As eluent, use a mixture of ethyl acetate and hexane (100% hexane progressively brought to 1:1 ethyl acetate/hexane).

(vii) Analyze the structure and purity of the product by GCMS, HRMS and NMR spectral analysis.

(D) **Synthesis of *N*-methylamines: reaction between 4-(phenoxymethyl)benzaldehyde and dimethylamine ● Timing 24 h)**

(i) Place a magnetic stir bar in an 8-mL reaction vial and add 3 mL of *t*-buOH solvent (Fig. 17).

(ii) Add 100 μL of aqueous dimethylamine (40 wt% in H_2O) and 111.2 mg of 4-(phenoxymethyl) benzaldehyde to the glass vial.

(iii) Add 25 mg of the cobalt-based catalyst (3.5 mol%) prepared in Step 8 to the glass vial containing the reaction mixture.

(iv) Flush the autoclave with hydrogen at 40-bar pressure twice and pressurize it with hydrogen to 40 bar.

Box 2 | Reaction scale-up for the synthesis of 4-(3-aminobutyl)phenol hydrochloride ● Timing 15 h

The reaction described in the Procedure is scaled up to 20 g. This scaled-up method generates 17.6 g of product (4-(3-aminobutyl)phenol) hydrochloride. In scaling up any of these reactions, the steps below need to be optimized.
For other upscaling reactions (5- to 20-g scale), the amounts of catalyst and solvent need to be altered. An amount of catalyst equivalent to 3.5 mol% and an amount of solvent equivalent to 10 mL for 1 g of substrate. Other parameters, such as reaction time, temperature, and pressure of hydrogen and ammonia, are applied in a manner similar to that used for small-scale reactions (0.5. mmol).

Procedure

1 Charge the Teflon or glass fitted 300-mL autoclave with a magnetic stir bar and 150 mL of THF solvent. Then add 20 g of 4-(4-hydroxyphenyl)butan-2-one (121.8 mmol).
2 Weigh 3.6 g (3.5 mol%) of the cobalt-based catalyst prepared in Step 8 of the main Procedure and add it to the autoclave.
3 Perform the reaction in an autoclave as described in Step 11A(iv–vi).
4 After completion of the reaction, let the autoclave cool to room temperature. Discharge the remaining ammonia and hydrogen and remove the reaction solution from the autoclave.
5 For purification, implement Step 11A(viii–xii). For purification, use a silica gel column with the following size: length, 1,000 mm; inner diameter, 75 mm; and volume, 200 mL. As eluent, use a mixture of ethyl acetate and hexane (1:10 ethyl acetate/hexane progressively brought to 1:5 ethyl acetate/hexane).

(v) Place the autoclave into an aluminum block preheated to 130 °C and stir the reaction mixture for 24 h at 130 °C (Fig. 17a). Set the stirring rate to 650–700 r.p.m.
▲ **CRITICAL STEP** The temperature of the aluminum block (heating system) should be verified by a temperature sensor to obtain the required reaction temperature. While heating up the reaction system, a temperature gradient between the aluminum block and the reaction vial inside the autoclave occurs. Preheat the autoclave for 30 min in order to achieve the desired reaction temperature before starting to count the reaction time.

(vi) Implement Step 11A(vi–xii) to obtain the pure product *N,N*-dimethyl-1-(4-(phenoxymethyl) phenyl)methanamine as a yellow gum. For the chromatographic purification of the desired product, use a silica gel column with the following size: length, 200 mm; inner diameter, 15 mm; and volume, 35 mL. As eluent, use a mixture of ethyl acetate and hexane (100% hexane progressively brought to 1:1 ethyl acetate/hexane).

(vii) Analyze the structure and purity of the product by GCMS, HRMS and NMR spectral analysis.

(E) **Synthesis of *N*-methylamines: reaction between 4-nitro-*N*-propylbenzamide and aqueous formaldehyde ● Timing 24 h**

(i) Charge an 8-mL glass vial with a magnetic stir bar and add 3 mL of a THF–H_2O (1:1) solvent mixture (Fig. 17).

(ii) Add 100 μL of aqueous formaldehyde (37% in water, stabilized with ~10% methanol), and 104.1 mg of 4-nitro-*N*-propylbenzamide to the glass vial.

(iii) Add 25 mg of the cobalt-based catalyst (3.5 mol%) prepared in Step 8 to the solution.

(iv) Flush the autoclave with hydrogen at 40-bar pressure twice and pressurize it with hydrogen to 40 bar.

(v) Place the autoclave into an aluminum block preheated to 130 °C and stir the reaction mixture for 24 h at 130 °C (Fig. 17a). Set the stirring rate to 650–700 r.p.m.
▲ **CRITICAL STEP** The temperature of the aluminum block (heating system) should be verified by a temperature sensor to obtain the required reaction temperature. While heating up the reaction system, a temperature gradient between the aluminum block and the reaction vial inside the autoclave occurs. Preheat the autoclave for 30 min in order to achieve the desired reaction temperature before starting to count the reaction time.

(vi) Implement Step 11A(vi–xii) to obtain the pure product 4-(dimethylamino)-*N*-propylbenzamide as brown solid. For the chromatographic purification of the desired product, use a silica gel column with the following size: length, 200 mm; inner diameter, 15 mm; and volume, 35 mL. As eluent, use a mixture of ethyl acetate and hexane (100% hexane progressively brought to 1:1 ethyl acetate/hexane).

(vii) Analyze the structure and purity of the product by GCMS, HRMS and NMR spectral analysis.

Troubleshooting

Troubleshooting advice can be found in Table 4.

Table 4 | Troubleshooting table

Step	Problem	Possible reason	Solution
2–4	The catalytic activity is lower than expected	Dissolving of both linkers and cobalt nitrate together or dissolving of TPA and cobalt nitrate together.	DABCO and cobalt nitrate should be dissolved in DMF first. Next, TPA that has already been dissolved in DMF should be added.
11A(xvi), 11B(v)	NH_2 peak in ^1H NMR observed	It is possible that the NH_2 peak merged with the residual solvent–water peak in DMSO	Convert amines into HCl salts and measure NMR in DMSO
11B(i)	The yield of the product is lower than expected	If an old bottle of THF was used, water might be present in the THF	Use fresh and dry THF
11C(iii)	The yield of the product is lower than expected	Less effective formation of the secondary imine	The Amberlite IR-120 is needed as an additive to form the corresponding imine effectively

Timing

Catalyst preparation

Steps 1–6, wet impregnation of Vulcan XC72R black carbon powder: 26 h

Step 7 and 8, heat treatment of the adsorbed Co-DABCO-TPA MOF on carbon: 8 h

Steps 9 and 10, catalyst characterization: variable

Amination reactions

Step 11A, synthesis of (3,4,5-trimethoxyphenyl)methanamine hydrochloride: 15 h

Step 11B, synthesis of 4-(3-aminobutyl)phenol hydrochloride: 15 h

Step 11C, reductive amination of 2,3-dihydrobenzo[b][1,4]dioxine-6-carbaldehyde with 2-chloro-1-fluoro-4-nitrobenzene: 24 h

Step 11D, synthesis of *N*-methylamines: reaction between 4-(phenoxymethyl)benzaldehyde and dimethylamine: 24 h

Step 11E, synthesis of *N*-methylamines: reaction between 4-nitro-*N*-propylbenzamide and aqueous formaldehyde: 24 h

Box 1, catalyst-recycling experiments with 4-(4-hydroxyphenyl)butan-2-one: 15 h

Box 2, reaction scale-up for the synthesis of 4-(3-aminobutyl)phenol hydrochloride: 15 h

Anticipated results

Co-DABCO-TPA@C-800 catalyst

TEM analysis and data

Aberration-corrected STEM analysis of the most active material (Co-DABCO-TPA@C-800; Co/GS@C) shows the formation of mainly metallic cobalt particles with diameter ranging from <5 nm to 30 nm (Fig. 2 and Supplementary Fig. 1). The EDXS (Supplementary Fig. 1a, left) shows mainly the presence of metallic Co particles within the carbon matrix. Most of these particles are surrounded by a combination of some graphitic layers and short-range ordered graphitic shells (Supplementary Fig. 1a, middle). In addition, a smaller quantity of core–shell particles with cobalt oxide shells at metallic Co is also present (Supplementary Fig. 2a). In regions of short-range ordered carbon, we detected single Co atoms as bright dots in HAADF images (Supplementary Fig. 1a, right).

To get information on the cobalt–carbon–nitrogen relation, the parallel mapping of EDXS for all elements and EELS (Supplementary Fig. 1b) optimized for carbon, nitrogen and oxygen were performed. Because the nitrogen signal is superimposed on the carbon signal in EDXS, these maps were used only for the Co distribution. Figure 2b shows the maps of C, N and Co (left image) in the neighborhood of a metallic particle wrapped by graphitic carbon. The C–N overlay in the HAADF image (middle image) gives evidence that nitrogen is located not only in the graphitic shell on the Co particle but surprisingly also in short-range ordered carbon, which is not part of the graphitic shell and corresponds to features with single atoms shown in Supplementary Fig. 1a. Co traces are

detectable everywhere in the nitrogen-containing carbon at low concentrations. By contrast, the less active material, Co-DABCO@C-800, contained mainly hollow cobalt oxide (Co_3O_4) particles (Supplementary Fig. 2b). In addition to Co_3O_4, some Co–Co_3O_4 core–shell particles were also present. Although sub-nanometer Co structures were found in this material, no single Co atoms were detected. Similarly, Co-TPA@C-800 (Supplementary Fig. 2c) also contained mainly cobalt oxide (Co_3O_4) particles encapsulated within graphitic shells, along with a small quantity of metallic cobalt in Co–Co_3O_4 core–shell structures. No single Co atoms or sub-nanometer Co structures were detected in this material. Cobalt nitrate@C-800, which was completely inactive, contained hollow Co_3O_4 with short-range ordered carbon from the support in the vicinity (Supplementary Fig. 2d). To understand the formation mechanism of the active catalyst, materials pyrolyzed at lower temperatures were also characterized (Supplementary Fig. 3). In Co-DABCO-TPA@C-400, a minor amount of metallic cobalt was present in the core of cobalt–cobalt oxide core–shell structures, and no formation of graphitic shells was observed. Co-DABCO-TPA@C-600 contained more metallic cobalt, and incipient formation of graphitic shells enveloping the metallic Co was evident. Apparently, this structural process is critical to high activity and stability. For the most active Co-DABCO-TPA@C-800, single Co atoms within some of the graphitic structures were detected. In the case of Co-DABCO-TPA@C-1000, most of the Co was present in metallic crystallite morphology completely covered by graphitic structures. In all the active catalysts, cloudy regions of cobalt species in the 1- to 2-nm range were detected.

XRD analysis and data

The different phases of cobalt in both active and less active catalysts have been also confirmed by XRD data (Supplementary Figs. 7 and 8) that accorded with the TEM analysis.

XPS analysis and data

The nature and quantity of nitrogen in these materials were further explored by XPS (Supplementary Figs. 10 and 11). Surprisingly, the combination of the two linkers increased the quantity of nitrogen in the near-surface region compared to either linker alone (Supplementary Fig. 12). The N content in Co-DABCO-TPA@C-800 was three times higher than in Co-DABCO@C-800, whereas in Co-TPA@C-800, only traces of N were observed. In both Co-DABCO-TPA@C-800 and Co-DABCO@C-800, two N-states could be detected (Supplementary Fig. 10): one correlating with imine-like N known from pyridine (~398 eV)[41,42] and the other manifesting a higher binding energy, corresponding to N bonded to the metal. For the former sample a clear separation of the two peaks was observed due to the slightly higher binding energy. For Co-DABCO-TPA@C pyrolyzed at different temperatures, iminic N was observed, and the binding energy of the Co–N bond increased as pyrolysis temperature ascended to 800 °C (Supplementary Fig. 10). In comparison to all other samples, the observation of the two N states was unique to these active systems (Supplementary Fig. 11)[41,42]. It seems that for the optimal catalyst, the bonding between Co and N is most pronounced. In the material pyrolyzed at 1,000 °C, the formation of nitrides could be observed as well (Supplementary Fig. 11). In the un-pyrolyzed and 1,000 °C samples, the amount of Co in the near-surface region was too low for a reasonable peak fitting; for all other samples, the metal content was nearly the same.

(3,4,5-Trimethoxyphenyl)methanamine hydrochloride

Column chromatography on silica gel (method: 10% ethyl acetate/hexane−60% ethyl acetate/hexane; Fig. 15) yielded the free amine, which is further converted into the corresponding hydrochloride salt to obtain the title compound in solid form (88%, 173.5 mg). ^{1}H NMR (300 MHz, rt, DMSO-d_6) δ_H = 8.69 (br s, 3H, NH_2·HCl), 6.98 (s, 2H, 2x CH), 3.95 (s, 2H, CH_2), 3.78 (s, 6H, 2x OCH_3), 3.65 (s, 3H, OCH_3). ^{13}C NMR (75 MHz, rt, DMSO-d_6) δ_C = 153.25 (2x C), 137.72 (C), 130.12 (C), 107.07 (2x CH), 60.48(OCH_3), 56.50 (2x OCH_3), 42.86 (CH_2) p.p.m. HRMS (EI): calcd. for $C_{10}H_{15}O_3N_1$ [M]+ 197.1046; found 197.1042. White solid.

4-(3-Aminobutyl)phenol hydrochloride

Column chromatography on silica gel (method: 10% ethyl acetate/hexane−60% ethyl acetate/hexane; Fig. 18) yielded the free amine, which is further converted into the corresponding hydrochloride salt to get the title compound in solid form (89%, 146.8 mg). ^{1}H NMR (300 MHz, rt, DMSO-d_6) δ_H = 9.14 (br s, 1H, OH), 8.40 – 8.03 (br s, 3H, NH_2.HCl), 6.98 (d, J = 8.4 Hz, 2H, 2x CH),

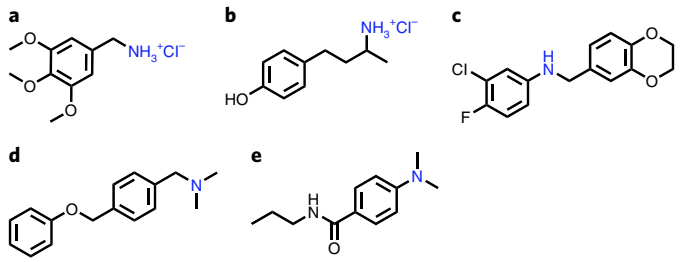

Fig. 18 | Structures of selected amines prepared in Step 11A–E. a–e, (3,4,5-trimethoxyphenyl)methanamine hydrochloride (Step 11A; **a**); 4-(3-aminobutyl)phenol hydrochloride (Step 11B; **b**); 3-chloro-*N*-((2,3-dihydrobenzo[b][1,4]dioxin-6-yl)methyl)-4-fluoroaniline (Step 11C; **c**); *N*,*N*-dimethyl-1-(4-(phenoxymethyl)phenyl)methanamine (Step 11D; **d**); A4-(dimethylamino)-*N*-propylbenzamide (Step 11E; **e**).

6.71 (d, $J = 8.4$ Hz, 2H, 2x CH), 3.20 – 2.93 (m, 1H, CH), 2.68 – 2.35 (m, 2H, CH_2), 2.00 – 1.80 (m, 1H, CH), 1.77 – 1.56 (m, 1H, CH), 1.22 (d, $J = 6.5$ Hz, 3H, CH_3). ^{13}C NMR (75 MHz, rt, DMSO-d_6) $\delta_C = 155.52$ (C), 130.79 (C), 128.94 (2x CH), 115.14 (2x CH), 46.37 (CH), 36.10 (CH_2), 29.96 (CH_2), 17.94 (CH_3) p.p.m. Traces of dioxane solvent peaks were observed in NMR. HRMS (ESI-TOF, *m*/*z*): calcd. for $C_{10}H_{15}NO$ [M+H]+ 166.1226; found 166.1226. Off white solid.

3-Chloro-N-((2,3-dihydrobenzo[b][1,4]dioxin-6-yl)methyl)-4-fluoroaniline

Column chromatography on silica gel (method: 0% ethyl acetate/hexane–40% ethyl acetate/hexane; Fig. 18) provided the title compound as colorless liquid (81%, 237.5 mg). ^{1}H NMR (300 MHz, rt, chloroform-d) $\delta_H = 6.79 – 6.74$ (m, 1H, CH), 6.71 – 6.68 (m, 1H, CH), 6.67 (d, $J = 0.4$ Hz, 1H, CH), 6.66 – 6.59 (m, 1H, CH), 6.42 (dd, $J = 6.1, 2.9$ Hz, 1H, CH), 6.24 (ddd, $J = 8.9, 3.8, 2.9$ Hz, 1H, CH), 4.05 (s, 4H, 2x CH_2), 3.95 (s, 2H, CH_2), 3.81 (br s, 1H, NH). ^{13}C NMR (75 MHz, rt, chloroform-d) $\delta_C = 150.90$ (d, $J = 237.3$ Hz, *ipso* C), 145.14 (d, $J = 2.1$ Hz, C), 143.73 (C), 142.94 (C), 131.99 (C), 120.99 (d, $J = 18.4$ Hz, C), 120.44 (CH), 117.49 (CH), 116.83 (d, $J = 21.9$ Hz, CH), 116.34 (CH), 113.76 (d, $J = 0.7$ Hz, CH), 112.08 (d, $J = 6.3$ Hz, CH), 64.40 (OCH_2), 64.35 (OCH_2), 47.99 (CH_2) p.p.m. HRMS (ESI-TOF, *m*/*z*): calcd. for $C_{15}H_{11}ClFNO_2$ [M+H]+ 292.0535; found 292.0529. Colorless liquid.

N,N-Dimethyl-1-(4-(phenoxymethyl)phenyl)methanamine

Column chromatography on silica gel (method: 10% ethyl acetate/hexane−50% ethyl acetate/hexane; Fig. 18) yielded the title compound in liquid form (86%, 207.7 mg). ^{1}H NMR (300 MHz, rt, chloroform-d) $\delta_H = 7.39 – 7.19$ (m, 5H, 5x CH), 7.13 (d, $J = 8.6$ Hz, 2H, 2x CH), 6.84 (d, $J = 8.6$ Hz, 2H, 2x CH), 4.94 (s, 2H, CH_2), 3.29 (s, 2H, CH_2), 2.14 (s, 6H, 2x CH_3). ^{13}C NMR (75 MHz, rt, chloroform-d) $\delta_C = 158.10$ (C), 137.11 (C), 130.75 (C), 130.45 (2x CH), 128.62 (2x CH), 127.98 (2x CH), 127.54 (CH), 114.65 (2x CH), 70.04 (CH_2), 63.62 (CH_2), 45.12 (2x CH_2) p.p.m. HRMS (EI): calcd. for $C_{16}H_{19}O1N1$ [M]+ 241.1461; found 241.1463. Yellow gum.

4-(Dimethylamino)-*N*-propylbenzamide

Column chromatography on silica gel (method: 10% ethyl acetate/hexane−70% ethyl acetate/hexane; Fig. 18) yielded the title compound in solid form (81%, 167.3 mg). ^{1}H NMR (300 MHz, rt, chloroform-d) $\delta_H = 7.61$ (d, $J = 8.9$ Hz, 2H, 2x CH), 6.57 (d, $J = 8.9$ Hz, 2H, 2x CH), 6.15 (br s, 1H, NH), 3.45 – 3.20 (m, 2H, CH_2), 2.92 (s, 6H, 2x CH_3), 1.73 – 1.40 (m, 2H, CH_2), 0.88 (t, $J = 7.4$ Hz, 3H, CH_3). ^{13}C NMR (75 MHz, rt, chloroform-d) $\delta_C = 167.49$ (CO), 152.32 (C), 128.33 (2x CH), 121.66 (C), 111.07 (2x CH), 41.59 (CH_2), 40.17 (2x CH_3), 23.13 (CH_2), 11.53 (CH_3) p.p.m. HRMS (EI): calcd. for $C_{12}H_{18}O1N_2$ [M]+ 206.1413; found 206.1415. Brown solid.

Reporting Summary

Further information on research design is available in the Nature Research Reporting Summary linked to this article.

References

1. Lawrence, S. A. *Amines: Synthesis, Properties and Applications* (Cambridge University Press, 2004).
2. Ricci, A. *Amino Group Chemistry: From Synthesis to the Life Sciences* (Wiley-VCH, 2008).

3. Smith, D. T., Delost, M. D., Qureshi, H. & Njarðarson, J. T. Top 200 pharmaceutical products by retail sales in 2016. https://njardarson.lab.arizona.edu/sites/njardarson.lab.arizona.edu/files/2016Top200PharmaceuticalRetailSalesPosterLowResV3_0.pdf (2017).
4. Roughley, S. D. & Jordan, A. M. The medicinal chemist's toolbox: an analysis of reactions used in the pursuit of drug candidates. *J. Med. Chem.* **54**, 3451–3479 (2011).
5. Dewick, P. M. *Medicinal Natural Products: A Biosynthetic Approach* 3rd edn (John Wiley & Sons, 2008).
6. Yan, T., Feringa, B. L. & Barta, K. Direct N-alkylation of unprotected amino acids with alcohols. *Sci. Adv.* **3**, eaao6494 (2017).
7. Froidevaux, V., Negrell, C., Caillol, S., Pascault, J.-P. & Boutevin, B. Biobased amines: from synthesis to polymers; present and future. *Chem. Rev.* **116**, 14181–14224 (2016).
8. Gomez, S. A., Peters, J. A. & Maschmeyer, T. The reductive amination of aldehydes and ketones and the hydrogenation of nitriles: mechanistic aspects and selectivity control. *Adv. Synth. Catal.* **344**, 1037–1057 (2002).
9. Alinezhad, H., Yavari, H. & Salehian, F. Recent advances in reductive amination catalysis and its applications. *Curr. Org. Chem.* **19**, 1021–1049 (2015).
10. Wakchaure, V. N., Zhou, J., Hoffmann, S. & List, B. Catalytic asymmetric reductive amination of α-branched ketones. *Angew. Chem. Int. Ed.* **49**, 4612–4614 (2010).
11. Gallardo-Donaire, J. et al. Direct asymmetric ruthenium-catalyzed reductive amination of alkyl-aryl ketones with ammonia and hydrogen. *J. Am. Chem. Soc.* **140**, 355–361 (2018).
12. Kadyrov, R. & Riermeier, T. H. Highly enantioselective hydrogen-transfer reductive amination: catalytic asymmetric synthesis of primary amines. *Angew. Chem. Int. Ed.* **42**, 5472–5474 (2003).
13. Tax, X. et al. Asymmetric synthesis of chiral primary amines by ruthenium catalyzed direct reductive amination of alkyl aryl ketones with ammonium salts and molecular H_2. *J. Am. Chem. Soc.* **140**, 2024–2027 (2018).
14. Chusov, D. & List, B. Reductive amination without an external hydrogen source. *Angew. Chem. Int. Ed.* **53**, 5199–5201 (2014).
15. Ogo, S., Uehara, K., Abura, T. & Fukuzumi, S. pH-Dependent chemoselective synthesis of α-amino acids. Reductive amination of α-keto acids with ammonia catalyzed by acid-stable iridium hydride complexes in water. *J. Am. Chm. Soc.* **126**, 3020–3021 (2004).
16. Nakamura, Y., Kon, K., Touchy, A. S., Shimizu, K.-i & Ueda, W. Selective synthesis of primary amines by reductive amination of ketones with ammonia over supported Pt catalysts. *ChemCatChem* **7**, 921–924 (2015).
17. Gross, T., Seayad, A. M., Ahmad, M. & Beller, M. Synthesis of primary amines: first homogeneously catalyzed reductive amination with ammonia. *Org. Lett.* **4**, 2055–2058 (2002).
18. Gallardo-Donaire, J., Ernst, M., Trapp, O. & Schaub, T. Direct synthesis of primary amines via ruthenium-catalysed amination of ketones with ammonia and hydrogen. *Adv. Synth. Catal.* **358**, 358–363 (2016).
19. Liang, G. et al. Production of primary amines by reductive amination of biomass derived aldehydes/ketones. *Angew. Chem. Int. Ed.* **56**, 3050–3054 (2017).
20. Wang, Z. Mignonac reaction. in *Comprehensive Organic Name Reactions and Reagents* (John Wiley & Sons, 2010).
21. Mao, F. et al. Heterogeneous cobalt catalysts for reductive amination with H_2: general synthesis of secondary and tertiary amines. *RSC Adv.* **6**, 94068–94073 (2016).
22. Santoro, F., Psaro, R., Ravasio, N. & Zaccheria, F. Reductive amination of ketones or amination of alcohols over heterogeneous Cu catalysts: Matching the catalyst support with the N-alkylating agent. *ChemCatChem* **4**, 1249–1254 (2012).
23. Jagadeesh, R. V. et al. Hydrogenation using iron oxide–based nanocatalysts for the synthesis of amines. *Nat. Protoc.* **10**, 548–557 (2015).
24. Jagadeesh, R. V. et al. Cobalt-based nanocatalysts for green oxidation and hydrogenation processes. *Nat. Protoc.* **10**, 916–926 (2015).
25. Jagadeesh, R. V. et al. MOF-derived cobalt nanoparticles catalyze a general synthesis of amines. *Science* **358**, 326–332 (2017).
26. Hahn, G., Kunnas, P., de Jonge, N. & Kempe, R. General synthesis of primary amines via reductive amination employing a reusable nickel catalyst. *Nat. Catal.* **2**, 71–77 (2019).
27. Filipponi, L. & Sutherland, D.S. *Nanotechnologies: Principles, Applications, Implications and Hands-on Activities* (European Commission, European Union, 2012).
28. Polshettiwar, V. & Asefa, T. *Nanocatalysis: Synthesis and Applications* (John Wiley & Sons, 2013).
29. Sankar, M. et al. Designing bimetallic catalysts for a green and sustainable future. *Chem. Soc. Rev.* **41**, 8099–8139 (2012).
30. Manoj., B. G. et al. Core-shell nanoparticles: synthesis and applications in catalysis and electrocatalysis. *Chem. Soc. Rev.* **44**, 7540–7590 (2015).
31. Munnik, P., de Jong, P. E. & de Jong, K. P. Recent developments in the synthesis of supported catalysts. *Chem. Rev.* **115**, 6687–6718 (2015).
32. Tao, F. *Metal Nanoparticles for Catalysis: Advances and Applications* (Royal Society of Chemistry, 2014).
33. van Schrojenstein Lantman, E. M., Deckert-Gaudig, T., Mank, A. J. G., Deckert, V. & Weckhuysen, B. M. Catalytic processes monitored at the nanoscale with tip-enhanced Raman spectroscopy. *Nat. Nanotechnol.* **7**, 583–586 (2012).

34. Jagadeesh, R. V. et al. Nanoscale Fe_2O_3-based catalysts for selective hydrogenation of nitroarenes to anilines. *Science* **342**, 1073–1076 (2013).
35. Liu, L. & Corma, A. Metal catalysts for heterogeneous catalysis: From single atoms to nanoclusters and nanoparticles. *Chem. Rev.* **118**, 4981–5079 (2018).
36. Wang, A., Li, J. & Zhang, T. Heterogeneous single-atom catalysis. *Nat. Rev. Chem.* **2**, 65–81 (2018).
37. Chen, Y. et al. Single-atom catalysts: Synthetic strategies and electrochemical applications. *Joule* **2**, 242–1264 (2018).
38. Yan, N. & Dyson, P. J. Nanocatalysis: synthesis, characterization, application and mechanisms. *Catal. Today* **183**, 1–178 (2012).
39. Dang, S., Zhu, Q.-L. & Xu, Q. Nanomaterials derived from metal-organic frameworks. *Nat. Rev. Mat.* **3**, 17075 (2017).
40. Shen, K., Chen, X., Chen, J. & Li, Y. Development of MOF-derived carbon-based nanomaterials for efficient catalysis. *ACS Catal.* **6**, 5887–5903 (2016).
41. Buchner, F. et al. Coordination of iron atoms by tetraphenylporphyrin monolayers and multilayers on Ag(111) and formation of iron-tetraphenylporphyrin. *J. Phys. Chem. C.* **112**, 15458–15465 (2008).
42. Jaouen, F. et al. Cross-laboratory experimental study of non-noble-metal electrocatalysts for the oxygen reduction reaction. *ACS Appl. Mater. Interfaces* **1**, 1623–1639 (2009).

Acknowledgements

We gratefully acknowledge the European Research Council (EU project 670986-NoNaCat) and the State of Mecklenburg-Vorpommern for financial and general support. We thank the analytical team of the Leibniz-Institute for Catalysis, Rostock, for their excellent service in the characterization of materials and reaction products.

Author contributions

R.V.J., K.M. and M.B. planned and developed the project. K.M. prepared catalytic materials and performed the experiments. V.G.C. and T.S. co-performed the experiments. R.V.J., K.M. and M.B. wrote the manuscript. R.V.J. and M.B. supervised the project.

Competing interests

The authors declare no competing interests.

Additional information

Supplementary information is available for this paper at https://doi.org/10.1038/s41596-019-0258-z.

Correspondence and requests for materials should be addressed to RV.J. or M.B.

Peer review information *Nature Protocols* thanks Bert Weckhuysen and the other, anonymous, reviewer(s) for their contribution to the peer review of this work.

Reprints and permissions information is available at www.nature.com/reprints.

Publisher's note Springer Nature remains neutral with regard to jurisdictional claims in published maps and institutional affiliations.

Received: 14 February 2019; Accepted: 21 October 2019;
Published online: 18 March 2020

Related link
Key references using this protocol
Jagadeesh, R. V., et al. *Science*, **358**, 326–332 (2017): https://science.sciencemag.org/content/358/6361/326

Chem Soc Rev

REVIEW ARTICLE

View Article Online
View Journal | View Issue

Cite this: *Chem. Soc. Rev.*, 2020, **49**, 6273

Catalytic reductive aminations using molecular hydrogen for synthesis of different kinds of amines

Kathiravan Murugesan, †[a] Thirusangumurugan Senthamarai,†[a] Vishwas G. Chandrashekhar, †[a] Kishore Natte, [b] Paul C. J. Kamer, [a] Matthias Beller *[a] and Rajenahally V. Jagadeesh *[a]

Reductive aminations constitute an important class of reactions widely applied in research laboratories and industries for the synthesis of amines as well as pharmaceuticals, agrochemicals and biomolecules. In particular, catalytic reductive aminations using molecular hydrogen are highly valued and essential for the cost-effective and sustainable production of different kinds of amines and their functionalization. These reactions couple easily accessible carbonyl compounds (aldehydes or ketones) with ammonia, amines or nitro compounds in the presence of suitable catalysts and hydrogen that enable the preparation of linear and branched primary, secondary and tertiary amines including *N*-methylamines and molecules used in life science applications. In general, amines represent valuable fine and bulk chemicals, which serve as key precursors and central intermediates for the synthesis of advanced chemicals, life science molecules, dyes and polymers. Noteworthily, amine functionalities are present in a large number of pharmaceuticals, agrochemicals and biomolecules, and play vital roles in the function of these active compounds. In general, reductive aminations are challenging processes, especially for the syntheses of primary amines, which often are non-selective and suffer from over-alkylation and reduction of carbonyl compounds to the corresponding alcohols. Hence, the development of suitable catalysts to perform these reactions in a highly efficient and selective manner is crucial and continues to be important and attracts scientific interest. In this regard, both homogeneous and heterogeneous catalysts have successfully been developed for these reactions to access various amines. There is a need for a comprehensive review on catalytic reductive aminations to discuss the potential catalysts used and applicability of this methodology in the preparation of different kinds of amines, which are of commercial, industrial and medicinal importance. Consequently, in this review we discuss catalytic reductive aminations using molecular hydrogen and their applications in the synthesis of functionalized and structurally diverse benzylic, heterocyclic and aliphatic primary, secondary and tertiary amines as well as *N*-methylamines and more complex drug targets. In addition, mechanisms of reductive aminations including selective formation of desired amine products as well as possible side reactions are emphasized. This review aims at the scientific communities working in the fields of organic synthesis, catalysis, and medicinal and biological chemistry.

Received 15th December 2019

DOI: 10.1039/c9cs00286c

rsc.li/chem-soc-rev

1. Introduction

Amines represent highly privileged chemicals extensively applied in different science areas such as chemistry, biology, medicine, energy, materials and environment (Fig. 1).[1–33] These important compounds serve both as fine and bulk chemicals as well as key precursors and central intermediates for the synthesis of advanced chemicals, pharmaceuticals, biomolecules, agrochemicals and polymers.[1–6] Notably, amine functionalities are present in the majority of drugs and biomolecules, and hence they form integral parts of these life science molecules (Fig. 2).[1–6] As an example, >80% of the 200 top selling drugs of 2018 contained amine and/or nitrogen moieties, which play significant roles in their activities.[3] Moreover, amines are involved in the creation of proteins, enzymes, nucleic acids and hormones in living beings (Fig. 2).[1–6] For the synthesis and functionalization of amines,

[a] *Leibniz-Institut für Katalyse e.V., Albert-Einstein-Straße 29a, 18059 Rostock, Germany. E-mail: matthias.beller@catalysis.de, jagadeesh.rajenahally@catalysis.de*

[b] *Chemical and Material and Sciences Division, CSIR-Indian Institute of Petroleum, Dehradun-248005, India*

† These authors contributed equally to this work.

Chem

CellPress

Article

A "universal" catalyst for aerobic oxidations to synthesize (hetero)aromatic aldehydes, ketones, esters, acids, nitriles, and amides

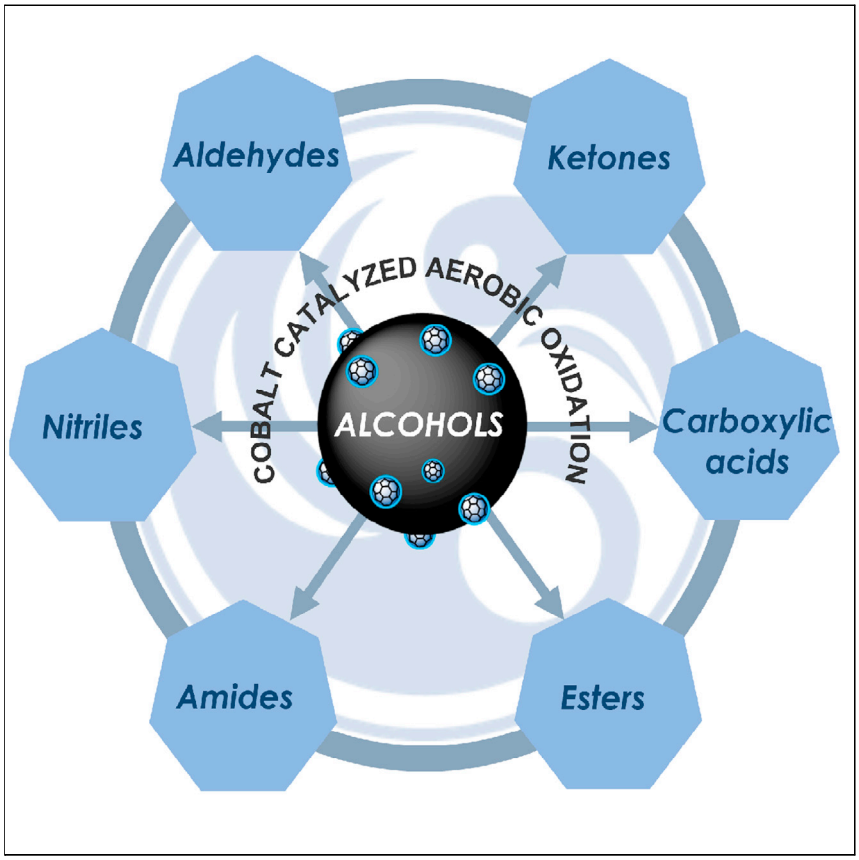

In catalysis, it is a common practice to develop catalysts for only one specific synthetic methodology. However, to save the time, energy, and resources, the development of more general catalysts applicable for many organic transformations to access different kinds of compounds offers interesting opportunities. In this respect, cobalt nanoparticles are presented as "universal" catalysts for aerobic oxidations of alcohols to synthesize aldehydes, ketones, carboxylic acids, esters, nitriles, and amides.

Thirusangumurugan Senthamarai, Vishwas G. Chandrashekhar, Nils Rockstroh, Jabor Rabeah, Stephan Bartling, Rajenahally V. Jagadeesh, Matthias Beller

jagadeesh.rajenahally@catalysis.de (R.V.J.)
matthias.beller@catalysis.de (M.B.)

Highlights

Development of a general and selective catalyst for manifold oxidations

Synthesis of a new class of Co-nanoparticles

Benign synthesis of aldehydes, ketones, acids, esters, nitriles, and amides

Kinetic and mechanistic investigations of catalytic aerobic oxidations

Senthamarai et al., Chem *8*, 1–24
February 10, 2022
https://doi.org/10.1016/j.chempr.2021.12.001

Please cite this article in press as: Senthamarai et al., A "universal" catalyst for aerobic oxidations to synthesize (hetero)aromatic aldehydes, ketones, esters, acids, nitriles, and amides, Chem (2021), https://doi.org/10.1016/j.chempr.2021.12.001

Chem

CellPress

Article

A "universal" catalyst for aerobic oxidations to synthesize (hetero)aromatic aldehydes, ketones, esters, acids, nitriles, and amides

Thirusangumurugan Senthamarai,[1] Vishwas G. Chandrashekhar,[1] Nils Rockstroh,[1] Jabor Rabeah,[1] Stephan Bartling,[1] Rajenahally V. Jagadeesh,[1,*] and Matthias Beller[1,2,*]

SUMMARY

Functionalized (hetero)aromatic compounds are indispensable chemicals widely used in basic and applied sciences. Among these, especially aromatic aldehydes, ketones, carboxylic acids, esters, nitriles, and amides represent valuable fine and bulk chemicals, which are used in chemical, pharmaceutical, agrochemical, and material industries. For their synthesis, catalytic aerobic oxidation of alcohols constitutes a green, sustainable, and cost-effective process, which should ideally make use of active and selective 3D metals. Here, we report the preparation of graphitic layers encapsulated in Co-nanoparticles by pyrolysis of cobalt-piperazine-tartaric acid complex on carbon as a most general oxidation catalyst. This unique material allows for the synthesis of simple, functionalized, and structurally diverse (hetero)aromatic aldehydes, ketones, carboxylic acids, esters, nitriles, and amides from alcohols in excellent yields in the presence of air.

INTRODUCTION

Catalysis is a key process in science that allows to control all kinds of chemical transformations. In the presence of a suitable catalytic material the reaction rate can be dramatically increased, which enables the optimal use of resources, increasing the yield of desired products and at the same time avoiding waste formation as well as reduce specific energy requirements.[1–10] Nowadays, 90% of all modern processes in the chemical industry apply catalytic technologies.[7–10] In addition to this crucial role in chemical sciences, catalysts also provide the basis of innovation for many other industries based on life and material sciences as well as energy technologies. Thus, new catalytic materials including molecularly defined and nanostructured systems are continuously prepared by scientists all over the world and tested for all kinds of transformations.[1–10] Regarding the potential new catalysts, in particular, 3D-metal-based systems are gaining increasing importance and provide the basis for an advanced and sustainable chemical synthesis.[11–17] Due to the inherent beneficial aspects such as stability, recycling, and reusability, heterogeneous nanostructured materials, especially, are of prime importance.[17–20]

Typically, for a specific benchmark reaction or more importantly for a given industrial process the "best" catalyst is desired. Especially, for the bulk chemical industry it is important to apply state-of-the-art catalysts with optimal activity (TOF, turnover frequency), productivity (TON, turnover number), and selectivity to be cost competitive on a global scale.[21] However, apart from such highly optimized systems, there is also significant interest in catalysts, which can be applied in a general way for various

The bigger picture

The development of a general and selective catalysts, which should be applicable not only for one specific class of products but also to the synthesis of different compound classes, has been scarcely investigated in catalysis research. Here, we present a "universal" catalyst that allows the synthesis of different kinds of functionalized and structurally diverse (hetero)aromatic compounds such as aldehydes, ketones, carboxylic acids, esters, nitriles, and primary amides. Key to success for this achievement is the application of carbon-supported graphitic-shell-encapsulated cobalt nanoparticles, which are prepared by immobilization and pyrolysis of cobalt-piperazine-tartaric acid template on carbon. We believe that the presented concept is not only valid for the here-described case of alcohol oxidations but also offers manifold opportunities for other chemical transformations.

processes. This is especially true for applications in organic synthesis, for drug discovery, and for basic sciences. Here, it is a common practice to develop new catalysts only for one specific synthetic methodology and the generality of a given catalyst is measured by its robustness toward different reaction conditions, but especially by its functional group tolerance and a wide substrate scope. Considering that elementary steps of many chemical processes are similar, we believe that "general" catalysts can be developed more efficiently by not only focusing on one specific transformation. As an example, in the oxidation of alcohols diverse compounds **B–F** can be formed. In general, alcohol (**A**) is oxidized to the corresponding aldehyde (**B**) first, which then can react with different nucleophiles such as H_2O, alcohol, and ammonia to generate either geminal diol (**X**), hemiacetal (**X**), hemiaminal (**X**), or primary imine (**Y**), respectively, as intermediates (**X** and **Y**). All these intermediates might be further oxidized to produce the corresponding acid (**C**), ester (**D**), primary amide (**F**), and/or nitrile (**E**), respectively (Figure 1).[22–28]

Looking at the individual steps of Figure 1, clearly the conversion of **A** to **B** and **X** to **C**, **D**, and **F** are mechanistically related and indeed can be performed with similar type of catalysts. However, traditionally each of these methodologies is studied separately using different catalyst systems, which is time and resource consuming.

Among the many kinds of chemicals, functionalized aromatic and heterocyclic compounds are most valuable, which provide the basis for countless products of our daily life. In fact, synthetic organic chemistry and drug discovery majorly rely on the valorization of such compounds.[29–31] Among these, (hetero)aromatic carbonyl compounds (**B**), carboxylic acids (**C**), esters (**D**), nitriles (**E**), and amides (**F**) represent valuable fine and bulk chemicals widely used in research laboratories and industries.[32–38] Notably, these compounds can be easily functionalized/upgraded. Hence, they serve as precursors and intermediates for the synthesis of advanced chemicals, pharmaceuticals, agrochemicals, biomolecules, and materials. Moreover, many life science molecules, natural products, fragrances, and cosmetics as well as other daily life products contain, –CHO, –C=O, –COOH, –COOR, –CN, and $–CONH_2$ functionalities, which play vital roles in their physical properties and functions.

In general, products **B–F** can be conveniently accessed by oxidation of benzylic alcohols and related heteroaromatic compounds,[39–102] which are broadly commercially available. As an example, more than >200 benzylic alcohols are available from Sigma-Aldrich.[103] Regarding potential oxidants, air is ideal because it is abundant, inexpensive, and green, and it produces only water as by-product.[104] Favorably, air is much safer and more convenient to use than dioxygen. To perform the oxidation of alcohols using molecular oxygen or air to produce **B–F**, both homogeneous and heterogeneous catalysts based on precious and non-precious metals were developed in the past (Figure 2).[39–102]

Despite these achievements, until now, there is no single general catalyst developed or applied for the oxidative conversion of alcohols to synthesize carbonyl compounds (aldehydes and ketones; **B**), carboxylic acids (**C**), esters (**D**), nitriles (**E**), and amides (**F**).

In this regard, here, we show that a general catalyst development can be achieved efficiently by directly including different related benchmark reactions and parallel testing of the catalyst materials under investigation. Following the presented strategy, we demonstrate that it is possible to develop graphitic-shell-encapsulated

[1]Leibniz-Institut für Katalyse e.V., Albert-Einstein-Straße 29a, 18059 Rostock, Germany

[2]Lead contact

*Correspondence: jagadeesh.rajenahally@catalysis.de (R.V.J.), matthias.beller@catalysis.de (M.B.)

https://doi.org/10.1016/j.chempr.2021.12.001

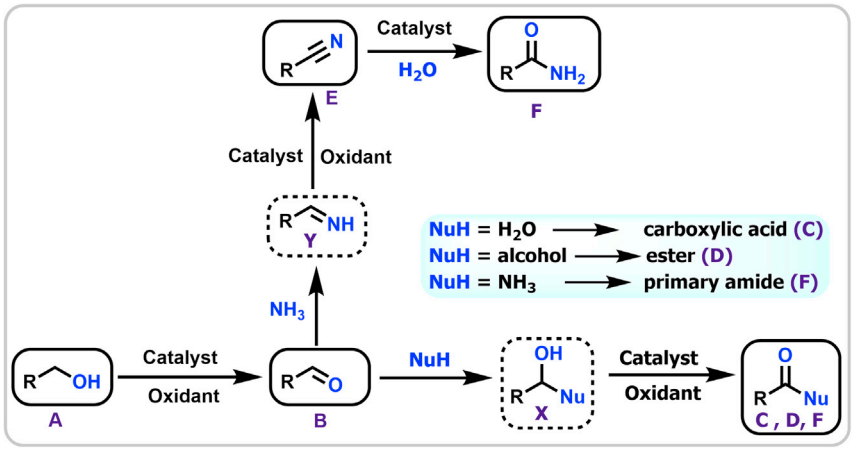

Figure 1. Possible products from alcohols by catalytic oxidation
Synthesis of aldehydes (B), carboxylic acids (C), esters (D), nitriles (E), and primary amides (F).

cobalt nanoparticles as a "most general" oxidation catalyst, which can not only be applied in one of the above-mentioned aerobic oxidation reactions but many related transformations. The highly stable and reusable catalyst allows for the synthesis of functionalized and structurally diverse aromatic and heterocyclic aldehydes, ketones, carboxylic acids, esters, nitriles, and primary amides in good to excellent yields.

RESULTS AND DISCUSSION

Preparation of materials and catalytic evaluations

In the past decade, we prepared a variety of nanostructured 3D-metal (Fe, Co, Ni, and Cu)-based materials by immobilization of either organometallic complexes or metal organic frameworks on inorganic supports and subsequent pyrolysis under inert atmosphere.[105–108] Some of these materials proved to be highly active and selective for catalytic hydrogenations, oxidations, and reductive amination reactions.[105–108] A typical feature of these active catalysts is the core-shell structure of the metal nanoparticles, which are embedded in graphene or graphitic layers.[105–108] To obtain this specific structure, ligated metal complexes have been used as precursors.[105–108] To be cost-efficient, the respective ligands should be as simple, abundant, and inexpensive as possible. In this respect, amines and carboxylic acids are interesting as a plethora of them is easily accessible.

In continuation of our previous work,[105–108] we started to prepare a library of supported 3D-metal nanoparticles using Co, Mn, Fe, and Cu salts with piperazine (PZ) and DL-tartaric acid (TA) as ligands, which will form metal coordination polymers or metal organic frameworks. As an example, $Co(NO_3)_2 \cdot 6H_2O$ was dissolved in DMF, and then this mixture was heated to 150°C. At this temperature, PZ and TA were added and stirring was continued for 30 min. After addition of the support (carbon; Vulcan XC72R) and 4 h of additional stirring, the solvent was removed, and the resulting dark solid material was grinded and pyrolyzed at different temperatures (400°C–1,000°C) under argon atmosphere for 2 h to provide the desired cobalt-based nanoparticles supported on carbon (Figure 3). Similarly, other 3D-metal nitrates ($Fe(NO_3)_3 \cdot 9H_2O$, $Mn(NO_3)_2 \cdot 6H_2O$, and $Cu(NO_3)_2 \cdot 3H_2O$) were applied following the same procedure. For comparison, metal salts without ligands were pyrolyzed on carbon, and Ru- as well as Pd-containing materials were made using PZ and TA ligands, too.

Please cite this article in press as: Senthamarai et al., A "universal" catalyst for aerobic oxidations to synthesize (hetero)aromatic aldehydes, ketones, esters, acids, nitriles, and amides, Chem (2021), https://doi.org/10.1016/j.chempr.2021.12.001

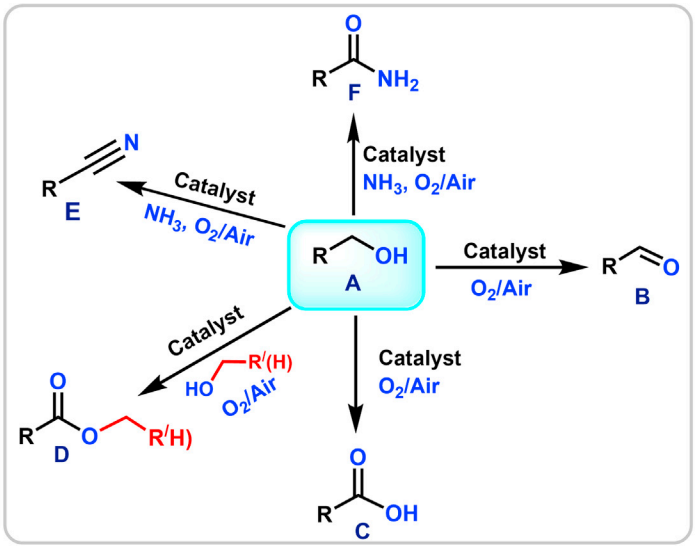

Previous works: Different catalysts were used for producing different products. Mainly molecular oxygen is used as oxidant in these cases.

Catalyst	Products				
	Aldehydes & ketones	Carboxylic acids	Esters	Nitriles	Primary amides
Homogeneous catalysts	Pd[39-40] Ru[41-43] Cu[44-48] Co[49] Mn[50-51] Fe[52-55]	Co[72] Fe[73]	Rh[78] Pd[79-80]	Cu[90-91] Fe[92]	
Heterogeneous catalysts	Pt[56-57] Pd[56,58-60] Au[56,59-62] Ru[63-64] Co[65-69] Mn[70] Fe[71]	Pt[56,74] Pd[56,75-76] Au[56,77]	Pt[56] Pd[56,81] Au[18,82-85] Co[65,86-89]	Pt[93] Au[94] Ru[95-96] Co[65, 97-99] Fe[97]	Au[100] Mn[101-102]

Present work: Single heterogeneous cobalt-based catalyst is used to produce all of these products. Air is used as oxidant.

Heterogeneous catalyst	Co-nanocatalyst	Co-nanocatalyst	Co-nanocatalyst	Co-nanocatalyst	Co-nanocatalyst

Figure 2. Synthesis of carbonyl compounds, carboxylic acids, esters, nitriles, and primary amides from alcohols by catalytic oxidations using molecular oxygen or air

Following our concept to develop a universal oxidation catalyst, we evaluated the generality and applicability of the prepared materials not only for one type of reaction, but five different aerobic oxidation reactions were chosen. More specifically, all potential catalysts as well as selected commercial ones were tested for their activities in the conversion of benzyl alcohol (A1) to benzaldehyde (B1), benzoic acid (C1), methyl benzoate (D1), benzonitrile (E1), and benzamide (F1) (Figure 4). In general, all these benchmark reactions were performed in the presence of air (1 bar or 10 bar) at 55°C–120°C using either alcohols, water, or heptane as solvent. Interestingly, aldehyde and ester formation are observed at ambient pressure and low temperature, while the formation of acid, amide, and nitrile proceeded at temperatures >100°C and 10 bar of air vide infra.

First, we tested in a parallel manner, the materials prepared by the pyrolysis of Fe-, Mn-, Co-, and Cu-nitrates on carbon ($Fe(NO_3)_3$@C-800, $Mn(NO_3)_2$@C-800,

Please cite this article in press as: Senthamarai et al., A "universal" catalyst for aerobic oxidations to synthesize (hetero)aromatic aldehydes, ketones, esters, acids, nitriles, and amides, Chem (2021), https://doi.org/10.1016/j.chempr.2021.12.001

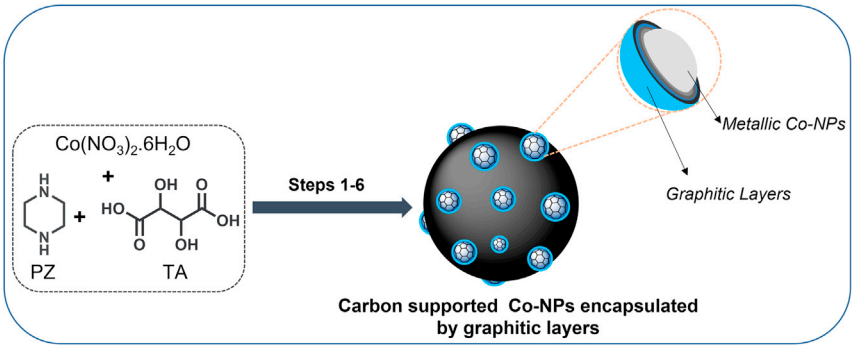

Figure 3. Preparation of Co-nanoparticles supported on carbon by the pyrolysis of cobalt-piperazine-tartaric acid complexes

Step 1: stirring in DMF at 150°C for 30 min. Step 2: addition of Vulcan XC72R. Step 3: stirring in DMF at 150°C for 4 h. Step 4: slow evaporation of DMF and drying. Step 5: grinding of Co-PZ-TA@C material into fine powder. Step 6: pyrolysis of Co-PZ-TA@C at 800°C for 2 h under Ar.

$Co(NO_3)_2$@C-800, and $Cu(NO_3)_2$@C-800) (Figure 4). All these materials exhibited no or poor activities for all the benchmark reactions (<16% yields of the corresponding products **B1–F1**). Next, we tested catalysts prepared by the impregnation and pyrolysis of PZ- and TA-ligated metal complexes (Fe-PZ-TA@C-800, Mn-PZ-TA@C-800, Co-PZ-TA@C-800, and Cu-PZ-TA@C-800) (Figure 4). Among these materials Fe-PZ-TA@C-800 was completely inactive for the formation of benzoic acid and methyl benzoate, whereas it showed low to moderate activity for the synthesis of benzaldehyde, benzonitrile, and benzamide in 16%, 20%, and 60%, respectively. Mn-PZ-TA@C-800 was even more specific producing only 20% of **B1**, while no or very little activity is observed in the other model reactions. Interestingly, Co-PZ-TA@C-800 exhibited remarkable activity and selectivity in all the benchmark reactions and produced almost quantitative of yields (>98%) of benzaldehyde, benzoic acid, methyl benzoate, benzonitrile, and benzamide. Finally, Cu-PZ-TA@C-800 was tested and showed no activity for the formation of **C1** and **D1** as well as very low activity for **B1** formation (30%). However, this material was found to be efficient for the preparation of benzonitrile (98%) and benzamide (97%). Because of the unique behavior of the cobalt-based material, variation of the pyrolysis temperature of the templated Co-PZ-TA@C was performed. However, materials prepared by pyrolysis at 400°C, 600°C, and 1,000°C showed lower activity. Similarly, pyrolysis of cobalt-complexes with single ligands either PZ or TA (Co-PZ@C-800 or Co-TA@C-800) gave less active materials and provided the desired products **B1–F1** in 50%–68% yields. Using the Fe, Mn, or Co salts in the absence and presence of PZ and TA under homogeneous conditions exhibited no or minor activity in all five benchmark tests (<5%) (Table S2). Likewise, the non-pyrolyzed supported pre-catalysts (metal-PZ-TA@C) behave. However, in the presence of the homogeneous Cu-PZ-TA system and its supported derivative some activity for the formation of benzaldehyde (10%–15%) is observed (Table S2).

To compare the activities and selectivities of the optimal system (Co-PZ-TA@C-800) with commercially available precious-metal-based catalysts, Ru/C and Pd/C were also applied in the benchmark reactions (Figure 4). Under similar conditions, Ru/C showed no activity for alcohol to ester oxidation, and in all other cases, product yields were lower compared with Co-PZ-TA@C-800, while Pd/C exhibited only high activity for the preparation of benzaldehyde. Likewise, Ru-PZ-TA@C-800 and Pd-PZ-TA@C-800, exhibited moderate to low activity for most reactions. Thus,

Please cite this article in press as: Senthamarai et al., A "universal" catalyst for aerobic oxidations to synthesize (hetero)aromatic aldehydes, ketones, esters, acids, nitriles, and amides, Chem (2021), https://doi.org/10.1016/j.chempr.2021.12.001

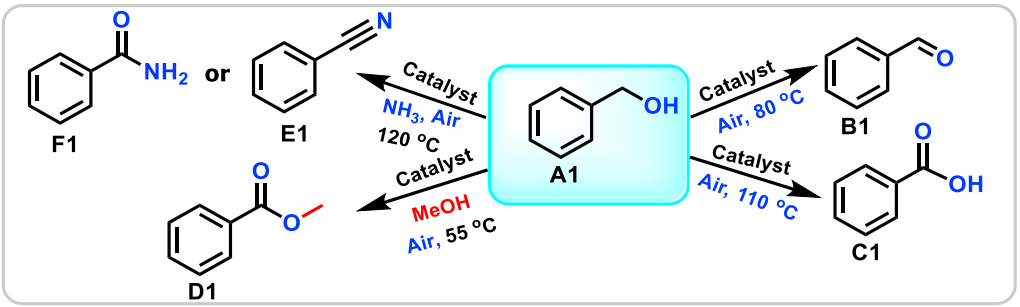

Catalyst	Product				
	Benzaldehyde (B1)	Benzoic acid (C1)	Methyl benzoate (D1)	Benzonitrile (E1)	Benzamide (F1)
$Fe(NO_3)_3$@C-800					
$Mn(NO_3)_2$@C-800					
$Co(NO_3)_2$@C-800					
$Cu(NO_3)_2$@C-800					
Fe-PZ-TA@C-800					
Mn-PZ-TA@C-800					
Co-PZ-TA@C-800					
Cu-PZ-TA@C-800					
Co-PZ-TA@C-400					
Co-PZ-TA@C-600					
Co-PZ-TA@C-1000					
Co-PZ@C-800					
Co-TA@C-800					
Ru/C (Commercial)					
Pd/C (Commercial)					
Ru-PZ-TA@C-800					
Pd-PZ-TA@C-800					

Yield of products: <2% | 5-10% | 15-40% | 50-70% | 75-90% | 95-99%

Figure 4. Synthesis of benzaldehyde, methyl benzoate, benzoic acid, benzonitrile, and benzamide by aerobic oxidation of benzyl alcohol: activity of different catalysts

Reaction conditions: for the synthesis of benzaldehyde (B) = 0.5 mmol benzyl alcohol, 35 mg catalyst (6.5 mol % of Co), 1 bar air, 10 mol % K_2CO_3, 2 mL n-heptane, 80°C, 24 h. For the synthesis of benzoic acid (C) = 0.5 mmol benzyl alcohol, 35 mg catalyst (6.5 mol % of Co), 10 bar air, 50 mol % KOH, 2 mL

Please cite this article in press as: Senthamarai et al., A "universal" catalyst for aerobic oxidations to synthesize (hetero)aromatic aldehydes, ketones, esters, acids, nitriles, and amides, Chem (2021), https://doi.org/10.1016/j.chempr.2021.12.001

Figure 4. *Continued*
water, 110°C, 24 h. For the synthesis of methyl benzoate (D) = 0.5 mmol benzyl alcohol, 35 mg catalyst (6.5 mol % of Co), 1 bar air, 10 mol % K_2CO_3, 2 mL methanol, 55°C, 24 h. For the synthesis of benzonitrile (E) = 0.5 mmol benzyl alcohol, 200 μL aqueous NH_3 (28%–30% NH_3 basis), 35 mg catalyst (6.5 mol % of Co), 10 bar air, 2 mL *t*-butanol, 120°C, 24 h. For the synthesis of benzamide (F) = 0.5 mmol benzyl alcohol, 200 μL aqueous NH_3 (28%–30% NH_3 basis), 35 mg catalyst (6.5 mol % of Co), 10 bar air, 2 mL water, 120°C, 24 h. GC yields using n-hexadecane as standard.

among all the tested materials Co-PZ-TA@C-800 was found to be the most general oxidation catalyst, which allows for diverse aerobic oxidations of benzyl alcohols to produce a variety of product classes in a selective manner.

To demonstrate the stability, recycling, and reusability of this Co-material (Co-PZ-TA@C-800), the synthesis of benzonitrile from benzyl alcohol in presence of aqueous ammonia and air was performed for seven times under standard conditions. Notably, in the presence of ammonia supported nanoparticles easily encounter stability and reusability problems. Nevertheless, as shown in Figure 5, Co-PZ-TA@C-800 was stable and is conveniently recycled and reused up to 7th run.

Characterization of Co-nanostructured catalysts

To know the structural features and to understand the catalytic activities, we carried out detailed characterizations of the most active (Co-PZ-TA@C-800), moderately active (Co-PZ@C-800), (Co-TA@C-800), and less active ($Co(NO_3)_2$@C-800) materials using X-ray powder diffraction (XRD), scanning transmission electron microscopy (STEM) with electron energy loss spectroscopy (EELS), and X-ray photoelectron spectroscopy (XPS). The XRD patterns of the most active catalyst, Co-PZ-TA@C-800, showed the presence of mainly metallic cobalt particles (Figure S1), while the moderately active catalysts Co-PZ@C-800 and Co-TA@C-800 contained a mixture of metallic cobalt and oxidic cobalt (Co_3O_4) particles (Figure S1). STEM analysis of

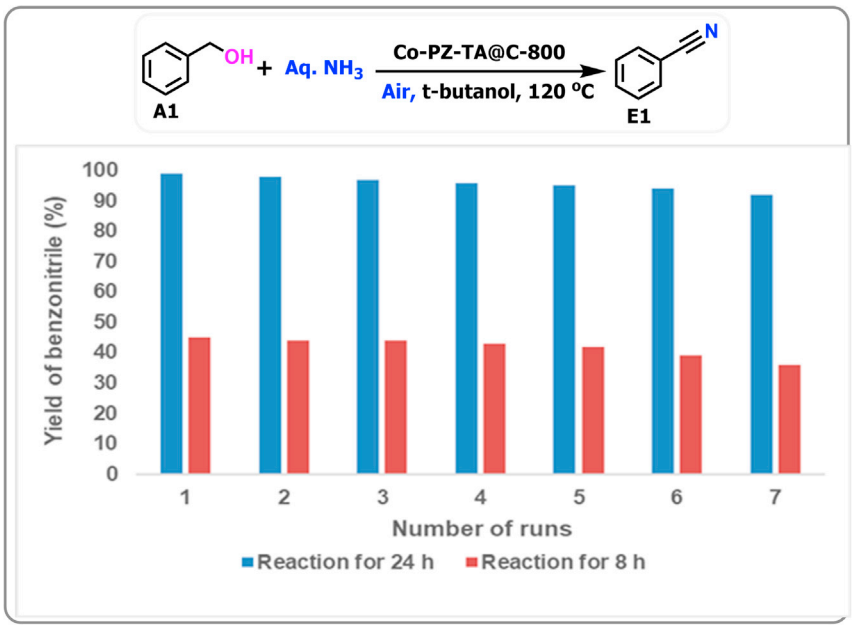

Figure 5. Recyclability and stability of Co-PZ-TA@C-800 catalyst for the synthesis of benzonitrile
Reaction conditions: 2 mmol benzyl alcohol, 140 mg catalyst (6.5 mol % Co), 800 μL aqueous NH_3 (28%–30% NH_3 basis), 10 bar air, 8 mL *t*-butanol, 120°C, 24 h and 8 h. Yields were determined by GC using n-hexadecane as standard.

Please cite this article in press as: Senthamarai et al., A "universal" catalyst for aerobic oxidations to synthesize (hetero)aromatic aldehydes, ketones, esters, acids, nitriles, and amides, Chem (2021), https://doi.org/10.1016/j.chempr.2021.12.001

Co-PZ-TA@C-800 proved the formation of metallic cobalt particles with different sizes ranging from 1 to 7 nm and from 25 to 40 nm (Figure 6A). However, some bigger particles with sizes up to 80 nm were also observed. The smaller particles are usually found in groups, while other areas of the material contained no cobalt. Interestingly, most of the particles in this material are surrounded by few layers of graphitic carbon (Figure 6A, right image). In addition to metallic cobalt, the presence of a very small amount of cobalt oxide is observed (Figures 7A, 7B, and S2). Co-PZ@C-800 contained also metallic and oxidic cobalt; however, the presence of the oxide seems to be more than in Co-PZ-TA@C-800, and it can be found either on the surface or as partially oxidized particles (see e.g., the biggest particle in the left image in Figures 6B and S3).The sizes of these particles are in the range between 25 and 60 nm with few particles being bigger up to 100 nm and fewer below 25 nm compared with Co-PZ-TA@C-800. In the case of metallic cobalt, these particles are covered by graphitic layers (Figure 6B, right image). Likewise, Co-TA@C-800 showed the presence of both metallic and oxidic cobalt particles with sizes of 15–50 nm and only very few below this size. Similar to Co-PZ-TA@C-800, the nanoparticles of metallic cobalt are surrounded by graphitic layers in both Co-PZ@C-800 and Co-TA@C-800 (Figure 6C). The least active material, cobalt nitrate@C-800, contained completely Co_3O_4 particles, which are not surrounded by graphitic layers (Figure S4). The material obtained after three reaction cycles using the active catalyst Co-PZ-TA@C-800 showed that there is not much difference in the structure compared with the fresh catalyst (Figure 6D). In this reused material, metallic nanoparticles with sizes of 3–10 and 25–40 nm are observed, which are in few cases partially oxidized at the surface. However, analysis of the material after 7 reaction cycles revealed that cobalt is oxidized in more proportion (Figure S5). This implies that the cobalt is successively oxidized during the reaction cycles. EELS was applied to analyze the elemental composition of a selected area in the most active material, Co-PZ-TA@C-800 (Figures 7A and 7B). Analysis of the edge features of the elements enables the visualization of the spatial distribution of the corresponding elements (C, N, O, and Co) in a single-color elemental map as shown in Figure 7 (right). As can be seen there the support mainly consists of carbon (Figure 7, red map, C-K edge) and some content of nitrogen, which is originated from the ligands (Figure 7, green map, N-K edge). Inspection of the distribution of the Co-L edge signal and the O-K edge signal (Figure 7, yellow and blue map, respectively) reveal that the two bigger particles consist of a metallic cobalt core and a shell of cobalt oxide. Two selected spectra that show different features of selected areas in the material are shown in Figure 7B.

To obtain further insights into the surface chemistry of these materials, we performed XPS analysis. The sample surfaces of all the four catalysts (Co-PZ-TA@C-800, Co-PZ@C-800, Co-TA@C-800, and Co-PZ-TA@C-800 recycled) consists mainly of C with small concentrations of Co, O, N, S, and Si (Table S1) with the last two probably originating from Vulcan XC-72R and N from the starting chemicals such as ligands and cobalt nitrate. As found by STEM the Co particles are surrounded by carbon layers leading to the very low surface concentrations of Co between 0.2 and 0.4 atom% for the fresh catalysts and 0.9 atom% for the recycled catalysts. The high-resolution Co 2p spectra of all four samples (see Figure 8A) confirmed the presence of metallic Co as sharp peaks at 778.7 (Co $2p_{3/2}$) and 793.8 eV (Co $2p_{1/2}$) as well as oxidic structures as broad peaks at higher binding energies.[109] Considering the satellite features at around 786 and 803 eV, a mixture of CoO and Co_3O_4 seems to be present. Looking at the recycled catalyst (three reaction cycles) Co-PZ-TA@C-800R (see Figure 8A) an oxidation of the surface can be observed so that only a minor part Co is still in the metallic state. Note that the Co concentration at the surface

Please cite this article in press as: Senthamarai et al., A "universal" catalyst for aerobic oxidations to synthesize (hetero)aromatic aldehydes, ketones, esters, acids, nitriles, and amides, Chem (2021), https://doi.org/10.1016/j.chempr.2021.12.001

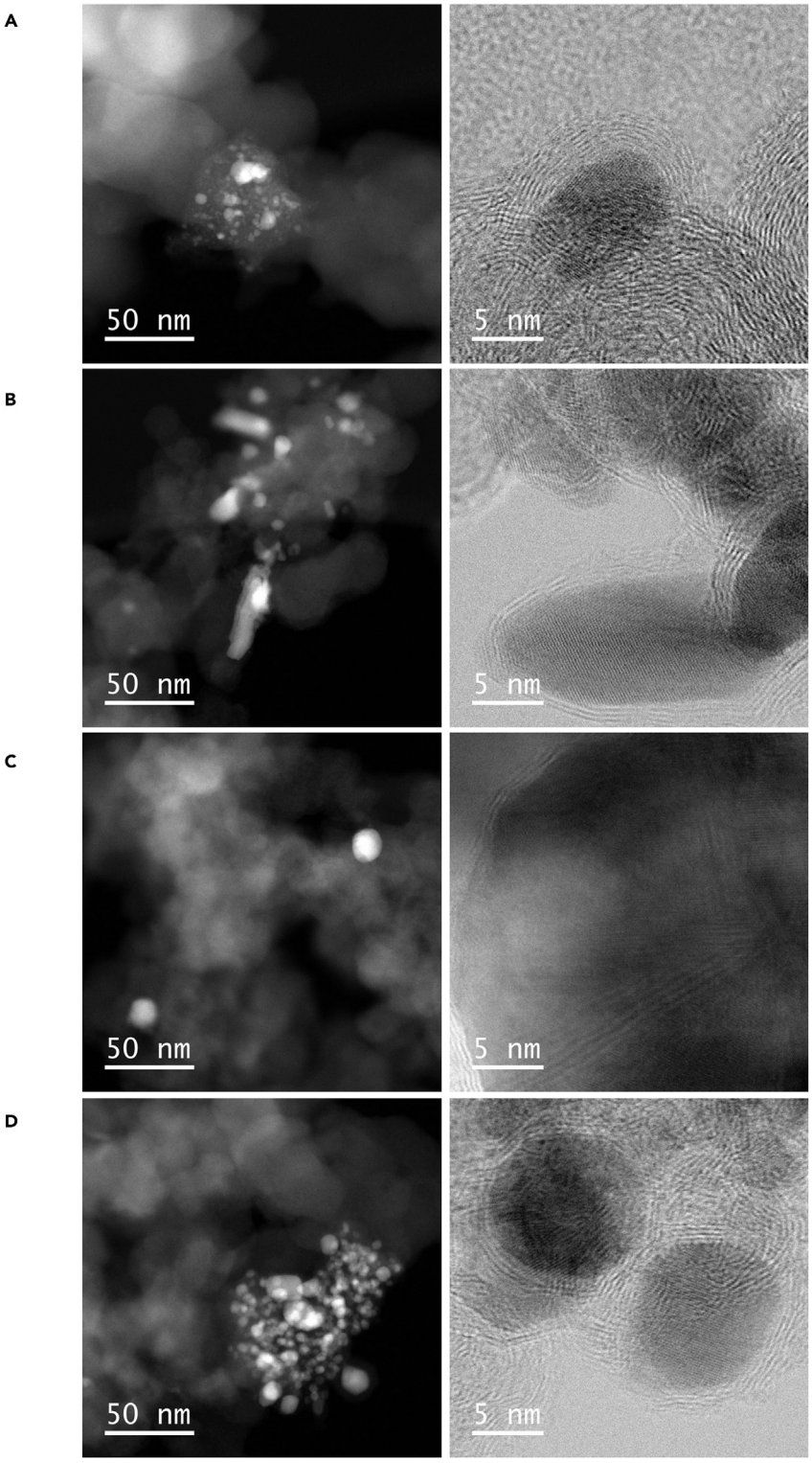

Figure 6. STEM-HAADF (high-angle annular dark-field) and ABF (annular bright field) images of cobalt-nanocatalysts

(A–D) (A) Co-PZ-TA@C-800, (B) Co-PZ@C-800, (C) Co-TA@C-800, and (D) Co-PZ-TA@C-800 recycled.
(Left) HAADF.
(Right) ABF.

Please cite this article in press as: Senthamarai et al., A "universal" catalyst for aerobic oxidations to synthesize (hetero)aromatic aldehydes, ketones, esters, acids, nitriles, and amides, Chem (2021), https://doi.org/10.1016/j.chempr.2021.12.001

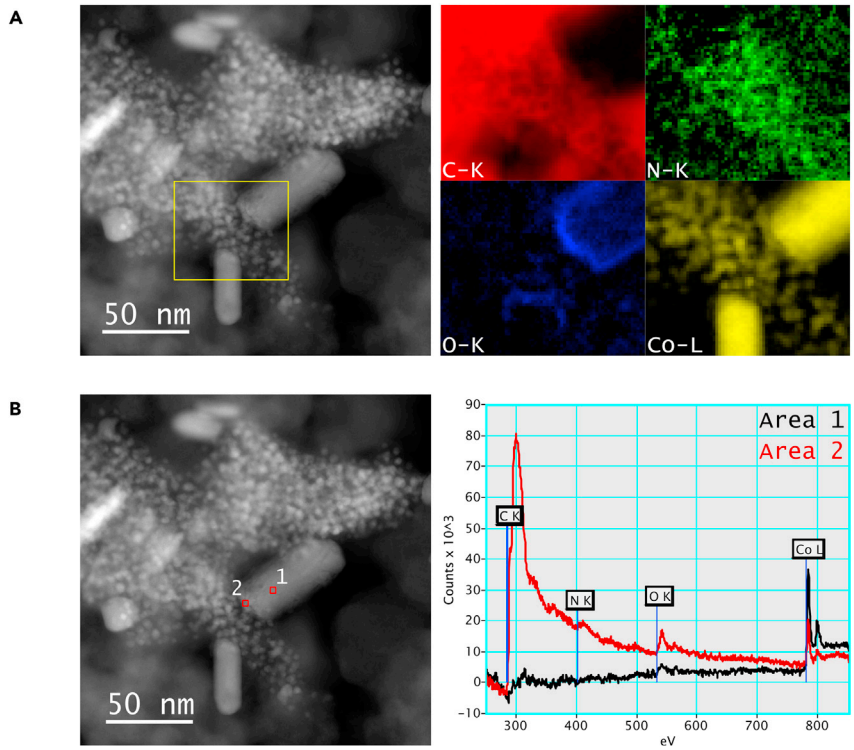

Figure 7. STEM and EELS images of Co-PZ-TA@C-800

(A) STEM-ADF image of Co-PZ-TA@C-800 (left). The highlighted area was investigated by EELS and the distribution of C, N, O, and Co is shown in the single-color elemental map on the right.

(B) STEM-ADF image of Co-PZ-TA@C-800 (left) and corresponding electron energy loss (EEL) spectra of the highlighted areas (right). Area 1 shows almost exclusively the signal edges of cobalt while in area 2, the signal edges of carbon, nitrogen, oxygen, and cobalt can be seen.

increases to 0.9 atom% (Table S1) in the recycled catalyst (three reaction cycles), which indicates a partial breakup of the protective carbon shell probably also leading to the observed oxidation during the use of the catalyst. In case of the recycled catalyst after 7th run, only oxidized Co is observed on the surface (Figure S6).

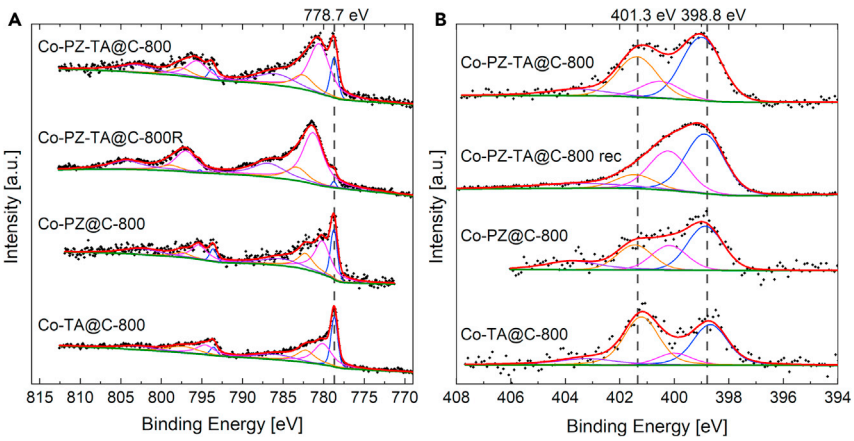

Figure 8. XPS spectra of Co-materials

(A and B) XPS Co 2p (A) and N 1s (B) spectra of Co-PZ-TA@C-800, Co-PZ-TA@C-800 recycled, Co-PZ@C-800, and Co-TA@C-800 from top to bottom.

Please cite this article in press as: Senthamarai et al., A "universal" catalyst for aerobic oxidations to synthesize (hetero)aromatic aldehydes, ketones, esters, acids, nitriles, and amides, Chem (2021), https://doi.org/10.1016/j.chempr.2021.12.001

The N 1s spectra in Figure 8B are fitted with four peaks which can be assigned to pyridinic-N at binding energies around 398.8 eV, pyrollic-N, and/or N bonded to a metal in a Me–N_x center (~400.1 eV), graphitic N (~401.3 eV) as well as oxidized pyridinic-N (~404 eV).[110] Interestingly the concentration of N is higher in Co-PZ-TA@C-800 (1.7 atom %) compared with the other fresh catalysts (0.6 and 0.7 atom%; Table S1). After recycling the N concentration becomes even higher (4.7 atom%) and is dominated by pyridinic and pyrollic-N/Me–N_x. This is explained by ammonia side-reactions on the catalyst surface.

All these characterization data revealed that the immobilization and pyrolysis of cobalt-complexes containing PZ and/or TA ligands produced dissimilar kinds of cobalt nanoparticles supported on carbon, which in turn revealed varying catalytic activities. The material (Co-PZ-TA@C-800) containing predominately metallic cobalt nanoparticles exhibited highest activity. Apparently, fully oxidized cobalt has a negative impact on the overall catalytic performance as such particles have not been observed in the most active catalyst, and even not in the recycled one. Catalytic performance likely depends on the particle nature, sizes, and their distribution. The combination of PZ and TA ligands seems to favor the formation of a higher share of smaller cobalt containing particles and thus induce an increased number of accessible active sites in the catalyst, Co-PZ-TA@C-800. Hereafter, we represent the most active catalyst Co-PZ-TA@C-800 as Co/GS@C, where GS denote graphitic shell.

Application of Co/GS@C (Co-PZ-TA@C-800) for the synthesis of aldehydes, ketones, acids, esters, nitriles, and amides

After having a general catalyst system Co/GS@C (Co-PZ-TA@C-800) in hand, we performed additional tests with >90 different alcohols. As shown in Figures 9, 10, 11, and 12, simple substituted as well as functionalized and structurally diverse aromatic and heterocyclic aldehydes, ketones, acids, esters, nitriles, and amides can be prepared in good to excellent yields. For example, alkyl- and phenyl-substituted alcohols produced the corresponding products **B–F** in up to 98% yield (Figure 9; products **B2**, **B6**, **B7**, **B11**, **C2**, **C3**, **C8–C10**, **D2–D5**, **E2–E4**, **F2–F4**, and **F8**).

Similarly, fluoro- and thio-trifluoromethyl-substituted products were obtained yields in up to 96% (Figure 9; products **B3–B5**, **B12**, **B13**, **C4–C7**, **D6**, **D7**, **E5–E7**, and **F5**). Such compounds are interesting building blocks for the discovery of new pharmaceuticals and agrochemicals.[111] In addition to benzyl alcohols, related condensed arenes gave corresponding products in up to 89% yields (Figure 9; products **B8**, **B9**, **D8**, **D9**, **E8–E10**, **F6**, and **F7**). Likewise, benzophenone, and 1-phenylbutan-1-one were obtained in 83%–85% yields (Figure 9; products **B14–B15**). Notably, in the oxidative cross-esterification reaction apart from methanol, other aliphatic alcohols can be used to provide ethyl, propyl, iso-propyl, butyl, and hexyl benzoates in up to 90% yields (Figure 9; products **D10–D14**). Interestingly, in case of ammoxidation to give nitriles, Co-PZ-TA@C-800 showed good activity for aliphatic alcohols at elevated temperature (140°C). As a result, 4-phenylbutanenitrile, and several alkyl nitriles were obtained in up to 78% yield (Figure 9; products **E12–E15**).

Next, the ability and selectivity of Co-PZ-TA@C-800 for the refinement of more complex molecules as well as the tolerance of functional and sensitive groups was studied. Thus, functionalized as well as multi-substituted benzylic alcohols were subjected to aerobic oxidation under the optimized conditions (Figure 10). Chloro-, bromo-, and iodo-substituted benzylic alcohols smoothly reacted to the corresponding halogenated benzaldehydes, acetophenones, benzoic acids, methyl benzoates, benzonitriles, and primary benzamides in good to excellent yields (Figure 10;

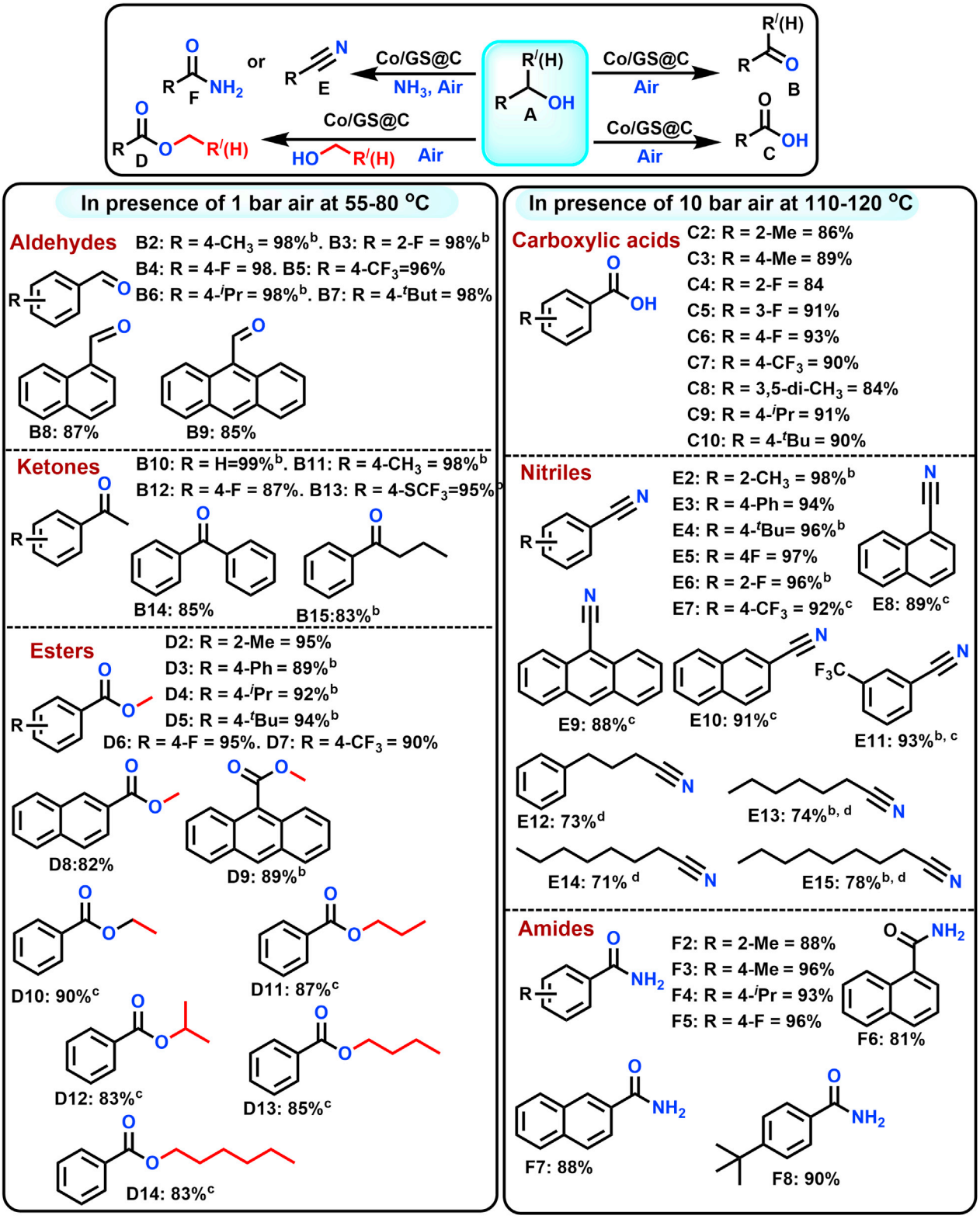

Figure 9. Synthesis of simple and substituted aldehydes, ketones, acids, esters, nitriles, and amides by Co/GS@C-catalyzed aerobic oxidation of alcohols

Reaction conditions: [a]for the synthesis of carbonyl compounds (**B**) = 0.5 mmol alcohol, 35 mg catalyst (6.5 mol % of Co), 1 bar air, 10 mol % K_2CO_3, 2 mL n-heptane, 80°C, 24 h, isolated yields. [b]GC yields using n-hexadecane as standard. [a]For the synthesis of carboxylic acids (**C**) = 0.5 mmol alcohol, 35 mg catalyst (6.5 mol % of Co), 10 bar air, 50 mol % KOH, 2 mL water, 110°C, 24 h, isolated yields. [a]For the synthesis of esters (**D**) = 0.5 mmol alcohol, 35 mg

Continued

Please cite this article in press as: Senthamarai et al., A "universal" catalyst for aerobic oxidations to synthesize (hetero)aromatic aldehydes, ketones, esters, acids, nitriles, and amides, Chem (2021), https://doi.org/10.1016/j.chempr.2021.12.001

Figure 9. *Continued*

catalyst (6.5 mol % of Co), 1 bar air, 10 mol % K_2CO_3, 2 mL methanol, 55°C, 24 h, isolated yields. [b]GC yields using n-hexadecane as standard. [c]In 2 mL different aliphatic alcohols as solvents instead of methanol. [a]For the synthesis of nitriles (**E**) = 0.5 mmol alcohol, 200 μL aqueous NH_3 (28%–30% NH_3 basis), 35 mg catalyst (6.5 mol % of Co), 10 bar air, 2 mL *t*-butanol, 120°C, 24 h, isolated yields. [b]GC yields using n-hexadecane as standard. [c]At 130°C, 24 h. [d]With 45 mg catalyst, 400 μL NH_3 (28%–30% NH_3 basis in water), 140°C, 48 h. [a]For the synthesis of amides (**F**) = 0.5 mmol benzyl alcohol, 200 μL aqueous NH_3 (28%–30% NH_3 basis), 35 mg catalyst (6.5 mol % of Co), 10 bar air, 2 mL water, 120°C, 24 h, isolated yields.

products **B16–B18**, **B27**, **B36–B38**, **C11–C14**, **C19**, **D15–D17**, **D25**, **E16–E19**, **F9–F13**, and **F18**). These further functionalized halogenated molecules are indispensable for many applications and serve as valuable starting materials and intermediates.[112] As an example, 2,6-dichloro-benzyl alcohol was reacted in presence of ammonia in water and produced the corresponding benzamide in 85% yield (**F18**). Substrates containing ether, hydroxyl, amine, nitro, ester, boronic ester, or nitrile substituents, were selectively converted to desired products **B19**, **B20**, **B23**, **B26–B33**, **B39**, **B40**, **C15**, **C16**, **C20**, **D18**, **D19**, **D21–D25**, **E21**, **E23**, **E27**, **F14**, **F15**, and **F17**. Interestingly, sulfur-containing alcohols were also selectively converted without oxidation of S-moiety (Figure 10; products **B24**, **B25**, **C17**, **D20**, **E25**, **E26**, and **F19**). In case of 1,3- and 1,4-benzenedimethanol, both CH_2–OH groups were selectively oxidized and produced terephthalaldehyde **B30** and terephthalonitrile **E24** in 95%–96% yields. In addition, di- and multi-substituted substrates, which possess additional challenges, were efficiently oxidized, and gave products **B21**, **B22**, **B26–B29**, **C18**, **C19**, **D23**, **D25**, **E20**, **E22**, and **F16–F18** in high yields (Figure 10). Even the dinitro-substituted benzyl alcohol produced the corresponding benzaldehyde **B28** in 85% yield. Sterically hindered tri-methyl benzyl alcohol also reacted to provide the corresponding benzonitrile in 86% yield (Figure 10; product **E22**). In addition to benzylic alcohols, allylic alcohols such as cinnamyl and perillyl alcohols can be efficiently transformed to cinnamaldehyde, perillyl aldehyde, and cinnamyl nitrile (Figure 10; products **B34**, **B35**, **E28**). Furthermore, aliphatic cyclic secondary alcohols were oxidized to produce cyclic ketones (Figure 10; products **B43** and **B44**).

Subsequently, the synthesis of heterocyclic carbonyl compounds, carboxylic acids, esters, nitriles, and amides from corresponding alcohols was explored. In general, heterocyclic compounds find wide range of applications, especially in life sciences. Indeed, such scaffolds are ubiquitous in pharmaceuticals, natural products, agrochemical, and other biomolecules. Thus, they play a pivotal role in modern small molecule drug discovery processes.[113,114] As shown in Figure 11, different kinds of heterocyclic alcohols were oxidized to give the desired compounds. Interestingly, nicotinic derivatives such as nicotinaldehyde, methyl nicotinate, nicotinonitrile, nicotinic acid (niacin), and nicotinamide—the latter two are used as food supplement and nutrition medications—as well as 3-acetylpyridine are smoothly prepared from 3-pyridinemethanol in up to 97% yield (Figure 11; products **B45**, **B61**, **C21**, **D26**, **E29**, **F20**). Similarly, bromo-, di-methoxy-, and di-chloro-substituted 2- and 3-pyridinemethanol are selectively oxidized to produce **B47–B49** and **D28**. Other N-heterocycles such 2-pyrazine and quinolinemethanol are well accepted and provided the respective products in 88%–94% (products **E30**, **E31**, and **F21**). Interestingly, 2-thiophenmethanol also allowed for selective oxidation in up to 95% yield (Figure 11; products **B50**, **B62**, **D29**, **E41**, and **F22**). At this point, it should be noted that sulfur-containing compounds constitute common poisons for most heterogeneous catalysts. However, Co-PZ-TA@C-800 tolerated the presence of many sulfur-containing molecules and a variety of sulfur-containing products, e.g., **B24**, **B25**, **B50**, **B52**, **B53**, **B62**, **C17**, **C22**, **D20**, **D29**, **E25**, **E26**, **E33**, **E34**, **E41**, **F19**, and **F22** were obtained in good to excellent yields. Apart from the oxidation of hydroxymethyl-substituted N-, O-, and S-heterocycles a variety of benzylic alcohol containing heterocyclic motifs

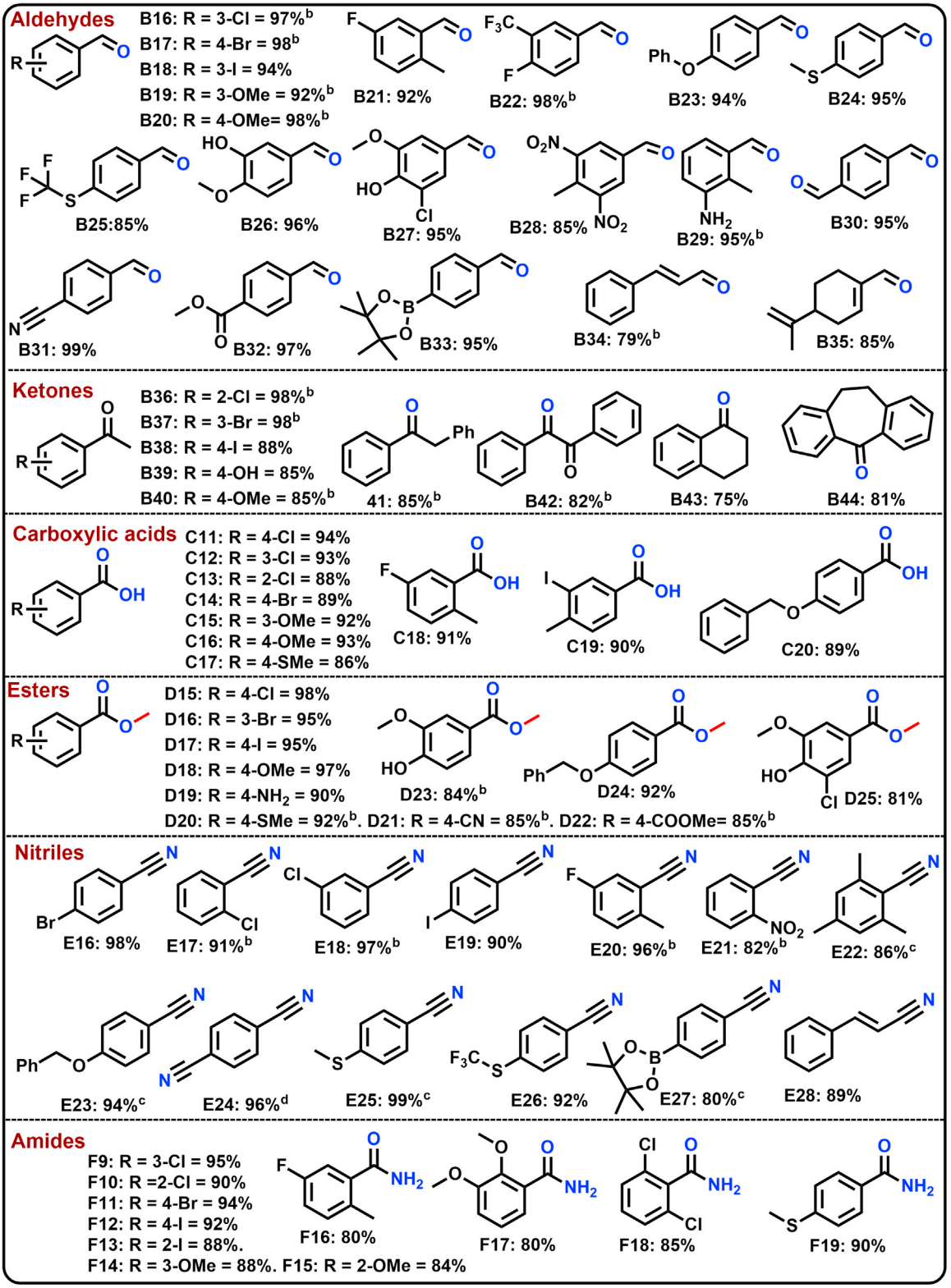

Figure 10. Co/GS@C-catalyzed synthesis of functionalized and challenging aldehydes, ketones, acids, esters, nitriles, and amides from alcohols

Reaction conditions: [a]for the synthesis of carbonyl compounds (**B**) = 0.5 mmol alcohol, 35 mg catalyst (6.5 mol % of Co), 1 bar air, 10 mol % K_2CO_3, 2 mL n-heptane, 80°C, 24 h, isolated yields. [b]GC yields using n-hexadecane as standard. [a]For the synthesis of carboxylic acids (**C**) = 0.5 mmol alcohol, 35 mg

Please cite this article in press as: Senthamarai et al., A "universal" catalyst for aerobic oxidations to synthesize (hetero)aromatic aldehydes, ketones, esters, acids, nitriles, and amides, Chem (2021), https://doi.org/10.1016/j.chempr.2021.12.001

Figure 10. *Continued*

catalyst (6.5 mol % of Co), 10 bar air, 50 mol % KOH, 2 mL water, 110°C, 24 h, isolated yields. [a]For the synthesis of esters (**D**) = 0.5 mmol alcohol, 35 mg catalyst (6.5 mol % of Co), 1 bar air, 10 mol % K_2CO_3, 2 mL methanol, 55°C, 24 h, isolated yields. [b]GC yields using n-hexadecane as standard. [a]For the synthesis of nitriles (**E**) = 0.5 mmol alcohol, 200 μL aqueous NH_3 (28%–30% NH_3 basis), 35 mg catalyst (6.5 mol % of Co), 10 bar air, 2 mL *t*-butanol, 120°C, 24 h, isolated yields. [b]GC yields using n-hexadecane as standard. [c]130°C. [d]With 70 mg catalyst, 400 μL NH_3 (28%–30% NH_3 basis in water), 48 h. [a]For the synthesis of amides (**F**) = 0.5 mmol benzyl alcohol, 200 μL aqueous NH_3 (28%–30% NH_3 basis), 35 mg catalyst (6.5 mol % of Co), 10 bar air, 2 mL water, 120°C, 24 h, isolated yields.

such as thiazole, morpholine, pyrazine, tetrahydropyran, diazepane, N-methyl diazepane, and triazole underwent aerobic oxidation under the previously optimized conditions and furnished the desired products (Figure 11; **B51–B53**, **B55–B60**, and **E33–E40**). As an example, 2,1,3-benzothiadiazol-5-yl-methanol gave corresponding aldehyde and nitrile (Figure 11; products **B52**, **E34**. Other notable examples include the oxidation of 3,4-(methylendioxy)-benzylalcohol, an important motif present in drugs and natural products (Figure 11, products **B51**, **C23**, **D30**, **E32**, **F23**) and 3,5-dimethyl-1-phenyl-1H-pyrazol-4-yl-methanol as well as 2-(2-morpholinoethoxy) phenyl-methanol (Figure 11, products **B54**, **B60**, **E40**, **E42**).

In recent years, the valorization of hydroxymethylfurfural (HMF, **A2**) and furfuryl alcohol (**A3**) attracted significant interest for the preparation of sustainable polymers and fuels (Figure 12).[115,116] Among these, the synthesis of 2,5-furandicarboxylic acid (FDCA) and dimethyl furan-2,5-dicarboxylate (FDCM) from HMF is of actual interest to produce poly(ethylenefuranoate) (PEF) polymer.[115] Applying our Co/GS@C catalyst FDCM, (**D31**) is prepared in up to 85% yield. More sensitive furan-2,5-dicarbaldehyde (**B66**) can be also obtained in up to 87% yield. Furthermore, furan-2,5-dicarbonitrile (**E43**) is available from this latter intermediate. Similarly, furfuryl alcohol (**A3**) was selectively transformed to corresponding aldehyde (**B67**), carboxylic acid (**C24**), methyl ester (**D32**), nitrile (**E44**), and amide (**F24**) in good to excellent yields (Figure 12). Again, these products have various interesting applications, for example, 2-furoic acid is a known preservative, flavoring ingredient, food, and color additive in food,[117] while 2-furonitrile has been suggested as a potential sweetening agent, which has about thirty times the sweetening power of sucrose.[118]

In general, catalytic oxidations were performed in 50–150 mg scale with respect to substrate. To demonstrate the utility of this catalyst system, reactions of five alcohols were also performed on 1–10 g (Figure 13). The yields of the desired products from these upscaling experiments were similar to those obtained from the smaller scale.

Further, we calculated TONs and TOFs of our Co-catalyst for the oxidation of benzyl alcohol to benzaldehyde (Table S3). Under standard conditions (0.5 mmol alcohol, 35 mg catalyst, 80°C, 24 h) these values are found to be 15.6 and 0.65 h^{-1}, while at 100°C and increased amount of substrate (2.5 mmol of benzyl alcohol, 35 mg catalyst, 24 h) both values increased (TOF and TON are 46.8 and 1.95 h^{-1}). These numbers are at least comparable to reported non-noble metal-based catalysts for the individual transformations (Table S3).

Kinetic and mechanistic investigations

We performed kinetic investigations on the Co/GS@C-catalyzed oxidation of benzyl alcohol to benzaldehyde and examined the effect of (1) reaction time, (2) reaction temperature, (3) catalyst amount, and (4) substrate (benzyl alcohol) concentration (Figure S7). By increasing the time, temperature, or catalyst loading the yield of benzaldehyde increased, and quantitative yield was obtained for 24 h, at 80°C with 35 mg of catalyst. On the other hand, increasing the substrate (benzyl alcohol) concentration, the yield of benzaldehyde is decreased. Next, we calculated the

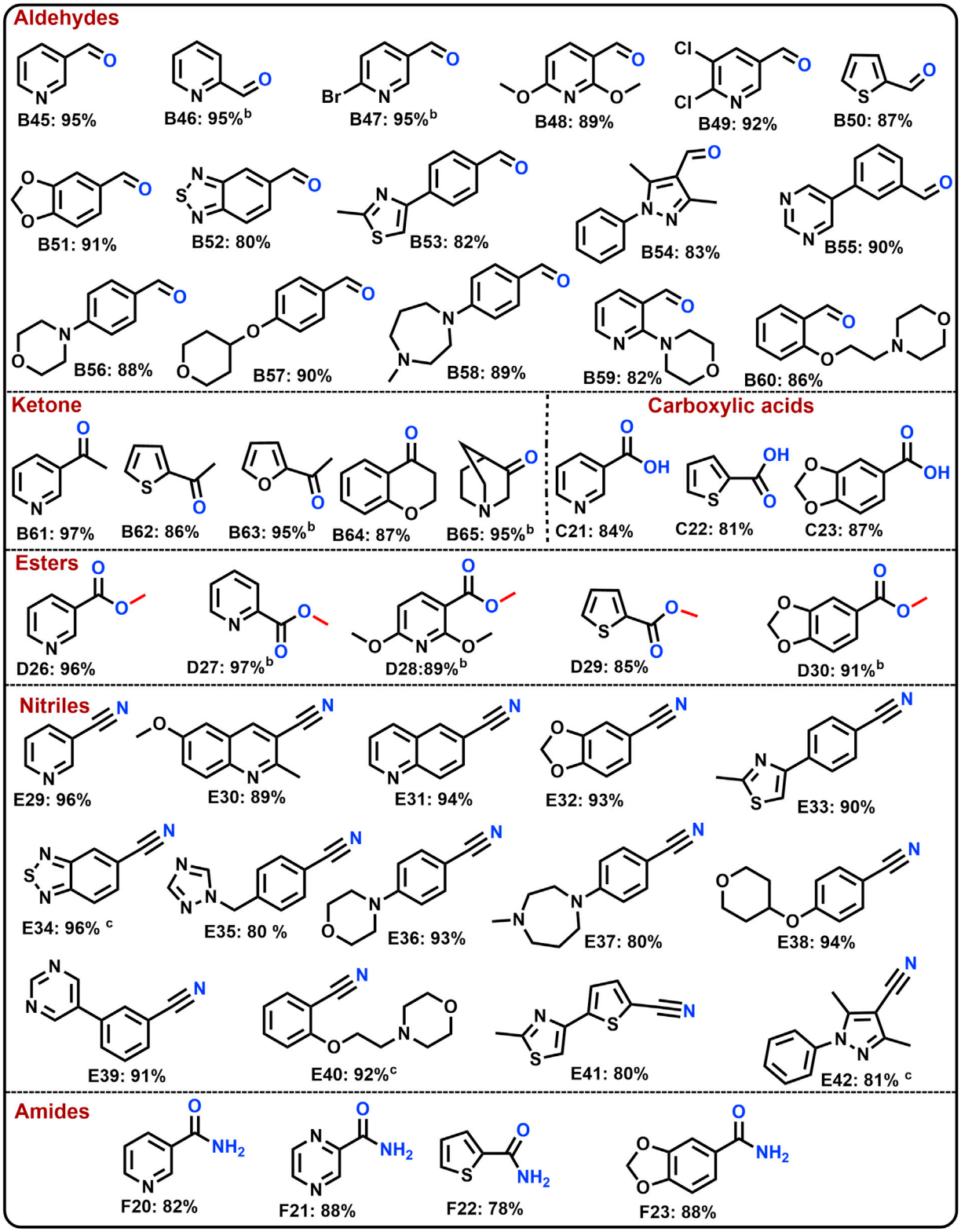

Figure 11. Synthesis of simple and substituted aromatic aldehydes, ketones, acids, esters, nitriles, and amides catalyzed by Co/GS@C catalyst

Reaction conditions: [a]for the synthesis of carbonyl compounds (**B**) = 0.5 mmol alcohol, 35 mg catalyst (6.5 mol % of Co), 1 bar air, 10 mol % K_2CO_3, 2 mL n-heptane, 80°C, 24 h, isolated yields. [b]GC yields using n-hexadecane. [a]For the synthesis of carboxylic acids (**C**) = 0.5 mmol alcohol, 35 mg catalyst (6.5 mol

Figure 11. *Continued*

% of Co), 10 bar air, 50 mol % KOH, 2 mL water, 110°C, 24 h, isolated yields. [a]For the synthesis of esters (**D**) = 0.5 mmol alcohol, 35 mg catalyst (6.5 mol % of Co), 1 bar air, 10 mol % K_2CO_3, 2 mL methanol, 55°C, 24 h, isolated yields. [b]GC yields using n-hexadecane as standard. [a]For the synthesis of nitriles (**E**) = 0.5 mmol alcohol, 200 μL aqueous NH_3 (28%–30% NH_3 basis), 35 mg catalyst (6.5 mol % of Co), 10 bar air, 2 mL *t*-butanol, 120°C, 24 h, isolated yields. [b]GC yields using n-hexadecane. [c]130°C. [a]For the synthesis of amides (**F**) = 0.5 mmol benzyl alcohol, 200 μL aqueous NH_3 (28%–30% NH_3 basis), 35 mg catalyst (6.5 mol % of Co), 10 bar air, 2 mL water, 120°C, 24 h, isolated yields.

reaction order with respect to substrate (benzyl alcohol), which is found to be −0.85 (Figure S7E). This also confirmed that the substrate has a negative effect on the rate of the reaction.

Next, we conducted experiments to identify the formation of possible reactive oxygen species (ROS) during the Co/GS@C-catalyzed aerobic oxidation reactions. For this purpose, under standard conditions, the oxidation of benzyl alcohol to benzaldehyde was tested in the presence of different radical quenchers/trapping agents such as NaN_3, i-PrOH, and p-benzoquinone (PBQ) (Table S4). All these reagents have been used to trap singlet oxygen ($^1O_2$), hydroxyl ($^{\bullet}OH$) or super oxide ($O_2^{\bullet-}$) radicals, which are considered as the ROS in aerobic oxidations. These experiments showed that there is no effect after adding i-PrOH or NaN_3 on the reactions. However, the reaction is inhibited after the addition of 80 mg PBQ. This makes the formation of super oxide ($O_2^{\bullet-}$) species likely. In addition, we performed an experiment for trapping super oxide ($O_2^{\bullet-}$) species using butylated hydroxytoluene (BHT) (Figure S8). Under similar experimental conditions, without the substrate (35 mg Co/GS@C, 0.5 mmol BHT, 1 bar air, 10 mol % K_2CO_3, 2 mL n-heptane, 80°C, 24 h), we performed the reaction with BHT and observed the formation of BHT-OOH, which is detected by GC-MS (Figure S8). These experiments indicate that super oxide ($O_2^{\bullet-}$) is formed during the reaction.

Further to prove the formation of a superoxide radical intermediate, EPR spin-trapping studies using 5,5-dimethyl-1-pyrroline N-oxide (DMPO) as spin-trap reagent were performed. The EPR spectrum of the reaction mixture containing a suspension of Co/GS@C catalyst, Cs_2CO_3 and benzyl alcohol in heptane after heating at 80°C for 3 min under bubbling of O_2 followed by addition of DMPO exhibited a signal at g = 2.006 characteristic of the DMPO-OOH spin adduct indicating again the formation of a superoxide radical intermediate during the catalytic reaction (Figure 14). It should be noted that no EPR signal is detected in the absence of benzyl alcohol suggesting that its adsorption on the surface of the Co/GS@C-800 catalyst induce the activation of molecular oxygen and superoxide formation.

Regarding the general mechanism, in all these oxidations, the first step is the Co/GS@C-catalyzed oxidative conversion of benzyl alcohol (**A**) to benzaldehyde (**B**). Thus, for the formation of carboxylic acid (**C**), ester (**D**), nitrile (**E**), and amide (**F**), (**B**) serves as the key intermediate (Figure S9). Indeed, for all transformations the formation of benzaldehyde was detected by GC-MS. In case of benzoic acid, the aldehyde reacts with water and generates benzaldehyde hydrate (**X**) as another intermediate, which is then oxidized in the presence of Co/GS@C and gives the corresponding acid. Similarly, in the formation of benzoic acid esters, aldehyde reacts with another alcohol and provides hemiacetal (**X′**) as another intermediate, which finally converts to the corresponding ester in presence of Co/GS@C and air. For the formation of nitrile, benzaldehyde couples with ammonia and generates primary imine (**Y**), which finally yields the corresponding nitrile. In case of amide synthesis, two pathways are possible: (1) the aldehyde can react with ammonia to form hemiaminal as the intermediate, which could be then oxidized to give the

Please cite this article in press as: Senthamarai et al., A "universal" catalyst for aerobic oxidations to synthesize (hetero)aromatic aldehydes, ketones, esters, acids, nitriles, and amides, Chem (2021), https://doi.org/10.1016/j.chempr.2021.12.001

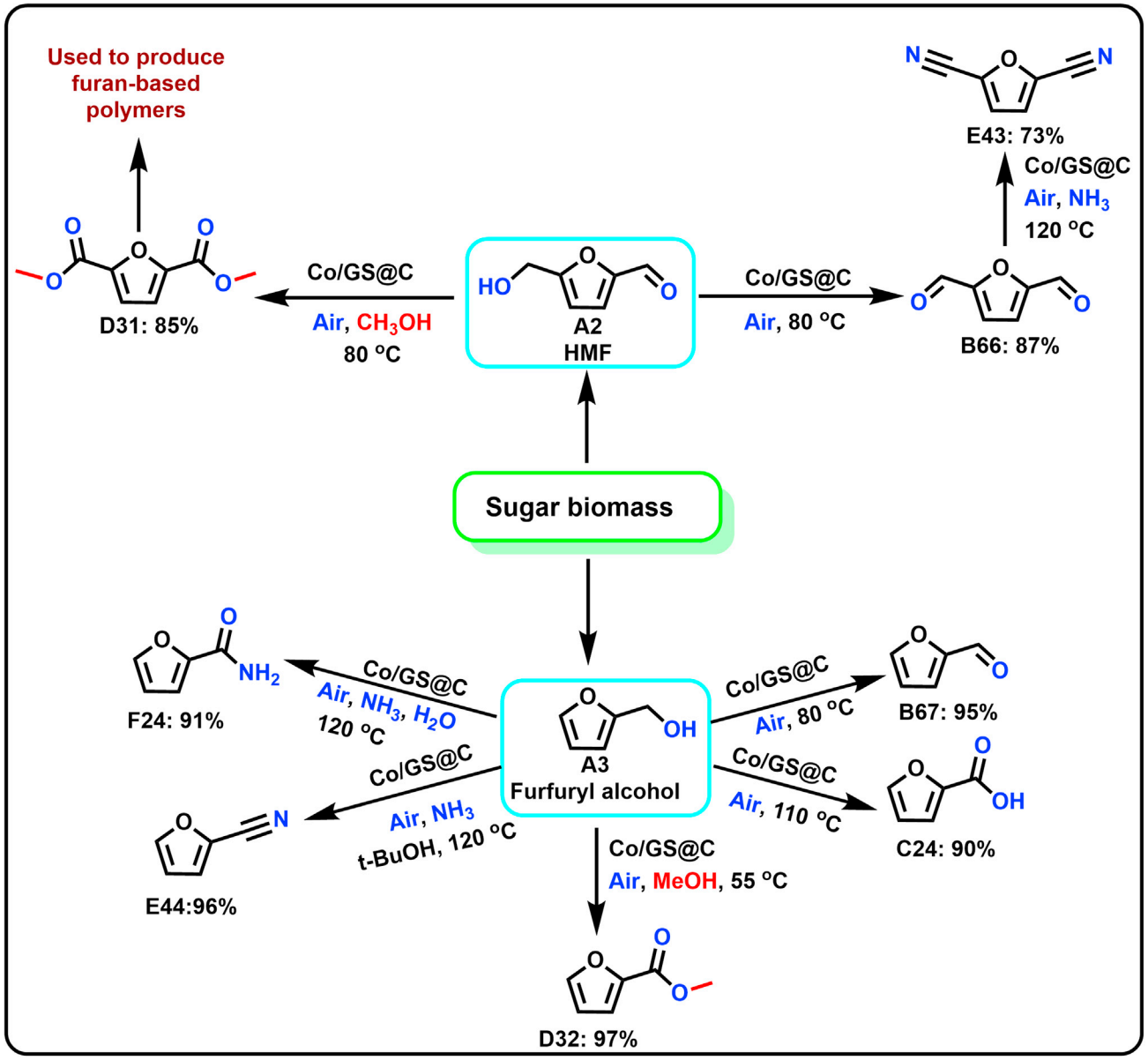

Figure 12. Co/GS@C-catalyzed aerobic oxidative conversion of HMF and 2-furfuryl alcohol to value-added products

Reaction conditions: "conversion of HMF": for the preparation of di-aldehyde (**B66**): 0.5 mmol HMF, 35 mg catalyst, 20 mol % K_2CO_3, 1 bar air, 2 mL of n-heptane, 80°C, 24 h, isolated yield. For the preparation of diester (**D31**): 0.5 mmol HMF, 70 mg catalyst, 40 mol % K_2CO_3, 1 bar air, 4 mL of methanol 80°C, 48 h, isolated yield. For the preparation of di-nitrile (**E43**): 0.5 mmol furan-2,5-dicarbaldehyde (**B66**, 400 μL aqueous NH_3 [28%–30% NH_3 basis], 70 mg catalyst, 5 bar air, 4 mL of *t*-butanol, 120°C), 24 h, isolated yield. "Conversion of 2-furfuryl alcohol": for the preparation of 2-furaldehyde (**B67**) = 0.5 mmol 2-furfuryl alcohol, 35 mg catalyst (6.5 mol % of Co), 1 bar air, 10 mol % K_2CO_3, 2 mL n-heptane, 80°C, 24 h, isolated yield. For the preparation of 2-furoic acid (**C24**) = 0.5 mmol 2-furfuryl alcohol, 35 mg catalyst (6.5 mol % of Co), 10 bar air, 50 mol % KOH, 2 mL water, 110°C, 24 h, isolated yield. For the preparation of methyl-2 furoate (**D32**) = 0.5 mmol 2-furfuryl alcohol, 35 mg catalyst (6.5 mol % of Co), 1 bar air, 10 mol % K_2CO_3, 2 mL methanol, 55°C, 24 h, isolated yield. For the preparation of 2-furonitrile (**E44**) = 0.5 mmol 2-furfuryl alcohol, 200 μL aqueous NH_3 (28%–30% NH_3 basis), 35 mg catalyst (6.5 mol % of Co), 10 bar air, 2 mL *t*-butanol, 120°C, 24 h, isolated yield. For the preparation of 2-furamide (**F24**) = 0.5 mmol 2-furfuryl alcohol, 200 μL aqueous NH_3 (28%–30% NH_3 basis), 35 mg catalyst (6.5 mol % of Co), 10 bar air, 2 mL water, 120°C, 24 h, isolated yield.

corresponding primary amide or (2) formation of benzonitrile takes place, which can undergo hydrolysis to form the primary amide. To prove these two pathways, we performed the reaction of benzonitrile in water in presence of ammonia and air using Co/GS@C catalyst at 120°C for 24 h. From this experiment, we obtained 98% of

Please cite this article in press as: Senthamarai et al., A "universal" catalyst for aerobic oxidations to synthesize (hetero)aromatic aldehydes, ketones, esters, acids, nitriles, and amides, Chem (2021), https://doi.org/10.1016/j.chempr.2021.12.001

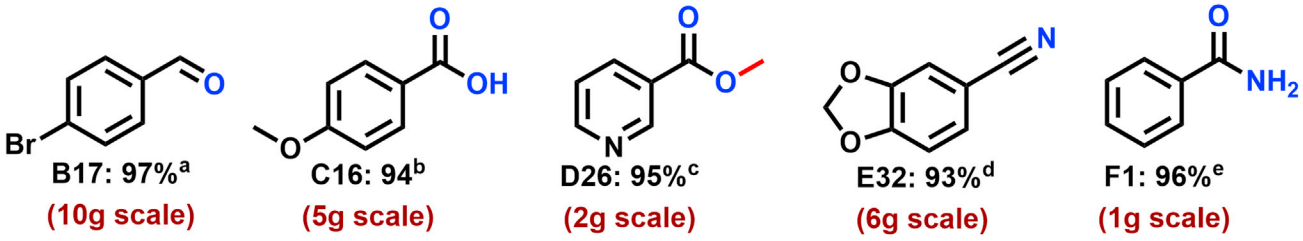

Figure 13. Scale up experiments for the synthesis of selected products B–F

Reaction conditions: [a]10 g 4-bromo benzyl alcohol, 3.7 g catalyst (6.5 mol% of Co), 1 bar air, 10 mol % K_2CO_3, 150 mL n-heptane, 80°C, 24 h. [b]5 g 4-methoxy benzyl alcohol, 2.5 g catalyst (6.5 mol % of Co), 10 bar air, 50 mol % KOH, 100 mL water, 110°C, 24 h. [c]2 g 3-pyridinemethanol, 1.2 g catalyst (6.5 mol % of Co), 1 bar air, 10 mol % K_2CO_3, 50 mL methanol, 55°C, 24 h. [d]6 g piperonyl alcohol, 15.5 mL aqueous NH_3 (28%–30% NH_3 basis), 2.7 g catalyst (6.5 mol% of Co), 10 bar air, 100 mL *t*-butanol, 120°C, 24 h. [e]1 g benzyl alcohol, 3.7 mL aqueous NH_3 (28%–30% NH_3 basis), 0.64 g catalyst (6.5 mol % of Co), 10 bar air, 25 mL water, 120°C, 24 h. All are isolated yields.

benzamide (Figure S10). Thus, we conclude the formation of amide occurred mainly by the hydrolysis of benzonitrile. It should be noted that the intermediates, aldehyde hydrate (X), hemiacetal (X′), and primary imine (Y) are unstable, and we were not able to detect or isolate them.

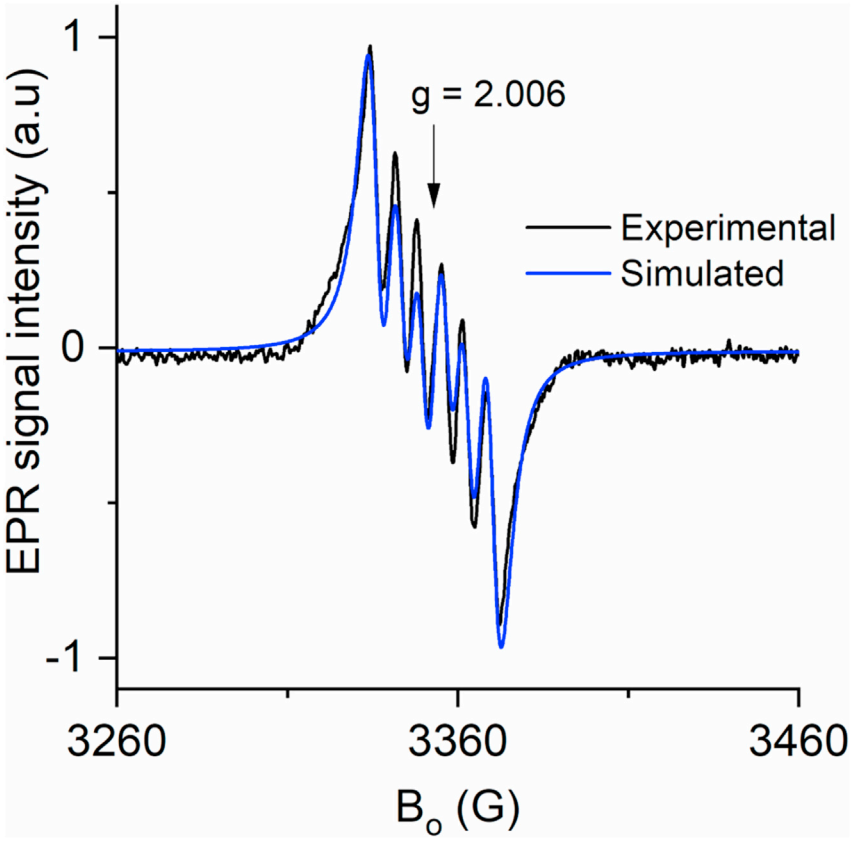

Figure 14. EPR spectrum

Measured at 20°C of Co/GS@C catalyst and benzyl alcohol suspension in heptane after heating at 80°C for 3 min under bubbling of O_2 followed by addition of DMPO (black-line); blue-line simulated spectrum. The EPR spectrum shows the formation of DMPO-OOH spin adduct.

Please cite this article in press as: Senthamarai et al., A "universal" catalyst for aerobic oxidations to synthesize (hetero)aromatic aldehydes, ketones, esters, acids, nitriles, and amides, Chem (2021), https://doi.org/10.1016/j.chempr.2021.12.001

Based on the identified active oxygen species and the proposed reaction pathways and intermediates, we suggest the following general mechanism for the different aerobic oxidations of primary alcohol in the presence of Co/GS@C (Figure 15). In the first step, (1) adsorption and activation of alcohol and oxygen takes place on the catalyst surface. During this process, the generation of the observed superoxide species occurs. In the next step (2), oxidation of the activated alcohol takes place. In the last step (3), the desorption of the product, aldehyde takes place by the regeneration of catalyst. Similar catalytic cycles for the formation of esters, carboxylic acid, and nitrile are proposed. The hydrolysis of benzonitrile to benzamide occurs best in presence of catalyst, water, ammonia, and air.

Conclusion

In conclusion, we demonstrate that a new catalyst can be efficiently developed not only for one specific synthetic transformation but also for related methodologies with similar elementary reaction steps. In particular, we show that the here presented cobalt catalyst is able to perform the selective aerobic oxidation of alcohols to a variety of functionalized aromatic products. This catalyst is based on carbon-supported graphitic-shell-encapsulated specific cobalt nanoparticles, which are prepared by immobilization of *in-situ*-generated cobalt-PZ-TA template on carbon and subsequent pyrolysis under argon at 800°C. Applying the optimal material, functionalized and structurally diverse (hetero)aromatic aldehydes, ketones, carboxylic acids, esters nitriles, and primary amides were prepared in selective manner from alcohols in the presence of air. The resulting compounds represent valuable fine and bulk chemicals, which serve as key starting materials and intermediates for the synthesis of advanced chemicals, pharmaceuticals, agrochemicals, and materials. We believe

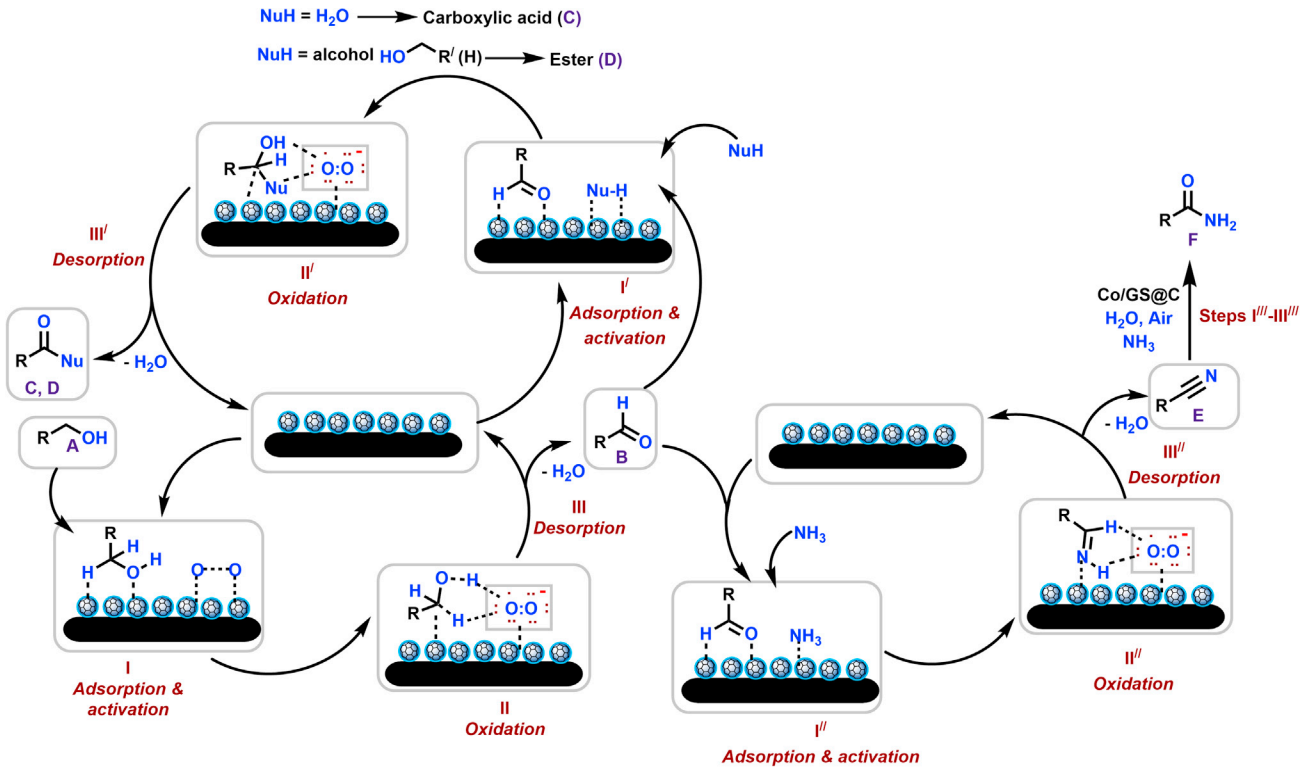

Figure 15. Proposed general mechanism for the Co/GS@C-catalyzed aerobic oxidative conversion of primary alcohols to products B–F

that the presented concept is not only valid for the here-described case of alcohol oxidations but offers manifold opportunities for other chemical transformations, too.

EXPERIMENTAL PROCEDURES

Resource availability

Lead contact

Further information and requests for resources should be directed to and will be fulfilled by the lead contact, Matthias Beller (matthias.beller@catalysis.de).

Materials availability

All materials generated in this study are available from the lead contact without restriction.

Data and code availability

This study did not generate any datasets.

SUPPLEMENTAL INFORMATION

Supplemental information can be found online at https://doi.org/10.1016/j.chempr.2021.12.001.

ACKNOWLEDGMENTS

We gratefully acknowledge the European Research Council (EU project 670986-NoNaCat) and the State of Mecklenburg-Vorpommern for financial and general support. We thank the analytical team of the Leibniz-Institut für Katalyse e.V. for their excellent service.

AUTHOR CONTRIBUTIONS

R.V.J. and M.B. supervised the project. T.S., R.V.J., and M.B. planned and developed the project. T.S. prepared catalysts and performed catalytic experiments. V.G.C. performed catalytic experiments and reproduced the results. N.R. performed TEM measurements and analysis. J.R. conducted EPR measurements. S.B. performed XPS measurements and analysis. R.V.J., T.S., M.B., and V.G.C. wrote the paper.

DECLARATION OF INTERESTS

The authors declare no competing interests.

Received: April 20, 2021
Revised: October 19, 2021
Accepted: November 30, 2021
Published: December 31, 2021

REFERENCES

1. Zecchina, A., and Califano, S. (2017). The Development of Catalysis: A History of Key Processes and Personas in Catalytic Science and Technology (Wiley).
2. Beller, M., and Bolm, C. (2008). Transition Metals for Organic Synthesis (Wiley-VCH).
3. Negishi, E.-I. (2011). Magical power of transition metals: past, present, and future (Nobel Lecture). Angew. Chem. Int. Ed. Engl. *50*, 6738–6764.
4. Rothenberg, G. (2011). Catalysis: Concepts and Green Applications (Wiley-VCH).
5. Beller, M., and Centi, G. (2009). Catalysis and sustainable development: the marriage for innovation. ChemSusChem *2*, 459–460.
6. Catlow, C.R., Davidson, M., Hardacre, C., and Hutchings, G.J. (2016). Catalysis making the world a better place. Philos. Trans. R. Soc. A *374*, 20150089.
7. Joshi, S., and Ranade, V. (2016). Industrial Catalytic Processes for Fine and Specialty Chemicals (Elsevier).
8. Roduner, E. (2014). Understanding catalysis. Chem. Soc. Rev. *43*, 8226–8239.
9. Hagen, J. (2006). Industrial Catalysis: A Practical Approach (Wiley-VCH).
10. Busacca, C.A., Fandrick, D.R., Song, J.J., and Senanayake, C.H. (2011). The growing impact

of catalysis in the pharmaceutical industry. Adv. Synth. Catal. *353*, 1825–1864.

11. Beller, M. (2019). Introduction: first row metals and catalysis. Chem. Rev. *119*, 2089.
12. Gandeepan, P., Müller, T., Zell, D., Cera, G., Warratz, S., and Ackermann, L. (2019). 3d transition metals for C–H activation. Chem. Rev. *119*, 2192–2452.
13. Gebbink, R.K., and Moret, M.-E. (2019). Non-Noble Metal Catalysis: Molecular Approaches and Reactions (Wiley-VCH).
14. Vogiatzis, K.D., Polynski, M.V., Kirkland, J.K., Townsend, J., Hashemi, A., Liu, C., and Pidko, E.A. (2019). Computational approach to molecular catalysis by 3d transition metals: challenges and opportunities. Chem. Rev. *119*, 2453–2523.
15. Bullock, R.M., Chen, J.G., Gagliardi, L., Chirik, P.J., Farha, O.K., Hendon, C.H., Jones, C.W., Keith, J.A., Klosin, J., Minteer, S.D., et al. (2020). Using nature's blueprint to expand catalysis with Earth-abundant metals. Science *369*, 786.
16. Schneider, U., and Thomas, S. (2020). Catalysis with Earth-Abundant Elements (Royal Society of Chemistry).
17. Wang, D., and Astruc, D. (2017). The recent development of efficient Earth-abundant transition-metal nanocatalysts. Chem. Soc. Rev. *46*, 816–854.
18. Liu, L., and Corma, A. (2018). Metal catalysts for heterogeneous catalysis: from single atoms to nanoclusters and nanoparticles. Chem. Rev. *118*, 4981–5079.
19. Buurmans, I.L.C., and Weckhuysen, B.M. (2012). Heterogeneities of individual catalyst particles in space and time as monitored by spectroscopy. Nat. Chem. *4*, 873–886.
20. Yang, X.-F., Wang, A., Qiao, B., Li, J., Liu, J., and Zhang, T. (2013). Single-atom catalysts: a new Frontier in heterogeneous catalysis. Acc. Chem. Res. *46*, 1740–1748.
21. Schneider, C., Leischner, T., Ryabchuk, P., Jackstell, R., Junge, K., and Beller, M. (2021). Development of bulk organic chemical processes—history, tatus, and opportunities for academic research. CCS Chem *3*, 512–530.
22. Parmeggiani, C., and Cardona, F. (2012). Transition metal-based catalysts in the aerobic oxidation of alcohols. Green Chem *14*, 547–564.
23. Piera, J., and Bäckvall, J.-E. (2008). Catalytic oxidation of organic substrates by molecular oxygen and hydrogen peroxide by multistep electron transfer—a biomimetic approach. Angew. Chem. Int. Ed. Engl. *47*, 3506–3523.
24. Mallat, T., and Baiker, A. (2004). Oxidation of alcohols with molecular oxygen on solid catalysts. Chem. Rev. *104*, 3037–3058.
25. Cao, Q., Dornan, L.M., Rogan, L., Hughes, N.L., and Muldoon, M.J. (2014). Aerobic oxidation catalysis with stable radicals. Chem. Commun. *50*, 4524–4543.
26. Matsumoto, T., Ueno, M., Wang, N., and Kobayashi, S. (2008). Recent advances in immobilized metal catalysts for environmentally benign oxidation of alcohols. Chem. Asian J. *3*, 196–214.
27. Parmeggiani, C., Matassini, C., and Cardona, F. (2017). A step forward towards sustainable aerobic alcohol oxidation: new and revised catalysts based on transition metals on solid supports. Green Chem *19*, 2030–2050.
28. Balaraman, E., Khaskin, E., Leitus, G., and Milstein, D. (2013). Catalytic transformation of alcohols to carboxylic acid salts and H2 using water as the oxygen atom source. Nat. Chem. *5*, 122–125.
29. Mortier, J. (2016). Arene Chemistry: Reaction Mechanisms and Methods for Aromatic Compounds (John Wiley & Sons).
30. Astruc, D. (2002). Modern Arene Chemistry (Wiley-VCH).
31. Quin, L.D., and Tyrell, J.A. (2010). Fundamentals of Heterocyclic Chemistry: Importance in Nature and in the Synthesis of Pharmaceuticals (Wiley).
32. Dickens, T.K., and Warren, S. (2018). Chemistry of the Carbonyl Group: A Step-by-Step Approach to Understanding Organic Reaction Mechanisms (Wiley).
33. Rai, K.M.L. (2020). Carbonyl Compounds—Chemistry and Synthetic Applications (Notion Press).
34. Badea, G.-I., and Radu, G.L. (2018). Carboxylic Acid: Key Role in Life Sciences (IntechOpen).
35. Patai, S., and Rappoport, Z. (2009). Patai's Chemistry of Functional Groups (Book Series 1964–1995) (Wiley).
36. Lemke, T.L., Roche, V.F., and Zito, S.W. (2011). Review of Organic Functional Groups: Introduction to Medicinal Organic Chemistry, Fifth Edition (Wolters Kluwer Health).
37. Fleming, F.F., Yao, L., Ravikumar, P.C., Funk, L., and Shook, B.C. (2010). Nitrile containing pharmaceuticals: efficacious roles of the nitrile pharmacophore. J. Med. Chem. *53*, 7902–7917.
38. Greenberg, A., Breneman, C.M., and Liebman, J.F. (2000). The Amide Linkage: Structural Significance in Chemistry, Biochemistry, and Materials Science (Wiley-Interscience).
39. ten Brink, G.-J., Arends, I.W.C.E., and Sheldon, R.A. (2000). Green, catalytic oxidation of alcohols in water. Science *287*, 1636–1639.
40. Wang, D., Weinstein, A.B., White, P.B., and Stahl, S.S. (2018). Ligand-promoted palladium-catalyzed aerobic oxidation reactions. Chem. Rev. *118*, 2636–2679.
41. Dijksman, A., Marino-González, A., Payeras, A.M.I., Arends, I.W.C.E., and Sheldon, R.A. (2001). Efficient and selective aerobic oxidation of alcohols into aldehydes and ketones using ruthenium/TEMPO as the catalytic system. J. Am. Chem. Soc. *123*, 6826–6833.
42. Ray, R., Chandra, S., Maiti, D., and Lahiri, G.K. (2016). Simple and efficient ruthenium-catalyzed oxidation of primary alcohols with molecular oxygen. Chemistry *22*, 8814–8822.
43. Csjernyik, G., Éll, A.H., Fadini, L., Pugin, B., and Bäckvall, J.E. (2002). Efficient ruthenium-catalyzed aerobic oxidation of alcohols using a biomimetic coupled catalytic system. J. Org. Chem. *67*, 1657–1662.
44. Marko, I.E., Giles, P.R., Tsukazaki, M., Brown, S.M., and Urch, C.J. (1996). Copper-catalyzed oxidation of alcohols to aldehydes and ketones: an efficient, aerobic alternative. Science *274*, 2044–2046.
45. Hoover, J.M., and Stahl, S.S. (2011). Highly practical copper(I)/TEMPO catalyst system for chemoselective aerobic oxidation of primary alcohols. J. Am. Chem. Soc. *133*, 16901–16910.
46. Steves, J.E., and Stahl, S.S. (2013). Copper(I)/ABNO-catalyzed aerobic alcohol oxidation: alleviating steric and electronic constraints of Cu/TEMPO catalyst systems. J. Am. Chem. Soc. *135*, 15742–15745.
47. Sasano, Y., Nagasawa, S., Yamazaki, M., Shibuya, M., Park, J., and Iwabuchi, Y. (2014). Highly chemoselective aerobic oxidation of amino alcohols into amino carbonyl compounds. Angew. Chem. Int. Ed. Engl. *53*, 3236–3240.
48. Xu, B., Lumb, J.-P., and Arndtsen, B.A. (2015). A TEMPO-free copper-catalyzed aerobic oxidation of alcohols. Angew. Chem. Int. Ed. Engl. *54*, 4208–4211.
49. Tovrog, B.S., Diamond, S.E., Mares, F., and Szalkiewicz, A. (1981). Activation of cobalt-nitro complexes by lewis acids: catalytic oxidation of alcohols by molecular oxygen. J. Am. Chem. Soc. *103*, 3522–3526.
50. Meng, S.-S., Lin, L.-R., Luo, X., Lv, H.-J., Zhao, J.-L., and Chan, A.S.C. (2019). Aerobic oxidation of alcohols with air catalyzed by decacarbonyldimanganese. Green Chem *21*, 6187–6193.
51. Lagerblom, K., Keskiväli, J., Parviainen, A., Mannisto, J., and Repo, T. (2018). Selective aerobic oxidation of alcohols with NO3– activated nitroxyl radical/manganese catalyst system. ChemCatChem *10*, 2908–2914.
52. Guðmundsson, A., Schlipköter, K.E., and Bäckvall, J.-E. (2020). Iron(II)-catalyzed biomimetic aerobic oxidation of alcohols. Angew. Chem. Int. Ed. Engl. *59*, 5403–5406.
53. Ma, S., Liu, J., Li, S., Chen, B., Cheng, J., Kuang, J., Liu, Y., Wan, B., Wang, Y., Ye, J., et al. (2011). Development of a general and practical iron nitrate/TEMPO-catalyzed aerobic oxidation of alcohols to aldehydes/ketones: catalysis with table salt. Adv. Synth. Catal. *353*, 1005–1017.
54. Liu, J., and Ma, S. (2013). Iron-catalyzed aerobic oxidation of allylic alcohols: the issue of C–C bond isomerization. Org. Lett. *15*, 5150–5153.
55. Wang, L., Shang, S., Li, G., Ren, L., Lv, Y., and Gao, S. (2016). Iron/ABNO-catalyzed aerobic oxidation of alcohols to aldehydes and ketones under ambient atmosphere. J. Org. Chem. *81*, 2189–2193.
56. Tang, L., Guo, X., Li, Y., Zhang, S., Zha, Z., and Wang, Z. (2013). Pt, Pd and Au nanoparticles supported on a DNA-MMT hybrid: efficient catalysts for highly selective oxidation of

primary alcohols to aldehydes, acids, and esters. Chem. Commun. *49*, 5213–5215.

57. Göksu, H., Burhan, H., Mustafov, S.D., and Şen, F. (2020). Oxidation of benzyl alcohol compounds in the presence of carbon hybrid supported platinum nanoparticles (Pt@CHs) in oxygen atmosphere. Sci. Rep. *10*, 5439.

58. Zhang, P., Gong, Y., Li, H., Chen, Z., and Wang, Y. (2013). Solvent-free aerobic oxidation of hydrocarbons and alcohols with Pd@N-doped carbon from glucose. Nat. Commun. *4*, 1593.

59. Kaizuka, K., Miyamura, H., and Kobayashi, S. (2010). Remarkable effect of bimetallic nanocluster catalysts for aerobic oxidation of alcohols: combining metals changes the activities and the reaction pathways to aldehydes/carboxylic acids or esters. J. Am. Chem. Soc. *132*, 15096–15098.

60. Enache, D.I., Edwards, J.K., Landon, P., Solsona-Espriu, B., Carley, A.F., Herzing, A.A., Watanabe, M., Kiely, C.J., Knight, D.W., and Hutchings, G.J. (2006). Solvent-free oxidation of primary alcohols to aldehydes using Au–Pd/TiO2 catalyst. Science *311*, 362–365.

61. Abad, A., Concepción, P., Corma, A., and García, H. (2005). A collaborative effect between gold and a support induces the selective oxidation of alcohols. Angew. Chem. Int. Ed. Engl. *44*, 4066–4069.

62. Tsukamoto, D., Shiraishi, Y., Sugano, Y., Ichikawa, S., Tanaka, S., and Hirai, T. (2012). Gold nanoparticles located at the interface of anatase/rutile TiO2 particles as active plasmonic photocatalysts for aerobic oxidation. J. Am. Chem. Soc. *134*, 6309–6315.

63. Vocanson, F., Guo, Y.P., Namy, J.L., and Kagan, H.B. (1998). Dioxygen oxidation of alcohols and aldehydes over a cerium dioxide-ruthenium system. Synth. Commun. *28*, 2577–2582.

64. Yasu-eda, T., Kitamura, S., Ikenaga, N., Miyake, T., and Suzuki, T. (2010). Selective oxidation of alcohols with molecular oxygen over Ru/CaO–ZrO2 catalyst. J. Mol. Catal. A Chem. *323*, 7–15.

65. Mao, F., Qi, Z., Fan, H., Sui, D., Chen, R., and Huang, J. (2017). Heterogeneous cobalt catalysts for selective oxygenation of alcohols to aldehydes, esters, and nitriles. RSC Adv *7*, 1498–1503.

66. Shaabani, A., Keshipour, S., Hamidzad, M., and Seyyedhamzeh, M. (2014). Cobalt(II) supported on ethylenediamine-functionalized nanocellulose as an efficient catalyst for room temperature aerobic oxidation of alcohols. J. Chem. Sci. *126*, 111–115.

67. Bai, C., Li, A., Yao, X., Liu, H., and Li, Y. (2016). Efficient and selective aerobic oxidation of alcohols catalysed by MOF-derived Co catalysts. Green Chem *18*, 1061–1069.

68. Zhu, J., Faria, J.L., Figueiredo, J.L., and Thomas, A. (2011). Reaction mechanism of aerobic oxidation of alcohols conducted on activated-carbon-supported cobalt oxide catalysts. Chemistry *17*, 7112–7117.

69. Zhu, J., Kailasam, K., Fischer, A., and Thomas, A. (2011). Supported cobalt oxide nanoparticles as catalyst for aerobic oxidation of alcohols in liquid phase. ACS Catal *1*, 342–347.

70. Sun, H.-Y., Hua, Q., Guo, F.-F., Wang, Z.-Y., and Huang, W.-X. (2012). Selective aerobic oxidation of alcohols by using manganese oxide nanoparticles as an efficient heterogeneous catalyst. Adv. Synth. Catal. *354*, 569–573.

71. Geng, L., Zhang, M., Zhang, W., Jia, M., Yan, W., and Liu, G. (2015). Rational design of carbon support to prepare ultrafine iron oxide catalysts for air oxidation of alcohols. Catal. Sci. Technol. *5*, 3097–3102.

72. Iwahama, T., Sakaguchi, S., Nishiyama, Y., and Ishi, Y. (1995). Aerobic oxidation of alcohols to carbonyl compounds catalyzed by *n*-hydroxyphthalimide (NHPI) combined with Co(acac)3. Tetrahedron Lett *36*, 6923–6926.

73. Jiang, X., Zhang, J., and Ma, S. (2016). Iron catalysis for room-temperature aerobic oxidation of alcohols to carboxylic acids. J. Am. Chem. Soc. *138*, 8344–8347.

74. Yamada, Y.M.A., Arakawa, T., Hocke, H., and Uozumi, Y. (2007). A nanoplatinum catalyst for aerobic oxidation of alcohols in water. Angew. Chem. Int. Ed. Engl. *46*, 704–706.

75. Ganji, N., Karimi, B., Najafvand-Derikvandi, S., and Vali, H. (2020). Palladium supported on a novel ordered mesoporous polypyrrole/carbon nanocomposite as a powerful heterogeneous catalyst for the aerobic oxidation of alcohols to carboxylic acids and ketones on water. RSC Adv *10*, 13616–13631.

76. Ahmed, M.S., Mannel, D.S., Root, T.W., and Stahl, S.S. (2017). Aerobic oxidation of diverse primary alcohols to carboxylic acids with a heterogeneous Pd–Bi–Te/C (PBT/C) catalyst. Org. Process Res. Dev. *21*, 1388–1393.

77. Zhou, L., Chen, M., Wang, Y., Su, Y., Yang, X., Chen, C., and Xu, J. (2014). Au/mesoporous-TiO2 as catalyst for the oxidation of alcohols to carboxylic acids with molecular oxygen in water. Appl. Catal. A *475*, 347–354.

78. Grigg, R., Mitchell, T.R.B., and Sutthivaiyakit, S. (1981). Oxidation of alcohols by transition metal complexes—iv: the rhodium catalysed synthesis of esters from aldehydes and alcohols. Tetrahedron *37*, 4313–4319.

79. Liu, C., Wang, J., Meng, L., Deng, Y., Li, Y., and Lei, A. (2011). Palladium-catalyzed aerobic oxidative direct esterification of alcohols. Angew. Chem. Int. Ed. Engl. *50*, 5144–5148.

80. Gowrisankar, S., Neumann, H., and Beller, M. (2011). General and selective palladium-catalyzed oxidative esterification of alcohols. Angew. Chem. Int. Ed. Engl. *50*, 5139–5143.

81. Mannel, D.S., Ahmed, M.S., Root, T.W., and Stahl, S.S. (2017). Discovery of multicomponent heterogeneous catalysts via admixture screening: PdBiTe catalysts for aerobic oxidative esterification of primary alcohols. J. Am. Chem. Soc. *139*, 1690–1698.

82. Wang, L., Li, J., Dai, W., Lv, Y., Zhang, Y., and Gao, S. (2014). Facile and efficient gold-catalyzed aerobic oxidative esterification of activated alcohols. Green Chem *16*, 2164–2173.

83. Oliveira, R.L., Kiyohara, P.K., and Rossi, L.M. (2009). Clean preparation of methyl esters in one-step oxidative esterification of primary alcohols catalyzed by supported gold nanoparticles. Green Chem *11*, 1366–1370.

84. Gopi, E., Gravel, E., and Doris, E. (2019). Direct aerobic oxidation of alcohols into esters catalyzed by carbon nanotube-gold nanohybrids. Nanoscale Adv *1*, 1181–1185.

85. Miyamura, H., Yasukawa, T., and Kobayashi, S. (2010). Aerobic oxidative esterification of alcohols catalyzed by polymer-incarcerated gold nanoclusters under ambient conditions. Green Chem *12*, 776–778.

86. Jagadeesh, R.V., Junge, H., Pohl, M.-M., Radnik, J., Brückner, A., and Beller, M. (2013). Selective oxidation of alcohols to esters using heterogeneous Co3O4–N@C catalysts under mild conditions. J. Am. Chem. Soc. *135*, 10776–10782.

87. Zhong, W., Liu, H., Bai, C., Liao, S., and Li, Y. (2015). Base-free oxidation of alcohols to esters at room temperature and atmospheric conditions using nanoscale Co-based catalysts. ACS Catal *5*, 1850–1856.

88. Su, H., Zhang, K.-X., Zhang, B., Wang, H.-H., Yu, Q.-Y., Li, X.-H., Antonietti, M., and Chen, J.-S. (2017). Activating cobalt nanoparticles via the Mott-Schottky effect in nitrogen-rich carbon shells for base-free aerobic oxidation of alcohols to esters. J. Am. Chem. Soc. *139*, 811–818.

89. Nandan, D., Zoppellaro, G., Medřík, I., Aparicio, C., Kumar, P., Petr, M., Tomanec, O., Gawande, M.B., Varma, R.S., and Zbořil, R. (2018). Cobalt-entrenched N-, O-, and S-tridoped carbons as efficient multifunctional sustainable catalysts for base-free selective oxidative esterification of alcohols. Green Chem *20*, 3542–3556.

90. Yin, W., Wang, C., and Huang, Y. (2013). Highly practical synthesis of nitriles and heterocycles from alcohols under mild conditions by aerobic double dehydrogenative catalysis. Org. Lett. *15*, 1850–1853.

91. Dornan, L.M., Cao, Q., Flanagan, J.C.A., Crawford, J.J., Cook, M.J., and Muldoon, M.J. (2013). Copper/TEMPO catalysed synthesis of nitriles from aldehydes or alcohols using aqueous ammonia and with air as the oxidant. Chem. Commun. *49*, 6030–6032.

92. Dighe, S.U., Chowdhury, D., and Batra, S. (2014). Iron nitrate/TEMPO: a superior homogeneous catalyst for oxidation of primary alcohols to nitriles in air. Adv. Synth. Catal. *356*, 3892–3896.

93. Preger, Y., Root, T.W., and Stahl, S.S. (2018). Platinum-based heterogeneous catalysts for nitrile synthesis via aerobic oxidative coupling of alcohols and ammonia. ACS Omega *3*, 6091–6096.

94. Ishida, T., Watanabe, H., Takei, T., Hamasaki, A., Tokunaga, M., and Haruta, M. (2012). Metal oxide-catalyzed ammoxidation of alcohols to nitriles and promotion effectof gold nanoparticles for one-pot amide synthesis. Appl. Catal. A *425*, 85–90.

95. Oishi, T., Yamaguchi, K., and Mizuno, N. (2009). Catalytic oxidative synthesis of nitriles directly from primary alcohols and ammonia. Angew. Chem. Int. Ed. Engl. *48*, 6286–6288.

96. Wang, H., Xu, D., Guan, E., Wang, L., Zhang, J., Wang, C., Wang, S., Xu, H., Meng, X., Yang, B., et al. (2020). Atomically dispersed Ru on manganese oxide catalyst boosts oxidative cyanation. ACS Catal *10*, 6299–6308.

97. Jagadeesh, R.V., Junge, H., and Beller, M. (2014). Green synthesis of nitriles using non-noble metal oxides-based nanocatalysts. Nat. Commun. *5*, 4123.

98. Shang, S., Wang, L., Dai, W., Chen, B., Lv, Y., and Gao, S. (2016). High catalytic activity of mesoporous Co–N/C catalysts for aerobic oxidative synthesis of nitriles. Catal. Sci. Technol. *6*, 5746–5753.

99. Sun, K.-K., Sun, J.-L., Lu, G.-P., and Cai, C. (2019). Enhanced catalytic activity of cobalt nanoparticles encapsulated with an N-doped porous carbon shell derived from hollow ZIF-8 for efficient synthesis of nitriles from primary alcohols in water. Green Chem *21*, 4334–4340.

100. Soulé, J.-F., Miyamura, H., and Kobayashi, S. (2011). Powerful amide synthesis from alcohols and amines under aerobic conditions catalyzed by gold or gold/iron, -nickel or -cobalt nanoparticles. J. Am. Chem. Soc. *133*, 18550–18553.

101. Yamaguchi, K., Kobayashi, H., Oishi, T., and Mizuno, N. (2012). Heterogeneously catalyzed synthesis of primary amides directly from primary alcohols and aqueous ammonia. Angew. Chem. Int. Ed. Engl. *51*, 544–547.

102. Nie, R., Shi, J., Xia, S., Shen, L., Chen, P., Hou, Z., and Xiao, F.-S. (2012). MnO2/graphene oxide: a highly active catalyst for amide synthesis from alcohols and ammonia in aqueous media. J. Mater. Chem. *22*, 18115–18118.

103. Merck, Methanol. (n.d.). https://www.sigmaaldrich.com/catalog/search?term=methanol&interface=All_DE&N0&mode=match%20partialmax&lang=de&region=DE&focus=product.

104. Stahl, S.S., and Alsters, P.L. (2016). Liquid Phase Aerobic Oxidation Catalysis: Industrial Applications and Academic Perspectives (Wiley-VCH).

105. Jagadeesh, R.V., Surkus, A.-E., Junge, H., Pohl, M.-M., Radnik, J., Rabeah, J., Huan, H., Schünemann, V., Brückner, A., and Beller, M. (2013). Nanoscale Fe2O3-based catalysts for selective hydrogenation of nitroarenes to anilines. Science *342*, 1073–1076.

106. Jagadeesh, R.V., Murugesan, K., Alshammari, A.S., Neumann, H., Pohl, M.-M., Radnik, J., and Beller, M. (2017). MOF-derived cobalt nanoparticles catalyze a general synthesis of amines. Science *358*, 326–332.

107. Ryabchuk, P., Agostini, G., Pohl, M.-M., Lund, H., Agapova, A., Junge, H., Junge, K., and Beller, M. (2018). Intermetallic nickel silicide nanocatalyst-a non-noble metal-based general hydrogenation catalyst. Sci. Adv. *4*, eaat0761.

108. Jagadeesh, R.V., Stemmler, T., Surkus, A.-E., Bauer, M., Pohl, M.-M., Radnik, J., Junge, K., Junge, H., Brückner, A., and Beller, M. (2015). Cobalt-based nanocatalysts for green oxidation and hydrogenation processes. Nat. Protoc. *10*, 916–926.

109. Biesinger, M.C., Payne, B.P., Grosvenor, A.P., Lau, L.W.M., Gerson, A.R., and Smart, R.S.C. (2011). Resolving surface chemical states in XPS analysis of first row transition metals, oxides, and hydroxides: Cr, Mn, Fe, Co, and Ni. Appl. Surf. Sci. *257*, 2717–2730.

110. Jaouen, F., Herranz, J., Lefèvre, M., Dodelet, J.-P., Kramm, U.I., Herrmann, I., Bogdanoff, P., Maruyama, J., Nagaoka, T., Garsuch, A., et al. (2009). Cross-laboratory experimental study of non-noble-metal electrocatalysts for the oxygen reduction reaction. ACS Appl. Mater. Interfaces *1*, 1623–1639.

111. Haufe, G., and Leroux, F. (2018). Fluorine in Life Sciences: Pharmaceuticals, Medicinal Diagnostics, and Agrochemicals (Elsevier).

112. de Meijere, A., and Diederich, F. (2004). Metal-Catalyzed Cross-Coupling Reactions, Second Edition (Wiley-VCH).

113. Pozharskii, A.F., Soldatenkov, A.T., and Katritzky, A.R. (2011). Heterocycles in Life and Society: an Introduction to Heterocyclic Chemistry, Biochemistry and Applications, Second Edition (Wiley).

114. Carey, J.S., Laffan, D., Thomson, C., and Williams, M.T. (2006). Analysis of the reactions used for the preparation of drug candidate molecules. Org. Biomol. Chem. *4*, 2337–2347.

115. van Putten, R.-J., van der Waal, J.C., de Jong, E., Rasrendra, C.B., Heeres, H.J., and de Vries, J.G. (2013). Hydroxymethylfurfural, a versatile platform chemical made from renewable resources. Chem. Rev. *113*, 1499–1597.

116. Zhao, D., Su, T., Wang, Y., Varma, R.S., and Len, C. (2020). Recent advances in catalytic oxidation of 5-hydroxymethylfurfural. Mol. Catal. *495*, 111133.

117. Burdock, G.A. (1996). Encyclopedia of Food and Color Additives, First Edition (CRC Press).

118. Jennings, T.J. (1966). Process for preparing furonitrile. US patent US3260731A, filed March 2, 1964, and granted, July 12, 1966.

7. Curriculum Vitae

Vishwas G. Chandrashekhar

Leibniz-Institute for Catalysis, University of Rostock (LIKAT)

Room 1.120, Albert-Einstein-Str. 29a, 18059 Rostock, Germany.

Phone: +49(381)1281-329

Email: vishwas.chandrashekhar@catalysis.de; vishwasgc9@gmail.com

Date of birth: 12 October 1991

Place of birth: Shivamogga, India

Nationality: Indian

Research Experience:

11/2018 — Present	PhD Scholar, Leibniz Institute for Catalysis at the University of Rostock, Germany. **Thesis title:** "Development of Fe- and Co-based catalysts for sustainable organic synthesis" **Supervisors:** Prof. Dr. Matthias Beller and Prof. Dr. Jagadeesh Rajenahally
08/2014 — 10/2018	Senior Associate Scientist, Drug Discovery Chemistry, Syngene International Ltd (A Biocon Company), Bangalore, India. **Supervisors:** Dr. Santosh Kulkarni and Dr. Runa Pal
01/2014 — 02/2014	Project trainee at Apotex Pharmachem India Pvt. Ltd., Bangalore, India. **Thesis tittle:** "Synthesis and Characterization of some Impurities of APIXABAN" **Supervisors:** Dr. K. V. Ramana and Dr. Shreenivasa H. N. Murthy

Education:

2012 — 2014	Master of Science in Organic Chemistry (79.6%), Manasagangotri, University of Mysore, Mysore, India.
2009 — 2012	Bachelor of Science in Physics, Chemistry, Mathematics (70%), SRNM National College, Kuvempu University, Shivamogga, India.

Publications:

1. Homogeneous cobalt-catalyzed reductive amination for synthesis of functionalized primary amines
   Kathiravan Murugesan, Zhihong Wei, **Vishwas G. Chandrashekhar**, Helfried Neumann, Anke Spannenberg, Haijun Jiao, Matthias Beller, Rajenahally V. Jagadeesh
   Nat Commun, 2019, **10,** 5443.

2. Ultra-small cobalt nanoparticles from molecularly-defined Co–salen complexes for catalytic synthesis of amines
   Thirusangumurugan Senthamarai, **Vishwas G. Chandrashekhar**, Manoj B. Gawande, Narayana V. Kalevaru, Radek Zbořil, Paul C. J. Kamer, Rajenahally V. Jagadeesh* and Matthias Beller*
   Chem. Sci., 2020, **11,** 2973-2981.

3. General and selective synthesis of primary amines using Ni-based homogeneous catalysts
   Kathiravan Murugesan, Zhihong Wei, **Vishwas G. Chandrashekhar**, Haijun Jiao,* Matthias Beller* and Rajenahally V. Jagadeesh*
   Chem. Sci., 2020, **11,** 4332-4339. (With back cover picture)

4. Catalytic reductive aminations using molecular hydrogen for synthesis of different kinds of amines
   Kathiravan Murugesan,† Thirusangumurugan Senthamarai,† **Vishwas G. Chandrashekhar**,† Kishore Natte, Paul C. J. Kamer, Matthias Beller* and Rajenahally V. Jagadeesh*
   Chem. Soc. Rev., 2020, **49,** 6273-6328. (†1st, 2nd & 3rd authors equal contribution)

5. Reductive amination using cobalt-based nanoparticles for synthesis of amines
   Kathiravan Murugesan, **Vishwas G. Chandrashekhar**, Thirusangumurugan Senthamarai, Rajenahally V. Jagadeesh* and Matthias Beller*
   Nat Protoc, 2020, **15,** 1313-1337.

6. A general catalyst based on cobalt core–shell nanoparticles for the hydrogenation of *N*-heteroarenes including pyridines
   Kathiravan Murugesan, **Vishwas G. Chandrashekhar**, Carsten Kreyenschulte, Matthias Beller,* and Rajenahally V. Jagadeesh*
   Angew. Chem. Int. Ed., 2020, **59,** 17408-17412.

7. Reductive amination, hydrogenation and hydrodeoxygenation of 5-hydroxymethylfurfural using silica-supported cobalt-nanoparticles
Vishwas G. Chandrashekhar, Kishore Natte, Asma M. Alenad, Ahmad S. Alshammari, Carsten Kreyenschulte, and Rajenahally V. Jagadeesh*
ChemCatChem, 2021, **13,** 1-10.

8. Silica-supported Fe/Fe–O nanoparticles for the catalytic hydrogenation of nitriles to amines in the presence of aluminium additives
Vishwas G. Chandrashekhar, Thirusangumurugan Senthamarai, Ravishankar G. Kadam, Ondřej Malina, Josef Kašlík, Radek Zbořil,* Manoj B. Gawande,* Rajenahally V. Jagadeesh* and Matthias Beller*
Nat Catal, 2022, **5,** 20-29.

9. A ‘‘universal’’ catalyst for aerobic oxidations to synthesize (hetero)aromatic aldehydes, ketones, esters, acids, nitriles, and amides
Thirusangumurugan Senthamarai, **Vishwas G. Chandrashekhar**, Nils Rockstroh, Jabor Rabeah, Stephan Bartling, Matthias Beller,* Rajenahally V. Jagadeesh*
Chem, 2022, **8,** 508-531.

10. Expanding the catalytic hydrogenation toolbox for synthesis of amines
Vishwas G. Chandrashekhar, Wolfgang Baumann, Matthias Beller* and Rajenahally V. Jagadeesh*
Submitted to Science on 17th December 2021 (under revision)

Conference:

- Poster presentation at **Cutting-Edge Homogeneous Catalysis 1** (CCIMC, European project, online 4th to 6th May 2021), poster entitled “Cobalt-catalyzed reductive amination for synthesis of functionalized primary amines”
- Poster presentation at **Hanse Chemistry Symposium 2019** (Rostock, Germany, May 2019), and poster entitled “Hydrogenation of nitriles and nitroarenes using cobalt nanoparticles”

Awards:

- DFG fellowship by NFDI4Cat, LIKAT, Rostock, Germany (July 2021-present)
- PhD fellowship by Leibniz-Institute für Katalyse, Rostock, Germany (Nov 2018-June 2021)
- As trainee gained a team award for successful completion of a library project from Syngene, India

- Won “TEAM EXCELENCY” award for separation of enantiomers by chiral resolution, from Syngene, India.

Research Interest:

Organic synthesis, Homogeneous and heterogeneous catalysis, Asymmetric synthesis, C-H activations, Aminations, Photocatalysis, Organocatalysis.

Research Skills:

- Organic synthesis (Small scale, Bulk scale)
- Library Synthesis
- Homogeneous and Heterogeneous catalysis
- Working in Glove box
- Operating analytical instruments: GC, GC-MS, HPLC, LCMS, IR, NMR.
- Pyrolysis Oven, Tubular Furnace, and Rotatory Furnace.
- Flash Chromatography (Biotage, Combiflash, Prep.HPLC)
- Microwave Reactor (Biotage)
- Electronic Lab Notebooks

Language Skills:

Kannada (mother language), English (fluent), Hindi (fluent), German (basic)

References:

Prof. Dr. Matthias Beller, Director, Leibniz Institute for Catalysis, Rostock, Germany.
Tel: +49 (381)1281-113; *email:* matthias.beller@catalysis.de

Prof. Dr. Jagadeesh Rajenahally, Group Leader, Synergy between Homogeneous and Heterogeneous Catalysis, Leibniz Institute for Catalysis, Rostock, Germany.
Tel: +49 (381)1281-210; *email:* jagadeesh.rajenahally@catalysis.de

Dr. Helfried Neumann, Group Leader, Catalysis for Life Sciences, Leibniz Institute for Catalysis, Rostock, Germany.
Tel: +49 (381)1281-171; *email:* helfried.neumann@catalysis.de

8. Selbstständigkeitserklärung

4. Erklärung gemäß § 4 Absatz 1 Buchstaben g und h der Promotionsordnung

Doktorandinnen/Doktoranden-Erklärung gemäß § 4 Absatz 1 Buchstaben g und h der Promotionsordnung der Mathematisch-Naturwissenschaftlichen Fakultät der Universität Rostock

Name ..... Vishwas Gajanor Chandrashekhar .....

(Name, Vorname)

Anschrift ..... Albert-Einstein-Str. 29a, 18059, Rostock .....

(Straße, PLZ, Wohnort)

Ich habe eine Dissertation zum Thema

..... Development of Fe- and Co-based catalysts for sustainable organic synthesis .....

.....

an der Mathematisch-Naturwissenschaftlichen Fakultät der Universität Rostock angefertigt. Dabei wurde ich von Frau/Herrn

..... Prof. Dr. Matthias Beller ..... betreut.

Ich gebe folgende Erklärung ab:

1. Die Gelegenheit zum vorliegenden Promotionsvorhaben ist mir nicht kommerziell vermittelt worden. Insbesondere habe ich keine Organisation eingeschaltet, die gegen Entgelt Betreuerinnen/Betreuer für die Anfertigung von Dissertationen sucht oder die mir obliegenden Pflichten hinsichtlich der Prüfungsleistungen für mich ganz oder teilweise erledigt.

2. Ich versichere hiermit an Eides statt, dass ich die vorliegende Arbeit selbstständig angefertigt und ohne fremde Hilfe verfasst habe. Dazu habe ich keine außer den von mir angegebenen Hilfsmitteln und Quellen verwendet und die den benutzten Werken inhaltlich und wörtlich entnommenen Stellen habe ich als solche kenntlich gemacht.

Rostock, den 21/03/22 ..... Vishwas G. C

(Unterschrift)